Novel Transition Metal Complexes based on N,N and N,P Ligands As Catalysts for Ethylene Transformation Reactions

By

Andrew John Swarts

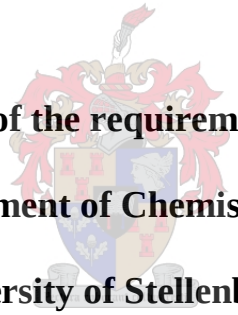

A dissertation in fulfilment of the requirement for the degree of Ph.D in Chemistry in the Department of Chemistry and Polymer Science, University of Stellenbosch.

Supervisor: Prof. S. F. Mapolie

April 2014

DECLARATION

By submitting this thesis/dissertation electronically, I declare that the entirety of the work contained therein is my own, original work, that I am the sole author thereof (save to the extent explicitly otherwise stated), that reproduction and publication thereof by Stellenbosch University will not infringe any third party rights and that I have not previously in its entirety or in part submitted it for obtaining any qualification.

December 2013

This PhD Dissertation is dedicated to the loving memory of my grandmother, Clara Simpson. Your legacy remains a source of inspiration and joy to us.

ACKNOWLEDGEMENTS

All thanks and praise goes to our Heavenly Father, who through His grace and mercy has carried me thus far and allowed me to complete this degree. His preservation is absolute and His mercy is all-encompassing. Thank you to the ministers in the congregation for their prayers and words of upliftment.

To my supervisor, Professor Selwyn F. Mapolie, I express my sincere gratitude for his guidance and mentorship throughout this research project. I complete this degree a better scientist and I owe it to your input and support.

A special thank you to my family: Andre Swarts, Roseline Swarts, Clara Simpson, Justin and Jason Swarts. Your love and support during this time is appreciated and my gratitude to you lives in my soul.

To my friends: Marco, Morph, Lyle, Paul, Wesley, Ludwig, Robin, Marlin, Angelique, Candice, Rene, Leanne, Nicole, Tracey, thank you for all your support and understanding throughout this degree. I love you guys!!

To the Organometallic Research Group at Stellenbosch University, Hennie Kotze, Drs. Gangadhar Bagihalli and Feng Zheng, Corli Joubert and Derik Wilbers, thank you for making the slaving in the lab a more pleasurable experience. Also, thank you for putting up with my stress-relief mechanism, singing and whistling very loudly.

I would like to thank Elsa Malherbe and Dr. Vincent Smith, for their assistance with NMR and SCD analyses.

Dr Feng Zheng is gratefully acknowledged for her assistance and guidance with the DFT calculations performed as part of this study.

ACKNOWLEDGEMENTS

Thank you to Drs Sadiq Cherutazekatt and Pritish Sinha, for their assistance with CRYSTAF and HT-SEC analyses and Solid State NMR on the polymer samples.

Thank to my friends and colleagues in Polymer Science, William and Divann, for the insightful discussions and assistance with all things polymer.

A big thank you to Sylette, Malcolm Taylor and Malcolm McLean, Johnny, Chalon and Moebarick for making our building the best building to work in, in the Chemistry Department. Period.

A special thank you to my good friend Dr Rehana Malgas-Enus, not only for your friendship, but also for proof-reading this thesis and providing constructive criticism throughout the writing process.

To my wife, Megan Samantha Swarts: You've been the voice of reason and calm when things became so difficult. You've carried me and supported me even when I thought that there was no light at the end of the tunnel. I thank you from the bottom of my heart for your love and encouragement. You are an angel in my life.

Oral contributions:

Andrew Swarts and Selwyn Mapolie

The application of novel iminophosphine-ligate Cr(III) complexes in ethylene polymerisation CATSA Annual Conference, Club Mykonos, Langebaan, South Africa, 2012.

Andrew Swarts and Selwyn Mapolie

Reactivity of cationic Pd N-alkyl dipyridylaldiminato complexes toward ethylene: Experimental and theoretical investigation. 246th American Chemical Society Fall Meeting, Indianapolis, Indiana USA, 2013.

Andrew Swarts and Selwyn Mapolie

Reactivity of cationic palladium N-alkyl dipyridylaldiminato complexes toward ethylene: Experimental and Theoretical Investigation. CATSA Annual Conference, Wild Coast Sun, Kwazulu-Natal, South Africa, 2013.

Reactivity of cationic Pd N-alkyl dipyridylaldiminato complexes toward ethylene: Experimental and theoretical investigation. Andrew Swarts, Feng Zheng, Ebbe Nordlander and Selwyn Mapolie. Submitted to *Organometallics.*

***The application of novel Cr(III) iminophosphine-ligated complexes in ethylene polymerisation: Insights from experiment and theory*.** Manuscript in preparation.

The application of novel Dinuclear Ni(II) N-alkyl dipyridylaldiminato complexes in selective ethylene dimerisation. Manuscript in preparation.

ABSTRACT

A series of largely novel *N*-alkyl 2,2′-dipyridylamine ligands of general formula $(2\text{-}C_5H_3NR)_2NR'$, (**a**): R = H, R′ = Me; (**b**): R = H, R′ = benzyl; (**c**): R = H, R′ = methylcyclohexyl; (**d**): R = H, R′ = neopentyl; (**e**): R = Me, R′ = Me) were prepared by a modified method involving base-mediated *N*-alkylation with the respective alkyl halide. The ligands were characterised by FT-IR spectroscopy, NMR (^{1}H and ^{13}C) spectroscopy, ESI-MS analysis, and in the case of the novel ligands, by elemental analysis. Reaction of ligands **a-e** with (COD)PdMeCl, generated the neutral methylpalladium complexes: [Pd(**a**)MeCl] (**2a**); [Pd(**b**)MeCl] (**2b**); [Pd(**c**)MeCl] (**2c**); [Pd(**d**)MeCl] (**2d**) and [Pd(**e**)MeCl] (**2e**). The neutral complexes were characterised by a range of spectroscopic and analytical techniques. The molecular structure of **2e** was established unambiguously by SCD analysis. To generate cationic methylpalladium complexes, **2a-2e** were subjected to chloride-abstraction by $NaBAr'_4$ in the presence of acetonitrile as coordinating solvent. Cationic acetonitrile adducts, **2f-2j** with general formula: $[PdMe(\mathbf{L})(MeCN)]^+[BAr'_4]^-$, where L = ligands **a-e** respectively, were isolated. Complexes **2f-2j** were found to be unstable over time, decomposing to palladium black both in the solid state and solution. The inherent instability of the complexes precluded unambiguous characterisation by SCD and elemental analysis. Despite this, satisfactory analytical data could be obtained by FT-IR spectroscopy, NMR (^{1}H and ^{13}C) spectroscopy and ESI-MS analysis. To generate more stable cationic complexes, the neutral analogues were reacted with $NaBAr'_4$ in the presence of pyridine as coordinating solvent. Cationic pyridine adducts, **2k-2o** with general formula $[PdMe\{\mathbf{a}\}(C_5H_5N)]^+[BAr'_4]^-$, where L = ligands **a-e** respectively, were isolated as air- and moisture-stable solids. The complexes were characterised by a range of analytical techniques, and in the case of **2o**, by SCD analysis. Employing an excess of pyridine during the synthesis of the cationic complexes led to the isolation of two species: the desired cationic pyridine-ligated complex and a cationic

tris(pyridine) methylpalladium complex. The molecular structure of the cationic tris(pyridine) methylpalladium analogue (**2o-A**) of complex **2o** was confirmed by SCD analysis.

The reactivity of the cationic acetonitrile complexes, **2f-2j**, toward ethylene was evaluated. Under 5 bar ethylene pressure and ambient reaction conditions, **2f-2j** were found to dimerise ethylene to a mixture of 1- and 2-butenes with low activities of up to 7.4 h^{-1}. In all cases, the observed selectivity was toward the formation of 2-butenes. Low temperature spectroscopic investigations of the reactivity of **2f** and **2j**, allowed for the determination of first-order $k_{insert,Me}$ and $k_{insert,Et}$ which demonstrated differences in palladium electrophilicity. In addition, DFT calculations supported the observed differences in associative olefin exchange behaviour and established differences in 1-butene isomerisation energetics for **2f** and **2j**.

Reaction of the ligands, **a-e**, with (DME)$NiCl_2$ allowed for the isolation of μ-Cl Ni(II) complexes: [Ni(μ-Cl){**a**}Cl]$_2$ (**4a**); [Ni(μ-Cl){**b**}Cl]$_2$ (**4b**); [Ni(μ-Cl){**c**}Cl]$_2$ (**4c**); [Ni(μ-Cl){**d**}Cl]$_2$ (**4d**) and [Ni(μ-Cl){**e**}Cl]$_2$ (**4e**). The complexes were characterised by FT-IR spectroscopy, magnetic susceptibility measurements, and in the case of **4a**, SCD analysis. Analysis by ESI-MS spectrometry led to the identification of solvent-dependent fragmentation and aggregation processes in solution. In the case of complex **4e**, an acid-mediated hydrolysis process was identified. The product of hydrolysis, the protonated ligand and a tetrachloronickelate salt (**4e-A**), was characterised by SCD analysis.

Activation of **4a-4e** with alkyl aluminium reagents generated highly active catalysts for the oligomerisation of ethylene, with activities of up to 864 $kg_{oligomers}.mol_{Ni}.h^{-1}$ and high selectivity toward the formation of butenes. In general, *trans* 2-butene was observed as the major isomer, with the exception of oligomers produced by **4e**. In the case of **4e**, the

selectivity for 1-butene was 98 %, thereby demonstrating the effect that the introduction of steric pressure in the coordination sphere of the catalyst has on selectivity.

A series of known and novel iminophosphine ligands of general formula {[RN=C-(*o*-PPh_2-C_6H_4)]}, (**5a**): R = *n*-propyl; (**5b**): R = 2,6-*i*Pr_2-C_6H_3; (**5c**): R = 2,4,6-Me_3-C_6H_2; (**5d**): R = *t*-Bu; (**5e**): R = 2,2-$(Me)_2$Pr were prepared by Schiff base condensation of the corresponding primary amine with *o*-(diphenylphosphino)benzaldehyde. Ligands **5a-5e** were characterised by FT-IR and NMR spectroscopy (^{1}H, ^{13}C and ^{31}P) as well as ESI-MS spectrometry and elemental analysis. Reaction of the ligands with $Cr(THF)_3Cl_3$ generated the mononuclear iminophosphine-ligated complexes: [$CrCl_3${**5a**}] (**5f**); [$CrCl_3${**5b**}] (**5g**); [$CrCl_3${**5c**}] (**5h**); [$CrCl_3${**5d**}] (**5i**) and [$CrCl_3${**5e**}] (**5j**). Complexes **5f-5j**, were characterised by FT-IR spectroscopy, magnetic susceptibility, ESI-MS spectrometry, elemental analysis and in the case of **5g**, SCD analysis. In the presence of alkyl aluminium reagents as co-catalysts, **5f-5j** were active catalysts for ethylene polymerisation. Under optimised conditions activities of up to 504 $kg_{PE}.mol_{Cr}^{-1}.h^{-1}$ were obtained. Characterisation of the polymer obtained by $^{13}C\{^{1}H\}$ NMR spectroscopy (solution and solid state), DSC, PXRD and HT-SEC analysis showed that the bulk material was high-density polyethylene and that the polymerisation was multi-modal in character. Fractionation techniques, followed by HT-SEC and DSC analysis, allowed for the identification of a soluble fraction present in the bulk polymer, with characterisation results indicative of linear low-density polyethylene. To probe whether ethylene oligomerisation or polymerisation was most favourable, DFT calculations were performed on a simplified model of **5f**. The DFT calculations showed that both a Cossee-Arlman and metallacycle mechanism could be operative in the gas phase and that the energy differences between key intermediates in each catalytic cycle were negligible.

‘n Reeks grootliks nuwe *N*-alkiel 2,2′-dipiridielamien ligande met die algemene formule $(2\text{-}C_5H_3NR)_2NR'$, **a**: R = H, R′ = Me; **b**: R = H, R′ = bensiel; **c**: R = H, R′ = metielsikloheksiel; **d**: R = H, R′ = neopentiel; **e**: R = Me, R′ = Me), is met behulp van ‘n aangepasde metode wat *N*-alkilering deur verskillende alkiel haliede in die teenswoordigheid van ‘n basis behels, berei. Die ligande is volledig met behulp van FT-IR, ^{1}H- en ^{13}C-KMR-spektroskopie, ESI-massaspektrometrie en in die geval van nuwe ligande, deur elementanalise gekarakteriseer. Die reaksie van die ligande **a-e** met [(COD)Pd(Cl)Me] het tot die vorming van ‘n reeks neutrale metielpalladiumverbindings gely: [Pd(**a**)Me(Cl)] (**2a**); [Pd(**b**)Me(Cl)] (**2b**); [Pd(**c**)Me(Cl)] (**2c**); [Pd(**d**)Me(Cl)] (**2d**) en [Pd(**e**)Me(Cl)] (**2e**). Die neutrale komplekse is volledig deur ‘n verskeidenheid spektroskopies en analities tegnieke gekarakteriseer. In die geval van verbinding **2e**, is ‘n kristal- en molekulêre struktuurbepaling uitgevoer. Ten einde kationiese metielpalladium komplekse te vorm, is **2a-2e** met die chloried-ontrekkingsmiddel, $NaBAr'_4$, in die teenswoordigheid van asetonitriel as stabiliserende ligand, gereageer. Kationiese asetonitriel komplekse $[PdMe\{\mathbf{a}\}(NCMe)]^+[BAr'_4]^-$ (**2f**), $[PdMe\{\mathbf{b}\}(NCMe)]^+[BAr'_4]^-$ (**2g**), $[PdMe\{\mathbf{c}\}(NCMe)]^+[BAr'_4]^-$ (**2h**), $[PdMe\{\mathbf{d}\}(NCMe)]^+[BAr'_4]^-$ (**2i**) en $[PdMe\{\mathbf{e}\}(NCMe)]^+[BAr'_4]^-$ (**2j**) is geïsoleer. Kationiese komplekse **2f-2j** was onstabiel mettertyd en het swart palladium neerslag gevorm, beide in oplossing en as vastestof. Die onstabiliteit het verhoed dat die komplekse met behulp van enkelkristal X-straaldiffraksie en elementanalise gekarakteriseer kon word. Ten spyte daarvan kon bevredigende analitiese data deur middel van FT-IR-, ^{1}H- en ^{13}C-KMR-spektroskopie, ESI-massaspektrometrie verkry word. Om meer stabiel kationiese verbindings te genereer, is **2a-2e** met $NaBAr'_4$ in die teenswoordigheid van piridien as stabiliserende ligand, gereageer. Kationiese piridien komplekse $[PdMe\{\mathbf{a}\}(C_5H_5N)]^+[BAr'_4]^-$ (**2k**), $[PdMe\{\mathbf{b}\}(C_5H_5N)]^+[BAr'_4]^-$ (**2l**),

[PdMe{**c**}(C_5H_5N)]$^+$[BAr′$_4$]$^-$ (**2m**), [PdMe{**d**}(C_5H_5N)]$^+$[BAr′$_4$]$^-$ (**2n**) en [PdMe{**e**}(C_5H_5N)]$^+$[BAr′$_4$]$^-$ (**2o**), is as stabiele vastestowwe geïsoleer en ten volle gekarakteriseer. In teenswoordigheid van ’n oormaat piridien, vorm twee verbindings: die gewenste kationiese piridien-gekoördineerde verbinding en ’n kationiese tris(piridien)metielpalladiumverbinding. Die molekulêre struktuur van die kationiese tris(piridien)metielpalladiumverbinding, **2o-A**, is deur X-straalkristallografie bepaal.

Die reaktiwiteit van die kationiese asetonitrielverbindings, **2f-2j**, teenoor etileen is geëvalueer. Teen ’n druk van 5 bar en by kamertemperatuur is gevind dat **2f-2j** etileen dimeriseer na ’n mengsel van 1-buteen en *cis*- en *trans*-2-buteen, met lae akitiwiteit van tot 7.4 h^{-1}. In alle gevalle begunstig die produkselektiwiteit van die katalisatore die vorming van *cis*- en *trans* 2-buteen. Die reaktiwiteit van **2f** en **2j** is deur middel van lae-temperatuur KMR-spektroskopie ondersoek. Dit het gelei tot eerste-orde $k_{\text{invoeging,Me}}$ and $k_{\text{invoegin,Et}}$ *k*-waardes, wat die verskil in die palladium elektrofilisiteit van **2f** en **2j** geïllustreer het. Verder is digtheidsfunksionaalteorie (DFT) gebruik om die eksperimenteelbepaalde waarnemings teoreties te ondersteun. Die berekeninge het onder andere die verskille in assosiatiewe olefienuitruiling beklemtoon en verskille in energie verbonde aan 1-buteenisomerisasie geïdentifiseer.

Die reaksie van ligande **a-e** met [(DME)$NiCl_2$] het die dikernige μ-Cl Ni(II)-komplekse gevorm: [Ni(μ-Cl){**a**}Cl]$_2$ (**4a**); [Ni(μ-Cl){**b**}Cl]$_2$ (**4b**); [Ni(μ-Cl){**c**}Cl]$_2$ (**4c**); [Ni(μ-Cl){**d**}Cl]$_2$ (**4d**) and [Ni(μ-Cl){**e**}Cl]$_2$ (**4e**). Die komplexkse is met behulp van FT-IR spektroskopie, magnetiese metings en, in die geval van **4a**, deur enkelkristal X-straaldiffraksie gekarakteriseer. Oplosmiddelafhanklike fragmentasie- en samevoegingsprosesse is deur middel van ESI-MS spektrometrie geïdentifiseer. In die geval van **4e**, was ’n suur-bemiddelde hidrolise proses geïdentifiseer. Die produk van hidrolise, ’n

tetrakloronikkel sout, **4e-A**, is deur middel van enkelkristal X-straaldiffraksie gekarakteriseer. Aktivering van **4a-4e** met alkielaluminiumreagense het hoogs aktiewe katalisatore gevorm vir die selektiewe oligomerisasie van etileen, met aktiwiteite so hoog as 864 $kg_{oligomers}.mol_{Ni}.h^{-1}$ vir die vorming van butene. Oor die algemeen is *trans*-2-buteen die isomeer wat hoofsaaklik gevorm word, behalwe in die geval van **4e**. In hierdie instansie is die selektiwiteit vir 1-buteen 98 %. Hierdie waarneming demonstreer die effek van steriese druk in die koordinasiesfeer van die katalisator op selektiwiteit.

Die reeks bekende en nuwe imino-fosfien ligande met die algemene formule: {[RN=C-(*o*-PPh_2-C_6H_4)]}, (**5a**): R = *n*-propiel; (**5b**): R = 2,6-*i*-Pr_2-C_6H_3; (**5c**): R = 2,4,6-Me_3-C_6H_2; (**5d**): R = *t*-Bu; (**5e**): R = 2,2-$(Me)_2$Pr, is deur middel van Schiffbasiskondensasie van die ooreenstemmende primêre amien en *o*-(difenielfosfieno)bensaldehied berei. Die ligande is volledig met behulp van FT-IR spektroskopie, KMR-(^{1}H, ^{13}C en ^{31}P) spektroskopie, ESI-massaspektrometrie en elementanalise gekarakteriseer. In die reaksie van die ligande met $[(THF)_3CrCl_3]$ het die monokernige Cr(III) iminofosfien komplekse $[CrCl_3${**5a**}] (**5f**), $[CrCl_3${**5b**}] (**5g**), $[CrCl_3${**5c**}] (**5h**), $[CrCl_3${**5d**}] (**5i**) en $[CrCl_3${**5e**}] (**5j**) gevorm. Komplekse **5f-5j**, is ten volle met behulp van FT-IR-spektroskopie, magnetiese metings, ESI-massaspektrometrie en, in die geval van **5g**, met enkelkristal X-straaldiffraksie gekarakteriseer. In die teenswoordigheid van alkielaluminiumreagense as ko-katalisatore, is **5f-5j** aktiewe katalisatore vir etileen polimerisasie. Onder optimale omstandighede is aktiwiteite so hoog as 504 $kg_{PE}.mol_{Cr}^{-1}.h^{-1}$ waargeneem. Die gevormde polimeer is deur middel van ^{13}C KMR spektroskopie (beide as oplossing en as vastestof), differensiële skanderingskalorimetrie (DSC), poeier X-straaldiffraksie (PXRD), HT-SEC-chromatografie gekarakteriseer, wat aangedui het dat die polimeer hoë-digtheid poliëtileen was. Daarbenewens het die analitiese data getoon dat die polimerisasie deur verskeie aktiewe sentra plaasvind. Fraksioneringstegnieke, gevolg deur DSC en HT-SEC kromatografie, het

die karakterisering van ’n oplosbare gedeelte van die polimeer moontlik gemaak. Die analitiese data het ooreengestem met wat tipies vir lineêre lae-digtheid poliëtileen verwag word. Om te bevestig of beide etileenoligomerisasie en etileenpolimerisasie moontlik is met die nuwe katalisator, is DFT-berekeninge op ’n vereenvoudigde model van **5f** uitgevoer. Die berekeninge toon dat beide ’n Cossee-Arlman meganisme en metallasikliese meganisme van toepassing op ons sisteem kan wees, en dat die verskil in energie tussen twee belangrike tussenverbindings in beide katalitiese meganismes baie klein is.

Table of Contents

Chapter 1: Mechanistic insight in transition metal-catalysed olefin transformations toward rational catalyst design.

Chapter 4: Synthesis and application of Ni(II) N-Alkyl Dipyridylaldiminato Complexes as Olefin Oligomerisation Precatalysts.

Chapter 5: Iminophosphine-ligated Cr(III) complexes and their application as catalyst precursors in ethylene polymerisation.

Chapter 1: Mechanistic insights in transition metal-catalysed olefin transformations toward rational catalyst design.

Chapter 2: Synthesis and Characterisation of neutral and cationic N-alkyl dipyridylaldiminato palladium methyl complexes.

Chapter 3: Reactivity of cationic N-alkyl dipyridylaldiminato complexes toward ethylene: Insights from experiment and theory.

Chapter 2: Synthesis and characterisation of neutral and cationic N-alkyl dipyridylaldiminato palladium methyl complexes.

Chapter 3: Reactivity of cationic N-alkyl dipyridylaldiminato complexes toward ethylene: Insights from experiment and theory.

Chapter 4: Synthesis and application of Ni(II) N-Alkyl Dipyridylaldiminato Complexes as Olefin Oligomerisation Precatalysts.

Chapter 5: Iminophosphine-ligated Cr(III) complexes and their application as catalyst precursors in ethylene polymerisation.

Å	Angstrom
MeCN	Acetonitrile
br.	broad
BAr'_4	tetrakis(bis-3,5-trifluoromethylphenyl)borate
δ	chemical shift
$CDCl_3$	deuterated chloroform
CD_2Cl_2	deuterated dichloromethane
COD	1,5-cyclooctadiene
CP/MAS	cross-polarisation magic-angle spinning
CRYSTAF	Crystallisation Analysis Fractionation
ESI-MS	Electrospray ionisation mass spectrometry
s	singlet
d	doublet
dd	doublet of doublets
dt	doublet of triplets
m	multiplet
dba	dibenzylideneacetone
DCM	dichloromethane
DFT	Density Functional Theory
QM	Quantum mechanics
MM	Molecular mechanics
ESI-MS	Electron Spray Ionisation Mass Spectrometry

FT-IR	Fourier Transform Infra Red Spectroscopy
GC-FID	Gas Chromatography Flame Ionisation Detector
h	hour(s)
Hz	hertz
^{i}Pr	*iso*-propyl
J	coupling constant
m	multiplet
MAO	methylaluminoxane
MMAO	modified methylaluminoxane
PMAO-IP	polymeric methylaluminoxane
DEAC	diethyl aluminium chloride
M.p.	melting point
min	minute(s)
m/z	mass to charge ratio
ml	millilitres
mmol	millimole
Me	methyl
MHz	megahertz
NMR	Nuclear Magnetic Resonance Spectroscopy
ppm	parts per million
PXRD	Powder X-ray diffraction
SCD	Single Crystal X-Ray Diffraction

1.1 Introduction.

One of the most significant scientific discoveries of the 20th century must without a doubt be that of polyolefins. These macromolecules, the microstructure of which directly affects its properties, have led to the manufacture of common household items without which life would be uncomfortable, to say the least. Historically this multi-billion rand global industry has its roots in the Max Planck Institut für Kohlensförschung in Mülheim an der Ruhr. Karl Ziegler and his co-workers made a fortuitous discovery during their studies of aluminium-alkyl catalysed olefin oligomerisation. During the course of their investigations they found that trace amounts of nickel present in the autoclave led to the dimerisation of ethylene to butene.[1] Further investigations showed that traces of acetylene present in the feed gas effectively stabilised the nickel catalyst from decomposition. The discovery of the so-called "nickel effect" led to the development of what can be termed "normal pressure" ethylene polymerisation, the product of which was high molecular weight polyethylene. Coupled to this was the development of catalytic propylene polymerisation. The stimulating effect this curiosity-driven research had and still has on the global chemistry community cannot be exaggerated. Using Ziegler catalysts, Giulio Natta demonstrated the utility of these complexes in stereospecific olefin polymerisation.[2] Thus this phenomenal success story culminated in the award of the Nobel Prize in Chemistry (1963) to Karl Ziegler and Giulio Natta with the following citation: "for their discoveries in the field of chemistry and technology of high polymers".[3] This is a prime example of the effect basic research can have on humanity.

Despite exceptional catalytic activity the Ziegler-Natta catalysts were undefined i.e. the exact nature of the catalytically active species was unknown.

Efforts to overcome this drawback led to the discovery that partially hydrated trimethyl aluminium,[4] which became known as MAO, in combination with well-defined zirconium or titanium metallocenes produced catalytic systems with unrivalled activity in olefin polymerisations (Scheme 1.1).[5]

Scheme 1.1 Active catalyst formed by a metallocene complex and MAO.

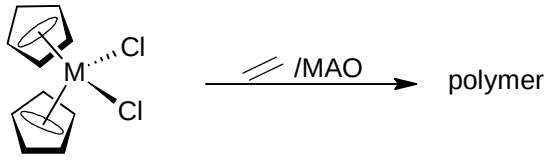

The result of these initial seminal studies was to provide significant research impetus which led to the development of various classes of olefin oligomerisation and homo-/co-polymerisation catalyst systems. These include the so-called constrained geometry (CGC), phenoxy-imine[6] and diimine-based catalyst systems (Fig. 1.1).[7]

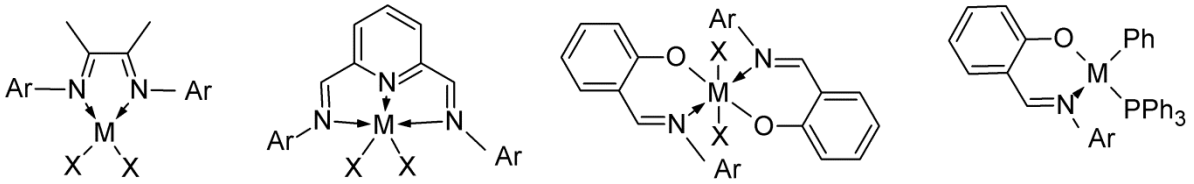

Fig. 1.1 Pre-catalysts developed in the so-called 'post-metallocene' era.

Coupled to this has been the development of quantum chemical techniques, which combined with increasing computational power, allows for the theoretical evaluation of catalytic reactions. This provided key insights into mechanistic features of catalytic reactions of various types.[8] In addition a synergistic approach of experiment and theory has become common-place in rational catalyst design.[9] This review will focus on reports which have provided significant insights into transition metal-catalysed olefin oligomerisation and

homo-/co-polymerisation. In addition, particular emphasis will be placed on the application of experimental and theoretical approaches to unraveling mechanistic features and directing rational catalyst design.

1.2 Catalyst systems derived from group 4 metals.

As mentioned, pre-catalysts generated from the group 4 metals, Ti; Zr and Hf, are known for their exceptional reactivity. This is observed in the case of metallocene as well as constrained geometry catalyst (CGC) systems. Despite their high activity, these catalyst systems generally show low levels of chain entrapment in ethylene homopolymerisation (to produce branched polyethylene) as well as low levels of co-monomer enchainment in ethylene/α-olefin co-polymerisation.[10] Marks and co-workers pioneered the development and application of multinuclear group 4 constrained geometry catalyst systems which displayed significantly enhanced cooperativity effects in ethylene homo- and co-polymerisation reactions.[11] Their initial report detailed the catalytic application of two constrained geometry catalysts, **1-I** and **1-II**, in the presence of a dianionic bisborate activator, $\mathbf{B_2}$, as an ethylene polymerisation catalyst system (Fig. 1.2).[12]

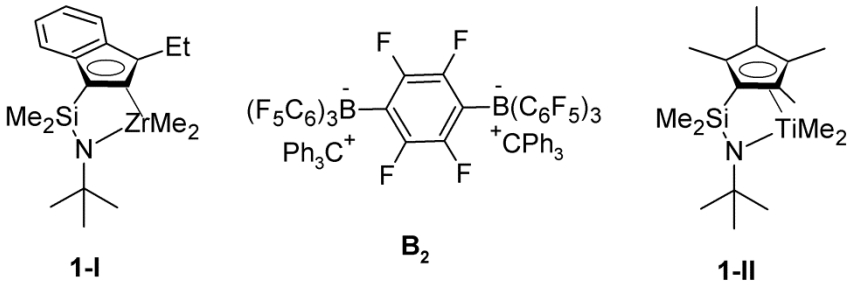

Fig. 1.2 Zr and Ti constrained geometry catalyst system displays cooperative effects due to ion-pairing with dianionic co-catalyst.[12]

Individually, complex **1-I** in the presence of $\mathbf{B_2}$ gave low molecular weight polyethylene as product, whereas complex **1-II** in the presence of $\mathbf{B_2}$ gave high-molecular

weight polyethylene. Employing a ratio of **1-I**:**1-II** of ≥ 20:1 in the presence of $\mathbf{B_2}$ allowed for the preparation of LLDPE (with branch lengths ≥ 6) as a result of the incorporation of the growing polymer chain on **1-I** into the growing polymer chain of **1-II**. The nature of the polyethylene formed also demonstrated the monomodal character of the polymerisation catalyst system. Their results demonstrated, for the first time, the ability of keeping two distinct catalytic centres in close proximity, via a dinuclear activator leading to the formation of strong catalyst-co-catalyst ion-pair. The advantage of such a system is a dramatic increase in the efficiency of chain incorporation in the production of LLDPE.

As an extension of their work, Marks and co-workers prepared a bimetallic Zr_2-CGC pre-catalyst, **1-III** (two diastereomers generated through differing orientations of the indenyl rings) and evaluated its catalytic activity for ethylene homo- and co-polymerisation in the presence of the abovementioned bisborate activator. The observed activity was compared that of the mononuclear analogue, **1-I** (Fig. 1.3).[13]

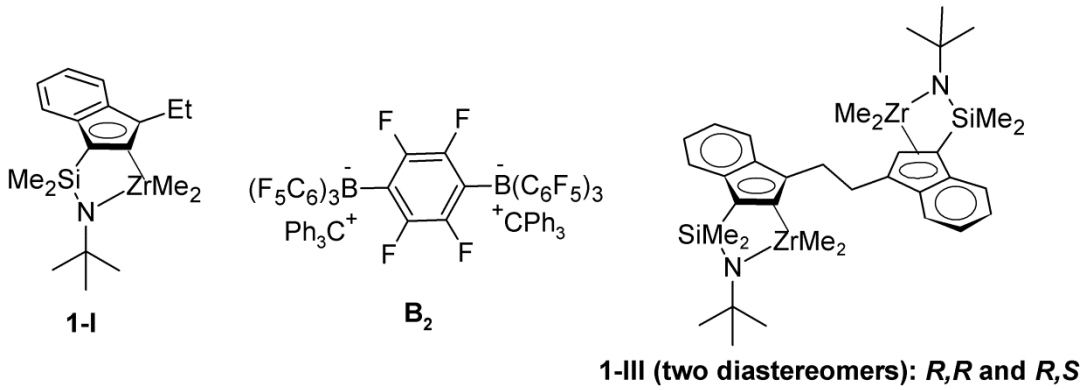

Fig. 1.3 Homobimetallic CGC-Zr catalyst developed by Marks and co-workers for cooperative ethylene homo- and co-polymerisation.[13]

Their goal was to determine whether bimetallic structures in which both catalytic centres provided access to incoming monomer *and* were in close proximity would allow for the isolation of novel polymeric material. It was envisaged that the novel polymers formed

would be generated as a result of enhanced/different selectivities for possible enchainment pathways in comparison to the mononuclear Zr-CGC pre-catalyst.

In the case of ethylene homopolymerisation, they found that the **1-III**/bisborate activator system showed a near 2-fold increase in the molecular weight of the polymer and significantly decreased catalytic activity in comparison to the mononuclear analogue, irrespective of ethylene pressure. Also, analysis of the polymer showed that for the **1-III**/bisborate activator system ethyl-branching within the polymer backbone dominated and that a greater than 11-fold increase in the number of ethyl branches per 1000 carbons was obtained in comparison to the mononuclear analogue. Significantly, no methyl, *n*-propyl or *n*-pentyl branching was observed, which would be indicative of 2,1-reinsertion of polymer. This observation led them to probe the reason for the observed increase in selective branch-formation more closely. The authors hypothesised that the **1-III**/bisborate catalyst system may display unusual binding/capture affinity for small/short-chain α-olefins. To test this hypothesis, both mononuclear and binuclear Zr-CGC/bisborate catalyst systems were evaluated in ethylene/1-pentene and ethylene/1-hexene co-polymerisation. Their results showed that for both co-polymerisation reactions, the incorporation of long-chain α-olefins was greatly enhanced in the case of **1-III**/bisborate; up to 4 times more for ethylene/1-pentene and 3 times more for ethylene/1-hexene co-polymerisation. The decrease between 1-pentene and 1-hexene was attributed to differences in steric pressure of retaining the α-olefin within the active site. In the case of ethylene/1-pentene co-polymerisation, *n*-propyl branches predominated while *n*-butyl branches predominated for ethylene/1-hexene co-polymerisation. Significantly, the same 11-fold increase in ethyl-branching was observed in both co-polymerisation reactions. Analysis of the microstructure of the obtained polymer in both homo- and co-polymerisation reactions allowed for the identification of a previously

unreported multi-metal centre enchainment pathway and the postulation of the following mechanistic scenario. In the case of the **1**-**III**/bisborate for ethylene homopolymerisation, chain transfer of the growing oligomeric chain generates a cationic bimetallic Zr-ethyl species in which the eliminated oligomer is bound to one metal centre and vacant coordination site of the other metal centre is stabilised via an agostic interaction with the eliminated oligomer (Scheme 1.2).

Scheme 1.2 Chain transfer processes at bimetallic CGC-Zr catalyst systems.[13]

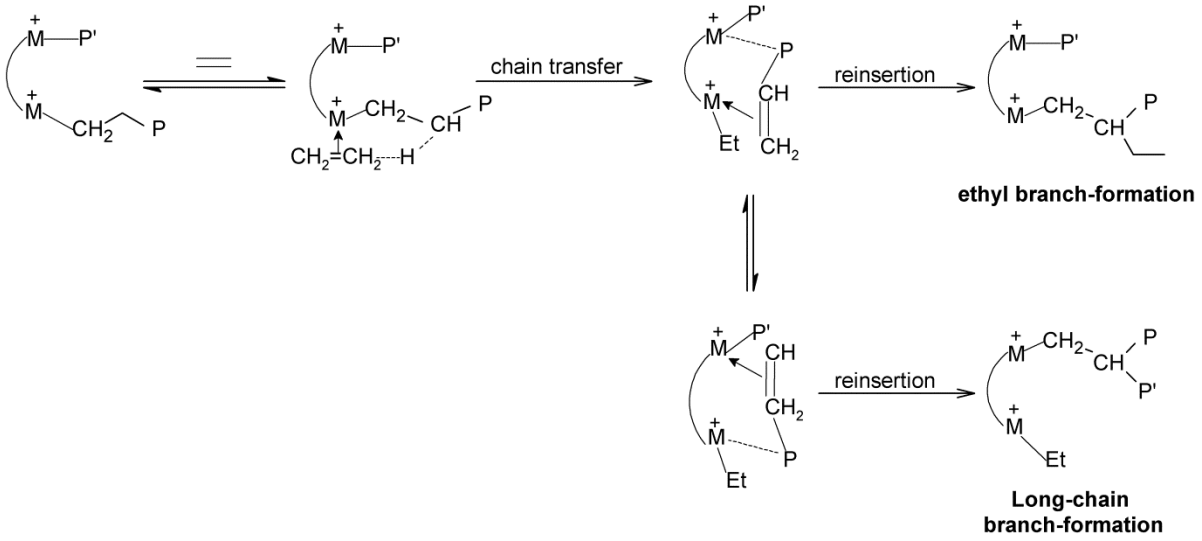

This species then undergoes subsequent reinsertion with 1,2-regiochemistry to generate ethyl-branched polyethylene. The same enchainment process is operative in the co-polymerisation, with competition between enchainment of ethylene and 1-pentene/hexene (smaller monomers leads to easier insertion in terms of steric pressure) being the reason for the same increase in ethyl-branching in co-polymerisation and homopolymerisation reactions. The main outcome of this study was that the rational design of multimetallic catalyst/co-catalyst systems could effect the preparation of polymeric materials with novel microstructures and enhanced physical properties.

Subsequently, Marks and co-workers demonstrated the generality of the multinuclear metal centre-mediated enchainment process.[14] They comparatively evaluated a mononuclear and binuclear Zr phenoxyiminato, **1-IVA** and **1-IVB** respectively, in ethylene homo- and ethylene/1-hexene co-polymerisation (Fig 1.4). Upon activation with MAO, complex **1-IVB** afforded high molecular weight polyethylene in ethylene homopolymerisation reactions. The observed catalytic activity was approximately 8 times that of the mononuclear analogue **1-IVA**.

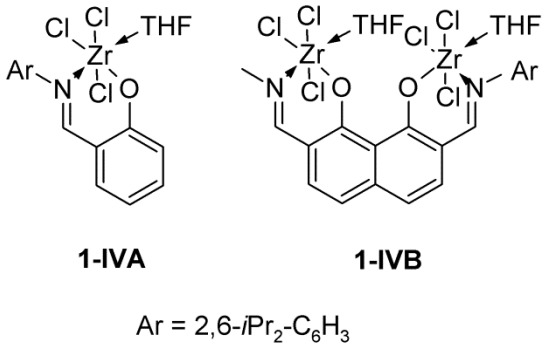

Fig. 1.4 Homo- and bimetallic FI-Zr complexes as ethylene homo- and ethylene/α-olefin co-polymerisation catalysts.[14]

In ethylene/1-hexene co-polymerisation mediated by **1-IVB**/MAO, 1-hexene incorporation was observed up to 5.8 % while **1-IVA** showed negligible activity under identical reaction conditions. Their results demonstrated that enhanced co-monomer enchainment as a result of proximal multinuclearity in catalyst systems was more general than initially anticipated. In addition, contrary to the observation made for bimetallic-CGC systems, increasing rigidity of the ligand framework and decreasing the M-M bond distance significantly enhances the observed catalytic activity.

Despite experimental observations which substantiated the proposed enchainment mechanism discussed above, key intermediates were not identified via experimental

techniques, which would provide unambiguous proof that the enchainment process was mediated by monomer-metal or polymer-metal interactions. Toward this end, Marks and Fragalà employed quantum mechanical techniques at the B3LYP level of theory in a comparative study of **1-I** and **1-III**/bisborate mediated ethylene homopolymerisation, using 1-octene as an oligoethylene model fragment.[15] They evaluated four key features of the proposed mechanism: (i) pre-catalyst geometries and methyl-abstraction/ion-pair formation energies, (ii) the nature of metal-oligoethylene interactions, (iii) insertion energetics via a Cossee-Arlman mechanism and (iv) chain-transfer processes via concerted β-hydrogen transfer. For the two diastereomers formed in the case of **1-III** (*R,R* and *R,S*) their calculations showed that methyl-group abstraction from either diastereomer was governed by geometrical constraints between the bimetallic complex and the bisborate activator and that methyl-group abstraction did not occur independently in each metal centre. In other words, the distance between methyl groups on adjacent metal centres needed to match the B-B distance within the activator and the required energy associated with this process was not cumulative. Accurate geometrical matching was found to result in significantly higher ion-pair stabilisation energies in **1-III** ($\Delta H_{\text{ion-pair stabilisation}(R,R)}$ = 271.9 kcal/mol and $\Delta H_{\text{ion-pair stabilisation}(R,S)}$ = 270.4 kcal/mol) than in **1-III** ($\Delta H_{\text{ion-pair stabilisation}}$ = 93.2 kcal/mol). This high ion-pair energy, essentially the energy barrier that needs to be overcome for olefin coordination/insertion, is the reason for the lower catalytic activity in ethylene homopolymerisation reported for **1-III**/bisborate in comparison to **1-I**/bisborate.[13]

Using 1-octene as a model for oligoethylene they calculated optimised geometries for bimetallic Zr-methyl π-^{n}octene species. Their calculations showed that orientation of the alkyl chain of the coordinated olefin had a significant effect on both charge densities at the metal centres as well as the ground state energy of the π-olefin species. In the species with

the alkyl-chain oriented toward the second Zr centre (Zr2, species **1-IIIA**), an agostic M-CH_3 interaction (evidenced by a slight elongation of the C-H bond length) resulted in a reduction in the positive charge of Zr2 (Fig. 1.5). The resultant charge density was comparable to the charge density on the Zr centre to which 1-octene was π-bonded. In comparison, the species in which the orientation of the alkyl-chain is away from Zr2 (species **1-IIIB**) showed no comparable decrease in electrophilicity. In addition, the calculated ground state energy was lower for **1-IIIA** than **1-IIIB**. These two distinct differences is the prerequisite for co-monomer/oligoethylene enchainment to be a dominant process in ethylene homo-/co-polymerisation with these catalyst systems.

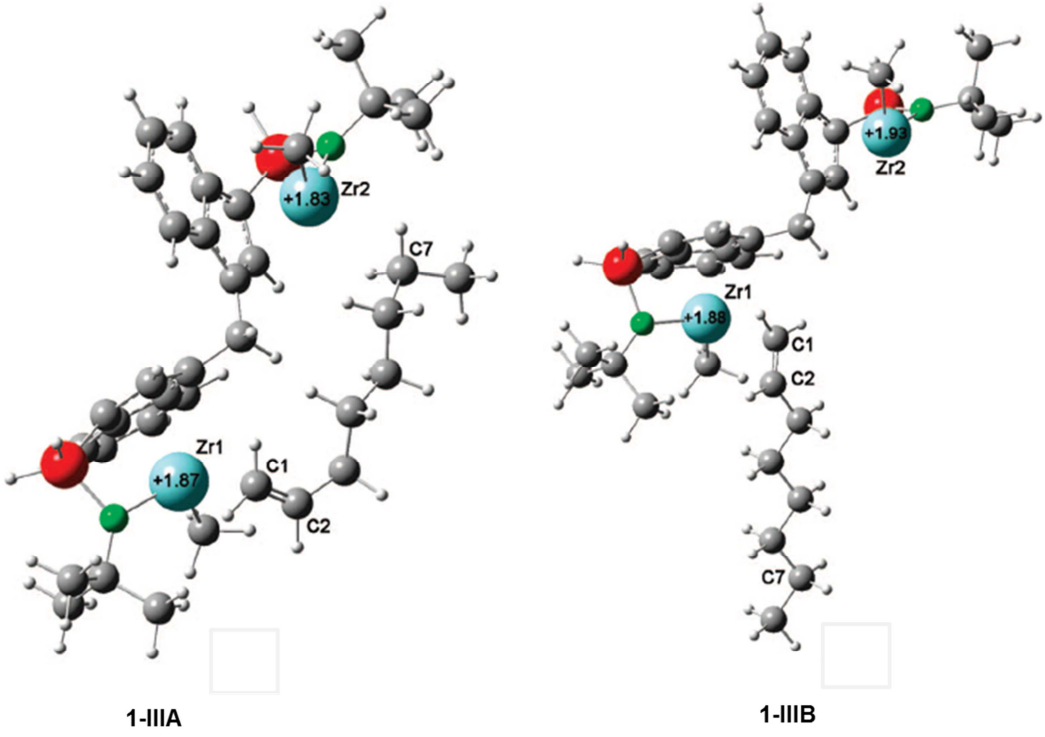

Fig. 1.5 Optimised structures of **1-IIIA** and **1-IIIB** showing the orientation of the olefin chain. Copyright 2009 American Chemical Society.[15]

Evaluation of the 1-octene insertion showed no distinct differences between the evaluated species as evidenced by comparable energies of the optimised transition state

structures. On the other hand, their evaluation of chain transfer via β-hydrogen transfer showed that chain transfer kinetics was significantly influenced by an elongation of the coordinated olefin moiety and that increasing chain length resulted in increases in the barrier for chain transfer. The result is that olefin insertion and subsequent chain propagation in the evaluated catalyst system was favored over chain transfer and chain termination. Their computational investigation showed a direct correlation between the stability of the Zr-methyl-π-olefin complex and Zr/C-H agostic interaction. In addition their calculations showed that the propensity for insertion of monomer versus reinsertion of oligoethylene produced during ethylene homo- and co-polymerisations was the reason for the observed selectivity toward ethyl-branched polyethylene.

The discussion above serves to reinforce the potential of homobimetallic group 4 catalyst systems to produce polymers with novel microstructures via cooperative effects between metal centres. The potential of heterobimetallic systems to induce novel enchainment processes which leads to new co-polymer syntheses was demonstrated recently by Marks, Delferro and co-workers.[16] They prepared and characterised a novel heterobimetallic group 4-group 6 pre-catalyst, **1-V**, consisting of a CGC-Ti centre covalently linked to a SNS-Cr centre (Fig. 1.6).

The titanium centre is known to be active in ethylene polymerisation while the chromium centre is known to be active as an ethylene trimerisation catalyst.[17] It was envisaged that the incorporation of selectively formed α-olefins at chromium into the growing polymer chain at titanium due to metal-metal proximity would generate LLDPE with unique microstructures.

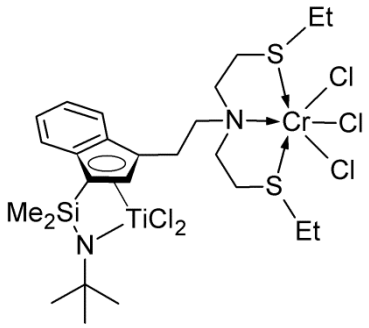

1-V

Fig. 1.6 Heterobimetallic Ti-Cr catalyst system developed by Marks and co-workers.[16]

A comparative study of the reactivity of **1-V** and a tandem catalysis system (CGC-Ti and SNS-Cr mixed together) toward ethylene in the presence of MAO was undertaken. Under optimised conditions **1-V**/MAO showed significantly lower activity in co-polymerising ethylene with formed 1-hexene in comparison to the tandem catalyst system, attributed to increased steric crowding of the active sites by the growing polymer chain and the eliminated 1-hexene product. The activity of 1-hexene formation was also significantly lower in the case of **1-V**/MAO while polymer molecular weights were approximately 20 times greater than for the tandem catalyst system. The molecular weights of the polymer produced by **1-V**/MAO showed little dependence on conversion even at longer reaction times. Also, the observed activity and molecular weight of the formed polymer in the **1-V**/MAO catalyst system showed little dependence on reaction time or the concentration of 1-hexene.

Analysis of the polymer microstructure showed that the selective formation of *n*-butyl branches within the polymer backbone occurred for polymers produced by **1-V**/MAO, with high branch densities of approximately 18.6 branches/1000 C atoms obtained. Also, the branch density of the formed polymer was observed to be independent of reaction time or

conversion. In contrast, the tandem catalyst system showed significantly decreased *n*-butyl branching, while branch densities were observed to be far more conversion-sensitive.

From these experimental results the authors concluded that the local concentration of 1-hexene i.e. the concentration of 1-hexene at the catalyst active site was constant and that spatial confinement between the heteronuclear metal centres increased the efficiency of the intramolecular co-monomer transfer process. The spatial proximity of the SNS-Cr moiety significantly altered the propagation and chain transfer rates operative at the CGC-Ti moiety.

1-pentene was added to probe the effect on 1-hexene enchainment for the **1-V**/MAO and tandem catalyst systems. In the case of the tandem catalyst system, co-polymer was produced in which the dominant branch corresponded to *n*-propyl, thereby demonstrating that *intermolecular* enchainment was operative. On the contrary, the **1-V**/MAO catalyst system produced co-polymer with significantly less *n*-propyl branching, with *no* change in the *n*-butyl branch density, demonstrating that *intramolecular* enchainment processes dominated, even in the presence of competing α-olefin.

The authors stated that the experimental data does not allow for discrimination between concerted or stepwise 1-hexene reductive elimination and 1-hexene reincorporation, or whether titanium impacts on the metallacycloheptane opening to form 1-hexene. A preliminary DFT investigation identified a low-energy structure in which 1-hexene is π-bound to the chromium centre while the alkyl chain interacts with titanium via a M-CH_3 agostic interaction, analogous to **1-IIIA** (Fig. 1.5).[15]

1.3 Catalyst systems derived from Chromium.

Catalytically active systems derived from chromium are known to display the greatest versatility toward product formation in olefin transformations. Generally introduced into the catalytic mixture as the trivalent species, this metal has been demonstrated to mediate selective[18] and non-selective[19] ethylene oligomerisation as well as ethylene polymerisation.[20] The difference in product formation from the same trivalent species generally introduced into the catalytic feed is as a result of the so-called redox dynamism of organochromium species.[19a,21] Alkylating agents added as co-catalysts generally reduce the metal to lower oxidation states, each of which possess unique reactivity. These reduced species, may then undergo disproportionation reactions, either reductive or oxidative, to regenerate the trivalent species. It is this redox dynamism and the presence of all three catalytically active oxidation states of chromium (+ I, + II and + III) which accounts for the observed versatility as well as switchable selectivity. Generally, it is accepted that Cr(II) species are active in polymerisation or non-selective oligomerisation, Cr(III) species are active in polymerisation and that Cr(I) and its Cr(III) redox couple is active for selective oligomerisation.[22]

The demand for high-purity 1-hexene and 1-octene as co-monomer for LDPE synthesis has resulted in significant research focus being directed toward selective ethylene oligomerisation.[23] As such, the reports of selective ethylene trimerisation[17,24] and tetramerisation[25] created huge hype within the catalysis community (Fig. 1.7).

Despite an understanding of the factors which lead to enhanced catalytic activity in Cr-catalysed trimerisation[18a] or tetramerisation,[26] an understanding of the Cr-oxidation state which governed selectivity toward trimerisation or tetramerisation remained a point of

contention. A case in point are reports regarding the active species present in the Phillips trimerisation catalyst system.[23b]

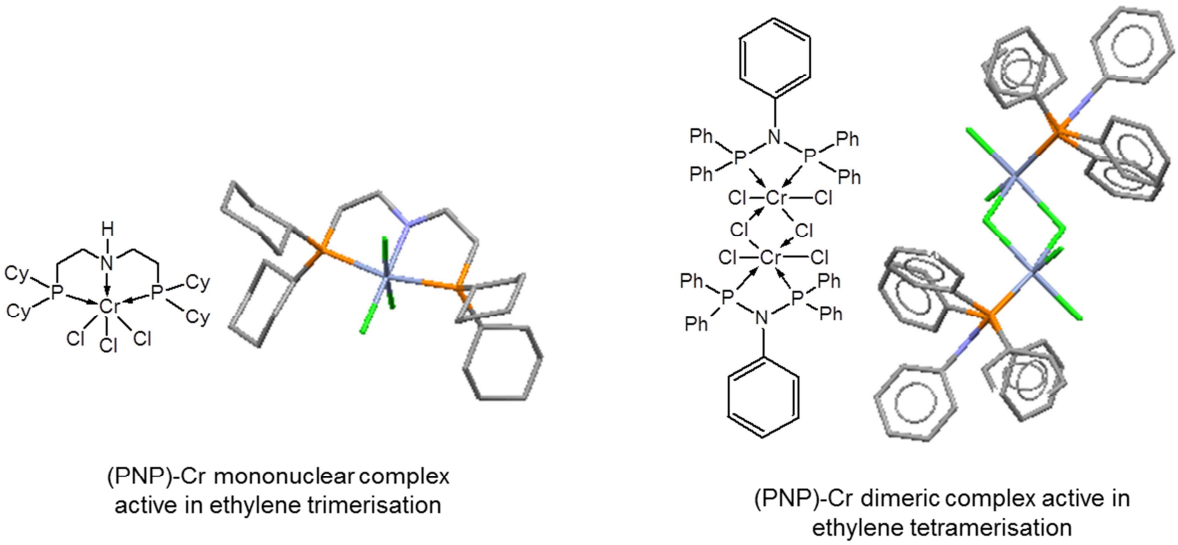

Fig. 1.7 Mononuclear and Dimeric PNP-Cr(III) complexes active in ethylene tri- and tetramerisation. Copyright Cambridge Structural Database 2013.[24-25]

Initial mechanistic proposals implicated a Cr(II)/Cr(IV) redox cycle in which the pyrrole ligand of the starting complex (Fig. 1.8) is thought to shuttle between η^1 and η^5 coordination throughout the catalytic cycle.[27] This shuttling serves to stabilise the active species during changes in the coordination environment of the metal.

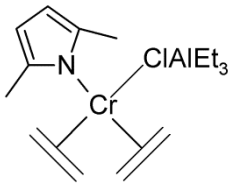

Fig. 1.8 Cr complex implicated in selective ethylene trimerisation using the Phillips catalyst system.[27]

Subsequently Gambarotta and co-workers provided evidence that a Cr(I)/Cr(III) redox cycle was operative in selective ethylene trimerisation, by isolating and characterising a

self-activating (η^6-pyrrole derivative)Cr complex (**1-VI**)[28] and a μ-Me Cr-dimer (**1-VII**, Fig. 1.9).[29]

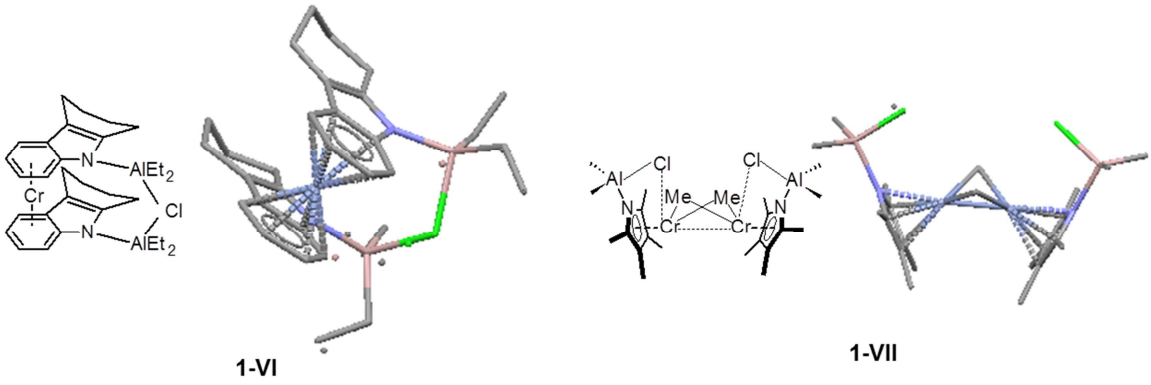

Fig. 1.9 Structures of isolated self-activating Cr(I) species relevant to the Phillips trimerisation catalyst system, Copyright 2013 Cambridge Structural Database.[28-29]

Further support for the Cr(I)/Cr(III) mechanism was provided by an in situ EPR study on the Phillips system, evidenced by the identification of Cr(III) and Cr(I) species present during catalysis.[30] On the other hand, a DFT study of mechanistic aspects of the Phillips systems suggested that a Cr(I)/Cr(II) mechanism was indeed feasible.[31]

The elaboration above clearly indicate that elucidation of the mechanism of Cr-catalysed selective oligomerisation is not a trivial exercise and that the interpretation of experimental and theoretical observations is often complicated further by multiple spin states for the different formal oxidation states of chromium. In addition, the paramagnetic nature of chromium makes NMR spectroscopic evaluation of mechanistic features near-impossible.

Toward elucidating the mechanism of selective ethylene trimerisation/tetramerisation, the groups of Bercaw[32] (**1-VIII**, Fig. 1.10) and Overett[33] employed deuterium-labelling studies to evaluate whether the metallacycle mechanism was operative.

Consistent with a metallacycle mechanism, analysis of the products of Cr-catalysed oligomerisation with a 1:1 mixture of C_2H_4 and C_2D_4 showed that the predicted and obtained isotopomer distributions for the oligomeric products were in excellent agreement. Furthermore, for selective tetramerisation, careful analysis of minor products formed during catalysis allowed for further mechanistic inference.

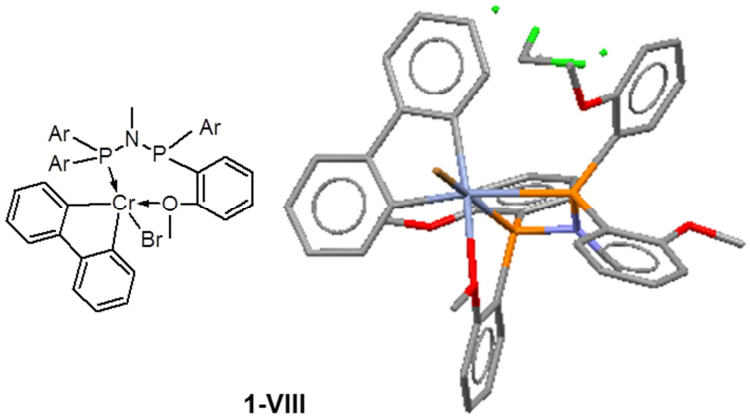

1-VIII

Fig. 1.10 Cr(III) P-O complex isolated by Bercaw and co-workers and employed in deuterium-labelling studies on catalytic ethylene trimerisation, Copyright 2013 Cambridge Structural Database.[32]

Firstly, the authors found that the metallacycloheptane species formed during ethylene tetramerisation displayed greater stability than the analogue formed during ethylene trimerisation. Coupled to this was a greater instability of the metallacyclononane species formed from subsequent ethylene insertion relative to the metallacycloheptane species. These two features accounted for the high tetramerisation selectivity as well as the observed product distributions. These distinct differences in the tetramerisation system with respect to the trimerisation system was attributed to ligand-mediated steric and electronic effects. The authors stated that these effects would be probed by molecular modelling studies but no reports have appeared in the literature as yet.

The activity of single-site early transition metal catalyst systems have been shown to be significantly affected by the nature of the ion-pair formed during the pre-catalyst activation step.[34] In the context of selective trimerisation, McGuinness evaluated a series of fluorinated alkyl- and aryloxymetalate anions, in which the metal was varied (metal = Al, Ta and B).[35] The evaluated anions were designed to vary in their coordinating strength, degree of steric protection and in their co-catalyst stability. Evaluation of the co-catalysts with an *in situ* generated pre-catalyst in ethylene tri-/tetramerisation established that the coordinating strength and stability of the co-catalyst had a significant effect on both activity and selectivity. Of the evaluated co-catalysts, $[Ph_3C][Al\{OC(CF_3)_3\}_4]$ in the presence of $Cr(THF)_3Cl_3$, bis(phosphino)amine ligand and $AlEt_3$ generated a highly active and selective ethylene tetramerisation catalyst system (Scheme 1.3).

Scheme 1.3 Catalytic system reported by McGuinness for selective ethylene tetramerisation.[35]

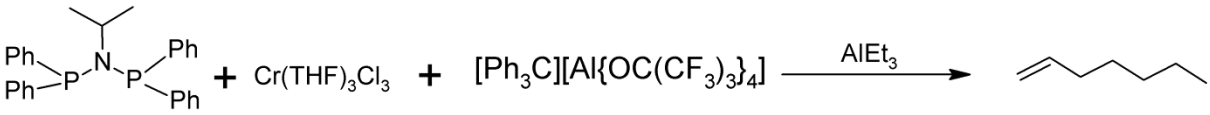

Janse van Rensburg and co-workers evaluated ion-pair interactions computationally in a model ethylene trimerisation/MAO catalyst system. Despite the poorly-defined nature of the co-catalyst,[36] their investigation evaluated the interaction of realistic MAO models with the $[CrCl_2(PNP)(\mu\text{-}Cl)_2]$ pre-catalyst and the effect of ion-pair formation on the catalytic process. In addition they evaluated the interaction of MAO models with chromacycloheptane intermediates to gain insight into the role that MAO plays during catalysis and evaluated the role of free trimethyl aluminium (TMA) in the catalytic process. Their computational results demonstrated that the role of TMA in catalysis is as a methylating agent and that MAO interacts with the methylated Cr-catalyst to generate ion-pairs. Also, MAO was found to form formally coordinated species with the chromacycloheptane species in the absence of ethylene

and that Me-abstraction to form a dissociated Cr catalyst-MAO ion-pair was the dominant pathway in the presence of ethylene. Their theoretical investigation provided significant insight into the role of MAO during the initial stages of the activation process as well as of the role MAO plays in stabilising reactive intermediates in the latter stages of the catalytic cycle.

Liu and co-workers recently sought to address mechanistic uncertainties related to the SNS-Cr ethylene trimerisation catalyst system employing quantum chemical techniques.[37] Experimental mechanistic investigations by McGuinness et al.[38] and Gambarotta, Duchateau et al.[39] raised points of contention as to whether the ligand N-H was deprotonated during the initial stages of the catalytic cycle. McGuinness and co-workers isolated deprotonated μ-ligand dimeric Cr(II) complexes (Scheme 1.4A) which were active ethylene trimerisation catalysts when activated with MAO, thereby postulating a Cr(II)/Cr(IV) metallacyclic mechanism.

Scheme 1.4 Deprotonated (A) and protonated SNS-Cr complexes isolated by McGuinness and Gambarotta, Duchateau, Copyright 2013 Cambridge Structural Database.[38-39]

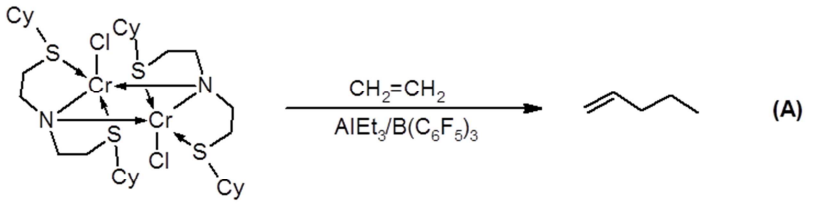

deprotonated Cr(II) dimer: 1-IX

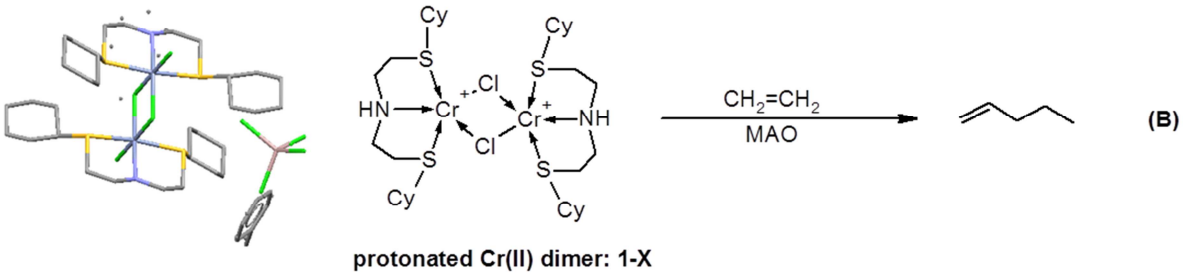

protonated Cr(II) dimer: 1-X

In contrast, Gambarotta, Duchateau and co-workers isolated μ-Cl Cr(III) complexes bearing protonated bis(thioether)amine ligands upon treatment of the starting complex with $AlMe_3$. The formation of these complexes after the reaction of the parent SNS-Cr complex with Al-activators was considered proof that deprotonation did not occur during catalysis (Scheme 1.4B). A point which may be raised here is that the SNS-Cr complex forms an active ethylene trimerisation catalyst (after activation with MAO) only at high temperatures, while the complexes isolated by Gambarotta et al. were prepared at ambient temperatures.

The computational investigation by Liu et al. addressed the issue regarding N-H deprotonation during catalysis and also incorporated the issue of spin-surface crossover[40] during catalysis. Simplistically, their calculations evaluated key intermediates taking into consideration all possible spin states for a given Cr oxidation state. Doing this would allow for the identification of low-energy points along the potential energy surface where changes between different spin states, and thus oxidation states, can occur. This is particularly relevant for chromium considering its intrinsic redox dynamism. Their computational investigation evaluated four mononuclear SNS-Cr models (Fig. 1.11).

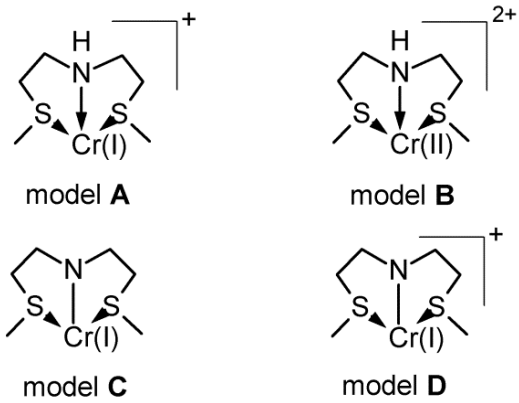

Fig. 1.11 Computational models **A-D** employed by Liu and co-workers to evaluate catalytic ethylene trimerisation.[37]

In models **A** and **C** the metal centre is in the + 1 oxidation state, with **A** containing a protonated ligand and **C** containing a deprotonated ligand. In models **B** and **D** the metal centre is in the + 2 oxidation state, with **B** containing a protonated ligand and **D** containing a deprotonated ligand. For models **A** and **C**, the spin states evaluated were doublet, quartet and sextet, while singlet, triplet and quintet spin states were evaluated for models **B** and **D**. Their computational results showed that on the basis of the metallacycle mechanism the energy barriers for chromacyclopentane and chromacycloheptane formation were turnover-limiting. Thus, without taking into consideration the effect of spin-surface crossover, the lowest energy pathway to 1-hexene formation was via model **C**. Spin-surface crossover was identified as a key feature of the catalytic cycle, corroborated by the identification of points along the potential energy surface where spin state changes were most facile, termed the minimum energy crossover point (MECP). In the case of models **A**, **C** {Cr(I)/Cr(III)} and **D** {Cr(II)/Cr(IV)} the MECP was located prior to chromacyclopentane formation and subsequent to chromacycloheptane formation. The resulting effect is a lowering of the energy barrier to chromacyclopentane and chromacycloheptane formation by more than 10 kcal/mol (relative to the energy barrier in the absence of spin-surface crossover). This reduction in the energy barrier was attributed to spin acceleration,[41] a phenomenon whereby the electrons involved in the spin-surface crossing exhibit high localisation on chromium. Spin acceleration increases the strength of spin-state mixing (required for spin crossover) and provides sufficient energy to overcome the forbidden nature of the reaction.[42] In the presence of spin-surface crossover, the lowest energy pathway to 1-hexene formation was identified as proceeding from model **A**, in which the oxidation state of the metal is +1 and the SNS ligand is protonated. Their computational investigation thus provided support for a Cr(I)/Cr(III)

redox cycle being operative for this class of ethylene trimerisation catalysts and corroborated the experimental observations made by Gambarotta, Duchateau and co-workers.

1.4 Catalysts derived from Palladium.

Mechanistically, details regarding palladium-diimine mediated ethylene homo- and ethylene/α-olefin co-polymerisation is well-established. This is as a result of seminal experimental and computational contributions which elucidated the key features in homo- and co-polymerisation reactions of this class of catalysts. Low temperature spectroscopic and computational investigations identified the catalyst resting states to be Pd-alkyl π-olefin species, establishing zero-order kinetics in olefin; barriers to insertion were determined to be in the range 17-18 kcal/mol; branching in homopolymerisation was established to proceed via the isomerisation of β-agostic Pd-alkyl species with isomerisation barriers of 8-9 kcal/mol; chain transfer proceeded via associative exchange of free olefin and that the degree of branching in the obtained polymer was independent of pressure while the morphology of the polymer was pressure dependent.[7a-c,43]

Researchers at Shell developed a novel class of late transition metal catalyst systems derived from a Pd(0) precursor and a zwitterionic phosphino-sulphonate ligand, capable of catalysing the alternating co-polymerisation of ethylene with MA (Scheme 1.5).

Scheme 1.5 First reported example of in situ generated catalyst system for ethylene/acrylate polymerisation.[44]

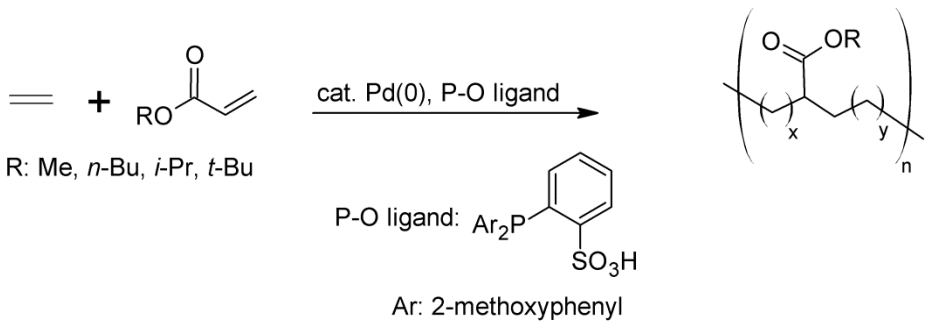

A distinct difference between this catalyst system and the Pd-diimine catalyst was the formation of a *linear* ethylene/MA co-polymer. Subsequently, Rieger[45] and Nozaki[46] isolated neutral and anionic Pd-phosphine sulphonate complexes, active for non-alternating co-polymerisation of ethylene/CO ethylene/MA respectively.

Experimentally, this class of Pd catalysts generate polymers which are highly linear, which is in direct contrast to the class of α-diimine Pd catalysts which usually generate highly-branched polymers. In addition, the Pd catalysts with P-O ligands demonstrate the unique ability of co-polymerising polar vinyl co-monomers such as acrylates,[47] acrylonitrile[48] and vinyl ethers[49] although the incorporation of vinyl co-monomers is accompanied by a significant decrease in catalytic activity.[50] The formation of linear polymers suggest that chain transfer processes via β-hydride elimination/reinsertion is much slower, in comparison to that observed for Pd-diimine and P-O Ni catalyst systems. Evidence for this was provided by Ziegler and co-workers.[43i] Their comparative investigation of ethylene/CO co-polymerisation catalysed by Pd-complexes bearing P-O and P-P ligands demonstrated that the rate of β-hydride elimination was much slower than the rate of propagation. In contrast, experimental investigations suggested that this was not the case. Jordan and co-workers reported the catalytic ethylene polymerisation, catalysed by Pd complexes bearing P-O ligands.[49] Microstructure analysis of the polymer product showed low levels of Me-branching suggesting that β-hydride elimination occurred, while a model reaction of the P-O ligated Pd-complex with 6-chloro-1-hexene gave products which were indicative of facile chain walking and β-Cl elimination (Scheme 1.6). In addition, a preliminary computational investigation by Nozaki and co-workers identified a low energy β-hydride elimination pathway.[48a]

To shed light on these contradictory observations regarding chain tranfer processes in P-O Pd-catalysed ethylene polymerisation, Nozaki and co-workers employed both experimental and computational techniques in an attempt to generate a complete mechanistic understanding of this catalytic process. Experimentally, the authors generated short- and long-chain Pd-alkyl species *in situ*, which were shown to exist as the Pd-^{n}alkyl species (Scheme 1.7).

Scheme 1.6 β-H and β-Cl elimination processes observed for P-O Pd complexes.[49]

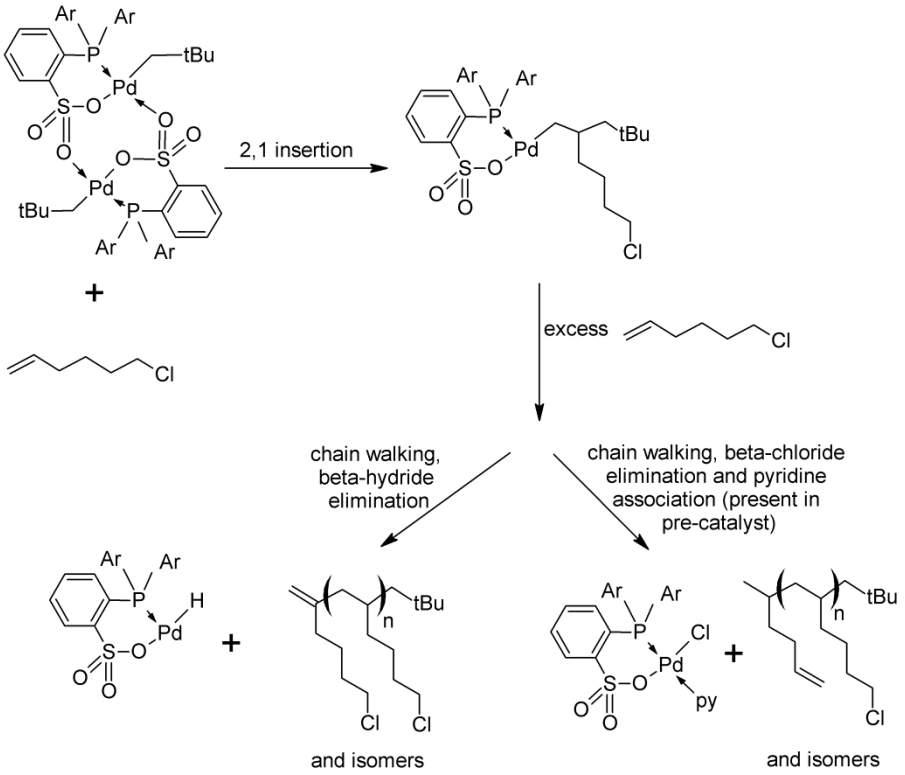

This is in stark contrast to the rapid isomerisation to *iso*-alkyl species generally observed for analogous diimine Pd-alkyls.[7c,43d] In addition, they showed that β-hydride elimination does occur, at elevated temperatures and in the absence of ethylene, as evidenced by the formation of hexene isomers following the reaction of the Pd-Me species with

1-hexene. DFT studies showed that the Pd-alkyl π-ethylene species, in which the alkyl group was *trans* to the sulphonate, was lower in energy than the *cis* isomer.

Scheme 1.7 Generation of linear Pd-alkyl species reported by Nozaki and co-workers.[51]

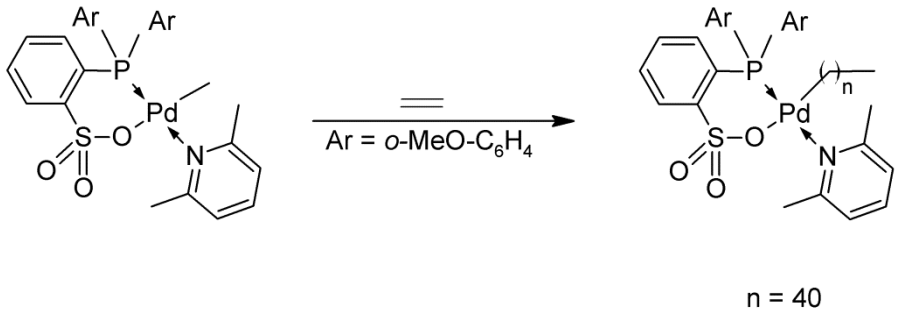

Ethylene insertion was calculated to proceed from the less stable *cis* isomer, with the interchange between *cis* and *trans* isomers demonstrated computationally to be governed by Berry pseudorotation[52] in comparison to a tetrahedral transition state,[53] whereby the second oxygen atom of the sulphonate moiety acts as an associative ligand (Scheme 1.8).

Scheme 1.8 Calculated pathway for *cis*/*trans* isomerisation via Berry pseudorotation.[51]

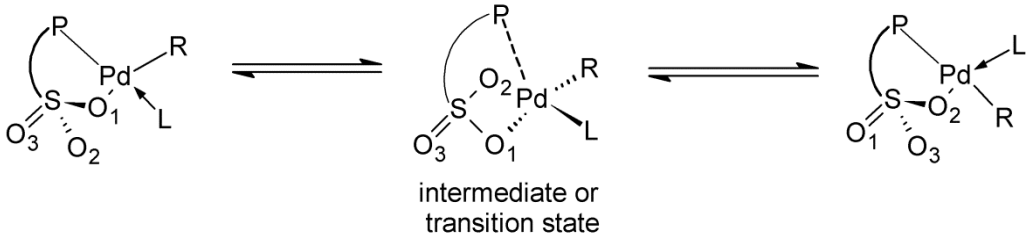

The isomerisation barriers were calculated to be in the range 17-21 kcal/mol. Ethylene insertion and β-hydride elimination proceeded via comparable energy barriers in the range 25-30 kcal/mol, although the pathway to generate the key *cis* Pd-alkyl intermediate was calculated to have to overcome high energy barriers of pyridine dissociation (27.4 kcal/mol); *cis*/*trans* isomerisation (31.7 kcal/mol) as well as ethylene dissociation (30.9 kcal/mol). Their

computational investigation also confirmed the likelihood of a low energy β-hydride elimination pathway, operative under low ethylene concentrations. The pathway is characterised by *cis-trans* isomerisation; pyridine dissociation and β-hydride elimination to generate a Pd-hydride π-olefin species (Scheme 1.9) and provided significant insight into the mechanistic features governing the formation of linear polyethylene by Pd-phosphine sulphonate complexes.

Scheme 1.9 Low energy β-hydride elimination pathway identified computationally.[51]

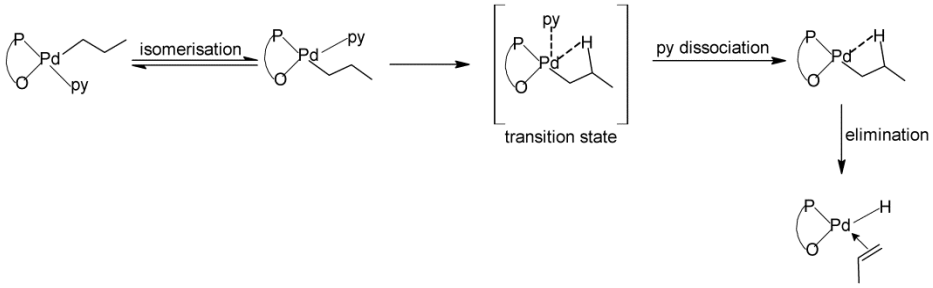

Bazan and co-workers have demonstrated the effect of incorporation of fluoroboranes into the ligand framework of SHOP-type Ni(II) oligomerisation catalysts (Fig. 1.12).[54] Incorporation of the fluoroboranes generated a zwitterionic species which displayed significantly enhanced activity in ethylene oligomerisation compared to the non-zwitterionic analogue as a result of increased electrophilicity at the metal centre.[55]

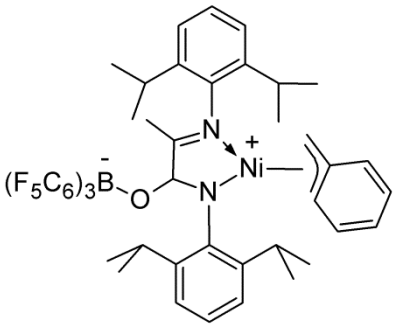

Fig. 1.12 Zwitterionic SHOP-type Ni(II) diimine complexes displaying enhanced catalytic activity in ethylene oligo-/polymerisation.[55b]

In an attempt to enhance the activity of Pd-phosphine sulphonate catalysts, Jordan and co-workers reported the preparation and evaluation of the reactivity of analogous zwitterionic species in ethylene polymerisation.[56] They isolated both neutral and zwitterionic dimeric complexes as well as mononuclear complexes after reaction of the neutral Pd-phosphine sulphonate complex with $B(C_6F_5)_3$ (Scheme 1.10).

Scheme 1.10 Formation of neutral and zwitterionic Pd-phosphine sulphonate complexes to enhance catalytic activity toward ethylene polymerisation.[56]

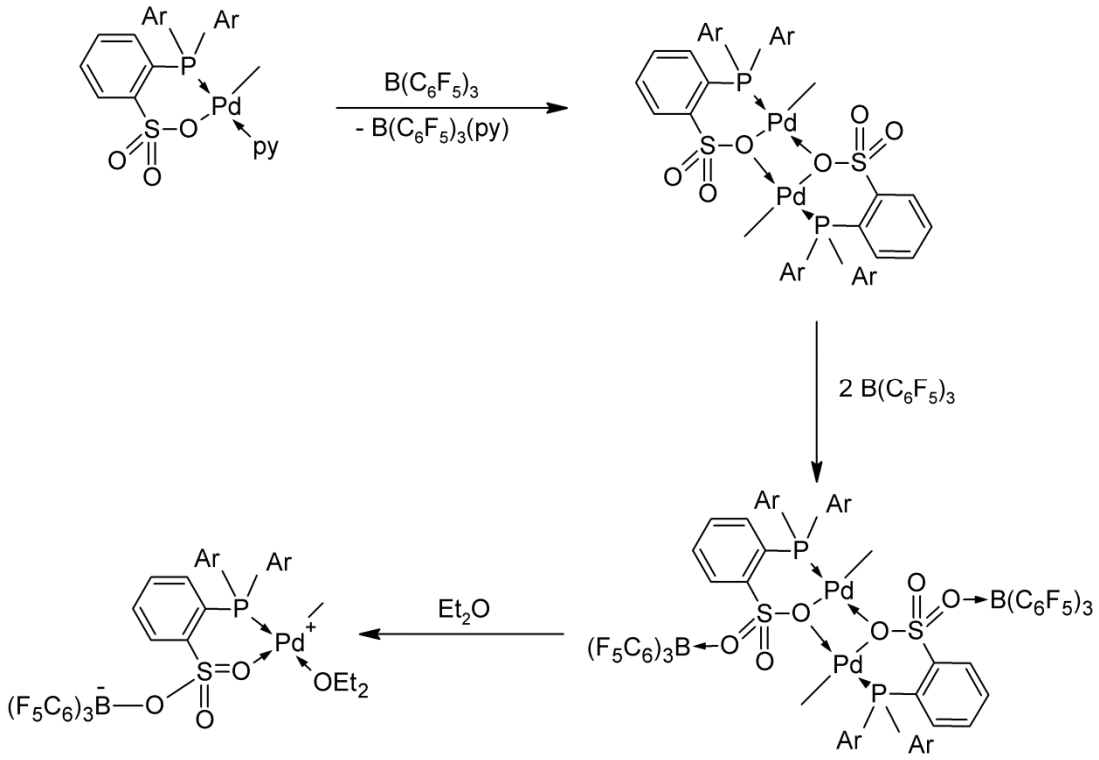

The formation of neutral and zwitterionic dimers was dependent on the ratio of $B(C_6F_5)_3$, while the zwitterionic dimer could be converted to the monomeric species in the presence of a coordinating solvent. Distinct differences in reactivity toward ethylene was observed. In the case of the neutral dimer, reactions with ethylene generated low-molecular weight polyethylene. In contrast, the zwitterionic dimer generated oligomers and trace amounts of polyethylene while displaying a 3-fold increase in activity under identical

conditions. The formation of oligomers as well as polyethylene was rationalised on the basis of $B(C_6F_5)_3$-dissociation, which was confirmed experimentally.

Low temperature spectroscopic investigations showed that the neutral dimer undergoes ethylene-promoted dissociation to generate the Pd-methyl π-ethylene species. The Pd-methyl π-ethylene species than undergoes multiple insertions to generate the long-chain Pd-alkyl π-ethylene species and no oligomers. The first-order rate constant for ethylene insertion into the Pd-methyl π-ethylene species was determined to be 1.1×10^{-4} s^{-1}. Identical experiments with the zwitterionic dimer determined a first-order rate constant for ethylene insertion into the Pd-methyl π-ethylene species of 3.0×10^{-4} s^{-1}, consistent with a 3-fold increase in activity. Only the formation of oligomers was observed with a concomitant decrease in the concentration of the Pd-methyl π-ethylene species. Generation of the zwitterionic Pd-phosphine sulphonate complex was thus shown to enhance both catalytic activity and chain transfer rates significantly.

1.5 Olefin polymerisation catalysts derived from Nickel.

Following the initial reports of Ni(II)-catalysed olefin polymerisation by sterically encumbered diimine ligands,[7a,57] a large number of reports detailing experimental[58] and theoretical[59] mechanistic investigations have appeared in the literature.[60]

These investigations established key mechanistic features for Ni(II)-catalysed olefin polymerisation and co-polymerisation which have led to the rational design of novel catalyst systems. To illustrate this point, a few examples will be highlighted.

The degree of branching within the polymer formed during Ni(II)-diimine catalysed polymerisation was found to differ significantly with varying reaction conditions and the

structure of the catalytically active species. The degree of branching was shown to be negligible at low reaction temperatures and high ethylene pressures when employing pre-catalysts with decreased steric bulk. In contrast, employing sterically encumbered pre-catalysts at high temperatures and low ethylene pressure led to the formation of highly branched polyethylene.[61] To probe this observed variation in polymer microstructure as a function of external factors, Brookhart and co-workers prepared a series of cationic Ni(II) alkyl complexes bearing α-diimine ligands and evaluated their reactivity and solution dynamics in the presence of ethylene (Scheme 1.11).[62] The initial product isolated was shown to be a cationic *β*-agostic Ni-propyl species, formed with a ratio of 20:1 *n*-propyl/*i*-propyl isomers. The experimentally determined ratio of isomers corrolated well with the isomer ratios determined computationally by Morokuma[59b] and Ziegler.[63]

Scheme 1.11 Observed isomerisation of Ni-alkyl complexes prepared by Brookhart and co-workers.[62]

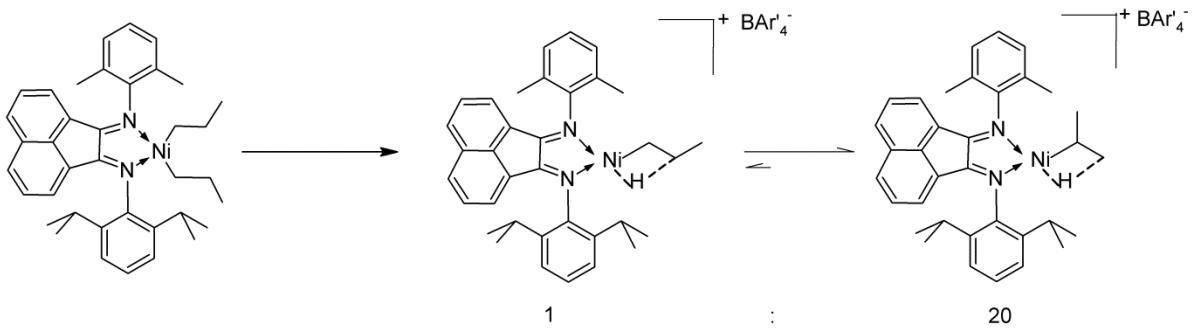

Variable temperature NMR studies on Ni-*i*Pr species revealed three distinct dynamic processes. In-place methyl rotation, characterised by hydrogen exchange through in-place rotation of the agostic Me group; and agostic methyl exchange, characterised by agostic Me/free Me group exchange by rotation about the Ni-C bond. Both processes were identified as being low in energy (energy barriers of 8 and 9 kcal/mol respectively).

The third process, methyl/methine hydrogen exchange, characterised by exchange of the methine hydrogen with the isopropyl methyl hydrogen, displayed a much higher energy barrier than the other two processes, calculated to be 14.0 kcal/mol. The overall dynamic behaviour of these species was similar to that reported for analogous Pd-alkyl species.[43b] Methyl/methine hydrogen exchange was identified as the process affecting the chain-walking ability of the Ni(II) complexes. In comparison to the palladium systems, the rotational barrier was 4-5 kcal/mol lower for these systems, thereby directly impacting on metal-migration along the growing polymer chain.

Trapping experiments with ethylene, acetonitrile and dimethyl sulphide demonstrated that the isomerisation between the Ni-*n*Pr and Ni-*i*Pr alkyl species was, in general, inversely dependent on the concentration of the trapping ligand, thereby providing evidence that isomerisation proceeded via a dissociative mechanism, analogous to that observed for palladium.[43d]

Ethylene insertion barriers, determined by low temperature NMR experiments, for both Ni-*n*Pr and Ni-*i*Pr alkyl species, were found to be 4-5 kcal/mol lower in energy in comparison to their Pd congeners, while the energy barriers for insertion from sterically encumbered analogues were slightly lower than the less sterically congested Ni-alkyl species. In addition the Ni-*n* alkyl species evaluated also displayed slightly lower barriers for ethylene insertion than the isopropyl analogues. These results were consistent with the observations made during bulk polymerisations as well as what has been established experimentally and theoretically regarding steric effects for nickel and palladium complexes of this type.[7a,59a]

Despite their exceptional catalytic activity toward ethylene homo- and ethylene/unactivated olefin polymerisation, Ni(II) complexes generally suffer from low

activity and/or rapid catalyst deactivation processes during attempted co-polymerisation of ethylene and polar vinyl monomers such as methyl acrylate.[64]

Mecking and co-workers recently employed spectroscopic techniques as a means to gain insight into the factors governing Ni(II)-mediated co-polymerisation of ethylene and polar vinyl monomers.[65] They reported the reaction of phenoxyimine-ligated Ni(II) hydride and Ni(II)-species with methyl acrylate (MA, Scheme 1.12A) and vinyl acetate (VA, Scheme 1.12B) as well as MA in the presence of ethylene. The reactions of the Ni(II)-hydride with MA and VA generated organometallic species as a result of regiospecific 2,1-insertion, characterised by a weak Ni-O interaction as evidenced by low temperature spectroscopic and *ab initio* DFT studies. The insertion product was shown to decompose in the presence of the Ni(II)-hydride species via a bimolecular pathway as well as at higher temperatures, generating methyl propanoate as the sole organic product, while displaying stability at low temperature in the absence of other Ni(II) species.

Scheme 1.12 The reactivity of N-O Ni(II)-hydride species toward polar vinyl monomers.[65]

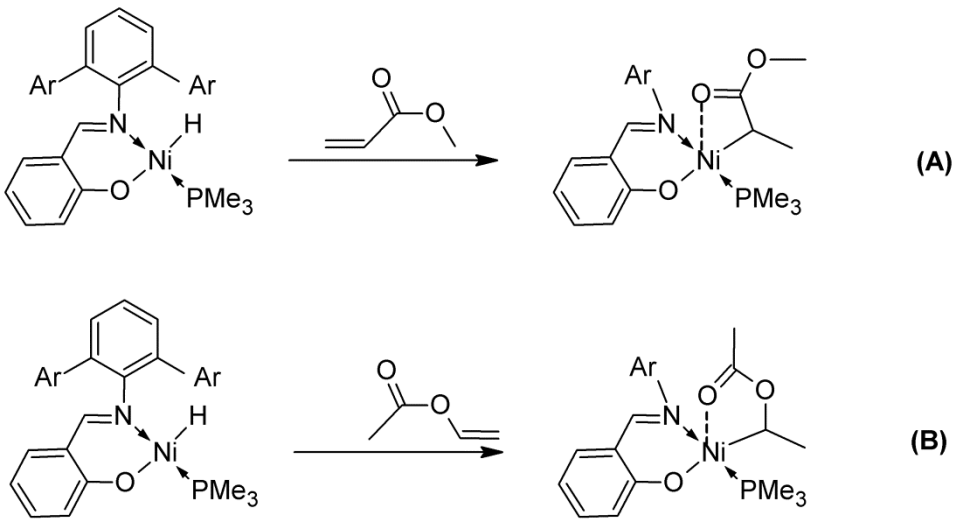

The stability at low temperature was confirmed by the absence of H/D scrambling during deuterium-labelling experiments with the organometallic insertion products. An

additional decomposition pathway was also identified as hydrolysis of the Ni-C bond of the insertion product in the presence of water. No further insertion was observed throughout this experimental investigation. The experimental results corroborated the observed lack of reactivity and provided key insights into decomposition pathways and reactivity profiles of Ni(II) intermediates generated during attempted co-polymerisation of ethylene with polar vinyl monomers.

Recently, Marks and co-workers demonstrated that the decomposition pathways identified by Mecking could be overcome by employing bimetallic catalysts in which the active metal sites are in close proximity with one another.[66] They prepared and characterised bimetallic phenoxyiminato-Ni_2 catalysts and evaluated their catalytic activity in ethylene homopolymerisation and in the co-polymerisation of ethylene and polar functionalised norbornenes, MA and methyl methacrylate (MMA, Fig. 1.13).

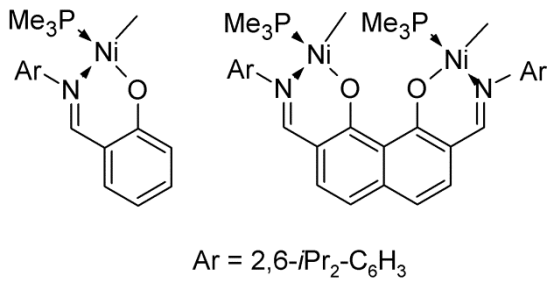

Fig. 1.13 Homo- and bimetallic phenoxyimine-Ni(II) pre-catalysts developed by Marks and co-workers for ethylene/α-olefin homo- and co-polymerisation.[66b]

The reported results demonstrated that the bimetallic catalysts showed significant increases in catalytic activity for ethylene homopolymerisation in comparison to the monometallic analogue. These catalysts also showed a significant increase in co-monomer incorporation during the co-polymerisation reactions, while displaying activity in the presence of diethyl ether, acetone and water. To gain mechanistic insight into the enhanced

enchainment selectivity, homo- (**1-XIA**) and bimetallic Ni(II) *n*-Bu species (**1-XIB**, Fig. 1.14) were prepared and low temperature spectroscopic techniques employed to evaluate differences in the dynamic behaviour of these species.

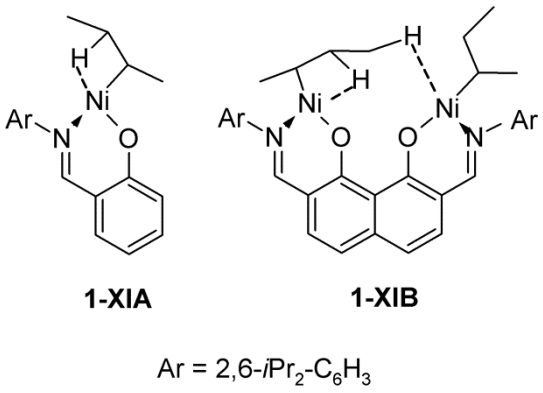

1-XIA **1-XIB**

Ar = 2,6-*i*Pr$_2$-C$_6$H$_3$

Fig. 1.14 Homo- and bimetallic Ni-butyl species and the differing cooperative effects evidenced by varying degrees of M-H agostic interactions.[66b]

Species **1-XIA** displayed a single Ni-H agostic interaction similar to that previously reported by Brookhart,[62] whereas the bimetallic species **1-XIB** displayed a Ni-H and a Ni-CH_3 agostic interaction. The origin of the second agostic interaction was probed and it was shown that it arose from the interaction of the terminal carbon atom of the alkyl group on one Ni centre, with the other Ni centre. In addition, radical trapping experiments and microstructure analysis showed that the co-polymerisation was indeed a coordinative polymerisation process and that the significantly enhanced co-monomer incorporation was due to cooperative effects between the proximal metal centres.

1.6 Objectives of the current study.

The field of transition metal-mediated olefin transformation has been driven by the need for catalytic systems which show enhanced activity and selectivity. The ability to

directly affect the nature of the products on a molecular level through rational catalyst design allows for the development of materials with novel properties.

The discussion above aimed to highlight how an understanding of the mechanism by which a particular catalyst system operates can be obtained by a combination of experimental and theoretical approaches. Firstly, this project aims to add to this body of knowledge by the synthesis, characterisation and catalytic application of early and late transition metal complexes. Secondly, it was envisaged that a combined experimental and computational approach would assist in providing insight into the mechanistic features associated with the application of these complexes as catalysts in olefin oligo-/polymerisation.

Chapter 2 details the synthesis and characterisation of novel neutral and cationic palladium methyl complexes ligated by alkyl-substituted 2,2′-dipyridyl-*N*-alkylamine ligands.

In **Chapter 3**, the application of the novel palladium methyl complexes as catalysts in ethylene oligomerisation is investigated, employing both low temperature spectroscopic techniques and DFT calculations to determine reaction kinetics and energy barriers associated with the ethylene oligomerisation process and to correlate the observed reactivity trends with those predicted by theory.

The preparation, characterisation and catalytic application in ethylene oligomerisation of neutral Ni(II) complexes ligated by alkyl-substituted 2,2′-dipyridyl-*N*-alkylamine ligands is reported in **Chapter 4**.

Chapter 5 details the synthetic and catalytic application of novel iminophosphine-ligated Cr(III) complexes in ethylene polymerisation. The results of a DFT

study on the reactivity of these complexes toward ethylene is correlated with the observed reactivity.

1.7 References

(1) Ziegler, K. *Brennst.-Chem.*, **1952**, *35*, 193.

(2) (a) Natta, V. G.; Corradini, P. *Die Makromolekulare Chemie*, **1955**, *16*, 77 (b) Natta, G.; Pino, P.; Mazzanti, G. *Atti, Accad. Naz. Lincei, Rend. Classe Sci. Fis. Mat. Nat*, **1958**, *25*, 3 (c) Natta, G.; Danusso, F.; Sianesi, D. *Die Makromolekulare Chemie*, **1958**, *28*, 253 (d) Natta, G.; Mazzanti, G.; Corradini, P.; Bassi, I. W. *Die Makromolekulare Chemie*, **1960**, *37*, 156.

(3) Nobelprize.org, The Nobel Prize in Chemistry 1963, 16 July 2013, <http://www.nobelprize.org/nobel_prizes/chemistry/laureates/1963/>

(4) Sinn, H.; Kaminsky, W. In *Adv. Organomet. Chem.*; Stone, F. G. A., West, R., Eds.; Academic Press, 1980; Vol. Volume 18, 99.

(5) (a) McKnight, A. L.; Waymouth, R. M. *Chem. Rev.*, **1998**, *98*, 2587 (b) Britovsek, G. J. P.; Gibson, V. C.; Wass, D. F. *Angew. Chem. Int. Ed.*, **1999**, *38*, 428.

(6) (a) Makio, H.; Kashiwa, N.; Fujita, T. *Adv. Synth. Catal.*, **2002**, *344*, 477 (b) Matsugi, T.; Fujita, T. *Chem. Soc. Rev.*, **2008**, *37*, 1264 (c) Makio, H.; Fujita, T. *Acc. Chem. Res.*, **2009**, *42*, 1532 (d) Makio, H.; Terao, H.; Iwashita, A.; Fujita, T. *Chem. Rev.*, **2011**, *111*, 2363 (e) Wang, C.; Friedrich, S.; Younkin, T. R.; Li, R. T.; Grubbs, R. H.; Bansleben, D. A.; Day, M. W. *Organometallics*, **1998**, *17*, 3149 (f) Younkin, T. R.; Connor, E. F.; Jason, I. H.; Friedrich, S. K.; Grubbs, R. H.; Bansleben, D. A. *Science*, **2000**, *287*, 460.

(7) (a) Johnson, L. K.; Killian, C. M.; Brookhart, M. *J. Am. Chem. Soc.*, **1995**, *117*, 6414 (b) Rix, F. C.; Brookhart, M.; White, P. S. *J. Am. Chem. Soc.*, **1996**, *118*, 4746 (c)

Tempel, D. J.; Johnson, L. K.; Huff, R. L.; White, P. S.; Brookhart, M. *J. Am. Chem. Soc.*, **2000**, *122*, 6686 (d) J. P. Britovsek, G.; C. Gibson, V.; J. McTavish, S.; A. Solan, G.; J. P. White, A.; J. Williams, D.; S. Kimberley, B.; J. Maddox, P. *Chem. Commun.*, **1998**, 849 (e) Small, B. L.; Brookhart, M.; Bennett, A. M. A. *J. Am. Chem. Soc.*, **1998**, *120*, 4049.

(8) (a) Schrock, R. R.; Luo, S.; Zanetti, N. C.; Fox, H. H. *Organometallics*, **1994**, *13*, 3396 (b) Bell, A. T.; Head-Gordon, M. *Annu. Rev. Chem. Biomol. Eng.*, **2011**, *2*, 453.

(9) (a) Arrieta, A.; de la Torre, M. C.; de Cózar, A.; Sierra, M. A.; Cossío, F. P. *Synlett*, **2013**, *24*, 535 (b) Wijma, H. J.; Janssen, D. B. *FEBS Journal*, **2013**, *280*, 2948 (c) Kumar, A.; Ghosh, P. *Eur. J. Inorg. Chem.*, **2012**, *2012*, 3955 (d) Bryliakov, K. P.; Talsi, E. P. *Coord. Chem. Rev.*, **2012**, *256*, 2994.

(10) (a) Devore, D. D.; Timmers, F. J.; Hasha, D. L.; Rosen, R. K.; Marks, T. J.; Deck, P. A.; Stern, C. L. *Organometallics*, **1995**, *14*, 3132 (b) Alt, H. G.; Föttinger, K.; Milius, W. *J. Organomet. Chem.*, **1999**, *572*, 21 (c) Frazier, K. A.; Froese, R. D.; He, Y.; Klosin, J.; Theriault, C. N.; Vosejpka, P. C.; Zhou, Z.; Abboud, K. A. *Organometallics*, **2011**, *30*, 3318.

(11) Delferro, M.; Marks, T. J. *Chem. Rev.*, **2011**, *111*, 2450.

(12) Abramo, G. P.; Li, L.; Marks, T. J. *J. Am. Chem. Soc.*, **2002**, *124*, 13966.

(13) Li, L.; Metz, M. V.; Li, H.; Chen, M.-C.; Marks, T. J.; Liable-Sands, L.; Rheingold, A. L. *J. Am. Chem. Soc.*, **2002**, *124*, 12725.

(14) Salata, M. R.; Marks, T. J. *J. Am. Chem. Soc.*, **2007**, *130*, 12.

(15) Motta, A.; Fragalà, I. L.; Marks, T. J. *J. Am. Chem. Soc.*, **2009**, *131*, 3974.

(16) Liu, S.; Motta, A.; Delferro, M.; Marks, T. J. *J. Am. Chem. Soc.*, **2013**, *135*, 8830.

(17) McGuinness, D. S.; Wasserscheid, P.; Keim, W.; Morgan, D.; Dixon, J. T.; Bollmann, A.; Maumela, H.; Hess, F.; Englert, U. *J. Am. Chem. Soc.*, **2003**, *125*, 5272.

(18) (a) Elowe, P. R.; McCann, C.; Pringle, P. G.; Spitzmesser, S. K.; Bercaw, J. E. *Organometallics*, **2006**, *25*, 5255 (b) Kim, S.-K.; Kim, T.-J.; Chung, J.-H.; Hahn, T.-K.; Chae, S.-S.; Lee, H.-S.; Cheong, M.; Kang, S. O. *Organometallics*, **2010**, *29*, 5805.

(19) (a) Albahily, K.; Licciulli, S.; Gambarotta, S.; Korobkov, I.; Chevalier, R.; Schuhen, K.; Duchateau, R. *Organometallics*, **2011**, *30*, 3346 (b) Albahily, K.; Gambarotta, S.; Duchateau, R. *Organometallics*, **2011**, *30*, 4655.

(20) (a) Zhang, M.; Wang, K.; Sun, W.-H. *Dalton. Trans.*, **2009**, 6354 (b) Wang, D.; Liu, S.; Zeng, Y.; Sun, W.-H.; Redshaw, C. *Organometallics*, **2011**, *30*, 3001 (c) Al Thagfi, J.; Lavoie, G. G. *Organometallics*, **2012**, *31*, 2463.

(21) Jabri, A.; Crewdson, P.; Gambarotta, S.; Korobkov, I.; Duchateau, R. *Organometallics*, **2006**, *25*, 715.

(22) Agapie, T. *Coord. Chem. Rev.*, **2011**, *255*, 861.

(23) (a) McGuinness, D. S. *Chem. Rev.*, **2010**, *111*, 2321 (b) Dixon, J. T.; Green, M. J.; Hess, F. M.; Morgan, D. H. *J. Organomet. Chem.*, **2004**, *689*, 3641.

(24) McGuinness, D. S.; Wasserscheid, P.; Keim, W.; Hu, C.; Englert, U.; Dixon, J. T.; Grove, C. *Chem. Commun.*, **2003**, 334.

(25) Bollmann, A.; Blann, K.; Dixon, J. T.; Hess, F. M.; Killian, E.; Maumela, H.; McGuinness, D. S.; Morgan, D. H.; Neveling, A.; Otto, S.; Overett, M.; Slawin, A. M. Z.; Wasserscheid, P.; Kuhlmann, S. *J. Am. Chem. Soc.*, **2004**, *126*, 14712.

(26) Blann, K.; Bollmann, A.; de Bod, H.; Dixon, J. T.; Killian, E.; Nongodlwana, P.; Maumela, M. C.; Maumela, H.; McConnell, A. E.; Morgan, D. H.; Overett, M. J.; Prétorius, M.; Kuhlmann, S.; Wasserscheid, P. *J. Catal.*, **2007**, *249*, 244.

(27) Janse van Rensburg, W.; Grové, C.; Steynberg, J. P.; Stark, K. B.; Huyser, J. J.; Steynberg, P. J. *Organometallics*, **2004**, *23*, 1207.

(28) Jabri, A.; Mason, C. B.; Sim, Y.; Gambarotta, S.; Burchell, T. J.; Duchateau, R. *Angew. Chem. Int. Ed.*, **2008**, *47*, 9717.

(29) Vidyaratne, I.; Nikiforov, G. B.; Gorelsky, S. I.; Gambarotta, S.; Duchateau, R.; Korobkov, I. *Angew. Chem. Int. Ed.*, **2009**, *48*, 6552.

(30) Skobelev, I. Y.; Panchenko, V. N.; Lyakin, O. Y.; Bryliakov, K. P.; Zakharov, V. A.; Talsi, E. P. *Organometallics*, **2010**, *29*, 2943.

(31) Budzelaar, P. *Can. J. Chem.*, **2009**, *87*, 832.

(32) Agapie, T.; Schofer, S. J.; Labinger, J. A.; Bercaw, J. E. *J. Am. Chem. Soc.*, **2004**, *126*, 1304.

(33) Overett, M. J.; Blann, K.; Bollmann, A.; Dixon, J. T.; Haasbroek, D.; Killian, E.; Maumela, H.; McGuinness, D. S.; Morgan, D. H. *J. Am. Chem. Soc.*, **2005**, *127*, 10723.

(34) (a) Chen, E. Y.-X.; Marks, T. J. *Chem. Rev.*, **2000**, *100*, 1391 (b) Zhou, J.; Lancaster, S. J.; Walker, D. A.; Beck, S.; Thornton-Pett, M.; Bochmann, M. *J. Am. Chem. Soc.*, **2000**, *123*, 223 (c) Rojas, R. S.; Peoples, B. C.; Cabrera, A. R.; Valderrama, M.; Fröhlich, R.; Kehr, G.; Erker, G.; Wiegand, T.; Eckert, H. *Organometallics*, **2011**, *30*, 6372.

(35) McGuinness, D. S.; Rucklidge, A. J.; Tooze, R. P.; Slawin, A. M. Z. *Organometallics*, **2007**, *26*, 2561.

(36) Ghiotto, F.; Pateraki, C.; Tanskanen, J.; Severn, J. R.; Luehmann, N.; Kusmin, A.; Stellbrink, J.; Linnolahti, M.; Bochmann, M. *Organometallics*, **2013**, *32*, 3354.

(37) Yang, Y.; Liu, Z.; Zhong, L.; Qiu, P.; Dong, Q.; Cheng, R.; Vanderbilt, J.; Liu, B. *Organometallics*, **2011**, *30*, 5297.

(38) McGuinness, D. S.; Brown, D. B.; Tooze, R. P.; Hess, F. M.; Dixon, J. T.; Slawin, A. M. Z. *Organometallics*, **2006**, *25*, 3605.

(39) Jabri, A.; Temple, C.; Crewdson, P.; Gambarotta, S.; Korobkov, I.; Duchateau, R. *J. Am. Chem. Soc.*, **2006**, *128*, 9238.

(40) Köhn, R. D. *Angew. Chem. Int. Ed.*, **2008**, *47*, 245.

(41) Poli, R. *J. Organomet. Chem.*, **2004**, *689*, 4291.

(42) Liu, Z.; Zhong, L.; Yang, Y.; Cheng, R.; Liu, B. *J. Phys. Chem. A*, **2011**, *115*, 8131.

(43) (a) Rix, F. C.; Brookhart, M. *J. Am. Chem. Soc.*, **1995**, *117*, 1137 (b) Tempel, D. J.; Brookhart, M. *Organometallics*, **1998**, *17*, 2290 (c) Mecking, S.; Johnson, L. K.; Wang, L.; Brookhart, M. *J. Am. Chem. Soc.*, **1998**, *120*, 888 (d) Shultz, L. H.; Tempel, D. J.; Brookhart, M. *J. Am. Chem. Soc.*, **2001**, *123*, 11539 (e) Woo, T. K.; Margl, P. M.; Blöchl, P. E.; Ziegler, T. *J. Phys. Chem. B*, **1997**, *101*, 7877 (f) Michalak, A.; Ziegler, T. *J. Am. Chem. Soc.*, **2001**, *123*, 12266 (g) Szabo, M. J.; Galea, N. M.; Michalak, A.; Yang, S.-Y.; Groux, L. F.; Piers, W. E.; Ziegler, T. *J. Am. Chem. Soc.*, **2005**, *127*, 14692 (h) Yang, S.-Y.; Szabo, M. J.; Michalak, A.; Weiss, T.; Piers, W. E.; Jordan, R. F.; Ziegler, T. *Organometallics*, **2005**, *24*, 1242 (i) Haras, A.; Michalak, A.; Rieger, B.; Ziegler, T. *Organometallics*, **2006**, *25*, 946.

(44) Drent, E.; van Dijk, R.; van Ginkel, R.; van Oort, B.; Pugh, R. I. *Chem. Commun.*, **2002**, 744.

(45) Hearley, A. K.; Nowack, R. J.; Rieger, B. *Organometallics*, **2005**, *24*, 2755.

(46) Kochi, T.; Yoshimura, K.; Nozaki, K. *Dalton. Trans.*, **2006**, *0*, 25.

(47) Guironnet, D.; Roesle, P.; Rünzi, T.; Göttker-Schnetmann, I.; Mecking, S. *J. Am. Chem. Soc.*, **2008**, *131*, 422.

(48) (a) Kochi, T.; Noda, S.; Yoshimura, K.; Nozaki, K. *J. Am. Chem. Soc.*, **2007**, *129*, 8948 (b) Nozaki, K.; Kusumoto, S.; Noda, S.; Kochi, T.; Chung, L. W.; Morokuma, K. *J. Am. Chem. Soc.*, **2010**, *132*, 16030.

(49) Vela, J.; Lief, G. R.; Shen, Z.; Jordan, R. F. *Organometallics*, **2007**, *26*, 6624.

(50) Nakamura, A.; Anselment, T. M. J.; Claverie, J.; Goodall, B.; Jordan, R. F.; Mecking, S.; Rieger, B.; Sen, A.; van Leeuwen, P. W. N. M.; Nozaki, K. *Acc. Chem. Res.*, **2013**, *46*, 1438.

(51) Noda, S.; Nakamura, A.; Kochi, T.; Chung, L. W.; Morokuma, K.; Nozaki, K. *J. Am. Chem. Soc.*, **2009**, *131*, 14088.

(52) (a) Deubel, D. V.; Ziegler, T. *Organometallics*, **2002**, *21*, 4432 (b) Casares, J. A.; Espinet, P. *Inorg. Chem.*, **1997**, *36*, 5428 (c) Casado, A. L.; Espinet, P. *Organometallics*, **1998**, *17*, 954.

(53) Zheng, F.; Hutton, A. T.; van Sittert, C. G. C. E.; Moss, J. R.; Mapolie, S. F. *Dalton. Trans.*, **2013**, *42*, 11163.

(54) Komon, Z. J. A.; Bu, X.; Bazan, G. C. *J. Am. Chem. Soc.*, **2000**, *122*, 1830.

(55) (a) Lee, B. Y.; Bazan, G. C.; Vela, J.; Komon, Z. J. A.; Bu, X. *J. Am. Chem. Soc.*, **2001**, *123*, 5352 (b) Boardman, B. M.; Bazan, G. C. *Acc. Chem. Res.*, **2009**, *42*, 1597.

(56) Cai, Z.; Shen, Z.; Zhou, X.; Jordan, R. F. *ACS Catal.*, **2012**, *2*, 1187.

(57) Killian, C. M.; Tempel, D. J.; Johnson, L. K.; Brookhart, M. *J. Am. Chem. Soc.*, **1996**, *118*, 11664.

(58) (a) Svejda, S. A.; Johnson, L. K.; Brookhart, M. *J. Am. Chem. Soc.*, **1999**, *121*, 10634 (b) Jenkins, J. C.; Brookhart, M. *J. Am. Chem. Soc.*, **2004**, *126*, 5827.

(59) (a) Deng, L.; Margl, P.; Ziegler, T. *J. Am. Chem. Soc.*, **1997**, *119*, 1094 (b) Musaev, D. G.; Froese, R. D. J.; Svensson, M.; Morokuma, K. *J. Am. Chem. Soc.*, **1997**, *119*, 367.

(60) Ittel, S. D.; Johnson, L. K.; Brookhart, M. *Chem. Rev.*, **2000**, *100*, 1169.

(61) Gates, D. P.; Svejda, S. A.; Oñate, E.; Killian, C. M.; Johnson, L. K.; White, P. S.; Brookhart, M. *Macromolecules*, **2000**, *33*, 2320.

(62) Leatherman, M. D.; Svejda, S. A.; Johnson, L. K.; Brookhart, M. *J. Am. Chem. Soc.*, **2003**, *125*, 3068.

(63) Deng, L.; Woo, T. K.; Cavallo, L.; Margl, P. M.; Ziegler, T. *J. Am. Chem. Soc.*, **1997**, *119*, 6177.

(64) Gibson, V. C.; Tomov, A. *Chem. Commun.*, **2001**, 1964.

(65) Berkefeld, A.; Drexler, M.; Möller, H. M.; Mecking, S. *J. Am. Chem. Soc.*, **2009**, *131*, 12613.

(66) (a) Rodriguez, B. A.; Delferro, M.; Marks, T. J. *Organometallics*, **2008**, *27*, 2166 (b) Rodriguez, B. A.; Delferro, M.; Marks, T. J. *J. Am. Chem. Soc.*, **2009**, *131*, 5902.

2.1 Introduction.

The development of olefin oligo- and polymerisation catalysts bearing neutral bidentate nitrogen donor ligands have seen phenomenal research interest over the past twenty years.[1,2,3] Of particular significance is the contributions by Brookhart and co-workers with respect to the development of diimine late transition metal catalysts of nickel and palladium, which dependent on catalyst structure, produced ethylene oligomers, polymers as well as copolymers of ethylene with polar and non-polar α-, internal and cyclic olefins (Chart 2.1).

Chart 2.1 Cationic α-diimine Pd catalysts developed by Brookhart and co-workers.

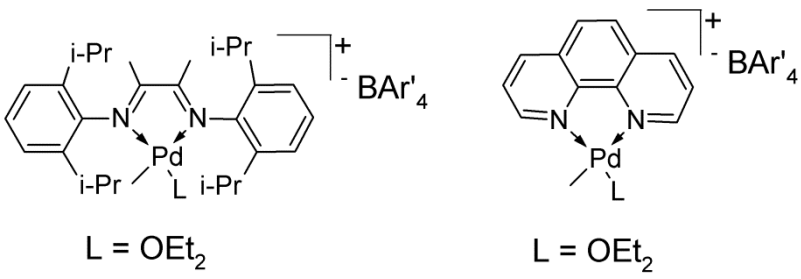

In particular, their research efforts gave fundamental insight into the mechanism of olefin oligo-/polymerisation employing these catalyst systems. It was demonstrated that chain transfer occurs via associative olefin exchange and that the introduction of steric bulk in the *ortho* position of the N,N-chelate ring positioned these substituents above and below the axial coordination sites within the square plane of the metal. This effectively inhibits associative ligand exchange, disfavoring chain transfer and allowing the production of polyolefins. In addition, it was demonstrated that in the catalytic dimerisation of ethylene by a (N,N)PdR$^+$ complex (N,N = phenanthroline) involves an insertion/β-H elimination mechanism and that the ethyl ethylene complex is the catalyst resting state.[4]

In relation to this, Jordan and co-workers examined the catalytic behaviour of a series of cationic palladium alkyl complexes bearing bis(heterocycle)methane ligands (Scheme 2.1).[5] They found that initial ethylene insertion rates increased with an increase in electrophilicity of the metal centre, as a result of a decrease in σ-donor ability of the ligand (imidazole > pyridine > pyrazole), as well as steric bulk at the metal center. Also, catalytic dimerisation proceeded via an analogous mechanism to that reported by Brookhart and co-workers. In addition, an increase in steric bulk around the metal centre led to branched polymer formation, thereby inhibiting associative chain transfer.

Scheme 2.1 Bis(heterocycle)methane Pd complexes evaluated in ethylene oligomerisation.[5a,b]

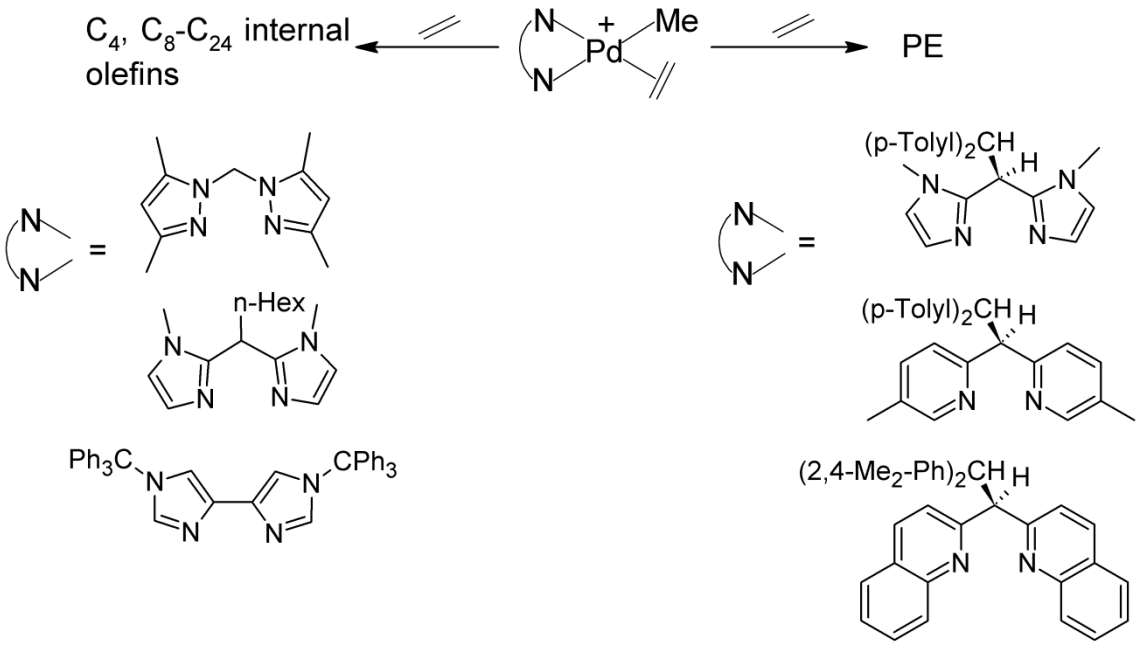

Herein we report the development of neutral and cationic palladium methyl complexes bearing *N*-alkyl-2,2′-dipyridylamine ligands to be employed in catalytic ethylene oligomerisation reactions.

2.2 Results and Discussion

2.2.1 Synthesis of N-alkyl-dipyridylamine ligands, 1a-1e.

A series of known and novel *N*-alkyl 2,2′-dipyridylamine ligands of general formula $(2\text{-}C_5H_3NR)_2NR'$, **a**: R = H, R′ = Me; **b**: R = H, R′ = benzyl; **c**: R = H, R′ = methylcyclohexyl; **d**: R = H, R′ = neopentyl; **e**: R = Me, R′ = Me) were prepared by a modified method involving base-mediated *N*-alkylation (Chart 2.2).[6] Ligands **a**,[7] **b**[6] and **d**[8] have been reported previously whereas **c** and **e** are novel. The ligands were isolated, after column chromatography, as yellow oils (**a**, **c**, **d**, **e**) or solid (**b**) in 60-90 % yield. The ligands displayed solubility in most organic solvents and were characterised by FT-IR and ^{1}H NMR spectroscopy (**a**, **b**, **d**) as well as ^{13}C{^{1}H} NMR spectroscopy, ESI-MS and elemental analysis (**c**, **e**).

Chart 2.2 *N*-alkyl 2,2′-dipyridylamine ligands prepared in this study; showing numbering scheme.

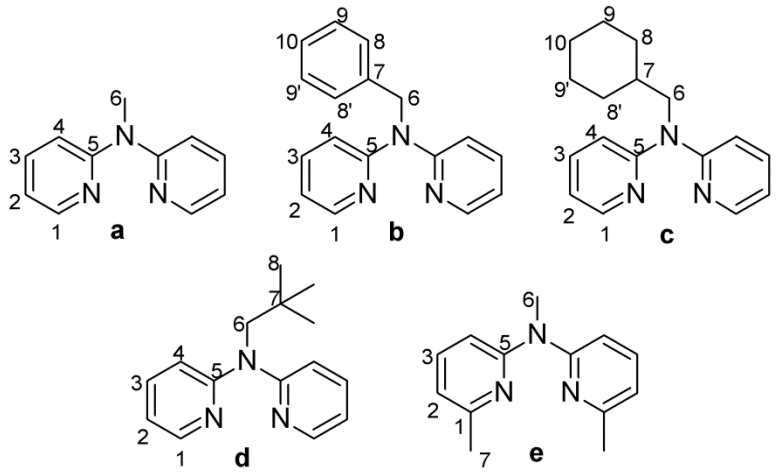

In the FT-IR spectra of the ligands, the $\upsilon_{C=N}$ absorption bands of the pyridyl ring were observed in the range 1591-1580 and 1566-1557 cm^{-1}. The ^{1}H NMR spectra of the ligands (Table 2.1) displayed the *ortho*-*N* proton resonances (**a**-**d**) in the range δ 8.31-8.32 ppm.

Table 2.1 ^{1}H NMR spectral data for 2,2′-dipyridyl-*N*-alkylamine ligands.[a]

Ligand	Aromatic Region	Aliphatic Region
a	δ 8.33-8.36 (dd, 2H, $^{3}J_{H\text{-}H}$ 7.92 Hz, H^{1}); δ 7.51-7.57 (m, 2H, H^{3}); δ 7.15-7.19 (dt, 2H, $^{3}J_{H\text{-}H}$ 8.51 Hz, H^{4}); δ 6.84-6.88 (m, 2H, H^{2})	δ 3.63 (s, 3H, H^{6})
b	δ 8.31-8.33 (dd, 2H, $^{3}J_{H\text{-}H}$ 7.63 Hz, H^{1}); δ 7.48-7.54 (m, 2H, H^{3}); δ 7.33-7.36 (br.d, 2H, $^{3}J_{H\text{-}H}$ 7.34 Hz, H^{4}); δ 7.25-7.28 (m, 2H, $H^{9,10}$); δ 7.15-7.20 (m, 3H, $H^{8,8',9}$); δ 6.82-6.87 (dt, 2H, $^{3}J_{H\text{-}H}$ 7.19 Hz, H^{2})	δ 5.51 (s, 2H, H^{6})
c	δ 8.32-8.34 (dd, 2H, $^{3}J_{H\text{-}H}$ 7.78 Hz, H^{1}); δ 7.48-7.54 (m, 2H, H^{3}); δ 7.06-7.10 (dt, 2H, $^{3}J_{H\text{-}H}$ 8.51 Hz, H^{4}); δ 6.82-6.86 (dt, 2H, $^{3}J_{H\text{-}H}$ 7.19 Hz, H^{2})	δ 4.06 (d, 2H, $^{3}J_{H\text{-}H}$ 7.34 Hz, H^{6}); δ 1.79-1.87 (m, 1H, H^{7}); δ 1.59-1.74 (m, 5H, $H^{8,9,10}$); δ 1.13-1.22 (m, 3H, $H^{9',10'}$); δ 0.92-1.03 (m, 2H, $H^{8'}$)
d	δ 8.31-8.34 (dd, 2H, $^{3}J_{H\text{-}H}$ 7.78 Hz, H^{1}); δ 7.47-7.53 (m, 2H, H^{3}); δ 7.03-7.06 (dt, 2H, $^{3}J_{H\text{-}H}$ 8.36 Hz, H^{4}); δ 6.82-6.87 (dt, 2H, $^{3}J_{H\text{-}H}$ 7.19 Hz, H^{2})	δ 4.20 (s, 2H, H^{6}); δ 0.88 (s, 9H, H^{7})
e	δ 7.40 (t, 2H, $^{3}J_{H\text{-}H}$ 7.48 Hz, H^{3}); δ 6.95 (d, 2H, $^{3}J_{H\text{-}H}$ 8.36 Hz, H^{4}); δ 6.70 (d, 2H, $^{3}J_{H\text{-}H}$ 7.19 Hz, H^{2})	δ 3.63 (s, 3H, H^{6}); δ 2.48 (s, 6H, H^{7})

[a] Spectra recorded in $CDCl_3$ at 25 °C. Chemical shifts reported as δ ppm values, referenced relative to residual proton signals of the solvent.

In addition the methylene protons (for **b**-**d**) were observed as a singlet or doublet (for **c**) in the range δ 4.06-5.51 ppm.

In the $^{13}C\{^{1}H\}$ NMR spectra of the novel ligands, **c** and **e**, the N=*C* carbon resonances of the pyridyl rings were observed in the range δ 157.00-158.05 ppm, while in the case of **c**, the methylene carbon resonance was observed at δ 54.18 ppm. Additionally, the ESI-MS spectra, in the case of **c** and **e**, showed the base peak and parent ion at *m/z* 268 and 214 respectively, corresponding to the proton adduct of the ligand.

2.2.2 Synthesis of neutral N-alkyl-dipyridylaldiminato methylpalladium complexes, 2a-2e.

The 2,2′-dipyridyl-*N*-alkylamine ligands, **a**-**e**, were reacted with the palladium precursor [(COD)Pd(Cl)Me][9] to afford the neutral methylpalladium complexes, **2a**-**2e** (Scheme 2.2). The novel complexes were isolated as pure orange and pale-yellow solids in 60-80 % yield, displaying solubility in chlorinated organic solvents while being insoluble in aromatic solvents, alkanes, alcohols and ethers. These complexes were characterised by FT-IR spectroscopy; ^{1}H and $^{13}C\{^{1}H\}$ NMR spectroscopy; mass spectrometry; melting point determination and elemental analysis.

The neutral complexes, **2a**-**2e**, showed a shift to slightly higher wavenumbers in their FT-IR spectra in comparison to those of the free ligands in the range 1594-1596 cm^{-1} and 1571-1574 cm^{-1} and was indicative of coordination of the ligand to the metal precursor via the pyridyl ring N-atoms (Table 2.2).[10]

The asymmetrical nature of these complexes was displayed in their NMR spectra (Table 2.3). In the ^{1}H NMR spectra of the complexes, the imine protons were observed as two resonances, one adjacent to chlorine and the other adjacent to carbon.

Scheme 2.2 Synthesis of neutral palladium methyl *N*-alkyl dipyridylaldiminato complexes.

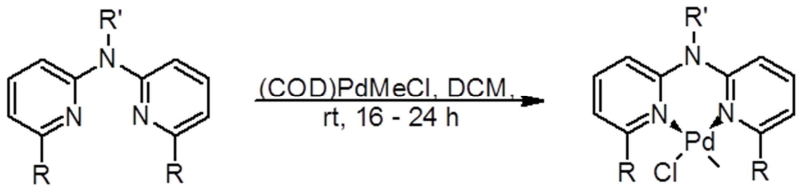

1a: R = H; R' = Me

1b: R = H; R' = benzyl

1c: R = H; R' = methylcyclohexyl

1d: R = H; R' = neopentyl

1e: R = Me; R' = Me

2a: R = H; R' = Me

2b: R = H; R' = benzyl

2c: R = H; R' = methylcyclohexyl

2d: R = H; R' = neopentyl

2e: R = Me; R' = Me

Table 2.2 Analytical data pertaining to neutral complexes, **2a**-**2e**.

Complex	M.p. (dec)[a]	FT-IR (cm^{-1}, C=N)[b]	ESI-MS (*m/z*)[c]
2a	196-198	1596, 1575	306
2b	152-153	1594, 1574	382
2c	178-179	1594, 1574	388
2d	180-181	1595, 1571	362
2e	205-207	1595, 1574	334

[a] Reported as uncorrected. [b] Recorded as neat spectra using a ZnSe ATR accessory. [c] Reported fragment corresponds to $[M\text{-}Cl]^{+}$.

In addition, these resonances were downfield shifted in comparison to those of the free ligand further confirming coordination to palladium. The *ortho-N* proton resonances were split into doublets of doublets in the range δ 7.69-8.85 ppm (proton adjacent to Cl) and δ 7.59-8.47 ppm (proton adjacent to Me). These resonance shifts are in the same range as those previously reported for analogous complexes. [5a,11]

Table 2.3 ^{1}H NMR spectral data of the neutral *N*-alkyl dipyridylaldiminato palladium complexes.[a]

Complex	Aromatic Region	Aliphatic Region
2a	δ 8.85 (dd, 1H, $^{3}J_{H\text{-}H}$ 5.9, $^{4}J_{H\text{-}H}$ 1.8, H^{1}); δ 8.47 (dd, 1H, $^{3}J_{H\text{-}H}$ 5.7, $^{4}J_{H\text{-}H}$ 1.8, $H^{1'}$); δ 7.86 (m, 1H, H^{3}); δ 7.77 (m, 1H, $H^{3'}$); δ 7.19 (d, 1H, $^{3}J_{H\text{-}H}$ 8.4, H^{4}); δ 7.11 (m, 3H, $H^{2,2',4'}$)	δ 3.56 (s, 3H, H^{6}); δ 0.83 (s, 3H, Pd-CH_3)
2b	δ 8.83 (dd, 1H, $^{3}J_{H\text{-}H}$ 4.1, $^{4}J_{H\text{-}H}$ 1.2, H^{1}); δ 8.45 (d, 1H, $^{3}J_{H\text{-}H}$ 5.9, $H^{1'}$); δ 7.70 (t, 2H, $^{3}J_{H\text{-}H}$ 7.9, $H^{3,3'}$); δ 7.61 (d, 2H, $^{3}J_{H\text{-}H}$ 7.62, $H^{4,4'}$); δ 7.30 (t, 2H, $^{3}J_{H\text{-}H}$ 7.62, $H^{2,2'}$); δ 7.21 (m, 1H, H^{10}); δ 7.17 (d, 1H, $^{3}J_{H\text{-}H}$ 8.20, H^{8}); δ 7.13 (d, 1H, $^{3}J_{H\text{-}H}$ 8.20, $H^{8'}$); δ 7.06 (m, 2H, $H^{9,9'}$)	δ 5.16 (s, 2H, H^{6}); δ 0.89 (s, 3H, Pd-CH_3)
2c	δ 8.80 (dd, 1H, $^{3}J_{H\text{-}H}$ 6.7, $^{4}J_{H\text{-}H}$ 1.5, H^{1}); δ 8.47 (dd, 1H, $^{3}J_{H\text{-}H}$ 5.7, $^{4}J_{H\text{-}H}$ 1.6, $H^{1'}$); δ 7.84 (dt, 1H, $^{3}J_{H\text{-}H}$ 7.3, $^{4}J_{H\text{-}H}$ 1.8, H^{3}); δ 7.73 (dt, 1H, $^{3}J_{H\text{-}H}$ 7.4, $^{4}J_{H\text{-}H}$ 1.9, $H^{3'}$); δ 7.22 (d, 1H, $^{3}J_{H\text{-}H}$ 8.2, H^{4}); δ 7.10 (m, 3H, $H^{2,2',4'}$)	δ 3.73 (d, 2H, $^{3}J_{H\text{-}H}$ 7.2, H^{6}); δ 2.13 (br.d, 2H, H^{8}); δ 1.70 (m, 2H, $H^{8'}$); δ 1.63 (m, 2H, H^{9}); δ 1.16 (m, 3H, $H^{7,9'}$); δ 1.05 (br.d, 2H, H^{10}); δ 0.84 (s,3H, Pd-CH_3)
2d	δ 8.79 (d, 1H, $^{3}J_{H\text{-}H}$ 5.3, H^{1}); δ 8.47 (d, 1H, $^{3}J_{H\text{-}H}$ 5.9, $H^{1'}$); δ 7.81 (m, 1H, H^{3}); δ 7.72 (m, 1H, $H^{3'}$); δ 7.40 (d, 1H, $^{3}J_{H\text{-}H}$ 8.2, H^{4}); δ 7.30 (d, 1H, $^{3}J_{H\text{-}H}$ 8.2, $H^{4'}$); δ 7.11 (m, 1H, H^{2}); δ 7.06 (m, 1H, $H^{2'}$)	δ 3.90 (br.d, 2H, H^{6}); δ 1.04 (s, 9H, H^{8}); δ 0.87 (s, 3H, Pd-CH_3)
2e	δ 7.69 (t, 1H, $^{3}J_{H\text{-}H}$ 7.69, H^{3}); δ 7.59 (t, 1H, $^{3}J_{H\text{-}H}$ 7.8, $H^{3'}$); δ 7.10 (d, 1H, $^{3}J_{H\text{-}H}$ 8.2, H^{4}); δ 6.96 (m, 3H, $H^{2,2',4'}$)	δ 3.58 (s, 3H, H^{6}); δ 2.97 (d, 6H, $^{4}J_{H\text{-}H}$ 5, $H^{7,7'}$); δ 0.58 (s, 3H, Pd-CH_3)

[a] Spectra recorded in $CDCl_3$ at 25 °C. Chemical shifts reported as δ ppm values, referenced relative to residual proton signals of the solvent. Coupling constant values in Hz

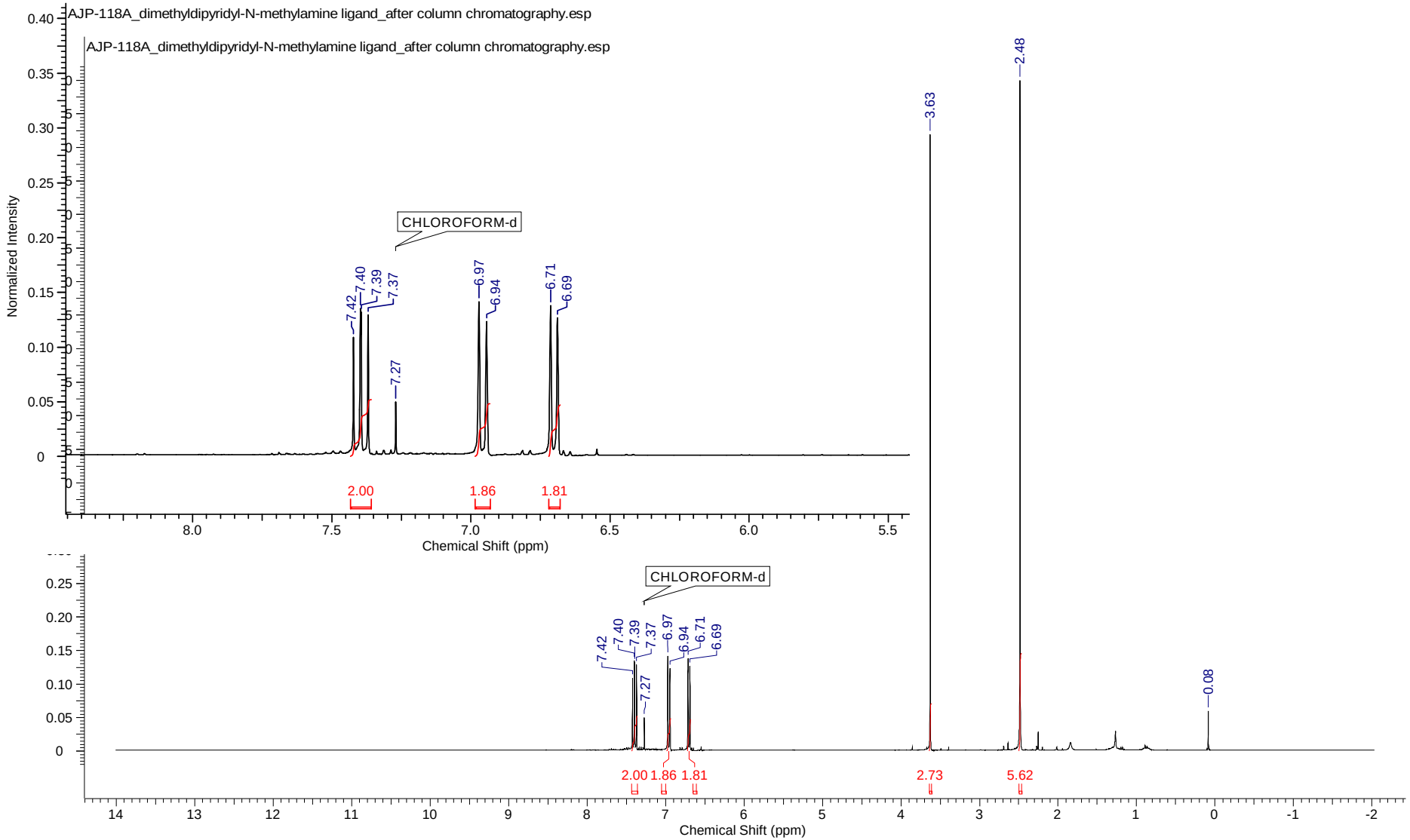

Fig. 2.1 ^{1}H NMR spectrum of complex **2e** in $CDCl_3$. Inset shows aromatic region.

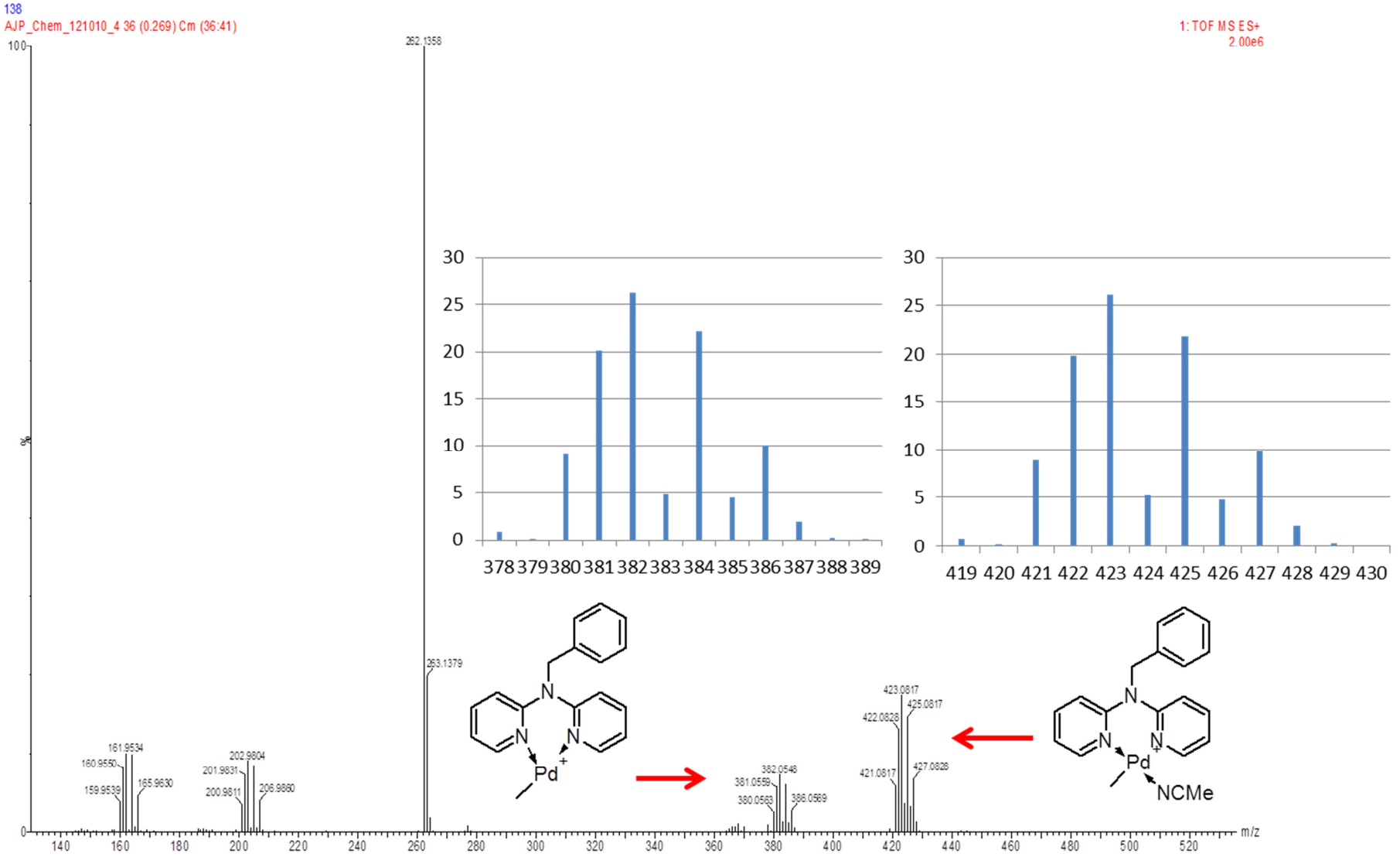

Fig. 2.2 ESI-MS spectrum of complex **2b** with the $[M\text{-}Cl]^+$ and $[M+MeCN\text{-}Cl]^+$ mass fragments highlighted. Inset shows simulated mass fragments.

In the case of complexes **2b**-**2d**, the methylene protons of the *N*-alkyl substituent were shifted slightly upfield in all cases in the range δ 3.73-5.16 ppm and resonated as singlets, except in the case of **2c** where this signal resonated as a broad doublet. The ^{1}H resonance of the Me-group bound to palladium was observed as a singlet in the range δ 0.58-1.04 ppm. The effect of introducting a Me-group in the 6-positions of the pyridyl rings is observed in the shift of the *Me*-resonance bound to palladium. For complex **2e** the *Me*-resonance is observed at δ 0.58 ppm, significantly high-field shifted in comparison to that observed for complexes **2a**-**2d**. This observation reflects the e^{-} -donating character of the Me-groups and their effect on the metal centre.

Scheme 2.3 Observed fragmentation pattern in the ESI-MS spectra of the neutral complexes.

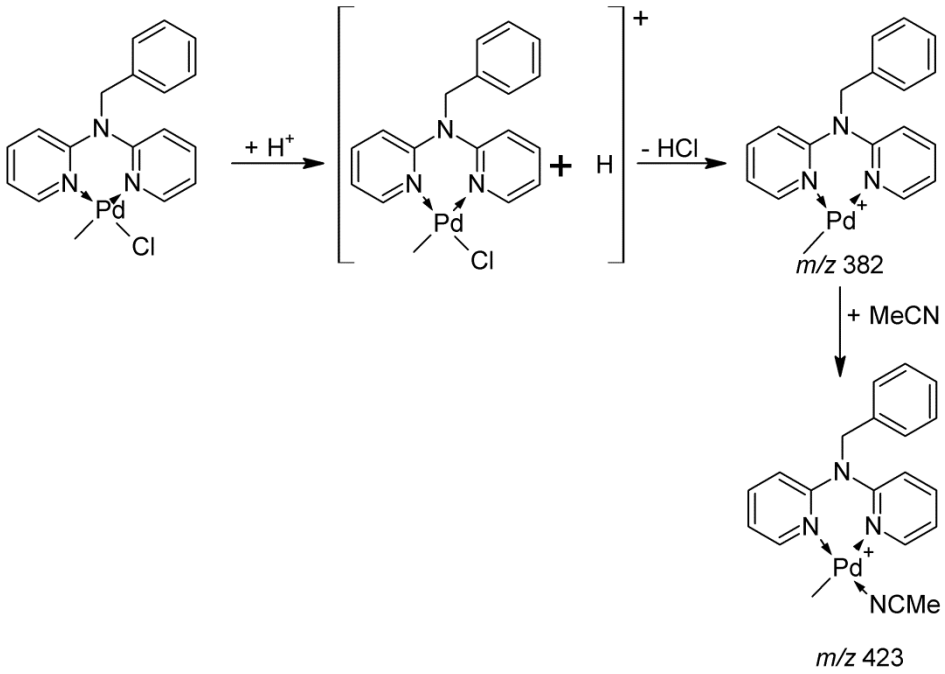

In the ^{13}C{^{1}H} NMR spectra, the N=*C* carbon resonances of the pyridyl rings were observed in the range δ 150.87-156.84 ppm (carbon adjacent to Cl) and δ 150.01-154.94 ppm

(carbon adjacent to Me), shifted downfield as a result of coordination to palladium via the pyridyl N-atoms.

The methylene carbon resonance (in the case of complex **2b**-**2d**) was observed in the range δ 55.27-64.97 ppm while the methyl carbon resonances (C_{Me}) bound to palladium of all the complexes were observed in the range δ -1.93 to -7.75 ppm, with the most high-field shifted Pd-*Me* resonance corresponding to complex **2e**.

The ESI-MS spectra showed characteristic isotope clusters corresponding to *m/z* $[M\text{-}Cl]^+$, which are typical fragments observed for these type of complexes (Fig. 2.2)[12] and for palladium-chloro complexes in general.[13] A possible fragmentation pattern is given (Scheme 2.3) which accounts for the observed formation of the higher than expected $[M+MeCN\text{-}Cl]^+$ mass fragment.

Single crystals of complex **2e** suitable for SCD analysis was grown by vapour diffusion of diethyl ether into a concentrated dichloromethane solution. The molecular structure of complex **2e** is shown in Figure 2.3 while selected crystallographic data as well as selected bond lengths and angles are listed in Tables 2.4 and 2.5 respectively.

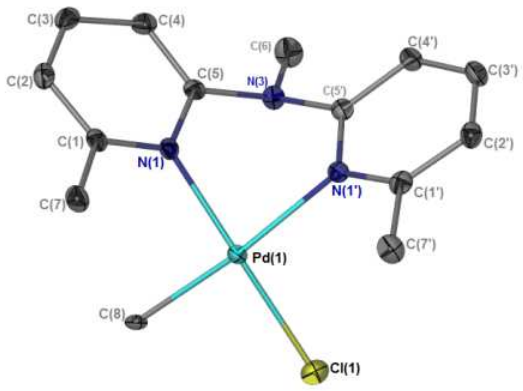

Fig. 2.3 Molecular structure of complex **2e**, drawn at 50 % probability ellipsoids. Hydrogen atoms omitted for clarity.

The geometry around palladium is distorted square planar, with geometric distortion as a result of diimine chelation. The *trans* influence of the *Me*-substituent on palladium is observed in the elongation of the Pd1-N1′ bond (*trans* to carbon) to 2.157 (5) Å in comparison to a value of 2.051 (5) Å for the Pd1-N1 bond (*trans* to chlorine).

Table 2.4 Crystallographic data for complex **2e**.

Complex	**2e**
Empirical Formula	$C_{14}H_{18}ClN_3Pd$
Temperature (K)	100(2)
Wavelength (Å)	0.71073
Crystal System	monoclinic
Space Group	$C_{2/c}$
***a* [Å]**	13.7860(7)
***b* [Å]**	9.6587(5)
***c* [Å]**	22.2882(13)
α [°]	90.00
β [°]	104.5240(10)
γ [°]	90.00
volume [Å^3]	2872.9(3)
Z	8
calc. density [Mg/m^3]	1.712
abs. coeff [mm^{-1}]	1.467
***F*(000)**	1488
crystal dimensions (mm)	0.25 x 0.22 x 0.17
Reflections [Fo > 4(Fo)	3234
Parameters	167
goodness-of-fit on F^2	1.101
Final R indices [I > 2σ/(I)]	R_1 = 0.0259
	wR_2 = 0.0620

Table 2.5 Selected bond lengths (°) and angles (Å) for complex **2e.**

Bond Lengths (Å)			Bond Angles (°)
Pd1-N1′ (*trans* to C)	2.157(6)	N1-Pd1-N1′	83.31(6)
Pd1-N1 (*trans* to Cl)	2.051(2)	N1-Pd1-C8	91.55(8)
Pd1- C8	2.070(2)	N1′-Pd1-Cl1	97.29(2)
Pd1- Cl1	2.321(6)	C8-Pd1-Cl1	87.20(6)
		N1-Pd1-Cl1	174.03(6)
		N1′-Pd1-C8	172.08(6)

The most significant bond lengths and angles are observed in the expected range for these types of complexes.[14]

2.2.3 Synthesis of cationic N-alkyl-dipyridylaldiminato palladium methyl acetonitrile complexes, 2f-2j.

The cationic palladium methyl complexes, **2f-2j**, were obtained by reaction of the neutral complexes with a chloride abstractor, $NaBAr'_4$ [Ar′ = 3,5-bis(trifluoromethyl)phenyl], in the presence of acetonitrile as coordinating solvent (Scheme 2.4).

Scheme 2.4 Synthesis of cationic *N*-alkyl dipyridylaldiminato palladium methyl acetonitrile complexes.

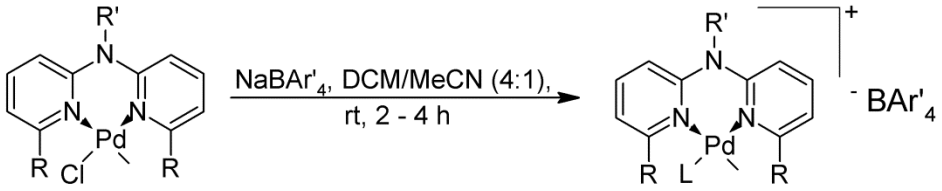

2a: R = H, R' = Me

2b: R = H, R' = benzyl

2c: R = H, R' = methylcyclohexyl

2d: R = H, R' = neopentyl

2e: R = Me, R' = Me

2f: R = H, R' = Me, L = MeCN

2g: R = H, R' = benzyl, L = MeCN

2h: R = H, R' = methylcyclohexyl, L = MeCN

2i: R = H, R' = neopentyl, L = MeCN

2j: R = Me, R' = Me, L = MeCN

The cationic complexes were isolated after work-up as solids in 60-80 % yield and displayed solubility in chlorinated solvents, ethers and were insoluble in alcohols, aromatic solvents and alkanes. The complexes are prone to decomposition to Pd-black as evidenced during the reaction and work-up procedures. In addition, decomposition of the isolated complexes was observed in solution and the solid state. The isolated cationic complexes were characterised by FT-IR spectroscopy, ^{1}H and ^{13}C{^{1}H} NMR spectrocopy, mass spectrometry and elemental analysis.

Table 2.6 Analytical data pertaining to cationic complexes, **2f-2j**.

Complex	M.p. (dec)[a]	FT-IR (cm^{-1}, C=N)[b]	ESI-MS (*m/z*)[c]
2f	97-98	1602, 1581	347
2g	110-111	1602, 1582	423
2h	108-109	1601, 1577	429
2i	117-118	1603, 1584	403
2j	120-121	1603, 1581	375

[a] Reported as uncorrected. [b] Recorded as neat spectra usinga ZnSe ATR accessory. [c] Reported fragment corresponds to the cationic component $[M\text{-}BAr'_4]^+$.

In the FT-IR spectra of the cationic complexes, **2f-2j**, the $\upsilon_{C=N}$ absorption band of the pyridyl rings was shifted to slightly higher wavenumbers in comparison to that of the neutral complexes and were observed in the range 1602-1603 cm^{-1} (Table 2.6), indicative of the formation of cationic species.

The formation of cationic complexes is also evidenced in shifts in their NMR spectra. In the ^{1}H NMR spectra of the complexes, the aromatic resonances of the ligand backbone were shifted to higher field in comparison to those observed for the neutral analogues (Table 2.7 and Fig. 2.4). The pyridyl ring imine resonances (complexes **2f-2i**) were observed in the range δ 8.22-8.27 ppm (for ^{1}H adjacent to MeCN) and δ 8.07-8.18 ppm

(for ^{1}H adjacent to Me).[5a] In addition broad resonances assigned to the BAr′$_4$ counterion were observed at approximately δ 7.70 ppm (*o*-H) and δ 7.50 ppm (*p*-H). In the aliphatic region no significant changes in the proton resonances were observed, indicative of continued coordination of the ligand to the metal centre. The *Me*-resonance of the coordinated acetonitrile molecule was observed in the range δ 2.17-2.34 ppm while a slight downfield shift was observed for the Pd-*Me* resonances in the range δ 0.67-0.94 ppm in comparison to the neutral analogues.

Analogous resonance shifts were observed in the ^{13}C{^{1}H} NMR spectra of the cationic complexes. The pyridyl ring N=*C* resonances were observed in the range δ 150.49-156.77 ppm (C-atom adjacent to MeCN) and δ 148.52-154.79 ppm (C-atom adjacent to Me). The methylene carbon resonance (complex **2g**-**2i**) was observed in the range δ 58.51-64.48 ppm, in the same range as for the neutral complexes. An analogous downfield shift of the Pd-*Me* carbon resonance was observed in the range δ -3.74 to 1.76 ppm, with the most highfield resonance observed for complex **2j** (δ -3.74 ppm).

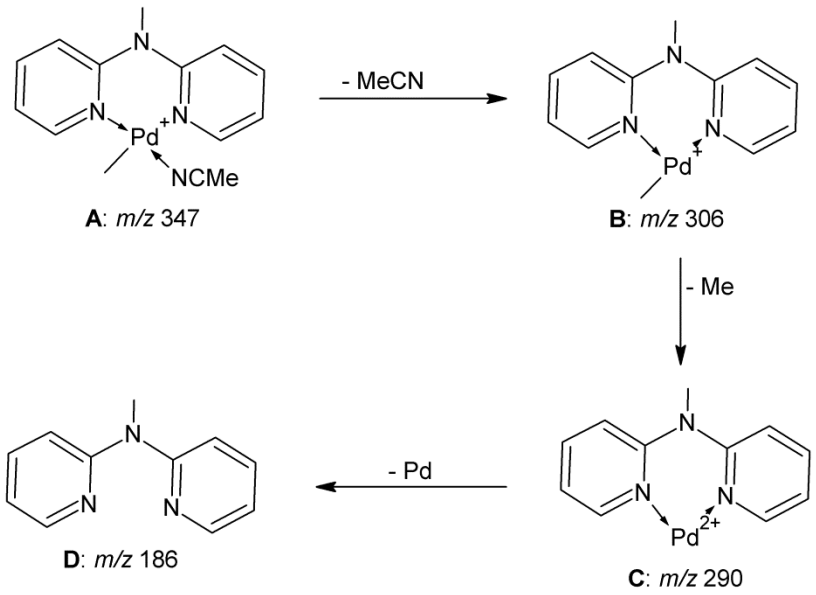

Fig. 2.4 Observed fragmentation pattern of complex **2f**.

Table 2.7 ^{1}H NMR spectral data of the cationic *N*-alkyl dipyridylaldiminato acetonitrile complexes.[a]

Complex	Aromatic Region	Aliphatic Region
2f	δ 8.23 (dd, 1H, $^{3}J_{H\text{-}H}$ 5.72, $^{4}J_{H\text{-}H}$ 1.76, H^{1}); δ 8.10 (dd, 1H, $^{3}J_{H\text{-}H}$ 5.43, $^{4}J_{H\text{-}H}$ 1.17, $H^{1'}$); δ 7.86 (t, 1H, $^{3}J_{H\text{-}H}$ 6.60, H^{3}); δ 7.74 (masked signal, 1H, $H^{3'}$); δ 7.70 (br.s, 8H, H2-BAr′$_4$); δ 7.52 (br.s, 4H, H4-BAr′$_4$); δ 7.12-7.21 (m, 4H, , $H^{2,4,4'}$); δ 6.98 (t, 1H, $^{3}J_{H\text{-}H}$ 6.46, $H^{2'}$)	δ 3.49 (s, 3H, H^{6}); δ 2.26 (s, 3H, C*H*$_3$CN); δ 0.83 (s, 3H, Pd-C*H*$_3$)
2g	δ 8.27 (dd, 1H, $^{3}J_{H\text{-}H}$ 5.86, $^{4}J_{H\text{-}H}$ 1.76, H^{1}); δ 8.18 (dd, 1H, $^{3}J_{H\text{-}H}$ 5.27, $^{4}J_{H\text{-}H}$ 1.76, $H^{1'}$); δ 7.82 (t, 1H, $^{3}J_{H\text{-}H}$ 7.03, H^{3}); δ 7.77 (t, 1H, $^{3}J_{H\text{-}H}$ 7.03, $H^{3'}$); δ 7.72 (br.s, 8H, H2-BAr′$_4$); δ 7.53 (br.s, 4H, H4-BAr′$_4$); δ 7.35 (t, 2H, $^{3}J_{H\text{-}H}$ 8.20, $H^{4,4'}$) δ 7.28 (m, 5H, NCH$_2$*Ph*); δ 7.17 (t, 1H, $^{3}J_{H\text{-}H}$ 6.44, H^{2}); δ 7.09 (t, 1H, $^{3}J_{H\text{-}H}$ 6.45, $H^{2'}$)	δ 5.16 (s, 2H, H^{6}); δ 2.34 (s, 3H, C*H*$_3$CN); δ 0.94 (s, 3H, Pd-C*H*$_3$)
2h	δ 8.23 (dd, 1H, $^{3}J_{H\text{-}H}$ 5.86, $^{4}J_{H\text{-}H}$ 1.56, H^{1}); δ 8.07 (dd, 1H, $^{3}J_{H\text{-}H}$ 5.47, $^{4}J_{H\text{-}H}$ 1.17, $H^{1'}$); δ 7.84 (t, 1H, $^{3}J_{H\text{-}H}$ 6.64, H^{3}); δ 7.73 (masked signal, 1H, $H^{3'}$); δ 7.70 (br.s, 8H, H2-BAr′$_4$); δ 7.51 (br.s, 4H, H4-BAr′$_4$); δ 7.25 (d, 1H, $^{3}J_{H\text{-}H}$ 8.20, H^{4}); δ 7.15-7.20 (m, 2H, $H^{2,4'}$); δ 6.98 (t, 1H, $^{3}J_{H\text{-}H}$ 6.25, $H^{2'}$)	δ 3.73 (d, 2H, $^{3}J_{H\text{-}H}$ 7.03, H^{6}); δ 2.29 (s, 3H, C*H*$_3$CN); δ 2.01 (br. d, 2H, H^{8}); δ 1.72 (m, 2H, $H^{8'}$); δ 1.65 (m, 2H, H^{9}); δ 1.15 (m, 3H, $H^{7,9'}$); δ 1.03 (m, 2H, H^{10}); δ 0.84 (s, 3H, Pd-C*H*$_3$)
2i	δ 8.22 (dd, 1H, $^{3}J_{H\text{-}H}$ 5.87, $^{4}J_{H\text{-}H}$ 1.32, H^{1}); δ 8.07 (dd, 1H, $^{3}J_{H\text{-}H}$ 5.43, $^{4}J_{H\text{-}H}$ 1.17, $H^{1'}$); δ 7.82 (t, 1H, $^{3}J_{H\text{-}H}$ 6.46, H^{3}); δ 7.70 (br.s, 8H, H2-BAr′$_4$); δ 7.67 (masked signal, 1H, $H^{3'}$); δ 7.51 (br.s, 4H, H4-BAr′$_4$); δ 7.35-7.41 (m, 2H, $H^{4,4'}$); δ 7.15 (t, 1H, $^{3}J_{H\text{-}H}$ 6.02, H^{2}); δ 6.97 (t, 1H, $^{3}J_{H\text{-}H}$ 6.31, $H^{2'}$)	δ 3.87-3.95 (br. m, 2H, H^{6}); δ 2.28 (s, 3H, C*H*$_3$CN); δ 0.97 (s, 9H, H^{8}); δ 0.88 (s, 3H, Pd-C*H*$_3$)
2j	δ 7.74 (br. s, 8H, H2-BAr′$_4$); δ 7.67 (t, 1H, $^{3}J_{H\text{-}H}$ 8.07 Hz, H^{3}); δ 7.60 (t, 1H, $^{3}J_{H\text{-}H}$ 7.92 Hz, $H^{3'}$); δ 7.53 (br. s, 4H, H4-BAr′$_4$); δ 7.10 (d, 1H, $^{3}J_{H\text{-}H}$ 7.40 Hz, H^{4}); δ 6.98 (m, 3H, $H^{4';2,2'}$)	δ 3.52 (s, 3H, H^{6}); δ 2.85 (s, 3H, H^{7}); δ 2.69 (s, 3H, $H^{7'}$); δ 2.17 (s, 3H, C*H*$_3$CN); δ 0.67 (s, 3H, Pd-C*H*$_3$)

[a] Spectra recorded in $CDCl_3$ at 25 °C. Chemical shifts reported as δ ppm values, referenced relative to residual proton signals of the solvent. Coupling constant values in Hz.

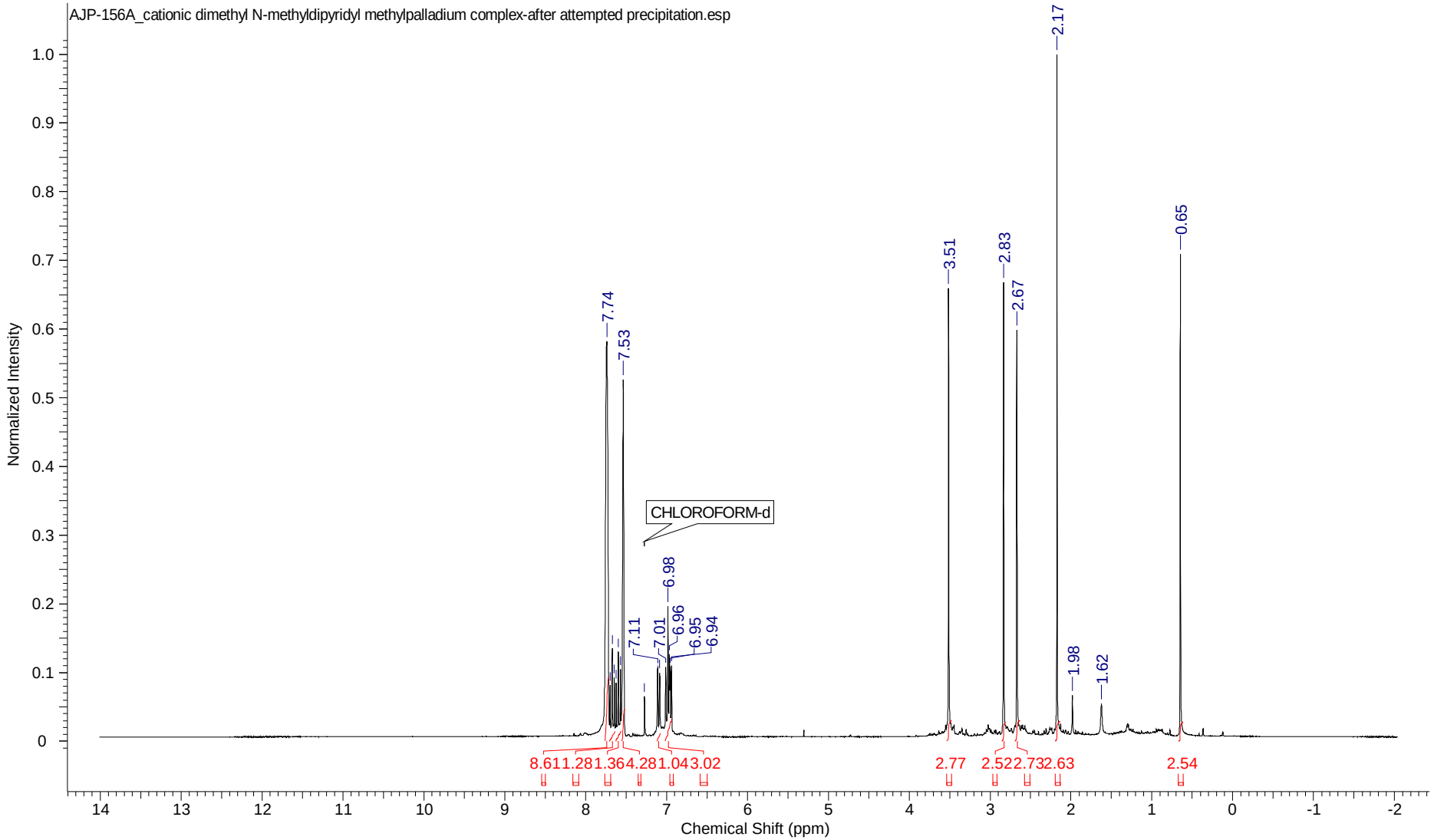

Fig. 2.5 ^{1}H NMR spectrum of cationic complex **2f** recorded in $CDCl_3$ at 25 °C.

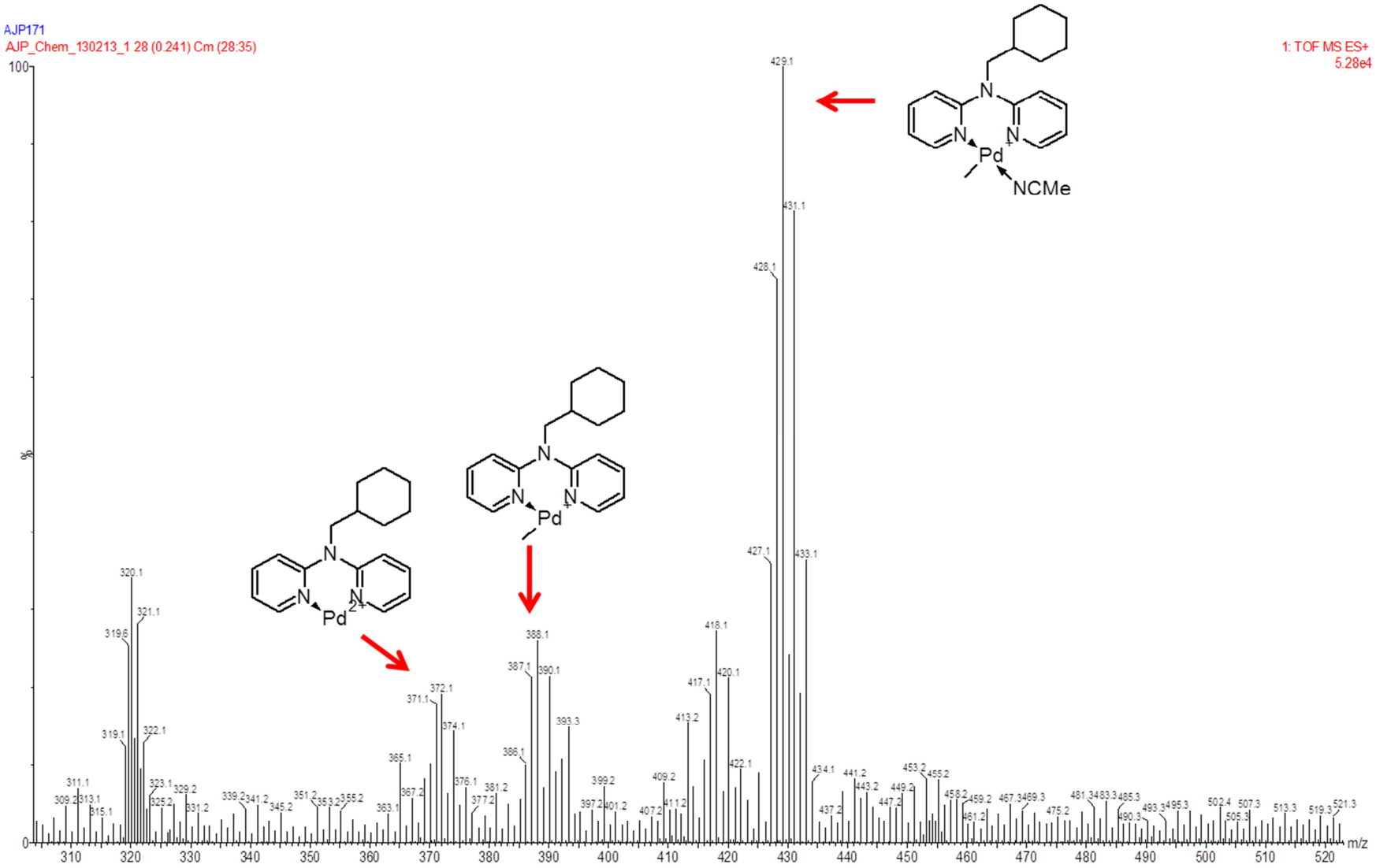

Fig. 2.6 ESI-MS spectrum of cationic complex **2j** recorded in acetonitrile.

The major fragment observed in the ESI-MS spectrum of complexes **2f-2j** corresponds to the cationic portion of the complex (Table 2.6 and Fig. 2.4). The observed fragmentation pattern for a representative example (complex **2f**) is shown in Figure 2.6. The complexes undergo sequential loss of coordinated acetonitrile and the methyl group to generate species **C**, followed by loss of palladium to generate the free ligand, species **D**.

2.2.4 Synthesis of cationic N-alkyl dipyridylaldiminato palladium methyl pyridine complexes, 2k-2o.

Following the observation that the cationic acetonitrile-ligated palladium methyl complexes undergo decomposition in the solid state and solution, an attempt was made to prepare more stable analogues. It was envisaged that an increase in the basicity of the coordinating ligand would enhance the stability of the electrophilic cationic metal centre and prevent the observed decomposition.

Scheme 2.5 Synthesis of cationic *N*-alkyl dipyridylaldiminato methylpalladium pyridine adducts.

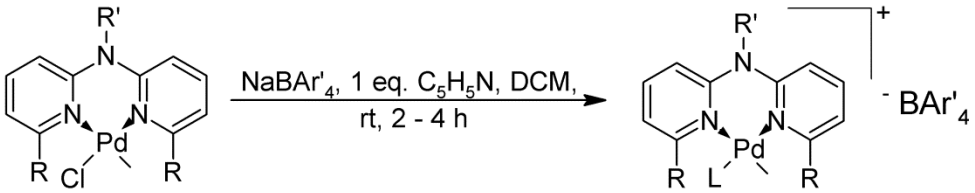

2a: R = H, R' = Me

2b: R = H, R' = benzyl

2c: R = H, R' = methylcyclohexyl

2d: R = H, R' = neopentyl

2e: R = Me, R' = Me

2k: R = H, R' = Me, L = C_5H_5N

2l: R = H, R' = benzyl, L = C_5H_5N

2m: R = H, R' = methylcyclohexyl, L = C_5H_5N

2n: R = H, R' = neopentyl, L = C_5H_5N

2o: R = Me, R' = Me, L = C_5H_5N

To this end, we reacted the neutral complexes, **2a-2e**, with $NaBAr'_4$ in the presence of pyridine (Scheme 2.5). The cationic pyridine analogues, **2k-2o**, were isolated after work-up

and recrystallisation from chloroform/pentane as off-white air- and moisture-stable crystalline solids in high yields. The isolated complexes displayed solubility in polar organic solvents and were insoluble in alkanes.

In the FT-IR spectra of the complexes, the $\upsilon_{C=N}$ absorption bands of the *N*-alkyl dipyridylamine ligands was observed in the range 1600-1604 cm^{-1} (Table 2.8), analogous to that observed for the cationic acetonitrile complexes and thereby confirming formation of the cationic complex.

In the ^{1}H NMR spectra of the complexes, the resonances were observed in the same region as for the acetonitrile analogues (Table 2.9). In the aromatic region, the pyridyl ring imine protons of the ligand scaffold (for complex **2k** to **2n**) were observed in the range δ 8.32-8.35 ppm (proton adjacent to pyridine) and δ 7.45-7.51 ppm (proton adjacent to methyl), integrating for a single proton.

Table 2.8 Analytical data pertaining to cationic complexes, **2k-2o**.

Complex	M.p. (dec)[a]	FT-IR (cm^{-1}, C=N)[b]	ESI-MS (*m/z*)
2k	131-132	1602, 1580	347[c]
2l	152-153	1601, 1576	423[c]
2m	156-157	1601, 1578	429[c]
2n	161-162	1601, 1571	403[c]
2o	179-180	1604, 1581	413[d]

[a] Reported as uncorrected. [b] Recorded as neat spectra on a ZnSe ATR accessory. [c] Reported fragment corresponds to cationic component [M-C_5H_5N+MeCN-B*Ar′*$_4$]. [d] Reported fragment corresponds to the cationic component [M-B*Ar′*$_4$]$^+$.

The B*Ar′*$_4$ proton resonances were observed as two broad singlets integrating for 8 (*o*-protons) and 4 (*p*-protons) protons at δ 7.71 and δ 7.51/7.50 ppm respectively. In the

aliphatic region the methylene protons bound to nitrogen were observed as a singlet (in the case of complex **2l** and **2m**) and as a doublet (in the case of complex **2n**) and integrated for two protons each. The proton resonances of the methyl group bound to palladium was observed as a singlet in the range δ 0.54-0.81 ppm, integrating for three protons each (Fig. 2.7).

Analogous resonances to that observed in the $^{13}C\{^{1}H\}$ NMR spectra of the acetonitrile analogues was observed in the $^{13}C\{^{1}H\}$ NMR spectra of the cationic pyridine complexes. The pyridyl ring N=*C* resonances was observed in the range δ 147.08-156.66 ppm (C-atom adjacent to pyridine) and δ 147.03-150.57 ppm (C-atom adjacent to Me).

The methylene carbon resonance (complex **2l**, **2m** and **2n**) was observed in the range δ 55.35-61.64 ppm, which resembles that for the acetonitrile analogues.

An analogous downfield shift of the Pd-*Me* carbon resonance was observed in the range δ -1.38 to 3.19 ppm, with the most highfield resonance observed for complex **2o** (-1.38 ppm).

Analysis of the complexes by ESI-MS (Table 2.8 and Fig. 2.8) in acetonitrile showed isotope clusters corresponding to the species in Scheme 2.6. The pyridine complex undergoes ligand exchange with acetonitrile to form the corresponding acetonitrile adduct, followed by protonation and elimination of methane to form the two-coordinate $[(N\text{-}N)Pd]^{2+}$ species.

The structure of complex **2o** was unambiguously determined by SCD analysis, with selected crystallographic data (Table 2.10) and metric parameters (Table 2.11) tabulated.

Table 2.9 ^{1}H NMR spectral data of the cationic *N*-alkyl dipyridylaldiminato pyridine complexes.[a]

Complex	Aromatic Region	Aliphatic Region
2k	δ 8.50 (d, 2H, $^{3}J_{H\text{-}H}$ 6.31, H_{py}); δ 8.35 (d, 1H, $^{3}J_{H\text{-}H}$ 5.72, H^{1}); δ 7.84 (m, 2H, $H^{3,3'}$); δ 7.71 (br. s, 8H, H-2, BAr′$_4$); δ 7.51 (br. s, 4H, H-4, BAr′$_4$); δ 7.45 (d, 1H, $^{3}J_{H\text{-}H}$ 5.58, $H^{1'}$); δ 7.40 (m, 2H, H_{py}); δ 7.20 (d, 2H, $^{3}J_{H\text{-}H}$ 7.78, $H^{4,4'}$); δ 7.18 (m, 2H, $H^{1,py}$); δ 6.86 (t, 1H, $^{3}J_{H\text{-}H}$ 6.46, $H^{2'}$)	δ 3.55 (s, 3H, H^{6}); δ 0.72 (2, 3H, Pd-CH_3)
2l	δ 8.42 (d, 2H, $^{3}J_{H\text{-}H}$ 6.31, H_{py}); δ 8.35 (d, 1H, $^{3}J_{H\text{-}H}$ 5.72, H^{1}); δ 7.83 (m, 2H, $H^{3,3'}$); δ 7.71 (br. s, 8H, H-2, BAr′$_4$); δ 7.64 (t, 1H, $^{3}J_{H\text{-}H}$ 7.34, H_{py}); δ 7.59 (d, 1H, $^{3}J_{H\text{-}H}$ 5.58, $H^{1'}$); δ 7.50 (br. s, 4H, H-4, BAr′$_4$); δ 7.36 (m, 5H, $H^{8,8',9,9',10}$); δ 7.25 (m, 4H, $H^{4,4',py}$); δ 7.18 (t, 1H, $^{3}J_{H\text{-}H}$ 7.04, H^{2}); δ 6.82 (t, 1H, $^{3}J_{H\text{-}H}$ 7.34, $H^{2'}$)	δ 5.19 (s, 2H, H^{6}); δ 0.81 (s, 3H, Pd-CH_3)
2m	δ 8.47 (d, 2H, $^{3}J_{H\text{-}H}$ 6.31, H_{py}); δ 8.32 (d, 1H, $^{3}J_{H\text{-}H}$ 5.72, H^{1}); δ 7.82 (m, 2H, $H^{3,3'}$); δ 7.71 (br. s, 8H, H-2, BAr′$_4$); δ 7.64 (t, 1H, $^{3}J_{H\text{-}H}$ 7.48, H_{py}); δ 7.51 (br. s, 4H, H-4, BAr′$_4$); δ 7.49 (masked signal, 1H, $H^{1'}$); δ 7.39 (m, 2H, H_{py}); δ 7.26 (d, 1H, $^{3}J_{H\text{-}H}$ 8.07, H^{4}); δ 7.22 (d, 1H, $^{3}J_{H\text{-}H}$ 8.36, $H^{4'}$); δ 7.17 (t, 1H, $^{3}J_{H\text{-}H}$ 7.04, H^{2}); δ 6.84 (t, 1H, $^{3}J_{H\text{-}H}$ 7.19, $H^{2'}$)	δ 3.80 (br. s, 2H, H^{6}); δ 2.18 (br. d, 2H, H^{8}); δ 1.76 (br. s, 2H, $H^{8'}$); δ 1.68 (br. s, 2H, H^{9}); δ 1.18 (m, 5H, $H^{7,9',10}$); δ 0.73 (s, 3H, Pd-CH_3)
2n	δ 8.50 (d, 2H, $^{3}J_{H\text{-}H}$ 6.46, H_{py}); δ 8.34 (d, 1H, $^{3}J_{H\text{-}H}$ 5.72, H^{1}); δ 7.85 (m, 2H, $H^{3,3'}$); δ 7.71 (br. s, 8H, H-2, BAr′$_4$); δ 7.65 (t, 1H, $^{3}J_{H\text{-}H}$ 7.34, H_{py}); δ 7.50 (br. s, 4H, H-4, BAr′$_4$); δ 7.46 (d, 1H, $^{3}J_{H\text{-}H}$ 5.58, $H^{1'}$); δ 7.41 (m, 4H, $H^{4,4',py}$); δ 7.17 (t, 1H, $^{3}J_{H\text{-}H}$ 7.19, H^{2}); δ 6.83 (t, 1H, $^{3}J_{H\text{-}H}$ 7.19, $H^{2'}$)	δ 3.96 (br. d, 2H, H^{6}); δ 1.07 (s, 9H, H^{8}); δ 0.78 (s, 3H, Pd-CH_3)
2o	δ 8.27 (d, 2H, $^{3}J_{H\text{-}H}$ 5.27, H_{py}); δ 7.81 (t, 1H, $^{3}J_{H\text{-}H}$ 7.62, H_{py}); δ 7.74 (t, 1H, $^{3}J_{H\text{-}H}$ 8.20, H^{3}); δ 7.69 (br. s, 8H, H-2, BAr′$_4$); δ 7.66 (t, 1H, $^{3}J_{H\text{-}H}$ 8.20, $H^{3'}$); δ 7.50 (br. s, 4H, H-4, BAr′$_4$); δ 7.32 (t, 2H, $^{3}J_{H\text{-}H}$ 7.62, $H^{4,4'}$); δ 7.15 (d, 1H, $^{3}J_{H\text{-}H}$ 7.62, H^{2}); δ 7.05 (d, 2H, $^{3}J_{H\text{-}H}$ 8.20, H_{py}); δ 6.87 (d, 1H, $^{3}J_{H\text{-}H}$ 7.62, $H^{2'}$)	δ 3.62 (s, 3H, H^{6}); δ 2.95 (s, 3H, H^{7}); δ 2.12 (s, 3H, $H^{7'}$); δ 0.54 (s, 3H, Pd-CH_3)

[a] Spectra recorded in $CDCl_3$ at 25 °C. Chemical shifts reported as δ ppm values, referenced relative to residual proton signals of the solvent. Coupling constant values in Hz.

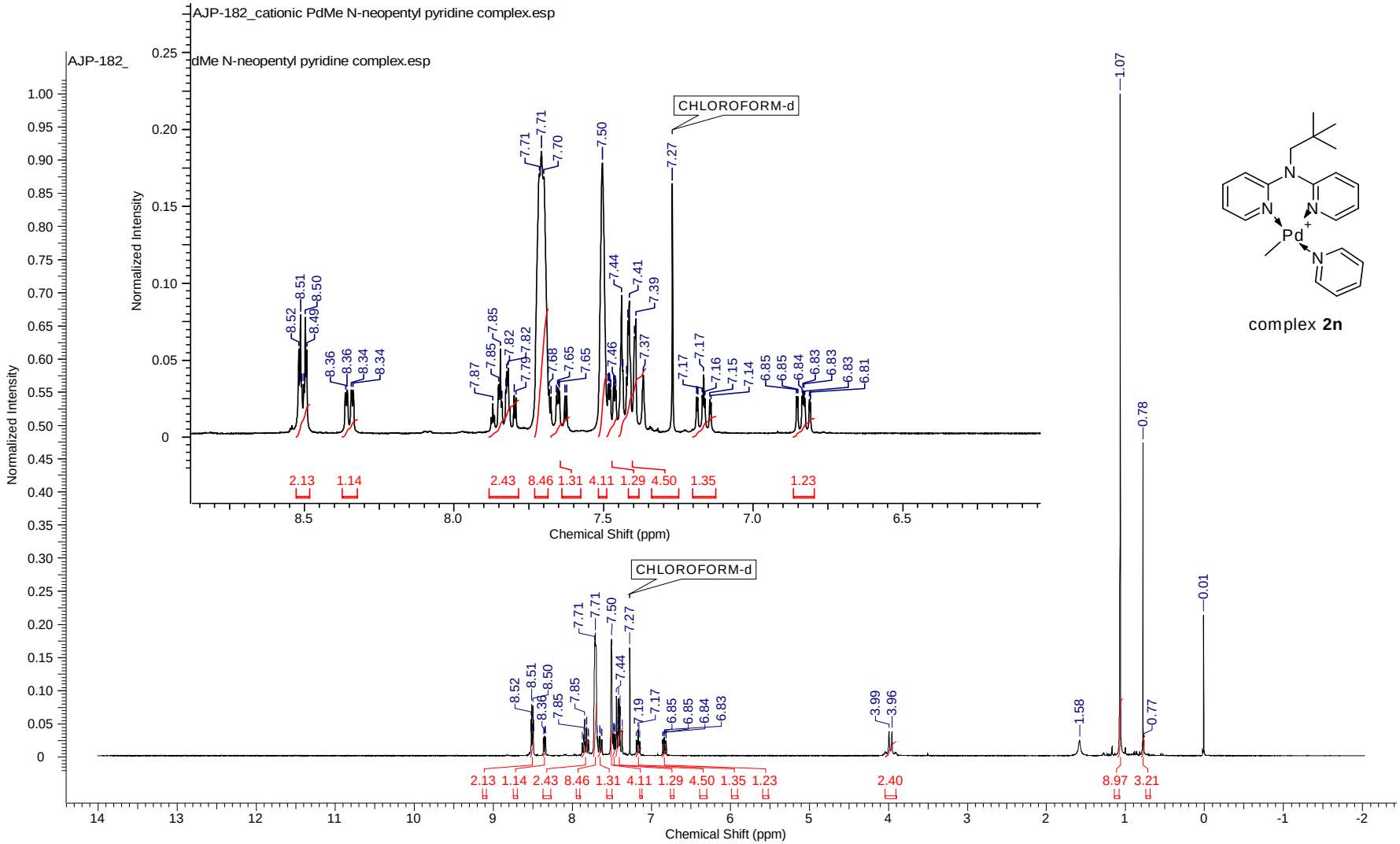

Fig. 2.7 ^{1}H NMR spectrum of cationic complex **2n** recorded in $CDCl_3$ at 25 °C.

Fig. 2.8 ESI-MS spectrum of cationic complex **2o** recorded in acetonitrile at 25 °C.

The molecular structure of the complex shows a dissociated ion-pair (Pd-B bond distance: 8.095 Å), with the cationic fragment in which the coordination sphere of the metal is occupied by the neutral *N*-alkyl dipyridylaldimine ligand and the anionic Me-group. The vacant coordination site is occupied by a pyridine molecule (Fig. 2.9).

Scheme 2.6 Observed fragmentation pattern in the ESI-MS spectra of the cationic pyridine adducts.

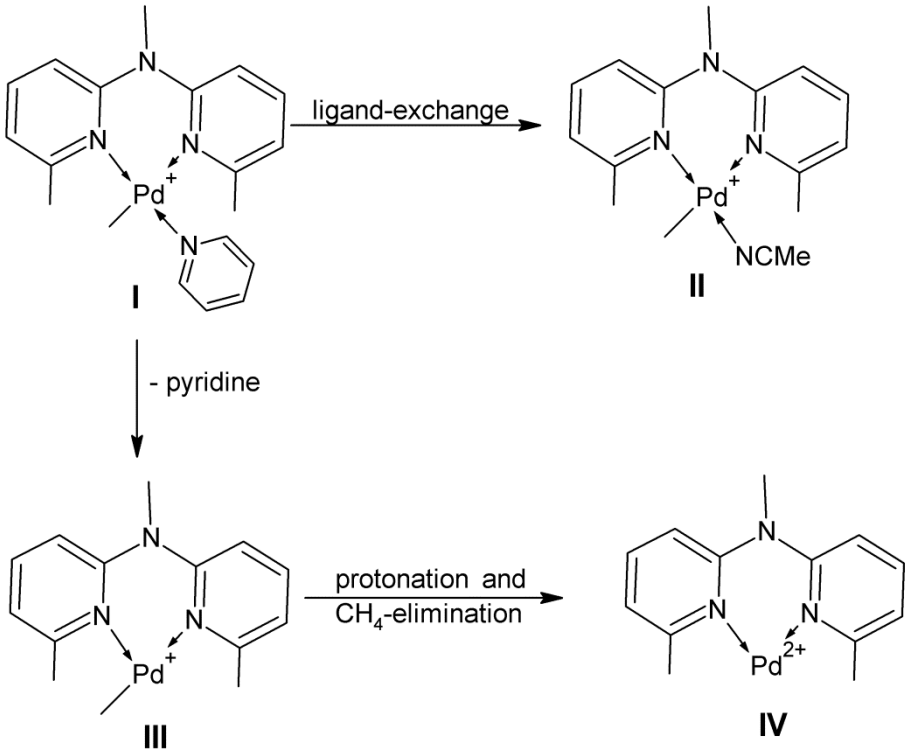

The geometry around the palladium centre is distorted square planar, with the largest deviation observed in the N1-Pd1-N1′ angle (83.41 °) as a result of complexation. The Pd1-N1 and Pd1-N8 bond lengths are 2.032 (2) and 2.034 (2) Å respectively, and are within the range observed for analogous complexes.[15] The Pd-N1′ bond length of 2.133 (2) Å is slightly longer than expected as a result of the *trans*-effect of the Me-group. The Pd-Me bond distance of 2.048 (2) Å is within the range previously reported for analogous complexes.[16] The anion consists of the four-coordinate B*Ar′*$_4$ anion with the B-coordination sphere occupied by four 3,5-bis(trifluoromethyl)phenyl groups.

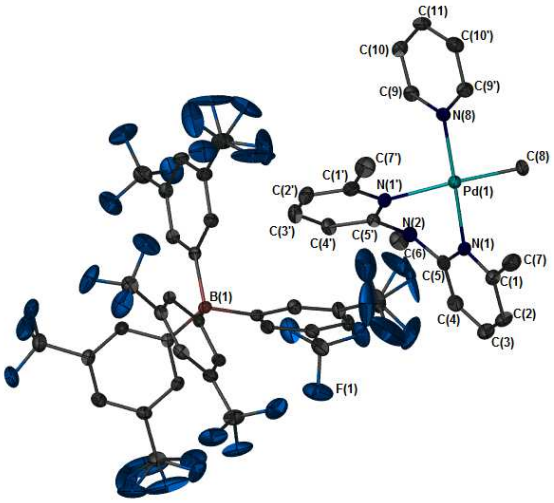

Fig. 2.9 Molecular structure of complex **2o**, drawn at 50 % probability ellipsoids. Hydrogen atoms omitted for clarity.

Table 2.10 Crystallographic data for complex **2o**.

Complex	**2o-A**
Empirical Formula	$C_{51}H_{35}BF_{24}N_4Pd$
Temperature (K)	150(2)
Wavelength (Å)	0.71073
Crystal System	monoclinic
Space Group	$P2_{1/n}$
***a* [Å]**	14.740(18)
***b* [Å]**	16.231(2)
***c* [Å]**	22.091(3)
α [°]	90.00
β [°]	98.847(2)
γ [°]	90.00
volume [Å^3]	5222.30(11)
Z	1
calc. density [Mg/m^3]	0.406
abs. coeff [mm^{-1}]	0.120
***F*(000)**	636
crystal dimensions (mm)	0.35 x 0.30 x 0.27
Reflections [Fo > 4(Fo)	12138
Parameters	818
goodness-of-fit on F^2	1.045
Final R indices [I > 2σ/(I)]	R_1 = 0.0419
	wR_2 = 0.1018

Table 2.11 Selected bond lengths (°) and angles (Å) for complex **2o.**

Bond Lengths (Å)			Bond Angles (°)
Pd1-N1	2.032(2)	N1-Pd1-N1′	83.41(8)
Pd1-N1′	2.133(1)	N1-Pd1-N8	175.80(8)
Pd1-N8	2.034(2)	N1-Pd1-C8	92.13(9)
Pd1-C8	2.048(1)	N1′-Pd1-N8	95.32(8)
		N1′-Pd1-C8	170.95(10)

The three fluorine atoms on C16, C18A and C18C shows positional disorder with each fluorine atom of the group occupying two positions within the crystal lattice as a result of rotational motion about the C_{Ph}-C_{CF3} bond.

2.2.4.1 Importance of coordinating solvent:neutral complex ratio in synthesis.

During the synthesis of the cationic pyridine analogues, **2k-2o**, it was observed that the ratio of pyridine to complex had a significant effect on the product formed. Figure 2.8 shows an ^{1}H NMR spectrum of the material isolated during attempted synthesis of complex **2o**, in which pyridine as coordinating solvent was added in excess (4:1 dichloromethane:pyridine, Scheme 2.7).

Scheme 2.7 Effect of pyridine on the reaction products obtained.

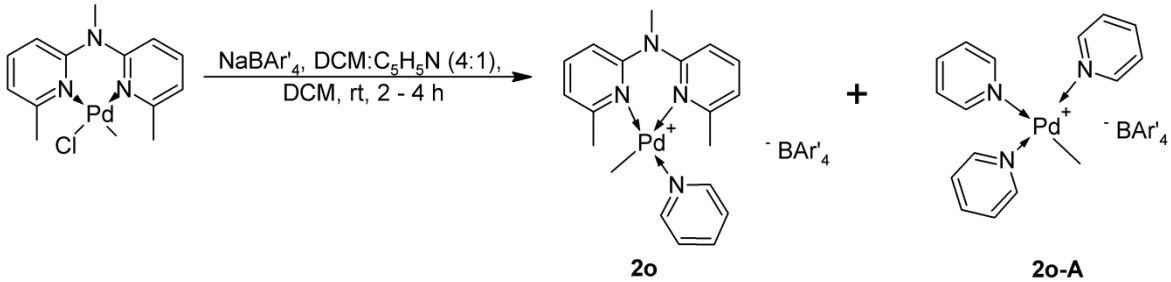

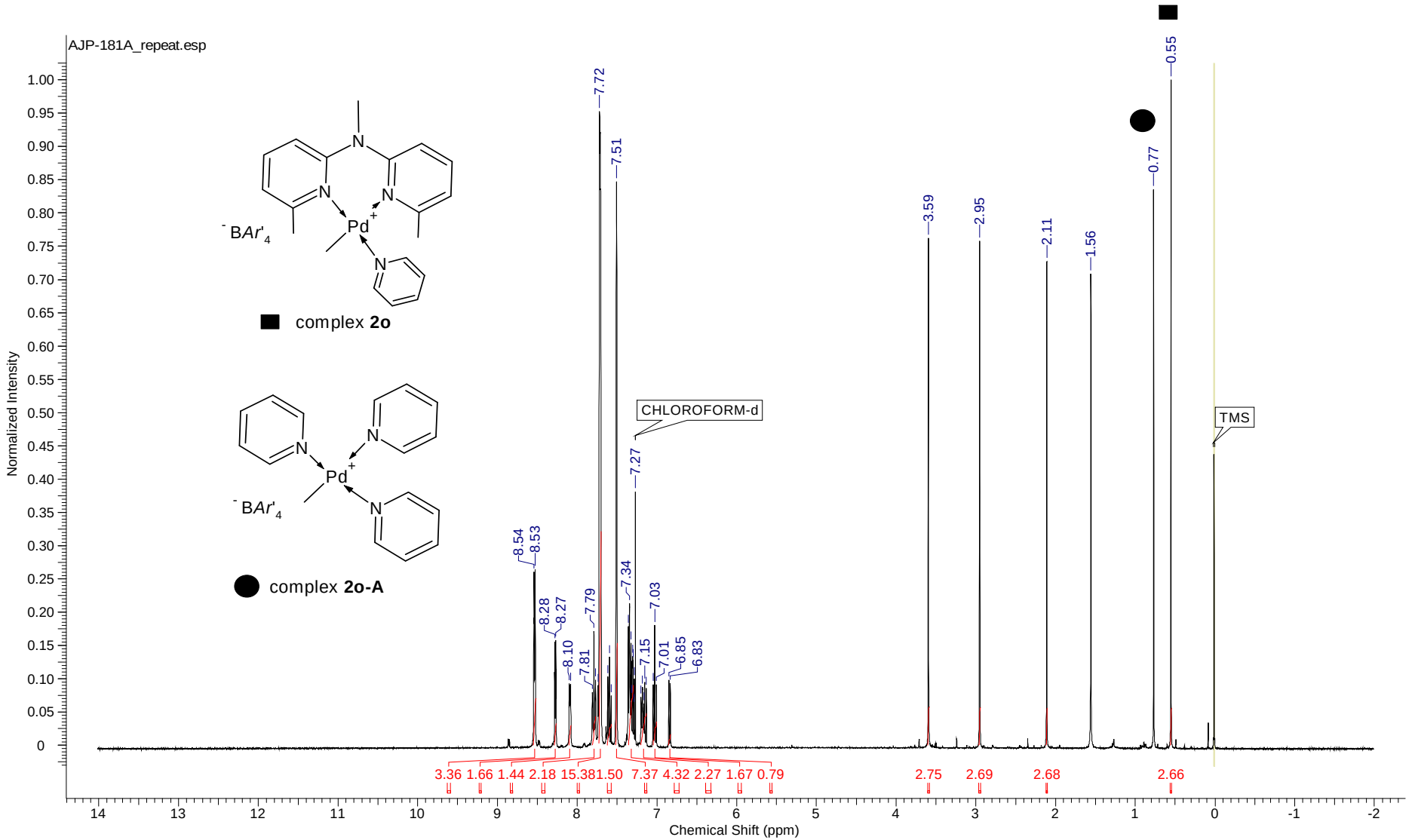

Fig. 2.10 ^{1}H NMR spectrum of the two cationic complexes **2o** and **2o-A** isolated, with key methyl resonance annotated. Spectrum recorded in $CDCl_3$ at 25 °C.

The observed proton resonances showed the formation of two products in approximately 1:1 ratio identified as the desired complex **2o** and a new complex **2o-A** (Fig. 2.10, key methyl resonance annotated).

The structure of complex **2o-A** was established by SCD analysis on crystals grown by diffusion of pentane into a solution of the isolated material in dichloromethane (Fig. 2.11). Selected metric parameters (Table 2.12) and crystallographic data (Table 2.13) are tabulated.

The molecular structure shows a cation-ion pair with the cation consisting of a slightly distorted square planar palladium(II) centre in which the coordination sphere is occupied by three neutral pyridine ligands and an anionic methyl group. The ion-pair is effectively dissociated as evidenced by the large Pd-B bond distance of 13.639 Å.

The anion consists of the four-coordinate BAr'_4 anion with the B-coordination sphere occupied by four 3,5-bis(trifluoromethyl)phenyl groups.

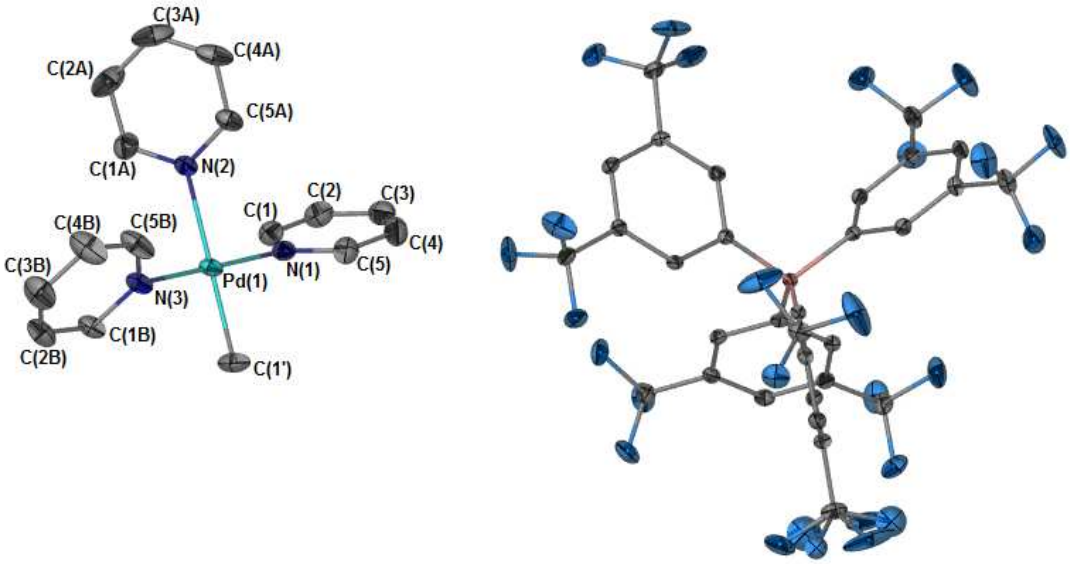

Fig. 2.11 Molecular structure of complex **2o-A**, drawn at 50 % probability ellipsoids. Hydrogen atoms omitted for clarity.

Table 2.12 Selected bond lengths (°) and angles (Å) for complex **2o-A.**

Bond Lengths (Å)			Bond Angles (°)
Pd1-N1	2.028(2)	N1-Pd1-N2	89.85(6)
Pd1-N2 (*trans* to Cl)	2.160(1)	N1-Pd1-N3	178.34(6)
Pd1-N3	2.030(2)	N1-Pd1-C1′	89.92(7)
Pd1-C1′	2.015(1)	N2-Pd1-C1′	179.34(7)
		N2-Pd1-N3	89.80(6)
		N3-Pd1-C1′	90.45(8)

Table 2.13 Crystallographic data for complex **2o-A**.

Complex	**2o-A**
Empirical Formula	$C_{48}H_{30}BF_{24}N_3Pd$
Temperature (K)	100(2)
Wavelength (Å)	0.71073
Crystal System	triclinic
Space Group	P-1
***a* [Å]**	13.021(3)
***b* [Å]**	13.101(3)
***c* [Å]**	16.199(4)
α [°]	84.145(4)
β [°]	87.023(4)
γ [°]	62.217(3)
volume [Å^3]	2432.01
Z	2
calc. density [Mg/m^3]	1.668
abs. coeff [mm^{-1}]	1.467
***F*(000)**	1212
crystal dimensions (mm)	0.41 x 0.49 x 0.57
Reflections [Fo > 4(Fo)	11198
Parameters	708
goodness-of-fit on F^2	1.029
Final R indices [I > 2σ/(I)]	R_1 = 0.0271
	wR_2 = 0.0641

The three fluorine atoms on C33B shows positional disorder with each fluorine atom of the group occupying two positions within the crystal lattice.

The Pd-N (pyridine) bond distances are 2.028(2) Å (Pd-N1); 2.160(1) Å (Pd-N2) and 2.030(2) Å (Pd-N3), with the Pd-N2 bond distance elongated due to the *trans* influence of the Me-group. The Pd-Me bond distance is 2.015(2) Å with both Pd-N and Pd-Me bond distances in the range previously observed for analogous Pd(II) complexes.[17]

Piers and co-workers made a similar observation during their attempted preparation of palladium complexes derived from aryltrifluoroborate-phosphine ligands with pyridine derivatives as coordinating solvents.[18] They found that reaction of the palladium precursor with the potentially bidentate trifluoroborate phosphine ligand in the presence of pyridine generated exclusively complexes of the type shown in Scheme 2.8, in which the coordination sphere of palladium is occupied by two pyridine molecules, the phosphine moiety of the ligand and the Me-group initially present in the precursor.

Scheme 2.8 Example of multiple pyridine-substitution during attempted during the preparation of cationic palladium complexes.[18]

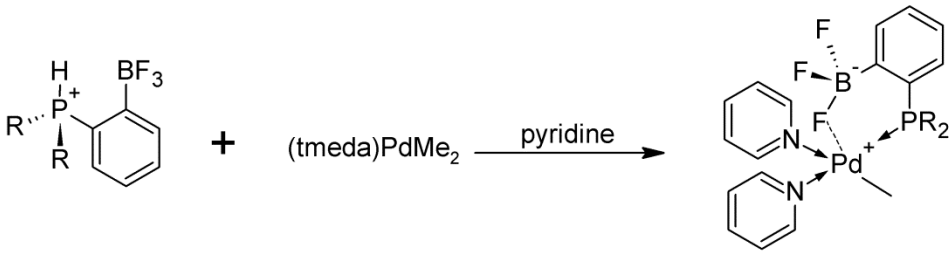

2.3 Conclusions

A series of *N*-alkyl-2,2′-dipyridylamine ligands and their neutral and cationic palladium methyl complexes were synthesised and characterised. In an attempt to prepare inherently more stable cationic complexes, pyridine was employed as coordinating solvent. It

was found that the ratio of pyridine to neutral metal complex had a significant effect on the product isolated. An excess of pyridine in the reaction mixture resulted in the isolation of a mixture of complexes with the cationic fragments, $[PdMe(N\text{-}N)(C_5H_5N)]^+$ and $[PdMe(C_5H_5N)_3]^+$, in a near 1:1 ratio. The structure of the tris(pyridine) analogue was unambiguously confirmed by SCD analysis.

2.4 Experimental Section

All transformations were performed using standard Schlenk techniques under a nitrogen atmosphere. Solvents were dried by refluxing over the appropriate drying agents followed by distillation prior to use and all other reagents were employed as obtained. NMR (^{1}H: 300 and 400 MHz; ^{13}C: 75 and 100 MHz) spectra were recorded on Varian VNMRS 300 MHz; Varian Unity Inova 400 MHz spectrometers and chemical shifts were reported in ppm, referenced to the residual protons of the deuterated solvents and tetramethyl silane (TMS) as internal standard. ESI-MS (positive and negative mode) analyses were performed on Waters API Quattro Micro and Waters API Q-TOF Ultima instruments by direct injection of sample. FT-IR analysis was performed on a Thermo Nicolet AVATAR 330 instrument, and spectra were recorded neat (ATR) unless otherwise specified. Melting point determinations were performed on a Stuart Scientific SMP3 melting point apparatus and are reported as uncorrected. $[(COD)PdCl_2]$ and [(COD)PdMe(Cl)] were prepared according to literature procedures.[9]

2.4.1 Synthesis of N-alkyl-2,2′-dipyridylamine ligands, 1a-1e.

2.4.1.1 2,2′-dipyridyl-N-methylamine (1a)

To a stirring slurry of KOH (786 mg, 14.018 mmol) in DMSO (10 ml) was added solid 2,2′-dipyridylamine (600 mg, 3.504 mmol). The reaction mixture was stirred for 45 min after which iodomethane (497 mg, 3.504 mmol) was added neat. The reaction mixture was stirred at room temperature for 20 h. After the allotted time the reaction mixture was quenched with water (50 ml) and the aqueous layer extracted with EtOAc (3 x 100 ml portions). The organic layer was separated, dried over $MgSO_4$ and the solvent removed *in vacuo*. The orange-brown crude oil was purified by flash chromatography employing EtOAc: Hexane (9:1) as eluent. The pure product was obtained as a yellow oil. Yield: 582 mg, 89 %. FT-IR (ATR, neat, ν): 1580 and 1557 cm^{-1} (C=N). Other spectral data in-text.

2.4.1.2 2,2′-dipyridyl-N-benzylamine (1b)

The same synthetic procedure as outlined above (**1a**) was employed for the synthesis of **1b**, using benzyl chloride as reagent. The product was isolated as a bright-yellow crystalline solid after recrystallisation from hexane. Yield: 755 mg, 82 %. FT-IR (ATR, neat, ν): 1581 and 1561 cm^{-1} (C=N). Other spectral data in-text.

2.4.1.3 2,2′-dipyridyl-N-methylcyclohexylamine (1c)

The same synthetic procedure as outlined above (**1a**) was employed for the synthesis of **1c**, using (bromomethyl)cyclohexane as reagent. The product was isolated as an orange oil after purification by flash chromatography (EtOAc: Hexane 1:4). Yield: 823 mg, 88 %. FT-IR (ATR, neat, ν): 1580 and 1558 cm^{-1}. $^{13}C\{^1H\}$ (75.38 MHz, $CDCl_3$): δ 158.05 (C^5); δ 148.17 (C^1); 136.95 (C^3); δ 116.73 (C^2); δ 114.86 (C^4); δ 54.18 (C^6); δ 37.24 (C^7); δ 30.98

($C^{8,8'}$); δ 26.54 (C^{10}); δ 26.00 ($C^{9,9'}$). ESI-MS: *m/z* 268.2 $[M+H]^+$. Elemental analysis: % Found (% calc.) for $C_{17}H_{21}N_3$: C: 76.01 (76.37); H: 7.80 (7.92); N: 15.38 (15.72).

2.4.1.4 2,2´-dipyridyl-N-neopentylamine (1d)

The same synthetic procedure as outlined above (**1a**) was employed for the synthesis of **1d**, using (bromomethyl)cyclohexane as reagent. The product was isolated as a colourless oil after purification by flash chromatography (EtOAc: Hexane 1:4). Yield: 823 mg, 88 %. FT-IR (ATR, neat, ν): 1581 and 1559 cm^{-1}. Other spectral data in-text.

2.4.1.5 (6,6´-dimethyl-2,2´-dipyridyl)-N-methylamine (1e)

To a stirring solution of 2-bromo-6-methylpyridine (499 mg, 2.9 mmol) and 2-amino-6-methylpyridine (345 mg, 3.19 mmol) in anhydrous PhMe (45 ml) was added $Pd_2(dba)_3$ (133 mg, 0.145 mmol), *rac*-BINAP (68 mg, 0.110 mmol) and KO*t*Bu (531 mg, 4.73 mmol) in rapid succession. The reaction mixture was heated for 15 h while stirring at 90 °C. After the allotted time the reaction mixture was quenched with EtOH (15 ml), filtered through celite and the solvent removed *in vacuo*. The crude product amine was isolated as a brown oil and was sufficiently pure (determined by ^1H NMR spectroscopy) and employed directly in the methylation step. The same synthetic procedure as outlined above (**1a**) was employed for the synthesis of **1e** using 6-methyl-N-(6-methylpyridin-2-yl)pyridin-2-amine as starting amine and iodomethane as reagent. The product was isolated as a yellow oil after purification by flash chromatography employing pentane as eluent. Yield: 289 mg, 46 % overall. FT-IR (ATR, neat, ν): 1591 and 1568 cm^{-1}. $^{13}C\{^1H\}$ (75.38 MHz, $CDCl_3$): δ 157.45 (C^5); δ 157.00 (C^1); δ 137.13 (C^3); δ 115.83 (C^2); δ 111.10 (C^4); δ 35.84 (C^6); δ 24.43 (C^7).

ESI-MS (*m/z*): 214 $[M + H]^+$. Elemental analysis: % Found (% calc.) for $C_{12}H_{15}N_3$: C: 73.13 (73.21); H: 6.84 (7.09); N: 19.58 (19.70).

2.4.2 Synthesis of neutral N-alkyl dipyridylaldiminato methylpalladium complexes, 2a-2e.

2.4.2.1 [PdMe(2,2´-dipyridyl-N-methylamine)Cl] (2a)

To a stirring solution of (COD)PdMeCl (416 mg, 1.571 mmol) in dichloromethane was added ligand **1a** (291 mg, 1.751 mmol). The reaction mixture was stirred at room temperature for 16 h. After the allotted time the reaction mixture was filtered through celite, solvent volume reduced and Et_2O added to precipitate the product. The pale-orange solid obtained was filtered, washed with Et_2O and dried *in vacuo*. Yield: 458 mg, 85 %. $^{13}C\{^1H\}$ (75.38 MHz, $CDCl_3$): δ 155.99 (C^5); δ 155.69 ($C^{5'}$); δ 150.94 (C^1); δ 150.05 ($C^{1'}$); δ 139.38 (C^3); δ 139.28 ($C^{3'}$); δ 120.57 (C^4); δ 119.87 ($C^{4'}$); δ 115.48 (C^2); δ 112.47 ($C^{2'}$); δ 39.53 (C^6); δ - 1.93 (C^{Me}). Elemental analysis: % Found (% calc.) for $C_{12}H_{14}ClN_3Pd$: C: 42.46 (42.13); H: 4.14 (4.12); N: 12.36 (12.28).

2.4.2.2 [PdMe(2,2´-dipyridyl-N-benzylamine)Cl] (2b)

The same synthetic procedure as outlined above (**2a**) was employed for the synthesis of **2b**, using ligand **1b** as reagent. Yield: 505 mg, 77 %. $^{13}C\{^1H\}$ (75.38 MHz, $CDCl_3$): δ 155.19 (C^5); δ 153.84 ($C^{5'}$); δ 150.97 (C^1); δ 150.14 ($C^{1'}$); δ 139.38 (C^3); δ 138.70 ($C^{3'}$); δ 134.93 (C^7); δ 128.98 (C^8); δ 128.93 ($C^{8'}$); δ 128.69 (C^{10}); δ 128.01 (C^9); δ 127.85 ($C^{9'}$); δ 120.97 (C^4); δ 120.34 ($C^{4'}$); δ 117.46 (C^2); δ 114.07 ($C^{2'}$); δ 55.27 (C^6); δ - 2.26 (C^{Me}). Elemental analysis: % Found (% calc) for $C_{18}H_{18}ClN_3 \cdot 0.2CH_2Cl_2$: C: 50.58 (50.23); H: 4.06 (4.26); N: 9.67 (9.66).

2.4.2.3 [PdMe(2,2´-dipyridyl-N-methylcyclohexylamine)Cl] (2c)

The same synthetic procedure as outlined above (**2a**) was employed for the synthesis of **2c**, using ligand **1c** as reagent. Yield: 539 mg, 81 %. $^{13}C\{^{1}H\}$ (75.38 MHz, $CDCl_3$): δ 155.82 (C^{5}); δ 153.97 ($C^{5'}$); δ 150.93 (C^{1}); δ 150.01 ($C^{1'}$); δ 139.38 (C^{3}); δ 138.87 ($C^{3'}$); δ 120.90 (C^{2}); δ 120.04 ($C^{2'}$); δ 117.96 (C^{2}); δ 114.18 ($C^{2'}$); δ 58.08 (C^{6}); δ 35.97 (C^{7}); δ 31.11 ($C^{8,8'}$); δ 26.38 (C^{10}); δ 25.63 ($C^{9,9'}$); δ - 2.62 (C^{Me}). Elemental analysis: % Found (% calc) for $C_{18}H_{24}ClN_3Pd$: C: 50.76 (50.96); H: 5.26 (5.70); N: 9.83 (9.90).

2.4.2.4 [PdMe(2,2´-dipyridyl-N-neopentylamine)Cl] (2d)

The same synthetic procedure as outlined above (**2a**) was employed for the synthesis of **2d**, using ligand **1d** as reagent. Yield: 462 mg, 74 %. $^{13}C\{^{1}H\}$ (75.38 MHz, $CDCl_3$): δ 157.45 (C^{5}); δ 155.02 ($C^{5'}$); δ 150.87 (C^{1}); δ 150.05 ($C^{1'}$); δ 139.05 (C^{3}); δ 139.03 ($C^{3'}$); δ 120.91 (C^{4}); δ 120.09 ($C^{4'}$); δ 119.57 (C^{2}); δ 116.08 ($C^{2'}$); δ 64.97 (C^{6}); δ 36.34 (C^{7}); δ 27.96 (C^{8}); δ - 2.77 (C^{Me}). Elemental analysis: % Found (% calc) for $C_{16}H_{22}ClN_3Pd\cdot 0.25CH_2Cl_2$: C: 46.50 (46.53); H: 5.07 (5.41); N: 9.67 (10.02).

2.4.2.5 [PdMe(6,6´-dimethyl-2,2´-dipyridyl-N-methylamine)Cl] (2e)

The same synthetic procedure as outlined above (**2a**) was employed for the synthesis of **2e**, using ligand **1e** as reagent. Yield: 383 mg, 66 %. $^{13}C\{^{1}H\}$ (75.38 MHz, $CDCl_3$): δ 159.38 (C^{5}); δ 159.20 ($C^{5'}$); δ 156.84 (C^{1}); δ 154.74 ($C^{1'}$); δ 138.68 (C^{3}); δ 138.42 ($C^{3'}$); δ 120.77 (C^{4}); δ 120.23 ($C^{4'}$); δ 110.87 (C^{2}); δ 108.38 δ($C^{2'}$); δ 38.23 (C^{6}); δ 27.55 (C^{7}); δ 25.59 ($C^{7'}$); δ - 7.75 (C^{Me}). Elemental analysis: % Found (% calc) for $C_{14}H_{18}ClN_3Pd$: C: 45.34 (45.42); H: 4.83 (4.90); N: 11.21 (11.35).

2.4.3 Synthesis of cationic N-alkyl dipyridylaldiminato methylpalladium acetonitrile complexes, 2f-2i.

2.4.3.1 [PdMe{2,2′-dipyridyl-N-methylamine}(NCMe)]$^+$[BAr′$_4$]$^-$ (2f)

To a stirring solution of NaBAr′$_4$ (208 mg, 0.235 mmol) in MeCN (2 ml) was added a solution of [PdMe{2,2′-dipyridyl-*N*-methylamine}Cl] (100 mg, 0.235 mmol) in DCM (8 ml). The reaction mixture was stirred at rt for 120 min. After the allotted time the solvent was removed *in vacuo* and the yellow residue obtained stirred in Et_2O, filtered through celite, solvent removed *in vacuo* to yield an orange-brown solid. Yield: 368 mg, 69 %. $^{13}C\{^1H\}$ (75.38 MHz, $CDCl_3$): δ 161.63 (q, $J_{C\text{-}B}$ 49.59, C_{ipso}); δ 155.77 (C^5); δ 153.87 ($C^{5'}$); δ 150.75 (C^1); δ 148.02 ($C^{1'}$); δ 141.13 (C^3); δ 141.11 ($C^{3'}$); δ 134.96 (C_o); δ 129.01 (q, $J_{C\text{-}F}$ 31.79, C_m); δ 123.35 (q, $J_{C\text{-}F}$ 126.52, C_m); δ 121.61 (C^4); δ 121.65 ($C^{4'}$); δ 117.70 (C_p); δ 116.38 (C^2) δ 113.84 ($C^{2'}$); δ 39.27 (C^6); δ 3.18 (Pd-CH_3CN); δ 1.72 (Pd-CH_3). ESI-MS (+ve): *m/z* 347 $[M]^+$. ESI-MS (-ve): *m/z* 863.1 $[BAr'_4]^-$. The instability of the material precluded accurate elemental analysis.

2.4.3.2 [PdMe{2,2′-dipyridyl-N-benzylamine}(NCMe)]$^+$[BAr′$_4$]$^-$ (2g)

The same synthetic procedure as outlined above (**2f**) was employed for the synthesis of **2g** using complex **2b** as starting material. Yield: 207 mg, 70 %. $^{13}C\{^1H\}$ (75.38 MHz, $CDCl_3$): δ 162.38 (q, $J_{C\text{-}B}$ 49.59, C_{ipso}); δ 155.97 (C^5); δ 154.55 ($C^{5'}$); δ 151.45 (C^1); δ 148.87 ($C^{1'}$); δ 141.62 (C^3); δ 141.54 ($C^{3'}$); δ 135.63 (C_o); δ 135.15 (C^7); δ 129.98 ($C^{8,8'}$); δ 129.66 (q, $J_{C\text{-}F}$ 31.79, C_m); δ 128.62 ($C^{9,9'}$); δ 128.09 (C^{10}); δ 124.48 (q, $J_{C\text{-}F}$ 126.52, C_m); δ 122.68 (C^4); δ 121.71 ($C^{4'}$); δ 119.19 (C^2); δ 118.33 (C_p); δ 116.52 ($C^{2'}$); δ 58.51 (C^6); δ 3.71

(Pd-CH_3CN); δ 1.37 (Pd-CH_3). ESI-MS (+ve): *m/z* 429 $[M]^+$. ESI-MS (-ve): *m/z* 863.1 $[BAr'_4]^-$. The instability of the material precluded accurate elemental analysis.

2.4.3.3 [PdMe{2,2´-dipyridyl-N-methylcyclohexylamine}(NCMe)]$^+$[BAr´$_4$]$^-$ (2h)

The same synthetic procedure as outlined above (**2f**) was employed for the synthesis of **2h** using complex **2c** as starting material: 116 mg, 36 %. $^{13}C\{^1H\}$ (75.38 MHz, $CDCl_3$): δ 162.03 (q, $J_{C\text{-}B}$ 49.59, C_{ipso}); δ 156.20 (C^5); δ 154.55 ($C^{5'}$); δ 151.18 (C^1); δ 148.52 ($C^{1'}$); δ 141.38 (C^3); δ 141.35 ($C^{3'}$); δ 135.45 (C_o); δ 130.61 (C^4); δ 129.42 (q, $J_{C\text{-}F}$ 31.79, C_m); δ 127.00 ($C^{4'}$); δ 120.87 (q, $J_{C\text{-}F}$ 126.52, C_m); δ 119.09 (C^2); δ 118.17 (C_p); δ 116.38 ($C^{2'}$); δ 58.51 (C^6); δ 36.75 (C^7); δ 31.62 ($C^{8,8'}$); δ 26.85 (C^{10}); δ 26.11 ($C^{9,9'}$); δ 3.71 (Pd-CH_3CN); δ 1.37 (Pd-CH_3). ESI-MS (+ve): *m/z* 429 $[M]^+$. ESI-MS (-ve): *m/z* 863.1 $[BAr'_4]^-$. The instability of the material precluded accurate elemental analysis.

2.4.3.4 [PdMe{2,2´-dipyridyl-N-neopentylamine}(NCMe)]$^+$[BAr´$_4$]$^-$ (2i)

The same synthetic procedure as outlined above (**2f**) was employed for the synthesis of **2i** using complex **2d** as starting material. Yield: 154 mg, 68 %. $^{13}C\{^1H\}$ (75.38 MHz, $CDCl_3$): δ 161.99 (q, $J_{C\text{-}B}$ 49.59, C_{ipso}); δ 157.06 (C^5); δ 155.12 ($C^{5'}$); δ 150.49 (C^1); δ 147.82 ($C^{1'}$); δ 140.89 (C^3); 140.76 ($C^{3'}$); δ 134.74 (C_o); δ 129.10 (q, $J_{C\text{-}F}$ 31.79, C_m); δ 129.91 (C^4) δ 126.29 ($C^{4'}$); δ 120.87 (q, $J_{C\text{-}F}$ 126.52, C_m); δ 120.65 (C^2); δ 119.60 ($C^{2'}$); δ 117.39 (C_p); δ 64.48 (C^6); δ 36.18 (C^7); δ 27.72 (C^8); δ 3.05 (Pd-CH_3CN); δ 0.67 (Pd-CH_3). ESI-MS (+ve): *m/z* 403.1 $[M]^+$. ESI-MS (-ve): *m/z* 863.1 $[BAr'_4]^-$. The instability of the material precluded accurate elemental analysis.

2.4.3.5 [PdMe{6,6′-dimethyl-2,2′-dipyridyl-N-methylamine}(NCMe)]$^+$[BAr′$_4$]$^-$ (2j)

The same synthetic procedure as outlined above (**2f**) was employed for the synthesis of **2j** using complex **2e** as starting material. Yield: 154 mg, 68 %. %. $^{13}C\{^1H\}$ (75.38 MHz, $CDCl_3$): δ 162.02 (q, $J_{C\text{-}B}$ 49.59, C_{ipso}); δ 159.50 (C^5); δ 157.51 ($C^{5'}$); δ 156.77 (C^1); δ 154.79 ($C^{1'}$); δ 140.52 (C^3); 140.47 ($C^{3'}$); δ 134.77 (C_o); δ 129.14 (q, $J_{C\text{-}F}$ 31.79, C_m); δ 122.07 (q, $J_{C\text{-}F}$ 126.52, C_m); δ 120.63 (C^4); δ 119.08 ($C^{4'}$); δ 117.50 (C_p); δ 111.89 (C^2); δ 110.17 ($C^{2'}$); δ 38.12 (C^6); δ 27.67 (C^7); δ 24.95 ($C^{7'}$); δ 2.72 (Pd-CH_3CN); δ -3.74 (Pd-CH_3). ESI-MS (+ve): *m/z* 375 $[M]^+$. ESI-MS (-ve): *m/z* 863.1 $[BAr'_4]^-$. The instability of the material precluded accurate elemental analysis.

2.4.4 Synthesis of cationic N-alkyl dipyridylaldiminato methylpalladium pyridine complexes, 2k-2o.

2.4.4.1 [PdMe{2,2′-dipyridyl-N-methylamine}(C_5H_5N)]$^+$[BAr′$_4$]$^-$ (2k)

The same synthetic procedure outlined above (complex **2f**) was employed in the synthesis of **2k**, employing pyridine as coordinating solvent. Yield: 197 mg, 67 %. $^{13}C\{^1H\}$ (75.38 MHz, $CDCl_3$): δ 157.99 (q, $J_{C\text{-}B}$ 49.59, C_{ipso}); δ 152.19 (C^5); δ 150.64 ($C^{5'}$); δ 148.54 (C_{py}); δ 147.08 ($C^{1,1'}$); δ 143.56 (C_{py}); δ 137.33 (C^3); 137.18 ($C^{3'}$); δ 135.50 (C_{py}); δ 131.23 (C_o); δ 12.30 (q, $J_{C\text{-}F}$ 31.79, C_m); δ 124.48 (C^4); δ 123.73 (C_{py}); δ 123.67 ($C^{4'}$); δ 120.06 (q, $J_{C\text{-}F}$ 126.52, C_m); δ 118.25 ($C^{4'}$); δ 117.13 (C_{py}); δ 113.94 (C_p); δ 112.36 (C^2); δ 110.18 ($C^{2'}$); δ 35.65 (C^6); δ -0.03 (Pd-CH_3). ESI-MS (-ve): *m/z* 863.1 $[BAr'_4]^-$. % Found (Calc) for $C_{49}H_{31}BF_{24}N_4Pd\cdot 0.5CH_2Cl_2$: C: 45.99 (46.04); H: 2.49 (2.50); N: 4.59 (4.34).

2.4.4.2 [PdMe{2,2′-dipyridyl-N-benzylamine}(C_5H_5N)]$^+$[BAr′$_4$]$^-$ (2l)

The same synthetic procedure outlined above (complex **2f**) was employed in the synthesis of **2l**, employing pyridine as coordinating solvent. Yield: 217 mg, 70 %. $^{13}C\{^1H\}$ (75.38 MHz, $CDCl_3$): δ 161.63 (q, $J_{C\text{-}B}$ 49.59, C_{ipso}); δ 155.67 (C^5); δ 153.59 ($C^{5'}$); δ 152.02 (C_{py}); δ 151.81 (C^1); δ 150.57 ($C^{1'}$); δ 147.24 (C_{py}); δ 140.67 (C^3); δ 140.54 ($C^{3'}$); δ 134.75 (C_o); δ 129.16 (q, $J_{C\text{-}F}$ 31.79, C_m); δ 126.40 (q, $J_{C\text{-}F}$ 126.52, C_m); δ 122.68 (C_{py}); δ 121.97 (C^4); δ 121.22 ($C^{4'}$); δ 119.07 (C_{py}); δ 118.06 (C^2); δ 117.47 (C_p); δ 115.97 ($C^{2'}$); δ 55.35 (C^6); δ 3.19 (Pd-CH_3). ESI-MS (-ve): *m/z* 863.1 [B*Ar′*$_4$]$^-$. % Found (Calc) for $C_{55}H_{35}BF_{24}N_4Pd$: C: 49.53 (49.85); H: 2.47 (2.66); N: 4.02 (4.23).

2.4.4.3 [PdMe{2,2′-dipyridyl-N-methylcyclohexylamine}(C_5H_5N)]$^+$[BAr′$_4$]$^-$ (2m)

The same synthetic procedure outlined above (complex **2f**) was employed in the synthesis of **2m**, employing pyridine as coordinating solvent. Yield: 216 mg, 69 %. $^{13}C\{^1H\}$ (75.38 MHz, $CDCl_3$): δ 161.42 (q, $J_{C\text{-}B}$ 49.59, C_{ipso}); δ 155.71 (C^5); δ 154.17 ($C^{5'}$); δ 151.93 (C_{py}); δ 150.50 (C^1) δ 147.03 ($C^{1'}$); δ 140.60 (C^3); δ 140.51 ($C^{3'}$); δ 138.98 (C_{py}); δ 134.75 (C_o); δ 128.75 (q, $J_{C\text{-}F}$ 31.79, C_m); δ 128.55 (C^4); δ 126.42 (C_{py}); δ 125.84 ($C^{4'}$); δ 121.67 (q, $J_{C\text{-}F}$ 126.52, C_m); δ 120.41 (C_{py}); δ 118.14 (C^2); δ 117.45 (C_p); δ 116.08 ($C^{2'}$); δ 57.86 (C^6); δ 36.39 (C^7); δ 30.91 ($C^{8,8'}$); δ 26.15 (C^{10}); δ 25.41 ($C^{9,9'}$); δ 2.69 (Pd-CH_3). ESI-MS (-ve): *m/z* 863.1 [B*Ar′*$_4$]$^-$. % Found (Calc) for $C_{55}H_{41}BF_{24}N_4Pd$: C: 49.43 (49.78); H: 2.80 (3.24); N: 4.02 (4.18).

2.4.4.4 [PdMe{2,2′-dipyridyl-N-neopentylamine}(C_5H_5N)]$^+$[BAr′$_4$]$^-$ (2n)

The same synthetic procedure as outlined above (**2f**) was employed for the synthesis of **2n**, employing pyridine as coordinating solvent. Yield: 220 mg,76 %. $^{13}C\{^1H\}$ (75.38

MHz, $CDCl_3$): δ 158.78 (q, $J_{C\text{-}B}$ 49.59, C_{ipso}); δ 154.48 (C^5); δ 153.03 ($C^{5'}$); δ 149.24 (C_{py}); δ 147.81 ($C^{1,1'}$); δ 144.32 (C_{py}); δ 138.03 (C^3); 137.94 ($C^{3'}$); δ 136.29 (C_{py}); δ 132.02 (C_o); δ 126.29 (q, $J_{C\text{-}F}$ 31.79, C_m); δ 124.48 (C^4); δ 123.73 (C_{py}); δ 123.50 ($C^{4'}$); δ 120.86 (q, $J_{C\text{-}F}$ 126.52, C_m); δ 119.10 (C^2); δ 118.30 ($C^{2'}$); δ 117.12 (C_{py}); δ 114.71 (C_p); δ 61.64 (C^6); δ 33.39 (C^7); δ 25.05 (C^8); δ 0.01 (Pd-CH_3). ESI-MS (-ve): *m/z* 863.1 [B*Ar′*$_4$]$^-$. % Found (Calc) for $C_{53}H_{39}BF_{24}N_4Pd$: C: 48.43 (48.78); H: 2.76 (3.01); N: 3.99 (4.27).

2.4.4.5 [PdMe{6,6′-dimethyl-2,2′-dipyridyl-N-methylamine}(C_5H_5N)]$^+$[BAr′$_4$]$^-$ (2o)

The same synthetic procedure as outlined above (**2f**) was employed for the synthesis of **2o**, employing pyridine as coordinating solvent. Yield: 184 mg, 65 %. %. $^{13}C\{^1H\}$ (75.38 MHz, $CDCl_3$): δ 161.22 (q, $J_{C\text{-}B}$ 49.59, C_{ipso}); δ 159.47 (C^5); δ 157.46 ($C^{5'}$); δ 156.66 (C^1); δ 155.12 ($C^{1'}$); δ 151.69 (C_{py}); δ 140.60 (C^3); 140.23 ($C^{3'}$); δ 138.71 (C_{py}); δ 134.63 (C_o); δ 129.81 (C_{py}); δ 128.93 (q, $J_{C\text{-}F}$ 36.88, C_m); δ 126.19 (C^4); δ 126.02 (C_{py}); δ 122.03 (q, $J_{C\text{-}F}$ 126.52, C_m); δ 118.96 ($C^{4'}$); δ 117.33 (C_p); δ 111.85 (C^2); δ 110.03 ($C^{2'}$); δ 38.42 (C^6); δ 27.55 (C^7); δ 24.26 ($C^{7'}$); δ -1.38 (Pd-CH_3). ESI-MS (-ve): *m/z* 863.1 [B*Ar′*$_4$]$^-$. % Found (Calc) for $C_{49}H_{31}BF_{24}N_4Pd$: C: 46.84 (47.12); H: 2.23 (2.50); N: 4.07 (4.49).

2.4.5 X-Ray Crystal structure determination.

Single crystals of complexes **2e**, **2o** and **2o-A** were mounted on glass fibers or nylon loops and centred in a stream of cold nitrogen at 100(2) K or 150(2) K. Crystal evaluation and data collection was performed on a Bruker-Nonius SMART Apex II CCD diffractometer with Mo K_α radiation (λ = 0.71073 Å). Data collection, reduction and refinement were performed using SAINT[19] and SADABS,[20] which forms part of the APEX II software package. The structures were solved by direct methods and refined by full-matrix least-

squares on F^2 using SHELX-97[21] within the X-Seed graphic user interface.[22] All non-hydrogen atoms were refined anisotropically and all hydrogen atoms were placed using calculated positions and riding models.

2.5 References

(1) (a) Skupinska, J. *Chem. Rev.*, **1991**, *91*, 613 (b) Keim, W. *Angew. Chem. Int. Ed. Engl.*, **1990**, *29*, 235.

(2) (a) Johnson, L. K.; Killian, C. M.; Brookhart, M. *J. Am. Chem. Soc.*, **1995**, *117*, 6414 (b) Doherty, M. D.; Trudeau, S.; White, P. S.; Morken, J., P.; Brookhart, M. *Organometallics*, **2007**, *26*, 1261 (c) Killian, C. M.; Johnson, L. K.; Brookhart, M. *Organometallics*, **1997**, *16*, 2005 (d) Svejda, S. A.; Brookhart, M. *Organometallics*, **1999**, *18*, 65 (e) Tempel, D. J.; Johnson, L. K.; Huff, R. L.; White, P. S.; Brookhart, M. *J. Am. Chem. Soc.*, **2000**, *122*, 6686.

(3) (a) Britovsek, G. J. P.; Gibson, V. C.; Wass, D. F. *Angew. Chem. Int. Ed.*, **1999**, *38*, 428 (b) Gibson, V. C.; Spitzmesser, S. K. *Chem. Rev.*, **2002**, *103*, 283 (c) Mecking, S. *Angew. Chem. Int. Ed.*, **2001**, *40*, 534 (d) Domski, G. J.; Rose, J. M.; Coates, G. W.; Bolig, A. D.; Brookhart, M. *Prog. Polym. Sci.*, **2007**, *32*, 30 (e) Ittel, S. D.; Johnson, L. K.; Brookhart, M. *Chem. Rev.*, **2000**, *100*, 1169.

(4) (a) Rix, F. C.; Brookhart, M. *J. Am. Chem. Soc.*, **1995**, *117*, 1137 (b) Rix, F. C.; Brookhart, M.; White, P. S. *J. Am. Chem. Soc.*, **1996**, *118*, 4746.

(5) (a) Burns, C. T.; Jordan, R. F. *Organometallics*, **2007**, *26*, 6726 (b) Burns, C. T.; Jordan, R. F. *Organometallics*, **2007**, *26*, 6737 (c) Conley, M. P.; Burns, C. T.; Jordan, R. F. *Organometallics*, **2007**, *26*, 6750.

(6) Fakih, S.; Tung, W. C.; Eierhoff, D.; Mock, C.; Krebs, B. *Z. Anorg. Allg. Chem.*, **2005**, *631*, 1397.

(7) Rauterkus, M. J.; Fakih, S.; Mock, C.; Puscasu, I.; Krebs, B. *Inorg. Chim. Acta*, **2003**, *350*, 355.

(8) Licciulli, S.; Thapa, I.; Albahily, K.; Korobkov, I.; Gambarotta, S.; Duchateau, R.; Chevalier, R.; Schuhen, K. *Angew. Chem. Int. Ed.*, **2010**, *49*, 9225.

(9) Rulke, R. E.; Ernsting, J. M.; Spek, A. L.; Elsevier, C. J.; van Leeuwen, P. W. N. M.; Vrieze, K. *Inorg. Chem.*, **1993**, *32*, 5769.

(10) Onoue, H.; Moritani, I. *J. Organomet. Chem.*, **1972**, *43*, 431.

(11) (a) Delis, J. G. P.; Groen, J. H.; Vrieze, K.; van Leeuwen, P. W. N. M.; Veldman, N.; Spek, A. L. *Organometallics*, **1997**, *16*, 551 (b) Canovese, L.; Visentin, F.; Chessa, G.; Uguagliati, P.; Levi, C.; Dolmella, A.; Bandoli, G. *Organometallics*, **2006**, *25*, 5355.

(12) (a) Flapper, J.; Wormald, P.; Lutz, M.; Spek, A. L.; van Leeuwen, P. W. N. M.; Elsevier, C. J.; Kamer, P. C. J. *Eur. J. Inorg. Chem.*, **2008**, 4968 (b) Flapper, J.; Kooijman, H.; Lutz, M.; Spek, A. L.; van Leeuwen, P. W. N. M.; Elsevier, C. J.; Kamer, P. C. J. *Organometallics*, **2009**, *28*, 3272.

(13) (a) Tusek-Bozic, L.; Curic, M.; Traldi, P. *Inorg. Chim. Acta*, **1997**, *254*, 49 (b) Tusek-Bozic, L.; Komac, M.; Curic, M.; Lycka, A.; Alpaos, M. D.; Scarcia, V.; Furlani, A. *Polyhedron*, **2000**, *19*, 937.

(14) (a) Schätz, A.; Scarel, A.; Zangrando, E.; Mosca, L.; Carfagna, C.; Gissibl, A.; Milani, B.; Reiser, O. *Organometallics*, **2006**, *25*, 4065 (b) Delis, J. G. P.; Rep, M.; Rülke, R. E.; van Leeuwen, P. W. N. M.; Vrieze, K.; Fraanje, J.; Goubitz, K. *Inorg. Chim. Acta*, **1996**, *250*, 87 (c) Done, M. C.; Rüther, T.; Cavell, K. J.; Kilner, M.; Peacock, E. J.; Braussaud, N.; Skelton, B. W.; White, A. *J. Organomet. Chem.*, **2000**,

607, 78 (d) Mungwe, N.; Swarts, A. J.; Mapolie, S. F.; Westman, G. *J. Organomet. Chem.*, **2011**, *696*, 3527.

(15) (a) Kitson, P. J.; Song, Y.-F.; Gamez, P.; de Hoog, P.; Long, D.-L.; Parenty, A. D. C.; Reedijk, J.; Cronin, L. *Inorg. Chem.*, **2008**, *47*, 1883 (b) Kwon, S. S.; Cha, M. S.; Lee, J. E.; Lee, S. S.; Jung, O.-S. *Cryst. Growth. Des.*, **2008**, *8*, 2073.

(16) (a) Shi, P.-Y.; Liu, Y.-H.; Peng, S.-M.; Liu, S.-T. *Organometallics*, **2002**, *21*, 3203 (b) Tsoureas, N.; Danopoulos, A. A.; Tulloch, A. A. D.; Light, M. E. *Organometallics*, **2003**, *22*, 4750.

(17) (a) Mastropietro, T. F.; Aprea, A.; La Deda, M.; Aiello, I.; Ghedini, M.; Crispini, A. *Cryst. Growth. Des.*, **2012**, *12*, 2173 (b) Troff, R. W.; Hovorka, R.; Weilandt, T.; Lutzen, A.; Cetina, M.; Nieger, M.; Lentz, D.; Rissanen, K.; Schalley, C. A. *Dalton. Trans.*, **2012**, *41*, 8410 (c) Meduri, A.; Cozzula, D.; D'Amora, A.; Zangrando, E.; Gladiali, S.; Milani, B. *Dalton. Trans.*, **2012**, *41*, 7474 (d) Khlebnikov, V.; Meduri, A.; Mueller-Bunz, H.; Milani, B.; Albrecht, M. *New J. Chem.*, **2012**, *36*, 1552.

(18) Gott, A. L.; Piers, W. E.; Dutton, J. L.; McDonald, R.; Parvez, M. *Organometallics*, **2011**, *30*, 4236.

(19) SAINT data reduction software, 6.45, Bruker AXS Inc.,Madison, WI, 2003

(20) Blessing, R. H. *Acta Crystallogr. Sect. A: Found. Crystallogr.*, **1995**, *51*, 33.

(21) SHELX-97, 1997

(22) (a) Barbour, L. J. *J. Supramol. Chem.*, **2001**, *1*, 189 (b) Atwood, J. L.; Barbour, L. J. *Cryst. Growth. Des.*, **2003**, *3*, 3.

3.1 Introduction

The developments in chemistry i.e. new synthetic methodologies, catalytic reactions etc. have always been driven by a fundamental understanding of the mechanism involved with each transformation. In the context of olefin transformations, particularly those mediated by palladium, seminal work regarding mechanistic understanding of the processes has always involved a combination of experimental and theoretical investigations.[1] The combined experimental and theoretical approach to gaining a mechanistic understanding of chemical transformations has the advantage of providing a correlation between theoretical prediction and experimental observation. In addition, this approach generates new insights into rational catalyst design. To highlight this strategy a few key examples will be discussed.

Employing low-temperature synthetic and spectroscopic techniques, Brookhart and co-workers reported the first observation of an acyl π-olefin complex, **3-I**, (Fig. 3.1), identified as a key intermediate in CO/*p*-tert-butyl styrene copolymerisation.[2]

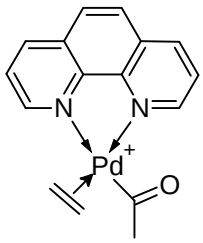

3-I

Fig. 3.1 Key intermediate in CO/*p*-tert-butyl styrene copolymerisation.[2]

In addition their investigation allowed for the determination of key insertion rates and insertion barriers which provided fundamental insight into the mechanism of Pd-mediated CO/*p*-tert-butyl styrene co-polymerisation.

Further work by the same research group demonstrated mechanistically how a family of aryl-substituted α-diiminato Pd(II) complexes were active as catalysts in olefin (α and internal) polymerisation.[3] Low-temperature NMR studies showed that Pd-alkyl π-olefin species were the catalyst resting states and that the migratory insertion barriers were in the range 17-19 kcal/mol. Detection of Pd-*n*/*iso*-propyl species and the evaluation of their reactivity provided fundamental insights into how "chain-walking"; to generate branched polymer occurred. Furthermore, the observation that an increase in steric bulk retarded the rate of associative exchange of free and coordinated ethylene, a distinguishing feature of this family of catalysts, have directed catalyst design up to now. Concurrent with these experimental investigations the groups of Ziegler,[4] Morokuma[5] and Siegbahn[6] evaluated the insertion/elimination behaviour of (N-N)NiR(olefin)$^+$ and (N-N)PdR(olefin)$^+$ species theoretically and showed excellent correlation with the mechanistic features determined experimentally.

Subsequently, Drent and co-workers reported an *in situ*-generated neutral catalyst system of a Pd(0) precursor and a P-O chelating ligand, **3-II** (Fig. 3.2), capable of copolymerising ethylene and alkyl acrylates.[7]

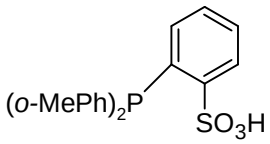

3-II

Fig. 3.2 Neutral P-O chelating ligand pioneered by Drent and co-workers.[7]

Building upon this foundation, Nozaki and others have demonstrated the catalytic utility of well-defined Pd-alkyl phosphine-sulphonate complexes in the copolymerisation of ethylene with acrylonitrile,[8] vinyl fluoride[9] and vinyl ethers.[10] In particular, Nozaki and

co-workers evaluated the above-mentioned catalytic system and its ability to produce linear polyethylene by experiment and theory.[11] Experimentally, long-chain Pd-alkyl complexes were prepared and their spectroscopic investigation showed that even in the presence of β-hydrogens, β-hydride elimination to generate α-olefins did not occur, or occurred to a negligible extent. Theoretically, they found that *cis*/*trans* isomerisation via Berry pseudo-rotation was a key step in the propagation process and that migratory insertion was likely to occur from the less stable Pd-alkyl π-olefin complex in which the growing polymer chain was located *trans* to phosphorus. Also, a correlation between experiment and theory established that for the evaluated catalyst system, chain transfer processes was dependent on ethylene pressure and that the generation of the key Pd-hydride π-olefin species only predominated under low ethylene pressures.

Nozaki and co-workers also conducted a comparative study of the Pd-phosphine sulphonate and Pd-diphenylphosphinoethane system in CO/methyl acrylate (MA) copolymerisation starting from the respective key Pd-chelate complexes, **3-IIIA** and **3-IIIB** (Fig. 3.3).[12]

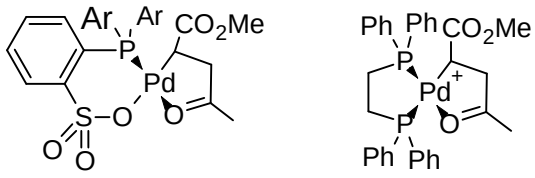

3-IIIA **3-IIIB**

Fig. 3.3 Species developed by Nozaki and co-workers to evaluate comparative CO/MA copolymerisation.[12]

Experimentally, they observed that species **3-IIIA** catalysed CO/MA copolymerisation as well as CO/MA/ethylene terpolymerisation while species **3-IIIB** was catalytically inert to the formation of the desired products in both reactions. Their catalytic

study showed that an increase in catalytic activity was observed with an increase in CO pressure. Further investigations showed that the initial coordinaton and insertion of CO to the chelate complex **3-IIIA** was reversible and that this process generated the acylpalladium species, **3-IV**, via coordination-insertion and *cis*/*trans* isomerisation (Fig. 3.4). The equilibrium constant $K_{4\text{-IV/V-IIIA}}$ was determined to be 3/2. In contrast, species **3-IIIB** was observed to undergo no reaction in the presence of CO.

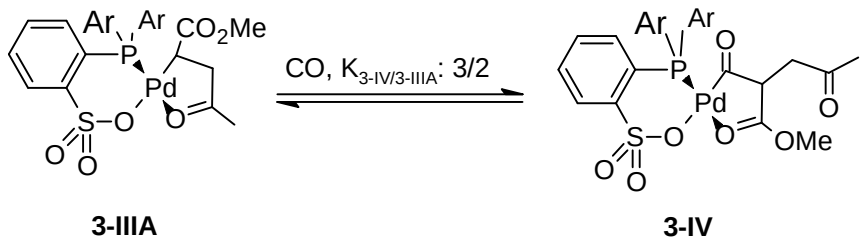

3-IIIA **3-IV**

Fig. 3.4 Equilibrium generated during the reaction of **3-IIIA** with CO.[12]

Their computational investigation showed that in comparison to species **3-IIIB**, MA insertion (rate-determining step) proceeded with a lower energy barrier as a result of decreased steric pressure of the sulphonate group in comparison to the phosphine group as well as enhanced back-donation from palladium to the coordinating olefin.

Here we report the experimental and theoretical evaluation of the reactivity of the cationic *N*-alkyl dipyridylaldiminato complexes reported in Chapter 2 toward ethylene.

3.2 Results and Discussion

3.2.1 Catalytic preparative-scale ethylene oligomerisation and low temperature kinetic studies of reactivity of cationic (N-N)Pd(Me)NCMe$^+$ species toward ethylene.

Preparative scale ethylene oligomerisation reactions were conducted at room temperature, employing cationic complexes **2f-2j** as precatalysts (Scheme 3.1, Table 3.1). It

was rationalised that olefin exchange with coordinated acetonitrile would be more facile in comparison to the pyridine-ligated analogues, owing to a decrease in basicity of the coordinated ligand.[13]

Scheme 3.1 Ethylene dimerisation catalysed by cationic palladium *N*-alkyl dipyridylaldiminato complexes.

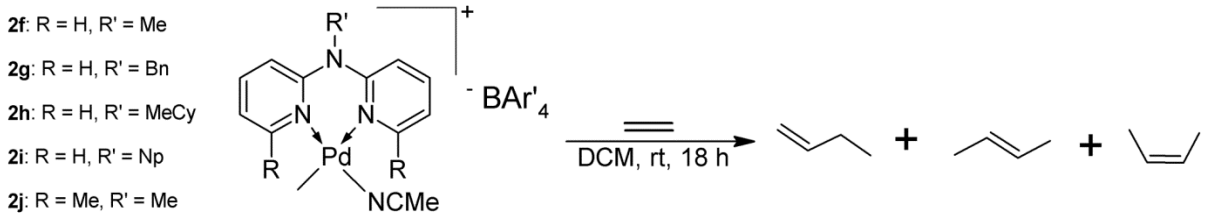

Our results showed that these complexes dimerise ethylene with relatively low activities, with the highest TOF value of 7.4 h^{-1} obtained for complex **2i**. The observed TOF values are significantly lower than what has been reported previously for a number of cationic palladium systems. Kress and co-workers reported the application of unsymmetrical diimine-ligated cationic palladium complexes in ethylene oligomerisation (Fig. 3.5).

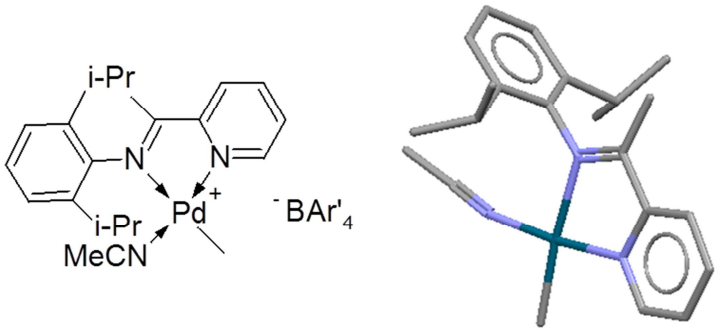

Fig. 3.5 Unsymmetrical cationic palladium-diimine complex found to be an active ethylene oligomerisation catalyst.[14] Copyright Cambridge Structural Database 2013.

Their catalytic system showed activities of up to 105 kg oligomer.$mol_{Pd}^{-1}.h^{-1}$ with a Schulz-Flory distribution of oligomeric products.[14] Brookhart and co-workers reported

ethylene oligomerisation catalysed by a cationic palladium phosphine-oxazoline complex (Fig. 3.6).[15]

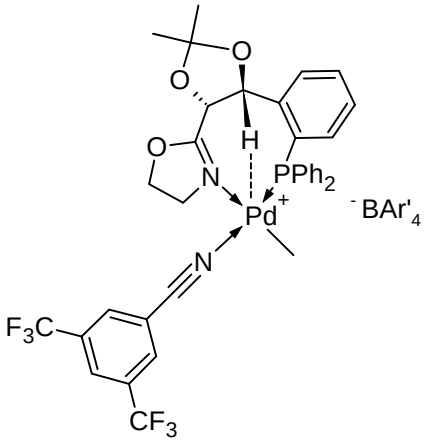

Fig. 3.6 Cationic phosphine-oxazoline complex active in ethylene oligomerisation.[15]

Complexes with no axial steric bulk yielded only butenes as oligomerisation products with no reported TOF values, while the complex with axial steric bulk yielded a Schulz-Flory distribution of α-olefins with TOF values of up to 15760 h^{-1}. It should be noted that the observed catalytic activity for **2f**-**2j** in ethylene oligomerisation is still higher than that reported for cationic palladium complexes bearing pyridine-phosphine ligands (Fig. 3.7).[16]

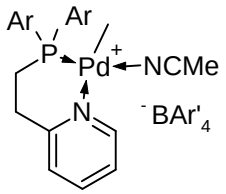

Fig. 3.7 Cationic palladium pyridine-phosphine complex which exhibits low activity in ethylene oligomerisation.[16a]

The comparatively low activity of the complexes **2f-2j** may be attributed to their inherent instability (as discussed in Chapter 2), and specifically, their thermal instability in solution; as evidenced by significant decomposition to palladium black during catalysis.

Table 3.1 Ethylene oligomerisation reactions employing complexes **2f**-**2j** as catalyst precursors.[a]

Entry	Pre-catalyst	V(ethylene consumed)	TOF[b]	Selectivity (1-C_4:2-C_4)[c]
1	**2f**	17	5.6	1:9
2	**2g**	15	5.5	1:8
3	**2h**	18	6.7	1:7
4	**2i**	20	7.4	1:9
5	**2j**	12	4.4	1:2

[a] Reaction parameters: Ethylene pressure: 5 bar; Solvent, V: DCM, 20 ml; Reaction temperature: 25 °C. Reaction time: 18 h. [b] TOF: $mol_{ethylene}.mol_{Pd}^{-1}.h^{-1}$. [c] Determined by GC-FID. *cis*/*trans* 2-butene ratio approximately 1:2 in all cases.

Jordan and co-workers have previously demonstrated the effect of temperature on the activity of Pd(II) bis(pyrazolyl)methane complexes in ethylene oligomerisation, and found that increased reaction temperatures (room temperature vs -10 °C) led to significant decreases in activity.[17] Analysis of the reaction products by GC-FID showed that the only catalysis products were 1-butene and *cis* and *trans* 2-butenes (Fig. 3.8). The selectivity for 1- and 2-butenes may be rationalised on the basis of an enhanced rate for chain termination in comparison to chain propagation. Chain termination rates have been shown to increase with a decrease in axial steric bulk of the coordinated ligand, even when the complexes with and without steric bulk have similar electronic properties.[2,3b,15,18] Considering complexes **2f** and **2j**, the Me-substituents in **2j** are orientated out of the plane of the palladium coordination sphere and as such only provides steric pressure in one face. Thus, even though the presence of the methyl groups may affect chain transfer processes (see below) its effect on selectivity is negligible and ethylene dimerisation predominates. This is illustrated more clearly in Figure 3.9, which compares axial steric bulk for neutral analogues of **2j** and the Brookhart diimine ethylene polymerisation system.

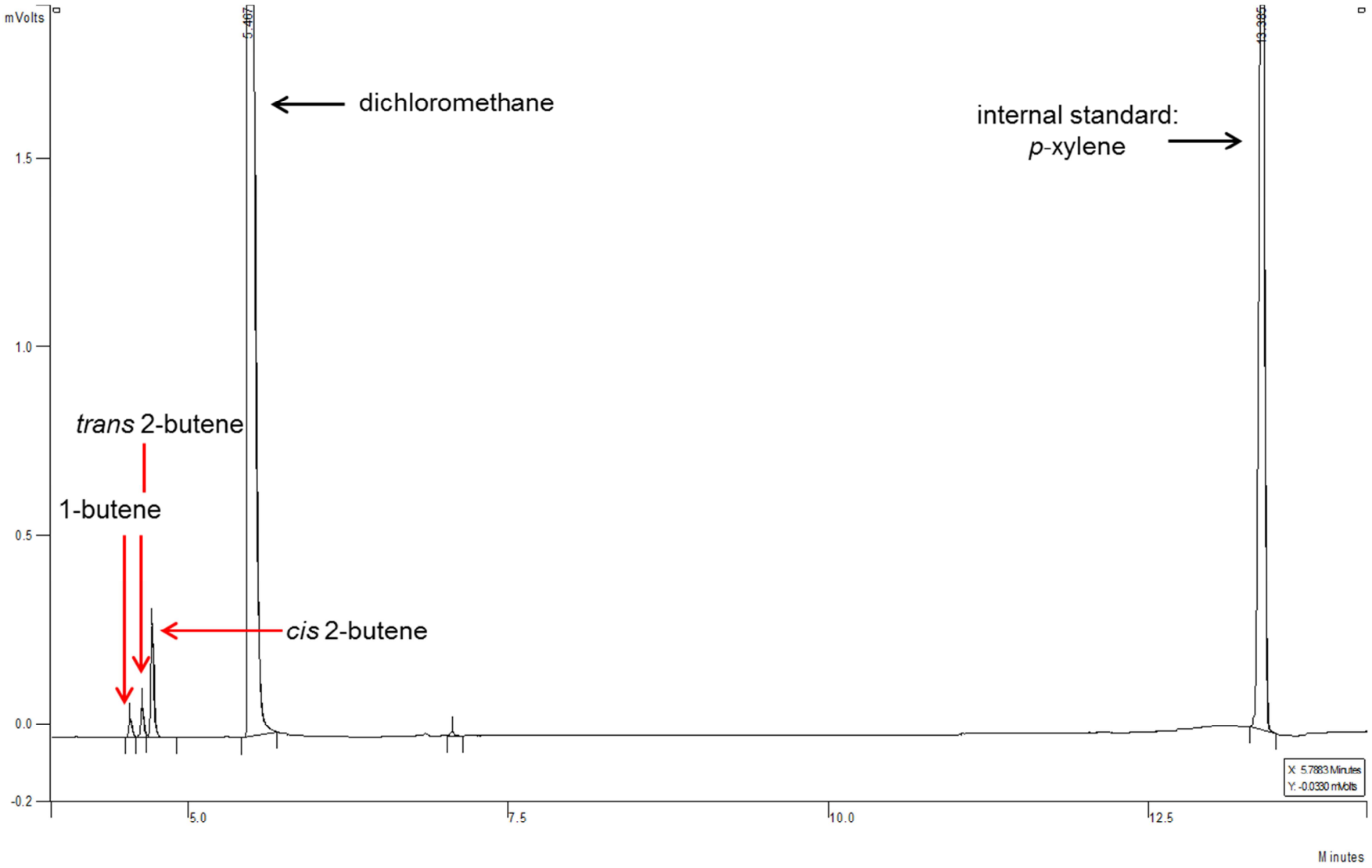

Fig. 3.8 Representative GC-trace of the oligomerisation products formed during catalysis.

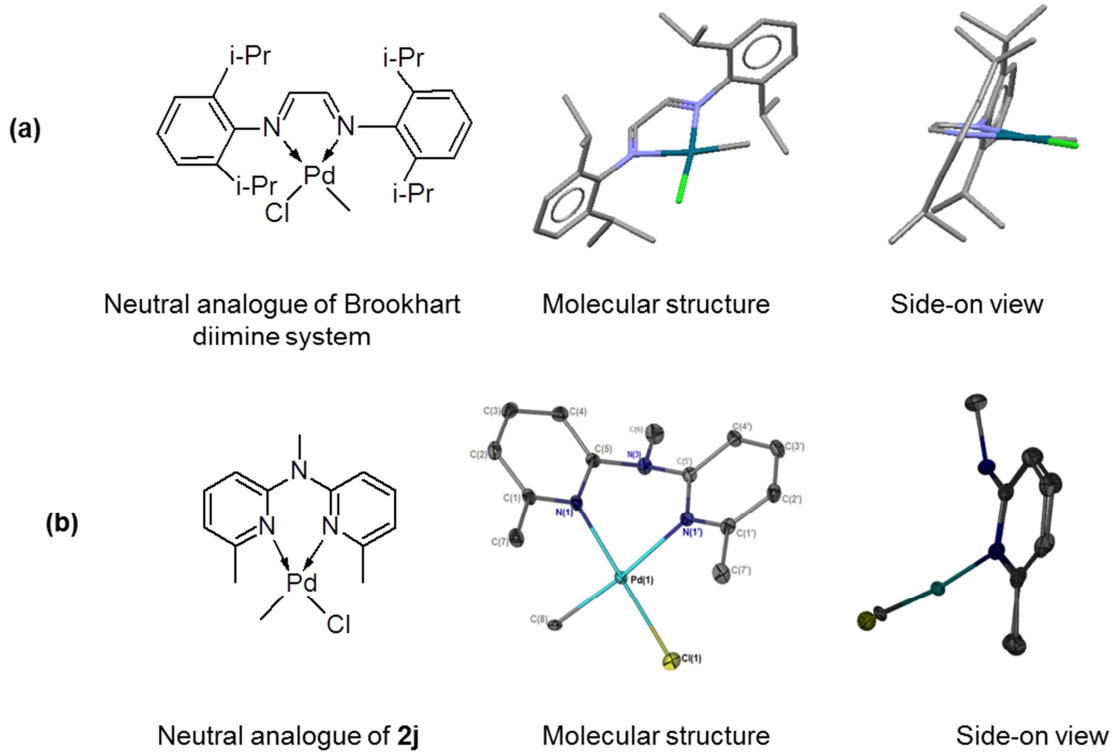

Fig. 3.9 Comparison of axial steric bulk for (a) the Brookhart diimine ethylene polymerisation system and (b) the neutral analogue of complex **2j**. Copyright Cambridge Structural Database.

No significant differences in the ratio of 1-butene to 2-butenes were observed for complexes **2f-2i** (Table 3.1, entries 1-4), while for **2j** this ratio was decreased (Table 3.1, entry 5). In addition, reactions at ambient and increased pressures (1 and 10 bar respectively) showed no increase in activity, thereby suggesting zero order kinetics in ethylene.[1c]

Our preparative scale catalytic results showed that the complexes displaying the most significant differences in activity were **2f** and **2j**. We postulated that the differences in steric bulk of the palladium metal centre may have an effect on initial ethylene coordination and insertion kinetics. To gain insight into these processes we reacted complexes **2f** and **2j** with excess ethylene at low temperatures and monitored the formation of the π-ethylene species and its subsequent insertion kinetics.

3.2.2 Generation of [PdMe(N-N)(CH_2=CH_2)]$^+$ species.

The reaction of the cationic acetonitrile-coordinated complexes **2f** and **2j** with ethylene at -78 °C generated the cationic π-ethylene species **3a** and **3b** respectively (Scheme 3.2).

Scheme 3.2 Generation of Pd-methyl π-ethylene species.

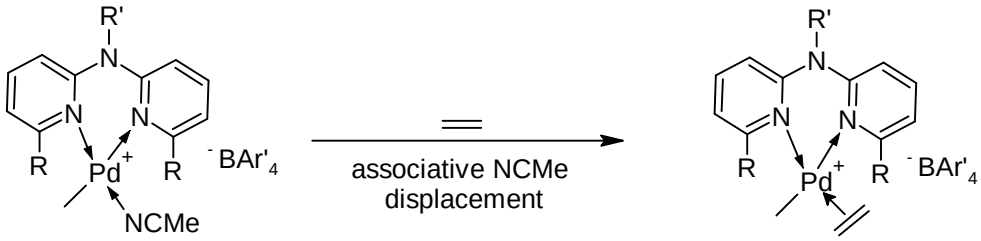

2f: R = H, R' = Me

2j: R = Me, R' = Me

3a: R = H, R' = Me

3b: R = Me, R' = Me

For both species **3a** and **3b** the ligand backbone remained inequivalent going from the acetonitrile to the π-ethene adduct, indicative that ethylene exchange is stereospecific (Table 3.2). This had been observed previously for analogous species.[19] For species **3a**, the pyridyl ring imine protons are observed as two poorly resolved doublets integrating for a single proton each at δ 8.20 and δ 7.93 ppm respectively. The remaining aromatic resonances are observed as a multiplet at δ 7.24 ppm ($H^{2,4,4'}$) and a poorly resolved triplet at δ 7.16 ppm ($H^{2'}$). The Pd-*Me* resonance shifted upfield in comparison to that of the acetonitrile adduct and was observed as a singlet at δ 0.60 ppm. In the case of species **3b**, the pyridyl ring aromatic resonances corresponding to $H^{3/3'}$ were observed as two broad triplets at δ 7.74 and δ 7.67 ppm respectively, while the remaining aromatic proton resonances were observed as a multiplet integrating for four protons at δ 7.09 ppm ($H^{2,2',4,4'}$). An analogous upfield shift of the Pd-*Me* resonance was observed as a singlet at δ 0.47 ppm. In addition, ethylene exchange

on the NMR chemical shift time scale is fast for species **3a** at -78 °C, as evidenced by a broad resonance at δ 5.40 ppm corresponding to free and coordinated ethylene. In contrast, ethylene exchange is slower for species **3b** at this temperature as evidenced by two resonances at δ 4.50 and 4.82 ppm corresponding to coordinated ethylene and a large resonance at δ 5.40 ppm assigned to free ethylene.

Consistent with differing ethylene exchange rates, complexes **2f** and **2j** displayed significantly different rates of formation of the Pd-methyl π-ethylene species, **3a** and **3b**. In the case of **2f** in the presence of ethylene, quantitative formation of **3a** was observed after 90 minutes at -78 °C, while in the case of **2j** the ratio of the starting acetonitrile complex to π-ethylene species was approximately 1:3 after 150 minutes at -78 °C (Fig. 3.10).

Analogous to what was observed by Brookhart and co-workers,[3a,20] the introduction of steric bulk in the coordination sphere of the palladium centre (in our case a Me-group) significantly decreased initial ethene associative exchange rates. By increasing the temperature from -78 °C to approximately -40 °C quantitative acetonitrile-ethylene exchange could be observed for both complexes.

3.2.3 Determination of ethylene insertion kinetics for species [PdMe(N-N)(CH_2=CH_2)]$^+$ (3a and 3b).

The rate of ethylene insertion into the Pd-Me bond was determined for both species **3a** and **3b** at -10 °C (Scheme 3.3). By monitoring the disappearance of the methyl resonance in species **3a**/**3b** at -10 °C, the formation of the Pd-propyl species could be observed. It should be noted that the proton resonances for this species was not assigned, except for the terminal Me-group. The kinetic plots of ethylene insertion into the Pd-Me bond of species **3a** and **3b** is shown in Figures 3.11 and 3.12 respectively.

Table 3.2 ^{1}H NMR spectral data for species [(N-N)PdMe($H_2C{=}CH_2$)]$^{+}$, **3a** and **3b** and [(N-N)PdEt($H_2C{=}CH_2$)]$^{+}$, **3e** and **3f**.[a]

Species	Aromatic Region	Aliphatic Region
3a	δ 8.20 (poorly resolved d, 1H, $H^{1/1'}$); δ 7.93 (poorly resolved d, 1H, $H^{1/1'}$); δ 7.83 (br. m, 2H, $H^{3/3'}$); δ 7.24 (m, 3H, $H^{4/4'/2}$); δ 7.16 (poorly resolved t, 1H, $H^{2'}$)	δ 5.39 (br. s, coordinated and free ethylene); δ 3.49 (s, 3H, H^{6}); δ 1.97 (s, 3H, free MeCN); δ 0.60 (s, 3H, Pd-*Me*)
3b	δ 7.74 (masked t, 1H, $H^{3'}$); δ 7.67 (poorly resolved t, 1H, H^{3}); δ 7.09 (m, 4H, $H^{2,2',4,4'}$);	δ 5.41 (br. s, free ethylene); δ 4.82 ppm (br. s, 2H, coordinated ethylene); δ 4.50 (br. s, 2H, coordinated ethylene); δ 3.50 (s, 3H, H^{6}); δ 2.74 (s, 3H, $H^{7'}$); δ 2.51 (s, 3H, H^{7}); δ 0.47 (s, 3H, Pd-*Me*)
3e	δ 8.41 (poorly resolved d, 1H, $H^{1'}$); δ 7.95 (poorly resolved t, 1H, $H^{3/3'}$); δ 7.84 (br. d, 1H, H^{1}); δ 7.32 (m, 2H, $H^{4,4'}$); δ 7.20 (br. d, 1H, $H^{2'}$); δ 7.16 (poorly resolved t, 1H, H^{2})	δ 5.41 (br. s, coordinated and free ethylene); δ 3.50 (s, 3H, H^{6}); δ 2.06 (poorly resolved pent., 1H, Pd-CH_2Me); δ 1.35 (poorly resolved pent., 1H, Pd-CH_2Me); δ 0.58 (s, 3H, Pd-CH_2*Me*)
3f	δ 7.90 (poorly resolved t, 1H, $H^{3'}$); δ 7.71 (masked t, 1H, H^{3}); δ 7.05 (m, 4H, $H^{2,2',4,4'}$);	δ 5.41 (br. s, free ethylene); δ 4.64 (poorly resolved d, 2H, coordinated ethylene); δ 4.44 (poorly resolved d, 2H, coordinated ethylene); δ 3.56 (s, 3H, H^{6}); δ 2.84 (s, 3H, $H^{7'}$); δ 2.60 (s, 3H, H^{7}); δ 1.90 (poorly resolved pent., 1H, Pd-CH_2Me); δ 1.44 (poorly resolved pent., 1H, Pd-CH_2Me); δ 0.57 (s, 3H, Pd-CH_2*Me*)

[a] Spectra recorded in CD_2Cl_2 at -60 °C. Chemical shifts reported as δ ppm values, referenced relative to residual proton signals of the solvent. BAr′$_4$-counterion resonances omitted for clarity.

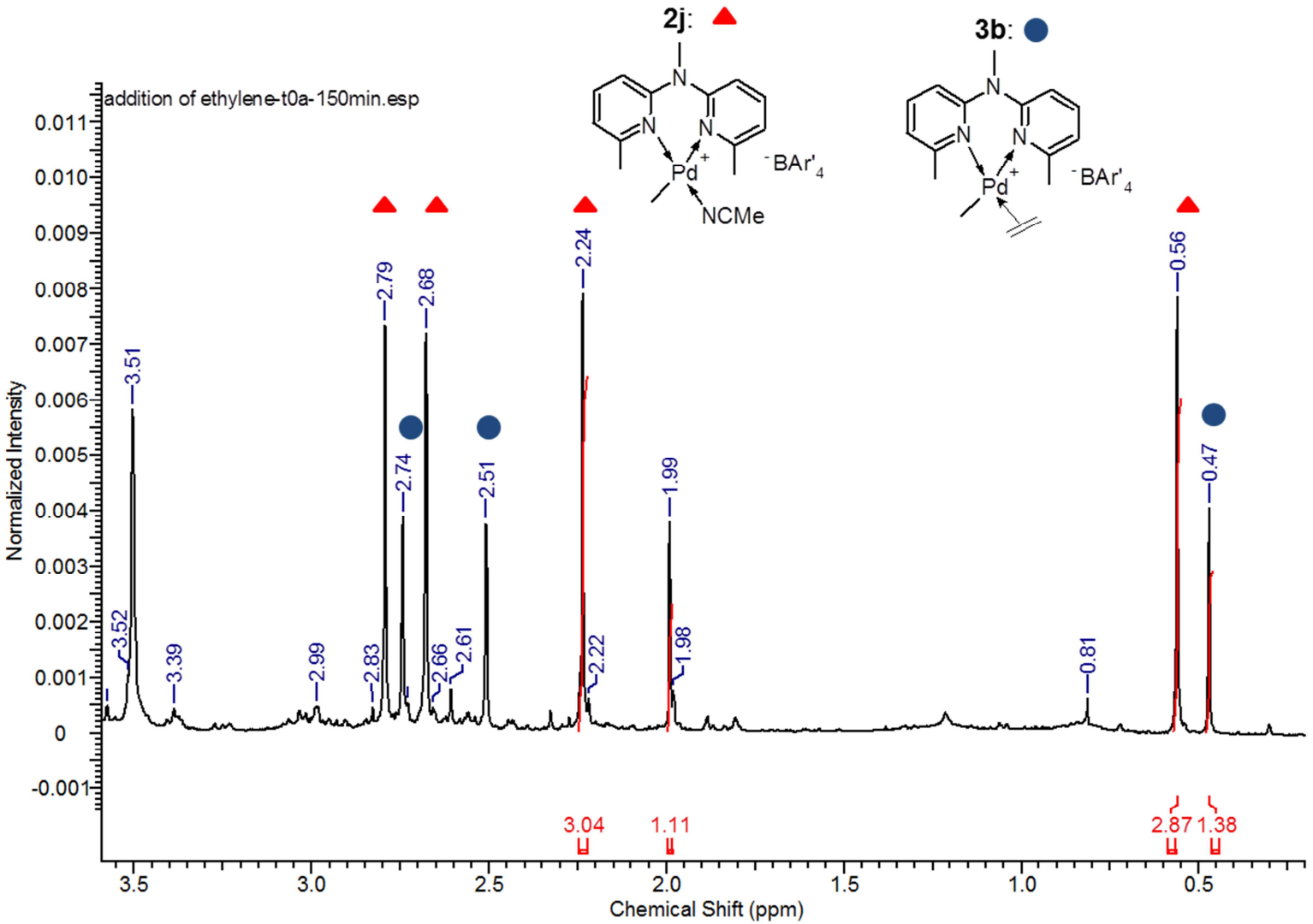

Fig. 3.10 ^{1}H NMR spectrum (aliphatic region) of the conversion of **2j** to **3b** after 150 min at -78 °C showing relative formation of species **3b**.

Scheme 3.3 Determination of ethylene insertion kinetics for Pd-methyl π-ethylene species, **3a** and **3b**.

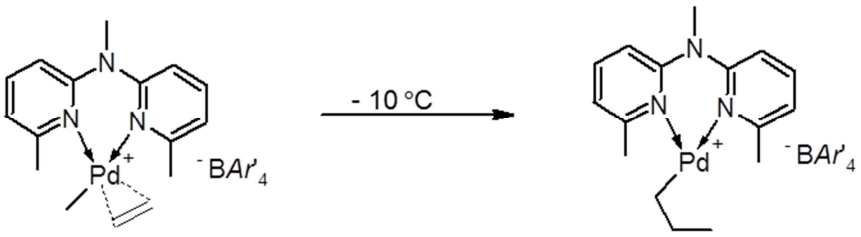

For species **3a**, $k_{insert,Me}$ was found to be 9 (± 1) x 10^{-4} s^{-1}. This value is in a similar range reported for the insertion of ethylene into the Pd-Me bond of cationic bis(5-methylpyridyl)methane palladium complexes and suggests that changing the bridgehead atom from carbon to nitrogen has negligible effect on the electronic nature of the metal centre.[19] In the case of species **3b**, $k_{insert,Me}$ was found to be 5.5 (± 0.5) x 10^{-4} s^{-1}. In comparison to species **3a** the insertion rate is approximately 1.5 times slower for species **3b**.

This decrease may be attributed to a decrease in the electrophilicity of the metal centre due to the e^--donating ability of the methyl substituents with a concomitant decrease in reactivity toward ethylene. A similar observation was made by Milani and co-workers when evaluating the insertion aptitude of methyl-substituted phenanthroline palladium complexes.[21] They found that the ethylene insertion rate decreased with an increase in the number of methyl substituents on the phenanthroline moiety, thereby increasing the basicity of the phenanthroline ligand.

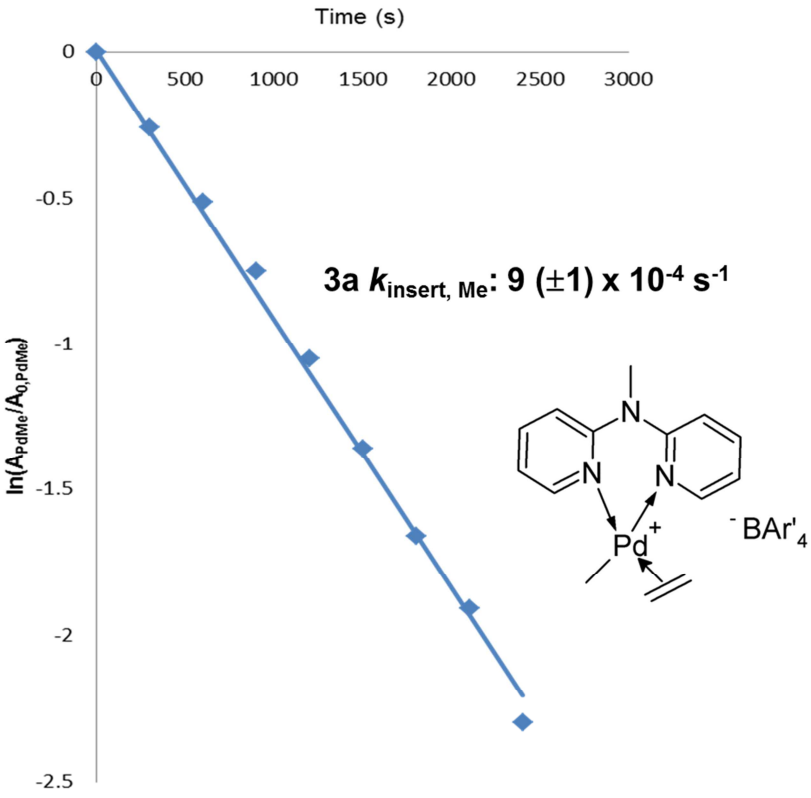

Fig. 3.11 Kinetic plot of ethylene insertion into Pd-Me bond of species **3a**.

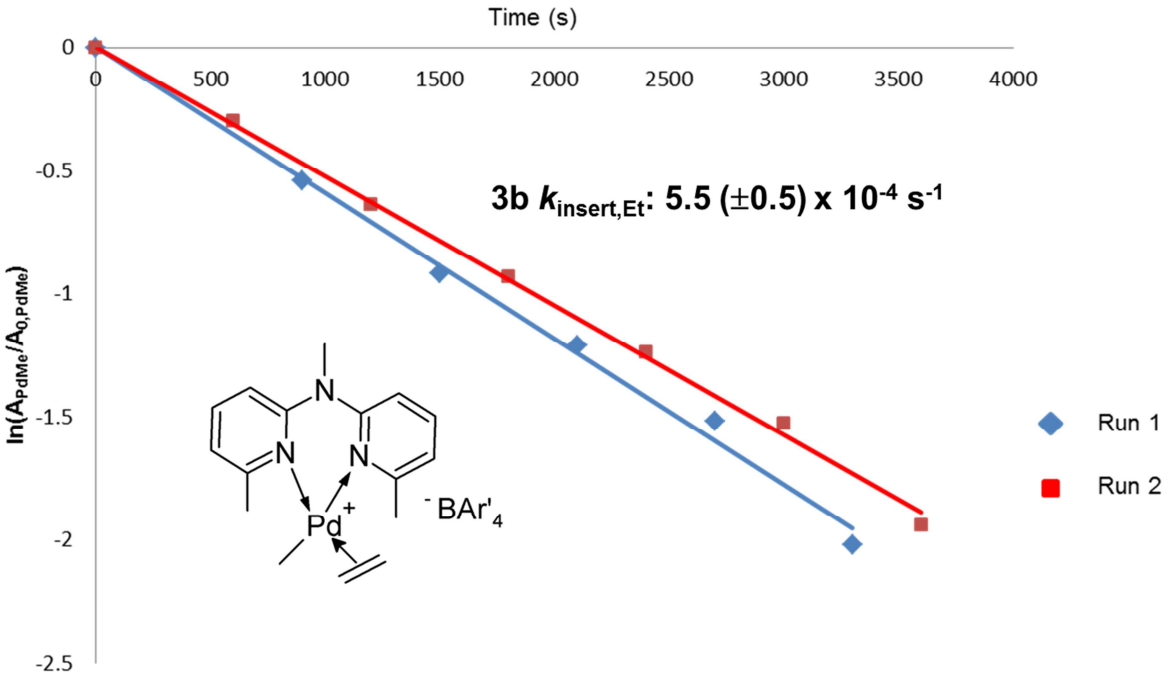

Fig. 3.12 Kinetic plot of ethylene insertion into Pd-Me bond of species **3b**.

3.2.4 Identification of the catalyst resting state [PdEt(N-N)(CH_2=CH_2)]$^+$ (3e and 3f).

The reaction of species **3c** and **3d** with ethylene at -10 °C allowed for the detection of ethylene oligomers and determination of the catalyst resting state (Scheme 3.4).

Scheme 3.4 Determination of the Pd-ethyl π-ethylene species as the catalyst resting state.

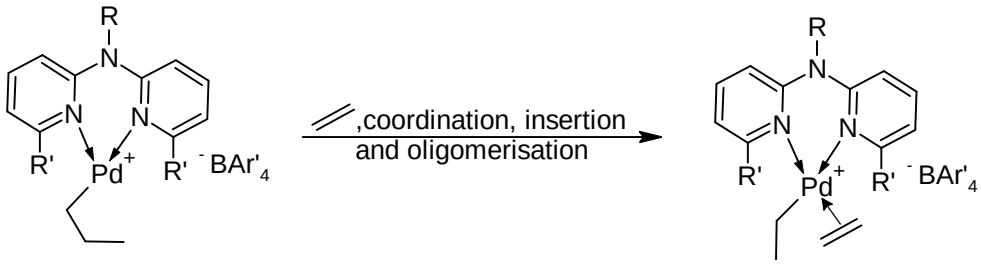

3c: R = Me, R' = H

3d: R = Me, R' = Me

3e: R = Me, R' = H

3f: R = Me, R' = Me

The resting state was identified as the [(N-N)Pd(Et)(H_2C=CH_2)]$^+$ species (**3e** and **3f**) by ^{1}H NMR spectroscopy (Table 3.2, Fig. 3.13 and 3.14). In species **3e** the PdC*H*$_2$Me resonances are diastereotopic and thus observed as poorly resolved pentets at δ 2.06 and δ 1.35 ppm respectively. The PdCH$_2$*Me* resonance was observed as a triplet ($^3J_{H-H}$ 7.42) at δ 0.58 ppm. Analogously, for species **3f** the PdC*H*$_2$Me resonances was observed at δ 1.90 and δ 1.44 ppm, while the PdCH$_2$*Me* resonances was observed as a triplet ($^3J_{H-H}$ 7.42) at δ 0.57 ppm. The identification of the Pd-ethyl π-ethylene species as the resting state confirms the nature of the reaction being first-order in palladium and zero-order in ethylene.[1c,3b,18]

The decreased reactivity of species **3b**/**3d** in comparison to **3a**/**3c** was also observed when quantifying the moles of butenes formed per mole of catalyst as a function of time. Our results allowed for an estimate of the rate of insertion of ethylene into the Pd-Et bond, $k_{insert,Et}$, of the catalyst resting state (Fig. 3.15 and 3.16).

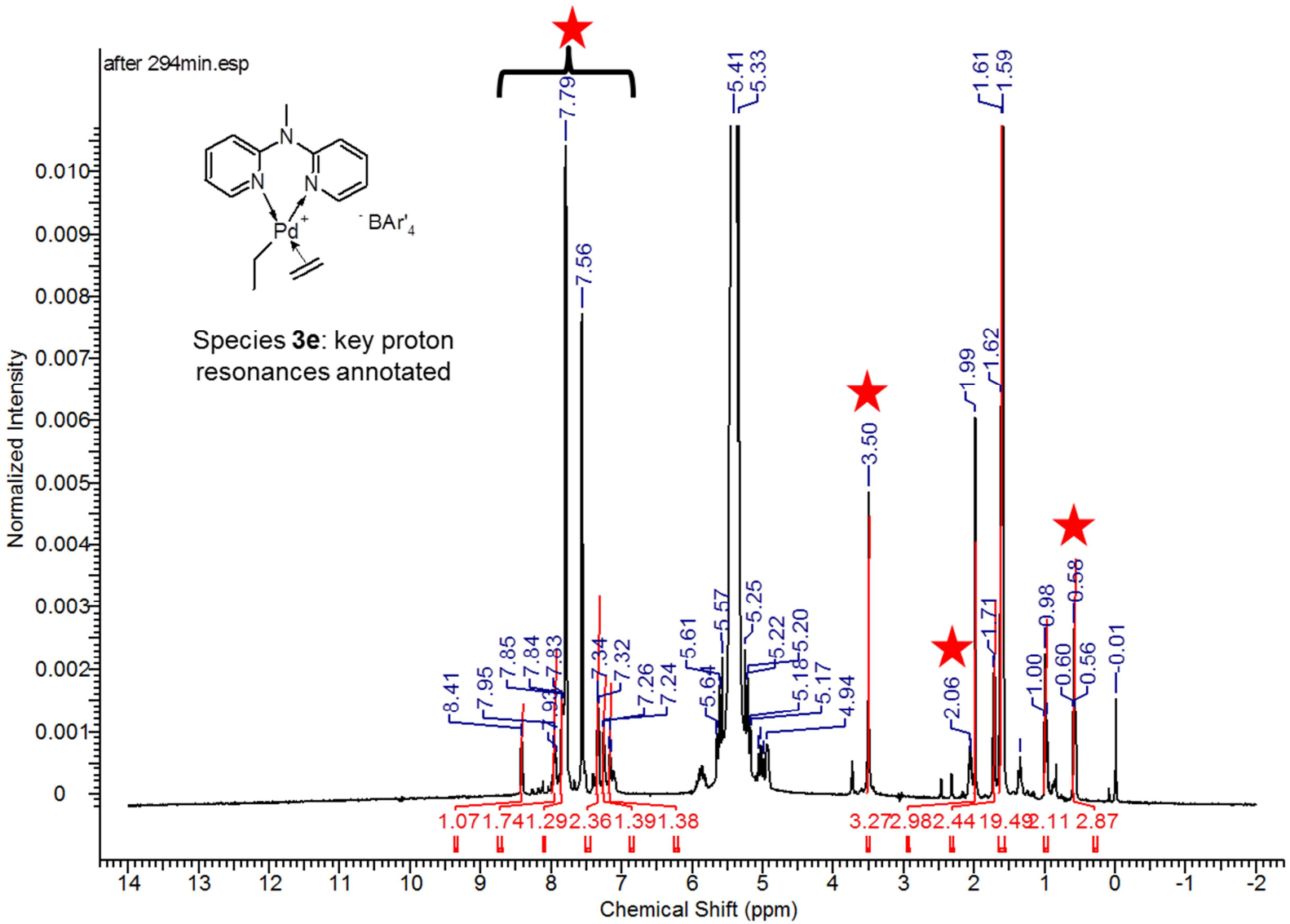

Fig. 3.13 ^{1}H NMR spectrum of the reaction of species **3c** with ethylene (after 294 min), generating species **3e** and oligomers.

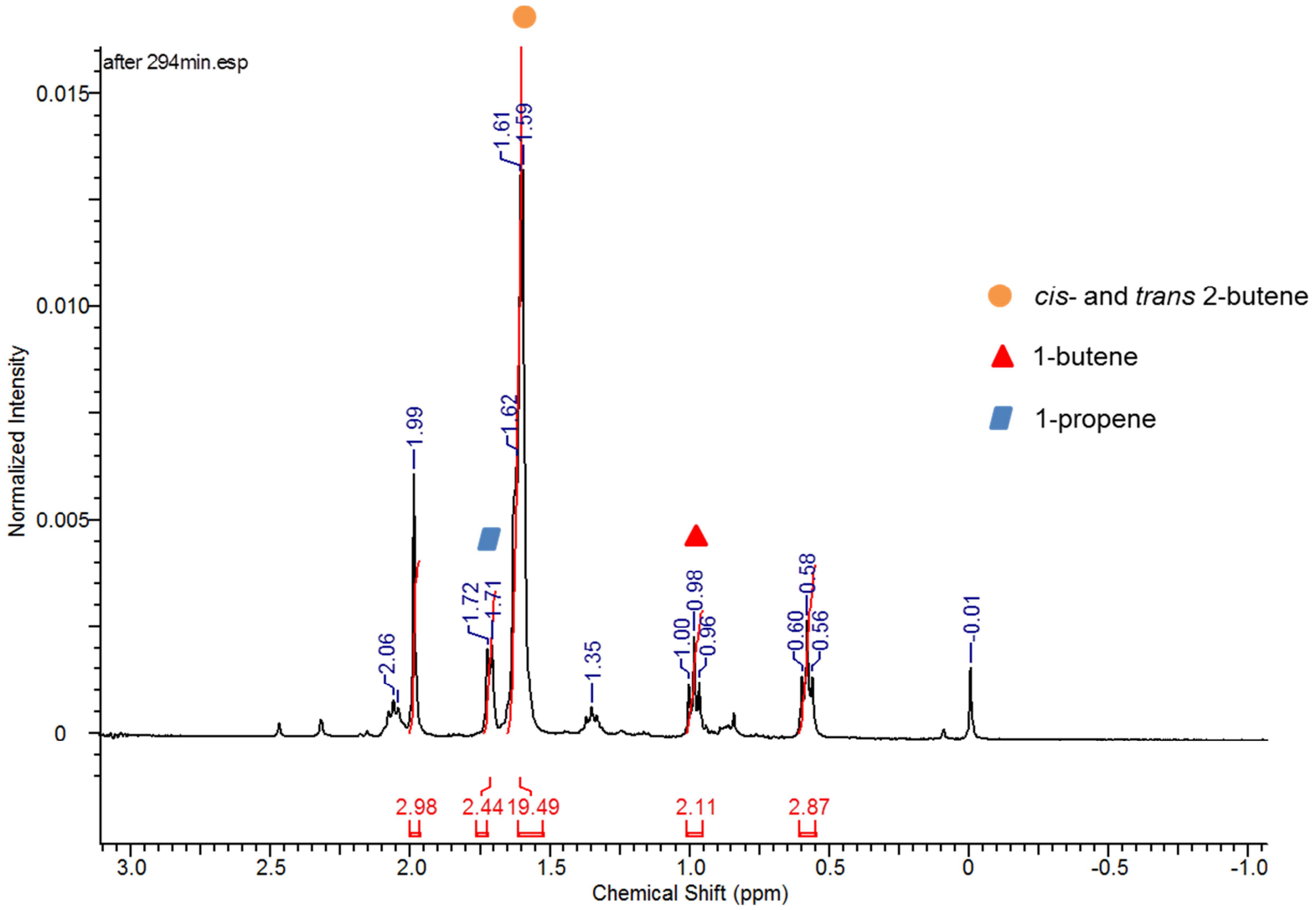

Fig. 3.14 ^{1}H NMR spectrum of the reaction of species **3c** with ethylene, with the oligomers annotated.

In the case of species **3e**, the insertion of ethylene, $k_{insert,Et}$ was estimated to be 4.0 x 10^{-4} s^{-1}, while for species **3f** this was estimated to be 0.8 x 10^{-4} s^{-1}. Consistent with our earlier observation relating to differences in ethylene insertion rates, ethylene insertion for **3e** is approximately twice as fast in comparison to **3f**.

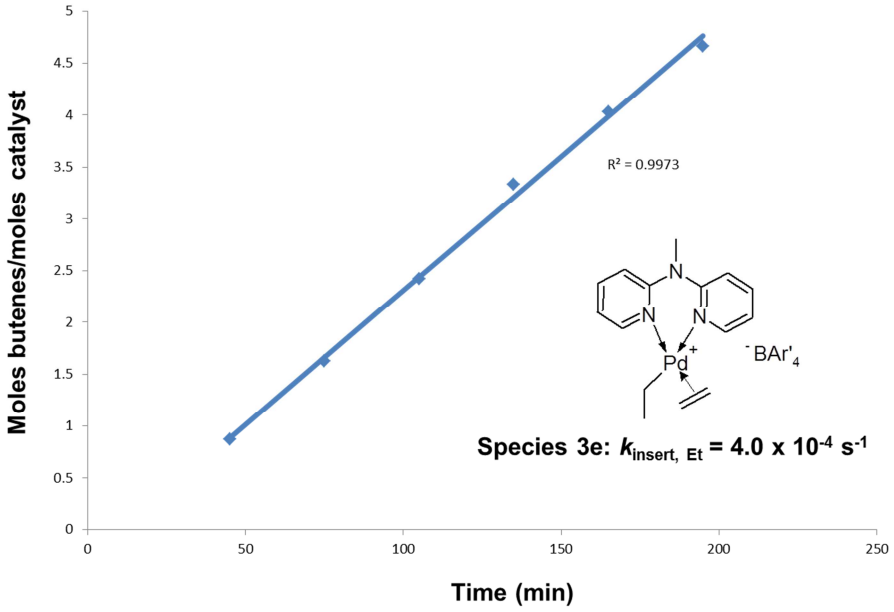

Fig. 3.15 Kinetic plot of ethylene insertion into the Pd-Et bond of species **3e** at -10 °C.

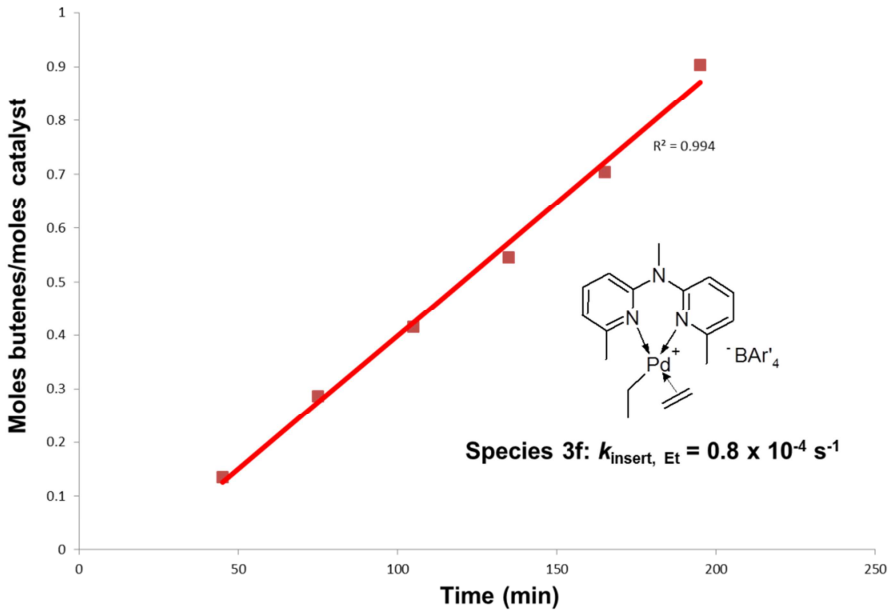

Fig. 3.16 Kinetic plot of ethylene insertion into the Pd-Et bond of species **3f** at -10 °C.

Again, this may be rationalised on the basis of a decrease in the electrophilicity of the metal centre in **3f** as a result of the electron-donating ability of the *o*-Me substituents. Our experimental comparison of the insertion kinetics provide a number of insights. Firstly, ethylene-acetonitrile exchange to generate the Pd-methyl π-ethylene species, is slower for **2j** in comparison to **2f**. For **2j**, this process also requires higher energy (-40 °C versus -78 °C), suggesting that ethylene exchange has a higher energy barrier for **2j** than for **2f**. Also, ethylene insertion and subsequent oligomerisation via the catalyst resting state, Pd-ethyl π-ethylene species, is significantly slower for **2j** than for **2f**. This observation suggests that steric bulk in the investigated catalytic systems results in a decrease in both ethylene exchange rates as well as the rate of formation of the catalyst resting state and the rate of ethylene oligomerisation. To gain further insight, the ethylene oligomerisation mechanism was investigated by density functional theory (DFT) calculations.

3.3 DFT investigation of the ethylene oligomerisation mechanism and correlation with experimental observations.

3.3.1 Rationale of the theoretical investigation.

A theoretical evaluation of the catalytic mechanism was undertaken in an attempt to correlate the observed reactivity with what would be predicted from a theoretical perspective. Experimentally, the cationic palladium methyl complexes are active as ethylene dimerisation catalysts, forming 2-butenes as major products. From a theoretical perspective the following experimental observations were probed using DFT:

1. Are there differences in the energetics of ethylene exchange to generate the first species in the catalytic cycle i.e. the Pd-methyl π-ethylene species?

2. Does ethylene dimerisation proceed via a lower energy pathway relative to longer-chain oligo-/polymerisation and what are the factors influencing selective ethylene dimerisation?
3. How facile is the 1st olefin-formation step i.e. propylene-formation, relative to chain propagation and does olefin formation proceed via β-hydrogen transfer (BHT) or β-hydride elimination (BHE)?
4. Can the observed reactivity trends between the evaluated cationic Pd-methyl catalysts be rationalised using a theoretical approach?

The kinetic results and low-temperature experiments confirmed that the Cossee-Arlman mechanism for chain growth was operative, thus our point of departure for the theoretical investigation was the cationic acetonitrile-adducts, **2f** and **2j**.

3.3.2 Functional Validation for Pd-catalysed ethylene oligomerisation.

3.3.2.1 Functional Validation.

The neutral complex **2e** and its atomic coordinates, bond lengths and angles have been reported in Chapter 2 as determined by SCD analysis. A prerequisite for reliable quantum-chemical computational evaluations is the use of accurate molecular geometries.[22]

Thus three nonlocal Generalised Gradient Approximation (GGA) exchange-correlation functionals available in the Dmol^3 density functional theory (DFT) code, which forms part of Materials Studio (Accelrys)[23] software package and the Double Numeric Polarization (DNP) basis set was employed to reproduce three structures derived from the SCD data for complex **2e**. The calculated bond distances and angles are tabulated (Table 3.3), which shows that the average deviation from the experimentally determined bond lengths is smallest for the PW91 and PBE functionals. When comparing the bond angles the

average deviation is much less for the PW91 functional in comparison to the PBE functional, thus our choice of functional and basis set for all the computations evaluated was Dmol^3/PW91/DNP.

Table 3.3 Functional validation based on comparative experimental and calculated molecular geometry parameters.

	Experimental	**PW91**	**PBE**	**RPBE**
Pd1-N1 (*trans* to Cl)	2.051	2.142	2.143	2.191
Pd1-N1 (*trans* to Me)	2.157	2.275	2.274	2.347
Pd1-C8	2.070	2.067	2.067	2.081
Pd1-Cl1	2.321	2.354	2.353	2.375
A.D[a]	0	0.060	0.060	0.099
N1-Pd1-N1′	83.31	81.187	80.811	79.527
N1-Pd1-C8	91.54	94.675	94.903	95.456
N1-Pd1-Cl1	174.03	176.758	176.749	176.115
N1′-Pd1-Cl1	97.29	96.723	97.236	97.408
N1′-Pd1-C8	172.08	169.584	170.341	169.163
Cl1-Pd1-C8	87.20	86.967	86.630	87.159
A.D[a]	0	0.074	0.203	-0.622

[a] Average deviation from experimental values.

3.3.2.2 Associative or dissociative ethylene exchange from the cationic acetonitrile-adduct, 2f and 2j.

Our initial calculations were directed toward a comparative examination of acetonitrile displacement by ethylene and whether it would occur preferentially by an associative or dissociative mechanism (Scheme 3.5). Our low-temperature experiments showed that this process was more facile for complex **2f** than **2j** and we sought to confirm

this theoretically. Our computational results showed that in the case of **2f**, associative displacement of acetonitrile by ethylene was facile and proceeded via the five-coordinate species, **2f-π$_{ethylene}$** with no maximum along the potential energy surface (Fig. 3.17). Dissociative exchange was calculated to proceed via a three-coordinate intermediate, **2f-MeCN**, endothermic by 9.2 kcal/mol.

Scheme 3.5 Associative or dissociative ethylene-acetonitrile exchange operative for complexes **2f** and **2j**.

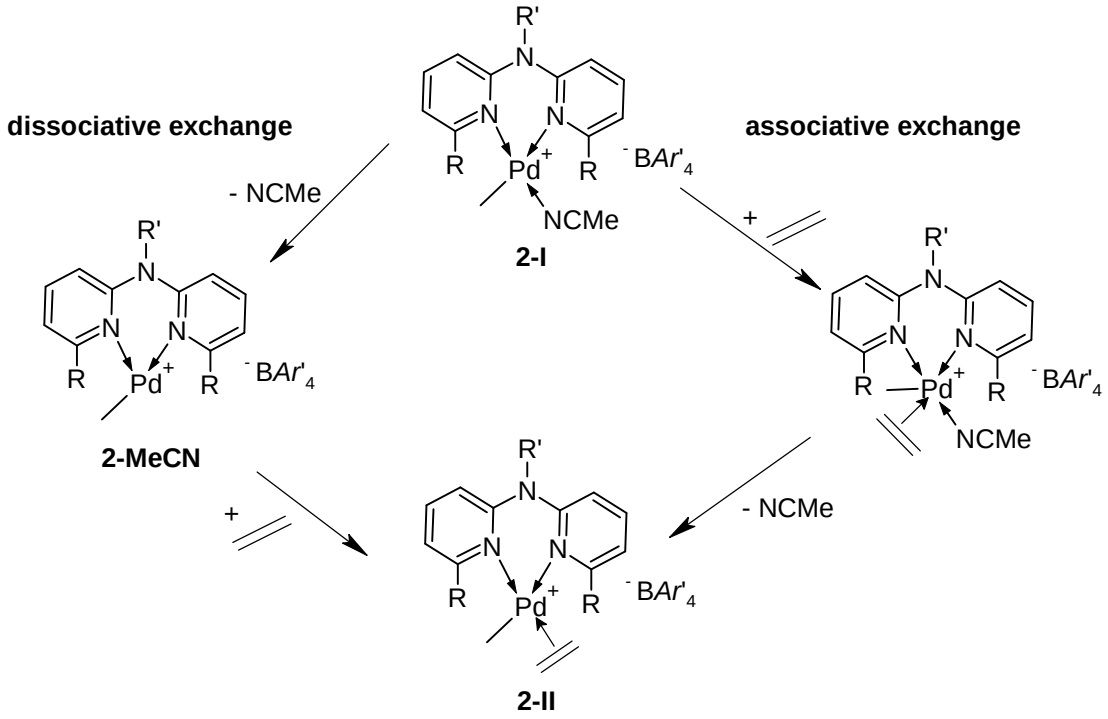

The product of associative/dissociative exchange, the Pd-methyl π-ethylene species; **2f-II**, was calculated to be exothermic by 10.3 kcal/mol relative to **2f-I**. In contrast to **2f**, our computational evaluation of the transformation of **2j-I** to **2j-II** shows that associative exchange via species **2j-π$_{ethylene}$** is endothermic by 4.2 kcal/mol. In addition the energy difference between associative exchange, **2j-π$_{ethylene}$**, and dissociative exchange via the three-coordinate intermediate, **2j-MeCN** ($\Delta G_{298.15K}$ +5.0 kcal/mol), is 0.8 kcal/mol. The

product of associative/dissociative exchange, **2j-II**, was calculated to be exothermic by 10.5 kcal/mol relative to **2j-I**.

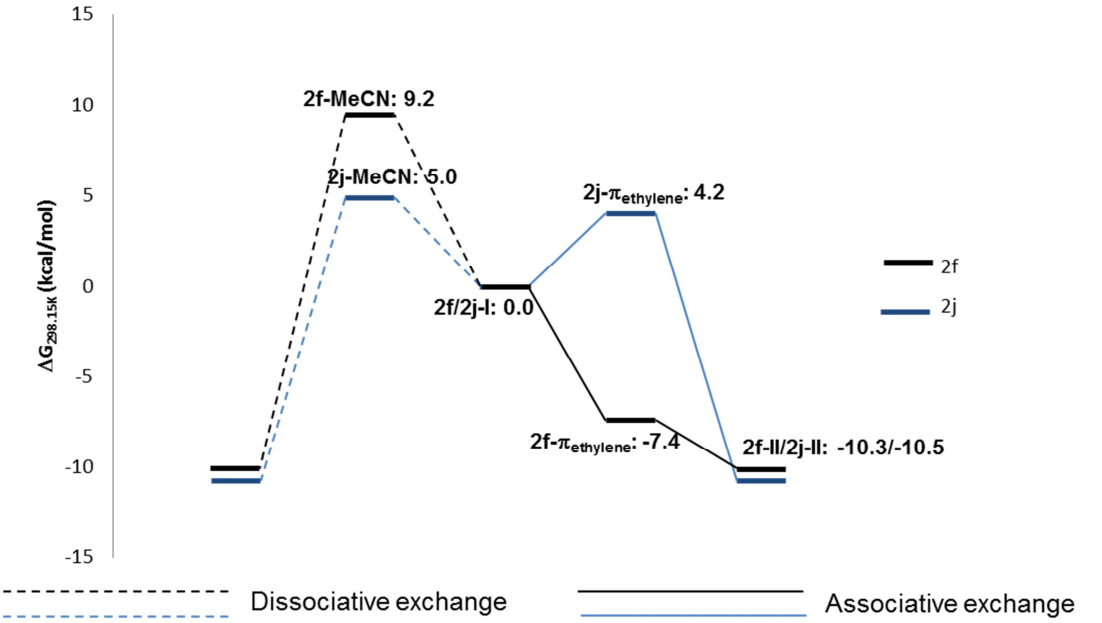

Fig. 3.17 Energy profile of comparative associative and dissociative ethylene exchange from complex **2f** and **2j**. Calculated Gibbs free energies ($\Delta G_{298.15K}$) reported at 298.15 K and 1 atm.

Our results firstly confirmed the more facile associative displacement of acetonitrile in **2f** in comparison to **2j** oberved in the kinetic experiments and provided a theoretical correlation that ethylene coordination to the cationic metal centre proceeds via associative exchange and that steric bulk increases the energy barrier associated with the exchange process.[2,20] Secondly, it showed that in the case of **2j**, associative exchange was only slightly more exothermic than the dissociative alternative. It should be noted that in each case no transition state structure for associative or dissociative exchange could be located. The optimised structures for the species shown in Scheme 3.5 are shown in Figure 3.18.

3.3.2.3 Ethylene insertion from species 2-II to generate the cationic Pd-propyl species, 2-III.

Our next consideration was the comparative ethylene insertion behaviour for species **2-II** (Fig. 3.19). Because of the symmetrical nature of the complex, discrimination between different insertion pathways was not necessary.[24]

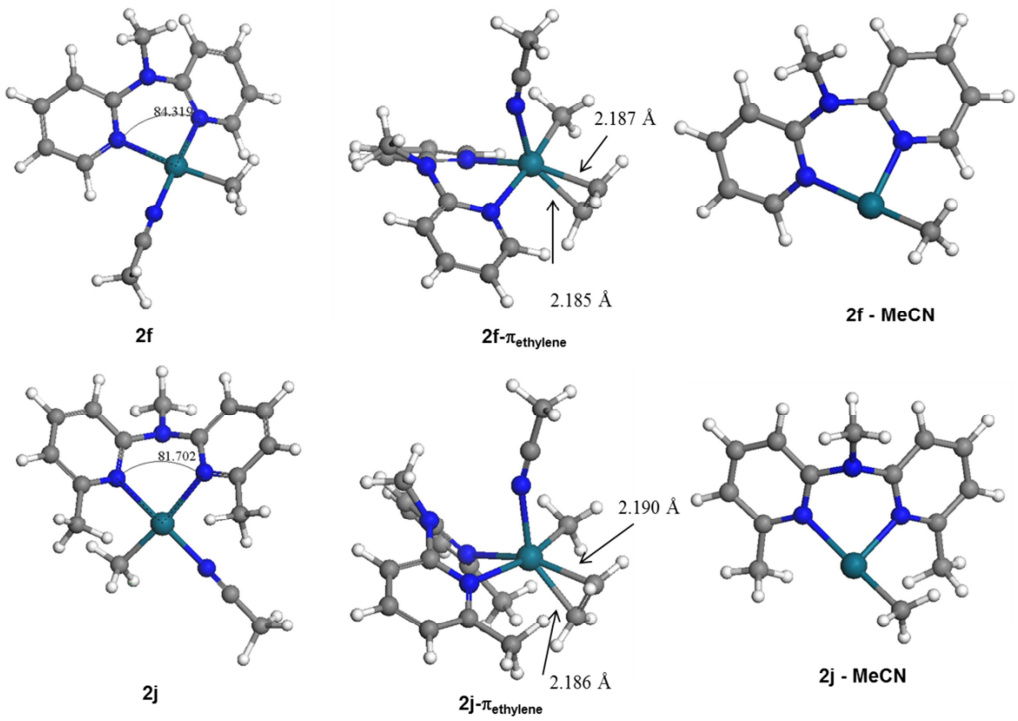

Fig. 3.18 Optimised structures of the species shown in Scheme 3.4.

Our calculations showed that ethylene insertion from **2-II** proceeded via **TS[2-II-2-III]** which was endothermic by 17.5 kcal/mol (in the case of **2f**) and 16.6 kcal/mol (in the case of **2j**) (Fig. 3.19). The obtained transition state structures showed the ethylene moiety rotated in-plane with a C_{Me}-C_{β} bond distance of 2.102 Å, in the case of **TS[2f-II-2f-III]**, and 2.105 Å in the case of **TS[2j-II-2j-III]**. The calculated barrier for insertion is within the range generally observed by both experiment and theory for palladium catalyst systems (+17 to +18 kcal/mol).[1c,4a,5]

The products of insertion, **2-III**, was calculated to be the Pd-propyl species, in which the vacant coordination site of the metal was stabilised by a β-agostic interaction (Fig. 3.20).[25]

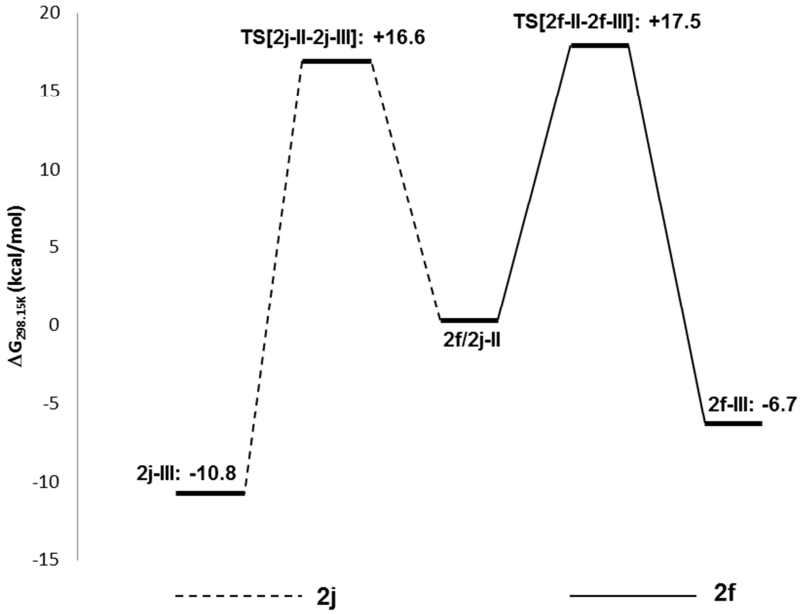

Fig. 3.19 Energy profile of comparative ethylene insertion for species **2f-II** and **2j-II**. Calculated Gibbs free energies ($\Delta G_{298.15K}$) reported at 298.15 K and 1 atm.

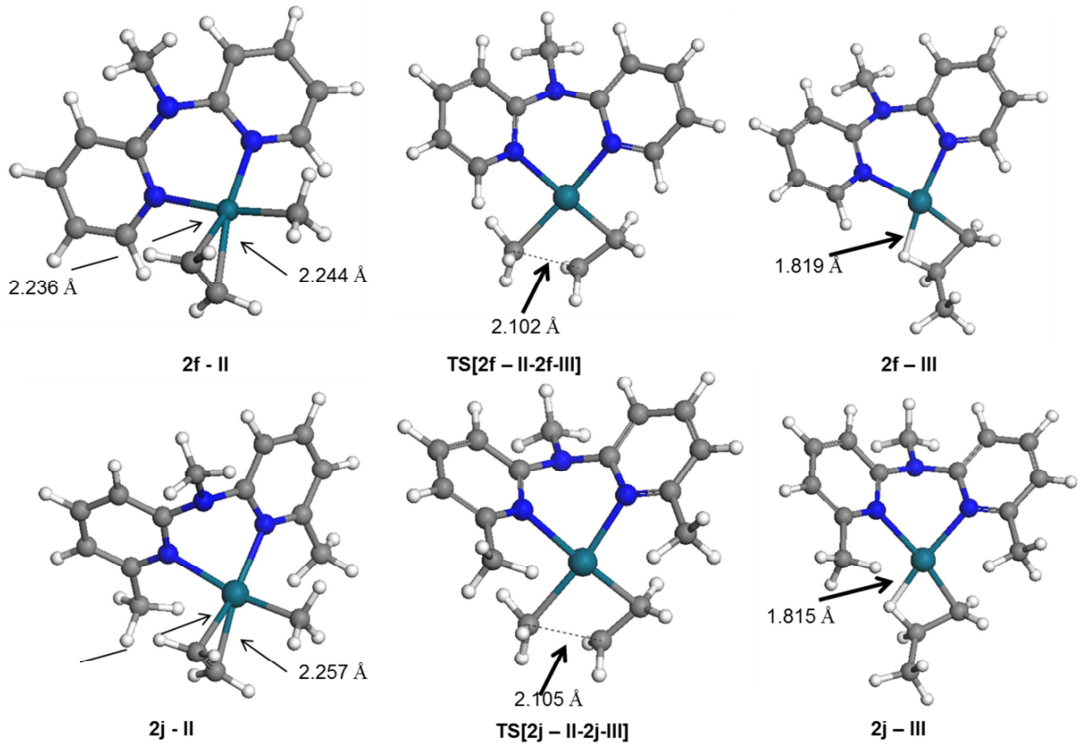

Fig. 3.20 Optimised structures of the minima and transition states for the transformation from **2-II** to **2-III**.

The optimised structure showed the propyl-chain rotated in-plane with a Pd-H_β bond length of 1.819 Å (in the case of **2f-III**) and 1.815 Å (in the case of **2j-III**). The insertion products **2f-III** and **2j-III** were calculated to be exothermic by 6.7 and 10.8 kcal/mol respectively (in comparison to **2-II**).

3.3.2.4 The propensity for chain termination via BHT or BHE, or further insertion.

A key step following insertion to generate the cationic Pd-propyl species, **2-III**, is chain termination via β-hydrogen transfer (BHT) or β-hydride elimination (BHE). The pathway which predominates has a direct impact on the termination process which is operative for a particular catalytic system. It has been demonstrated computationally to differ for nickel and palladium, with BHT being favored for nickel and BHE being favored for palladium.[3b,4b,26] Scheme 3.6 shows the products of each process.

Scheme 3.6 Possible chain-termination processes which may be operative during catalysis.

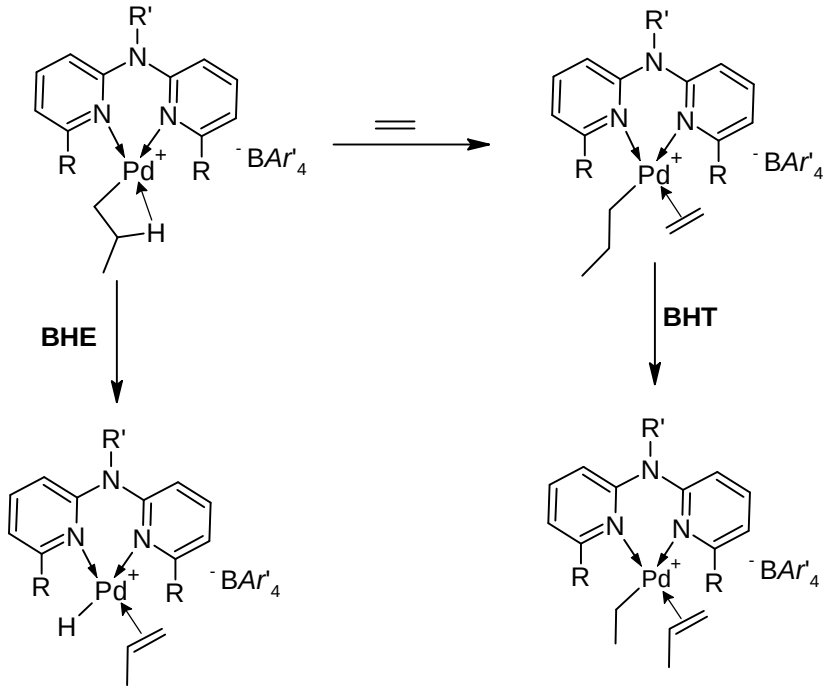

In the case of BHT, following coordination of ethylene to the Pd-propyl species, the product generated would be a Pd-ethyl π-propylene species, which could undergo

associative/dissociative olefin exchange with an incoming ethylene molecule to generate the Pd-ethyl π-ethylene species. Subsequent insertion would generate the Pd-butyl species. In the case of BHE, the product would be a Pd-hydride π-propylene species which could undergo associative/dissociative olefin exchange to generate the Pd-ethyl π-ethylene species. Further insertion would generate the Pd-butyl species. In addition, the Pd-propyl π-ethylene species generated in the BHT process can also undergo insertion to generate a Pd-pentyl species. With this in mind comparative chain termination via BHE and BHT and further insertion was evaluated computationally.

Our calculations showed that for both species **2f-III** and **2j-III** chain termination proceeded via β-hydride elimination (Fig. 3.21).

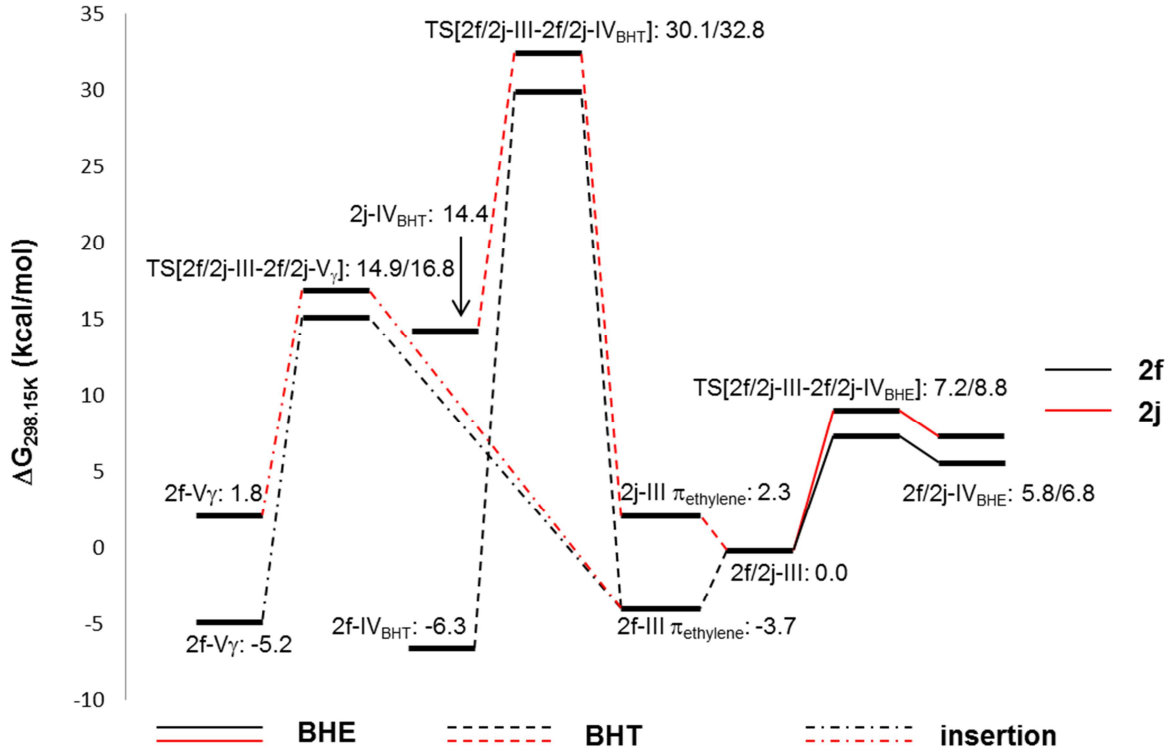

Fig. 3.21 Energy profile of comparative chain termination via BHE or BHT and olefin insertion. Calculated Gibbs free energies ($\Delta G_{298.15K}$) reported at 298.15 K and 1 atm.

A late transition state **TS[2f-III-2f-IV$_{BHE}$]** and **TS[2j-III-2j-IV$_{BHE}$]** was located in each case and was calculated to be endothermic by 7.2 kcal/mol (**TS[2f-III-2f-IV$_{BHE}$]**) and +8.8 kcal/mol (**TS[2j-III-2j-IV$_{BHE}$]**) relative to **2f/2j-III**. The transition state structure was characterised by a C_β-H bond distance of 2.435 Å (in the case of **2f**, Fig 3.22) and 2.056 Å (in the case of **2j**, Fig 3.23). In addition the C_α-C_β bond length of the eliminating olefin was calculated as 1.382 Å and 1.388 Å for **TS[2f-III-2f-IV$_{BHE}$]** and **TS[2j-III-2j-IV$_{BHE}$]** respectively. These values are slightly longer than that reported for free propylene (1.336 Å). The product of BHE, the Pd-hydride π-ethylene species **2f-IV$_{BHE}$** and **2j-IV$_{BHE}$**, was calculated to be endothermic relative to **2f/2j-III** by 5.8 and 6.8 kcal/mol respectively.

In the case of chain termination via BHT an initial intermediate, the Pd-propyl π-ethylene species (**2f/2j-III$_{\pi\text{-ethylene}}$**) was located. For **2f**, the coordination of ethylene is exothermic by 3.7 kcal/mol whereas this process proceeds via a low-energy barrier of 2.3 kcal/mol in the case of **2j**.

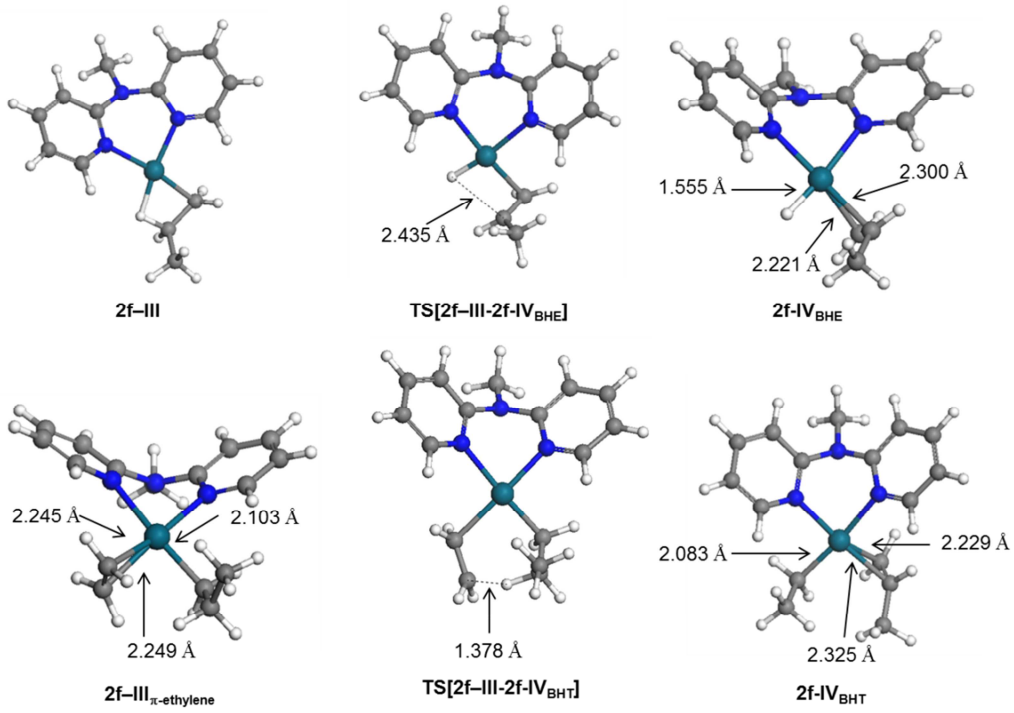

Fig. 3.22 Optimised minima and transition states for the chain termination of **2f-III** via BHE or BHT.

This difference in energetics may be attributed to an increase in steric bulk in the coordination sphere of the metal centre, which results in the destabilisation of the π-olefin complex and leads to a higher ground state energy.[25]

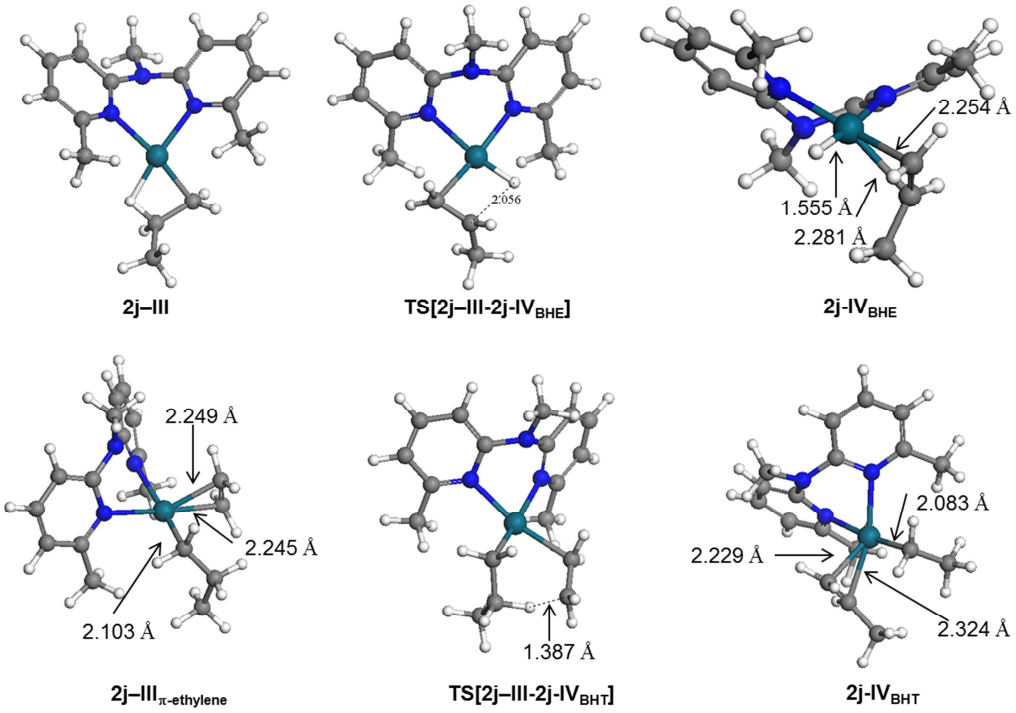

Fig. 3.23 Optimised minima and transition states for the chain termination of **2j-III** via BHE or BHT.

β-hydrogen transfer was calculated to proceed via transition state **TS[2f-III-2f-IV$_{BHT}$]** and **TS[2j-III-2j-IV$_{BHT}$]** with energy barriers of 30.1 and 32.8 kcal/mol (relative to **2f-III** and **2j-III**) respectively. In the transition state structures the ethylene and propylene moieties are oriented in-plane with a $C_{\beta(ethylene)}$-$H_{\beta(propylene)}$ bond distance of 1.378 Å and 1.387 Å for **TS[2f-III-2f-IV$_{BHT}$]** and **TS[2j-III-2j-IV$_{BHT}$]** respectively. The product of BHT, the Pd-ethyl π-propylene species (**2f-IV$_{BHT}$** and **2j-IV$_{BHT}$**) and their ground state energies relative to **2f** and **2j** demonstrated the significant impact steric pressure has on the energy of the located minima. In the case of **2f-IV$_{BHT}$** minimum was located 6.3 kcal/mol below **2f-III** whereas **2j-IV$_{BHT}$** was located 14.4 kcal/mol above **2j-III**. The resulting steric influence of

the ligand, ethyl and π-propylene moieties within the coordination sphere of the metal in **2j-IV$_{BHT}$** resulted in a significant increase in the ground state energy of **2j-IV$_{BHT}$** and accounts for the observed energy difference.

Since the formation of the Pd-propyl π-ethylene species, **2f/2j-III$_{\pi\text{-ethylene}}$**, is energetically favourable, the insertion of ethylene to form the Pd-pentyl species, **2-V**, was evaluated. Insertion was found to proceed via transition state structure **TS[2f-III$_{\pi\text{-ethylene}}$-2f-V]** and **TS[2j-III$_{\pi\text{-ethylene}}$-2j-V]**, endothermic by 14.9 and 16.8 kcal/mol respectively (relative to **2f/2j-III**, Fig. 3.24).

The transition state structures **TS[2f-III$_{\pi\text{-ethylene}}$-2f-V]** and **TS[2j-III$_{\pi\text{-ethylene}}$-2j-V]** was characterised by in-plane rotation of ethylene with $C_{\beta(ethylene)}$-$C_{\alpha(propyl)}$ bond distance of 2.112 Å. The observed bond distance is in the range observed for computed insertion transition states in Ni(II) Brookhart-type complexes.[4a] The product of insertion, **2f/2j-V**, was calculated to be exothermic by 5.2 kcal/mol (**2f-V**) and endothermic by 1.8 kcal/mol (**2j-V**) relative to **2f/2j-III**. The computed minima (**2f-V** and **2j-V**) are characterised by γ-agostic interaction with Pd-H_γ bond distances of 1.935 Å (**2f-V**) and 1.930 Å (**2j-V**).

The computational evaluation showed that the first olefin elimination proceeded exclusively via β-hydride elimination to eliminate 1-propylene and that β-hydrogen transfer to monomer was energetically unfavourable. In addition, our calculations showed that ethylene insertion into the Pd-propyl species was disfavoured relative to chain termination via BHE; thereby ruling out polymer-/long-chain oligomer formation from the Pd-propyl species.

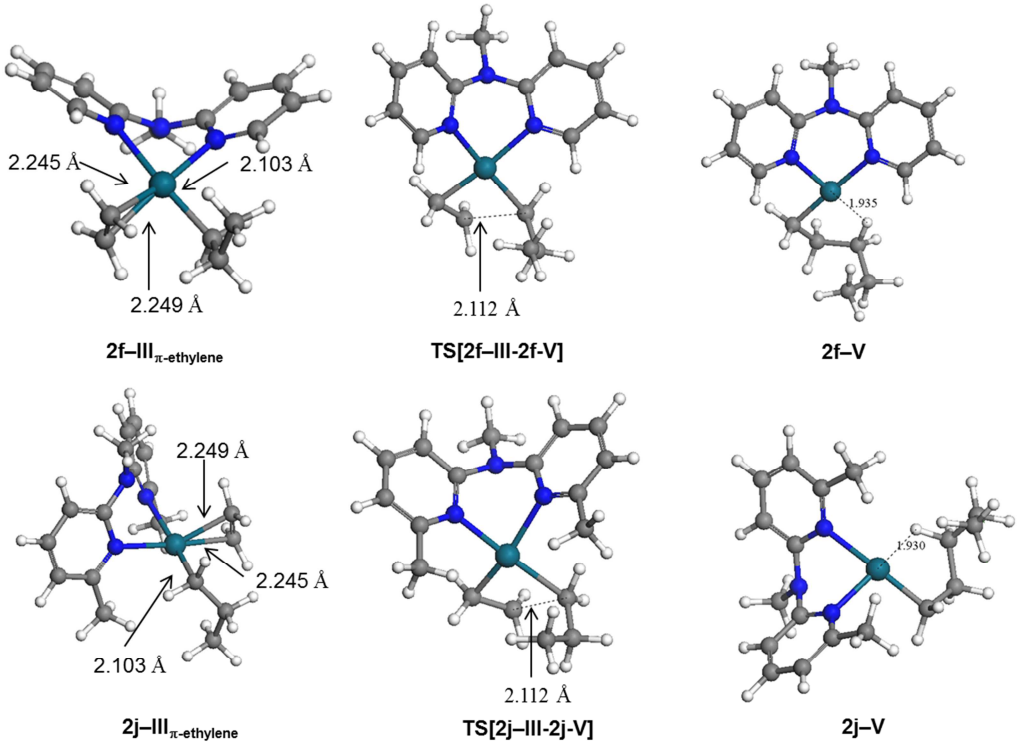

Fig. 3.24 Optimised minima and transition states for the chain propagation from **2f/2j-III$_{\pi\text{-ethylene}}$** to **2f/2j-V**.

3.3.2.5 Associative or Dissociative olefin exchange from Pd-hydride π-propylene species, 2-IV$_{BHE}$.

Previous mechanistic evaluations had established that olefin exchange of incoming ethylene with the coordinated olefin proceeds rapidly and that this exchange is governed by an associative mechanism (Scheme 3.7).[3b,5] Thus we evaluated whether olefin exchange would occur via an associative or dissociative mechanism and whether, in the case of associative olefin exchange, a low-lying intermediate or transition state could be located. Our computational results showed that the associative mechanism is favourable for both species **2f** and **2j** (Fig. 3.25). Associative olefin exchange was found to proceed via a five-coordinate intermediate located 3.2 kcal/mol (**2f-IV$_{\pi\text{-ethylene}}$**) and 14.3 kcal/mol (**2j-IV$_{\pi\text{-ethylene}}$**) above **2f/2j-IV$_{BHE}$**.

Scheme 3.7 Associative or dissociative chain transfer processes which may be operative during catalysis.

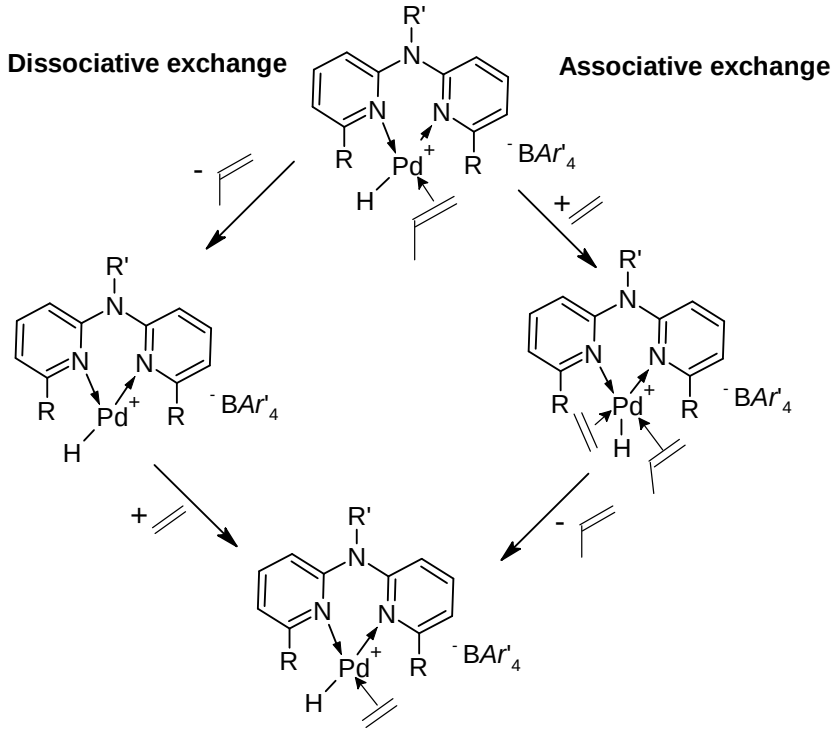

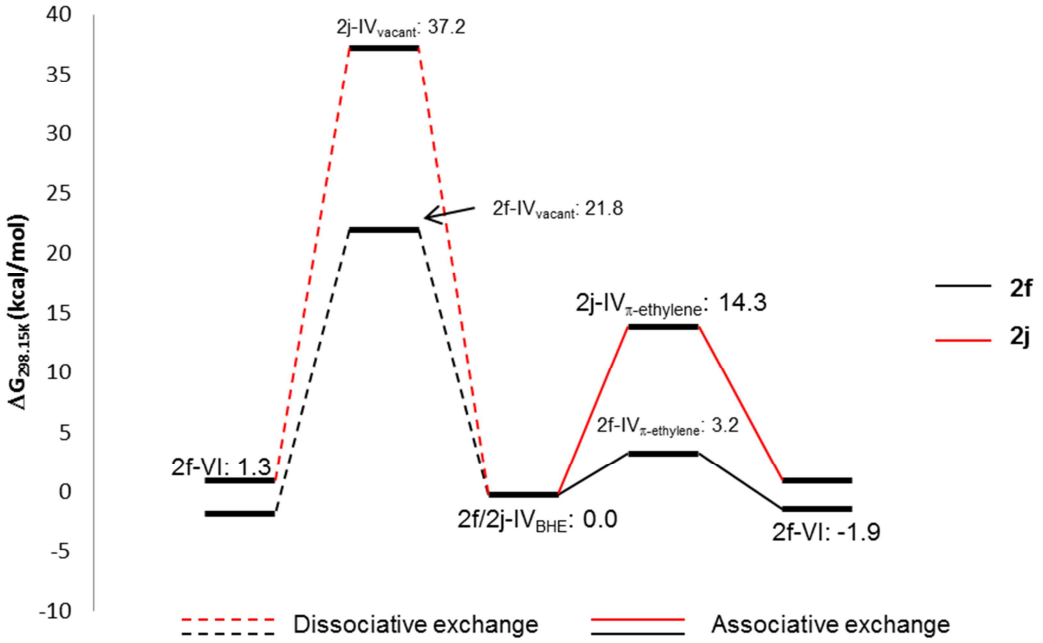

Fig. 3.25 Energy profile of comparative associative and dissociative olefin exchange from **2f/2j-IV$_{BHE}$**. Calculated Gibbs free energies ($\Delta G_{298.15K}$) reported at 298.15 K and 1 atm.

The difference in energy (ΔE = 11.1 kcal/mol if **2f/2j-IV$_{BHE}$** considered equal) between **2f-IV$_{\pi\text{-ethylene}}$** and **2j-IV$_{\pi\text{-ethylene}}$** can be attributed to differences in steric pressure in the optimised intermediates. In the optimised structures of the intermediates **2f-IV$_{\pi\text{-ethylene}}$** and **2j-IV$_{\pi\text{-ethylene}}$**, the coordinated ethylene and propylene moieties occupy the axial sites of the coordination sphere of the metal centre (Fig 3.26 and 3.27) with the angle between coordinated ethylene and propylene equal to 94.907 °. In both cases the propylene molecule displays transient coordination to the palladium centre via the $C_{[\beta(propylene)]}$ atom with a Pd-$C_{[\beta(propylene)]}$ bond distance of 2.385 Å. The C_α and C_β atoms of the coordinated ethylene (in the 5-coordinate intermediate) show elongated Pd-C bond lengths in comparison to the associative exchange product, **2-VI**, of 2.273 Å (C_α) and 2.281 Å (C_β) in comparison to 2.234 Å and 2.248 Å in **2f/2j-VI**. The Pd-H bond distances in the intermediate **2f/2j-IV$_{\pi\text{-ethylene}}$** (1.541 Å) and the associative exchange product **2f/2j-VI** (1.556 Å) does not undergo any significant elongation/contraction during the associative exchange process.

In the case of dissociative olefin exchange, the three-coordinate intermediate **2f/2j-IV$_{vacant}$** was successfully optimised. The three-coordinate intermediate was found to be endothermic by 21.8 kcal/mol in the case of **2f**, and 37.2 kcal/mol in the case of **2j**. Coordination of ethylene to the three-coordinate intermediate stabilises the highly electrophilic metal centre with a concomitant decrease in the ground state energy to generate the exchange product **2f-VI** and **2j-VI**. Thus our calculations showed that the Pd-hydride π-ethylene species, **2f/2j-VI**, was formed via associative exchange of ethylene with the Pd-hydride π-propylene species, **2f/2j-IV$_{BHE}$**.

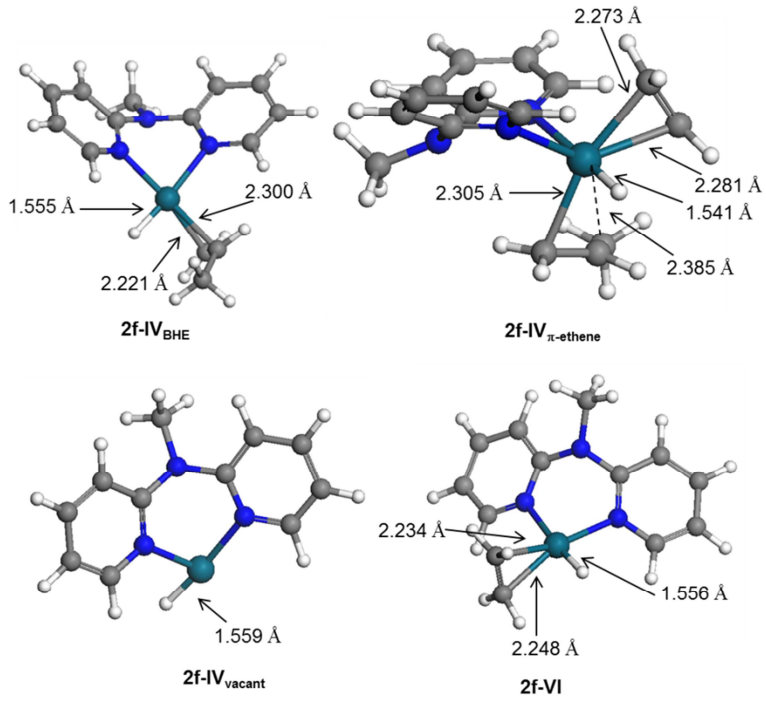

Fig. 3.26 Optimised minima and intermediates for comparative associative or dissociative olefin exchange from **2f-IV$_{BHE}$** to generate the Pd-hydride π-ethylene species, **2f-VI**.

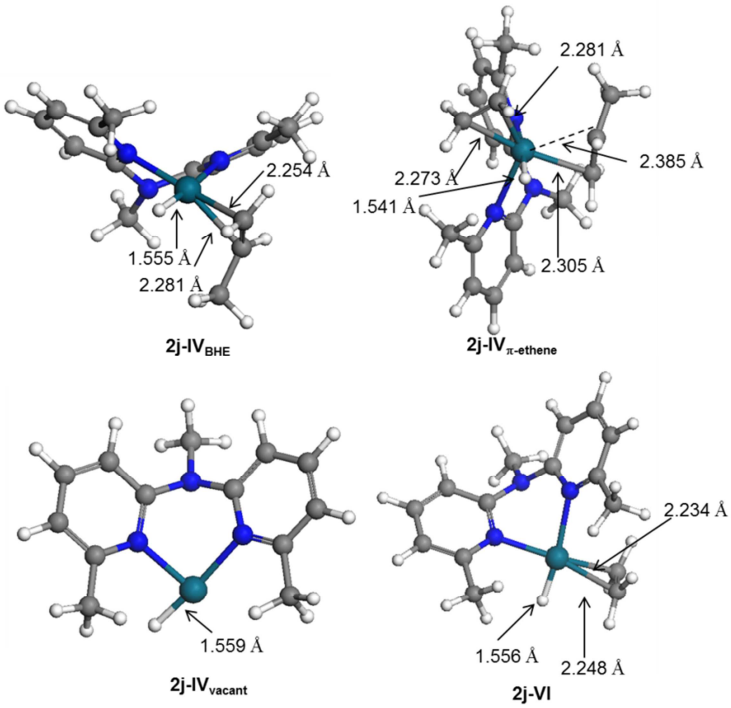

Fig. 3.27 Optimised minima and intermediates for comparative associative or dissociative olefin exchange from **2j-IV$_{BHE}$** to generate the Pd-hydride π-ethylene species, **2j-VI**.

3.3.2.6 Ethylene insertion from Pd-hydride π-ethylene species, 2-VI, to generate the Pd-butyl species, 2-IX.

Subsequently, we focussed our attention on the ease of insertion of ethylene into the Pd-H bond of the Pd-hydride π-ethylene species, **2f/2j-VI** (Scheme 3.8). Our kinetic experiments identified the Pd-ethyl π-ethylene species, **2f/j-VIII**, as the catalyst resting state. We envisaged that our computational investigation may provide insight into the energetics associated with its formation.

Scheme 3.8 Ethylene insertion from Pd-hydride species, **2-VI**.

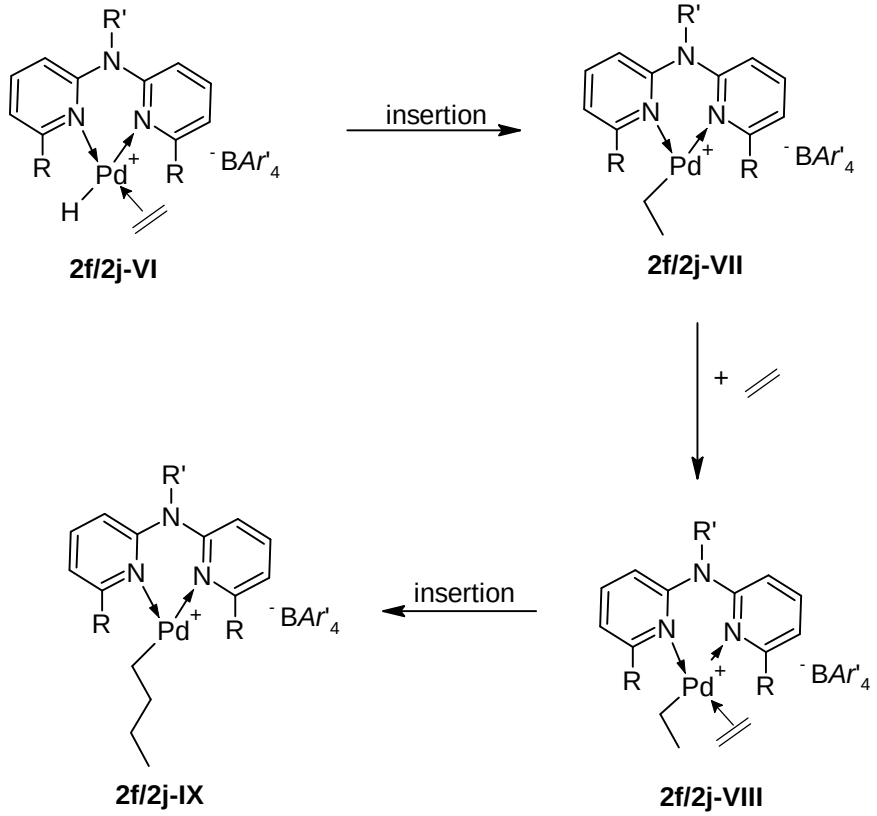

As a precursor to the catalyst resting state, insertion of ethylene into the Pd-hydride bond generated the Pd-ethyl species, **2fj/2j-VII** (Fig. 3.28). Our calculations showed that insertion proceeded via a low-energy intermediate, **2f/2j-VI$_{\text{in-plane}}$**, in which the coordinated

ethylene molecule was rotated into the plane of the palladium coordination sphere with the N,N-ligand; the coordinated hydrogen and the palladium centre being co-planar.

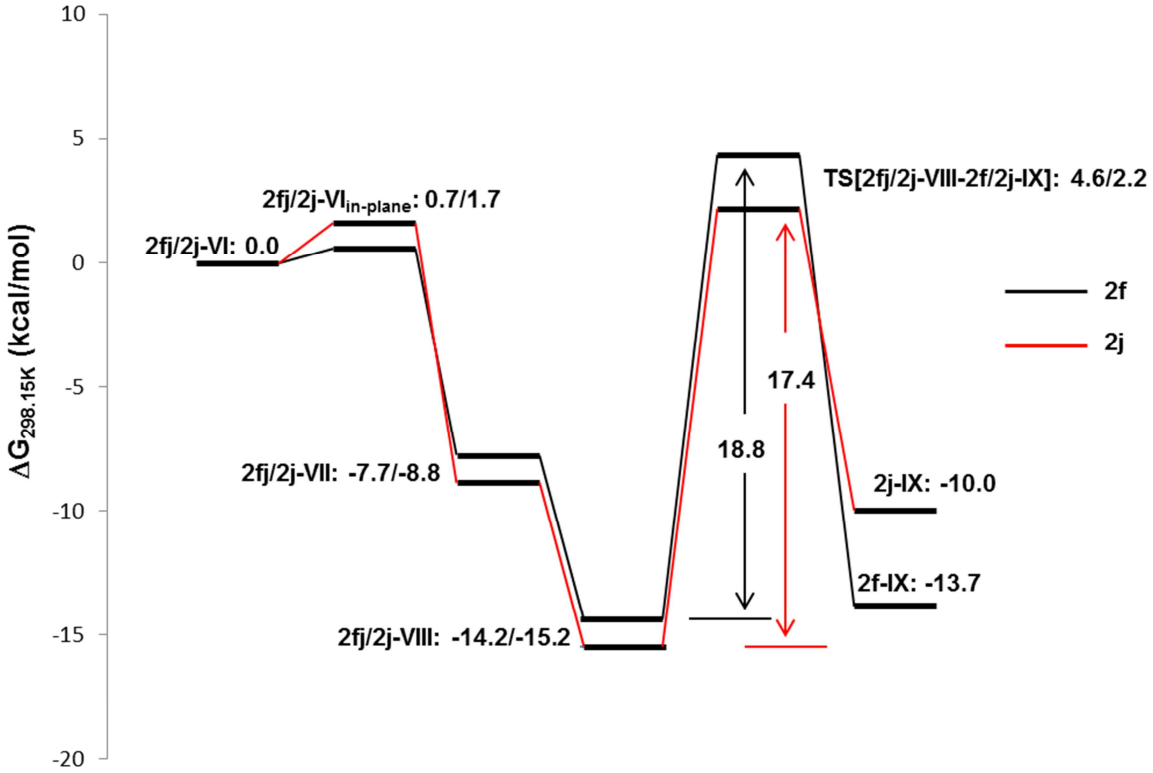

Fig. 3.28 Energy profile of comparative ethylene insertion from **2f/2j-VI;** generation of the catalyst resting state **2f/2j-VIII** and subequent insertion to generate **2f/2j-IX**. Calculated Gibbs free energies ($\Delta G_{298.15K}$) reported at 298.15 K and 1 atm.

In the case of **2f** the intermediate **2f-VI$_{in\text{-}plane}$** is 0.7 kcal/mol higher in energy than **2f-VI** whereas for **2j** the intermediate **2j-VI$_{in\text{-}plane}$** is 1.7 kcal/mol higher in energy than **2j-VI**. The insertion products, **2f-VII** and **2j-VII**, were optimised without locating a transition state structure. This suggests that ethylene insertion into **2j/2j-VI** proceeds with virtually no energy barrier. The insertion products **2f-VII** and **2j-VII** were calculated to be exothermic by 14.2 kcal/mol and 15.2 kcal/mol respectively. The optimised structures of **2f-VII** and **2j-VII** show that the cationic species is stabilised by a β-agostic interaction, with Pd-H$_\beta$ bond distances of 1.848 Å and 1.840 Å respectively (Fig. 3.29).

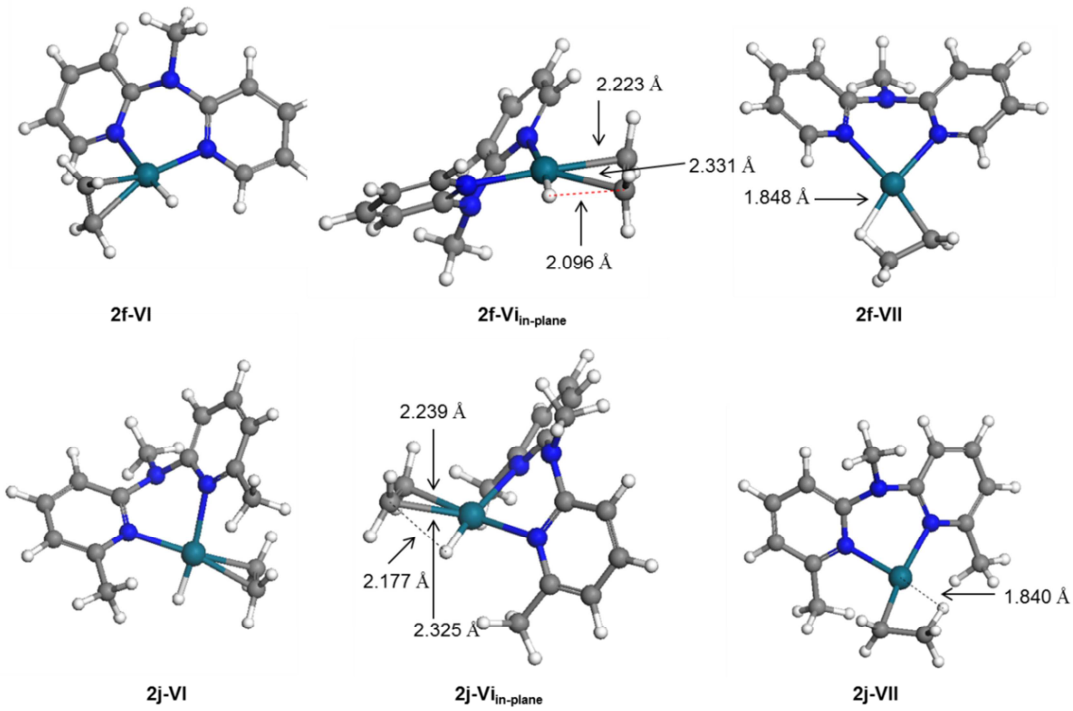

Fig. 3.29 Optimised minima and intermediates for ethylene insertion from **2f/2j-VI** to generate the Pd-ethyl species, **2f/2j-VII**.

Next we evaluated the coordination of ethylene to the Pd-ethyl species to generate the Pd-ethyl π-ethylene species, **2f/2j-VIII**. The formation of the catalyst resting states **2f-VIII** and **2j-VIII** were found to be exothermic by 14.2 and 15.2 kcal/mol respectively (relative to **2f/2j-VI**). The insertion of ethylene from **2f/2j-VIII** was calculated to proceed via **TS[2f-VIII-2f-IX]** and **TS[2j-VIII-2j-IX]**, endothermic by 18.8 kcal/mol (relative to **2f-VIII**) and 17.4 kcal/mol (relative to **2j-VIII**) respectively. As observed for analogous insertion transition state structures (see above), the coordinated ethylene is rotated in-plane with a $C_{\beta(ethylene)}$-$C_{\alpha(ethyl)}$ bond distance of 2.102 Å (for **2f**) and 2.098 Å (for **2j**, Fig. 3.30). The insertion products, **2f-IX** and **2j-IX** were optimised as cationic Pd-butyl species stabilised by a β-agostic interaction with Pd-H_β bond distance of 1.815 Å and 1.813 Å respectively.

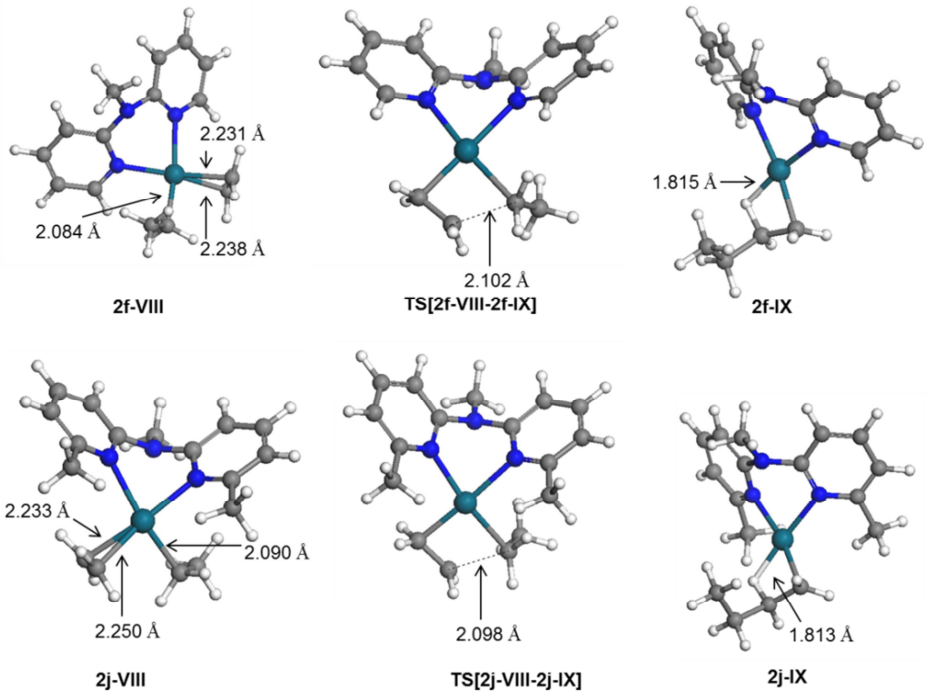

Fig. 3.30 Optimised minima and transition state structures for ethylene insertion from **2f/2j-VIII** to generate the Pd-butyl species, **2f/2j-IX**.

3.3.2.7 Comparative chain transfer via BHE or BHT, or further insertion to generate the Pd-hexyl species.

Scheme 3.9 Comparative chain transfer via BHE or BHT, or ethylene insertion from Pd-butyl species, **2f/2j-IX**.

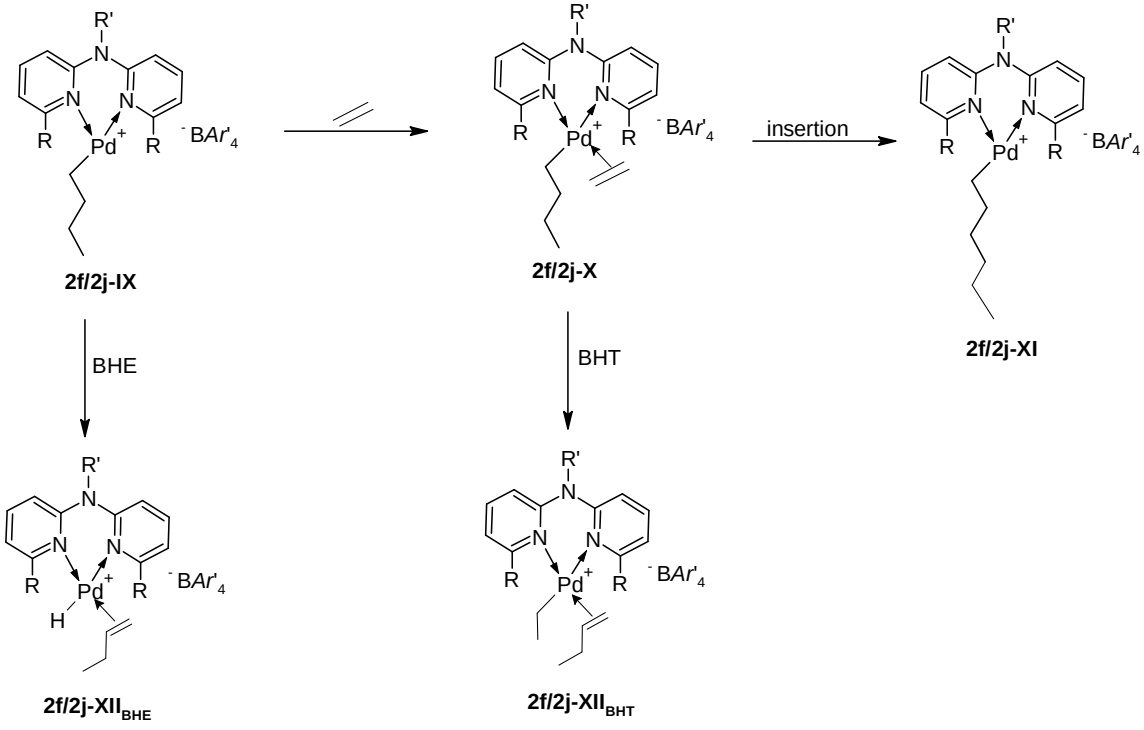

After generating the Pd-butyl species, **2f/2j-IX**, we evaluated the propensity for chain transfer via BHE or BHT as well as further coordination and insertion of ethylene to generate ethylene trimers (Scheme 3.9, Fig. 3.31).

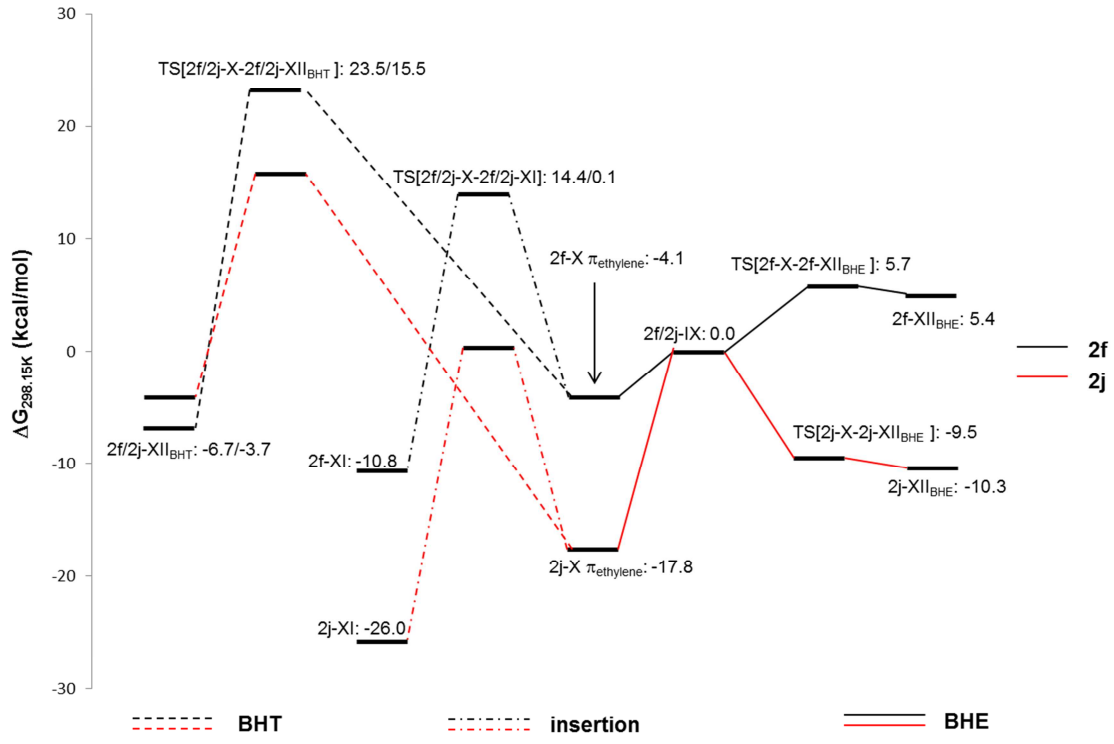

Fig. 3.31 Energy profile of comparative chain transfer via BHE or BHT from **2f/2j-IX;** as well as further ethylene insertion to generate the Pd-hexyl species. Calculated Gibbs free energies ($\Delta G_{298.15K}$) reported at 298.15 K and 1 atm.

Our calculations showed that BHE was the preferred elimination pathway from species **2f/2j-IX**, to generate the Pd-hydride π-butene species, **2f/2j-XII$_{BHE}$**. β-hydride elimination was calculated to proceed via a late-stage transition state, **TS[2f/2j-IX-2f/2j-XII$_{BHE}$]** and was calculated to be endothermic by 5.7 kcal/mol in the case of the species derived from complex **2f** while **TS[2j-IX-2j-XII$_{BHE}$]** was calculated to be exothermic by 9.5 kcal/mol relative to **2j-IX**. This significant difference in the propensity for BHE may be attributed to steric differences; whereas the driving force for elimination is the generation of a π-olefin complex in which the coordinated olefin is orientated perpendicular

to the square plane of the metal centre. This preferred orientation significantly reduces the *o*-Me/olefin interactions in species **2j**; interactions which are absent in the case of **2f**. The optimised structures of the transition states **TS[2f/2j-IX-2f/2j-XII$_{BHE}$]** are characterised by in-plane rotation of the butyl fragment; analogous to that observed for **TS[2f-III-2f-IV$_{BHE}$]** and **TS[2j-III-2j-IV$_{BHE}$]** (Fig. 3.32) and displayed a C_β-H_β interaction of 1.778 Å (in the case of **2f**) and 1.951 Å (in the case of **2j**).

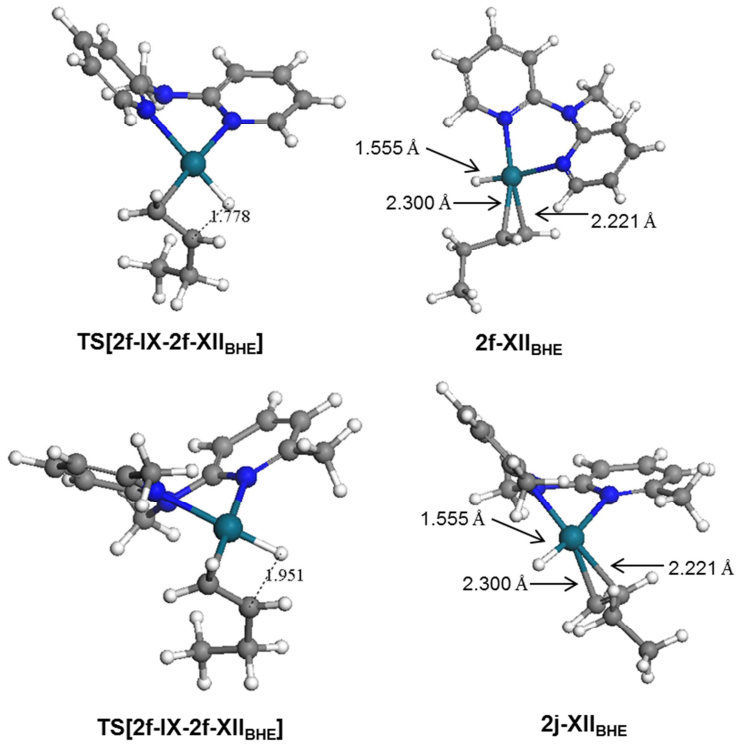

Fig. 3.32 Optimised minima and transition state structures for 1-butene elimination from **2f/2j-VIX** via β-hydride elimination to generate the Pd-hydride π-butene species, **2-XII$_{BHE}$**.

The product of BHE, **2f/2j-XII$_{BHE}$**, was calculated to be endothermic by 5.4 kcal/mol (in the case of **2f**) and exothermic by 10.3 kcal/mol (in the case of **2j**) and was characterised by the perpendicular orientation of the eliminated 1-butene as well as a Pd-H bond distance of 1.555 Å and a Pd-C_α and Pd-C_β bond distance of 2.221 and 2.300 Å respectively.

Both chain termination via BHT and chain growth via insertion proceed from the Pd-butyl π-ethylene species, **2f/2j-X$_{\pi\text{-ethylene}}$**, calculated to be exothermic by 4.1 kcal/mol (in the case of **2f-X$_{\pi\text{-ethylene}}$**, and 17.8 kcal/mol (in the case of **2j-X$_{\pi\text{-ethylene}}$**). β-hydrogen transfer was calculated to proceed via transition state **TS[2f/2j-X-2f/2j-XII$_{BHT}$]**, with a large elimination barrier of 27.6 kcal/mol (in the case of **2f**) and 33.5 kcal/mol (in the case of **2j**). The difference in the energies of the transition state structures may be attributed to differences in steric pressure. In the case of **2j**, increased steric bulk in the coordination sphere of the metal centre results in a dramatic increase in the minimum energy associated with the transition state structure; in an analogous manner to that observed in the case of **2-IV$_{BHT}$**. The optimised transition state structures are geometrically analogous to those discussed previously for **TS[2f/2j-III-2f/2j-IV$_{BHT}$]**, with a $C_{\beta(ethylene)}$-$C_{\beta(butyl)}$ bond distance of 1.286 Å (Fig. 3.33)

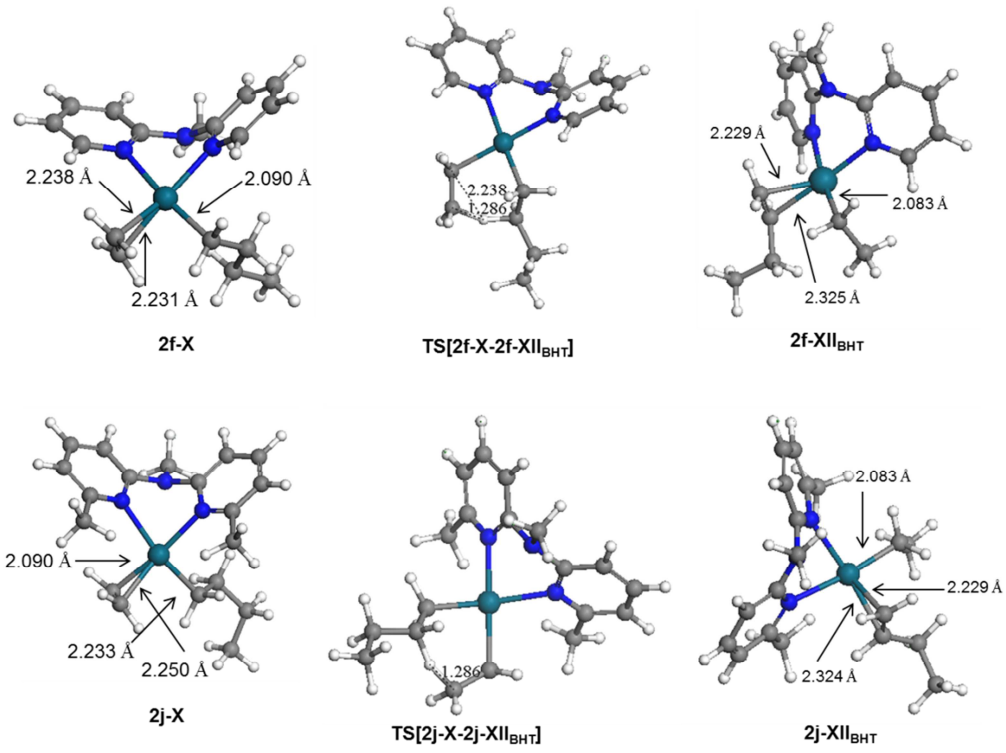

Fig. 3.33 Optimised minima and transition state structures for 1-butene elimination from **2f/2j-IX** via β-hydrogen transfer to generate the Pd-ethyl π-butene species, **2-XII$_{BHT}$**.

The product of BHT, the Pd-ethyl π-butene species **2f/2j-XII$_{BHT}$**, showed optimised geometries in which the π-butene fragment is perpendicular to the plane of the metal coordination sphere, with Pd-C_α and Pd-C_β bond distances of 2.229 and 2.325 Å (in the case of **2f-XII$_{BHT}$**); and 2.229 and 2.324 Å (in the case of **2j-XII$_{BHT}$**) respectively. Both species **2f-XII$_{BHT}$** and **2j-XII$_{BHT}$** was calculated to be exothermic by 6.7 and 3.7 kcal/mol (relative to **2f/2j-IX**) respectively.

Ethylene coordination and insertion from **2-X$_{\pi\text{-ethylene}}$** was calculated to proceed via transition states **TS[2f-X-2f-XI]** and **TS[2j-X-2j-XI]** with an insertion barrier of 18.5 and 17.9 kcal/mol respectively. The transition state was characterised by a $C_{\beta(ethylene)}$-$C_{\alpha(butyl)}$ distance of 2.094 (in the case of **2f**) and 2.102 Å (in the case of **2j**, Fig. 3.34).

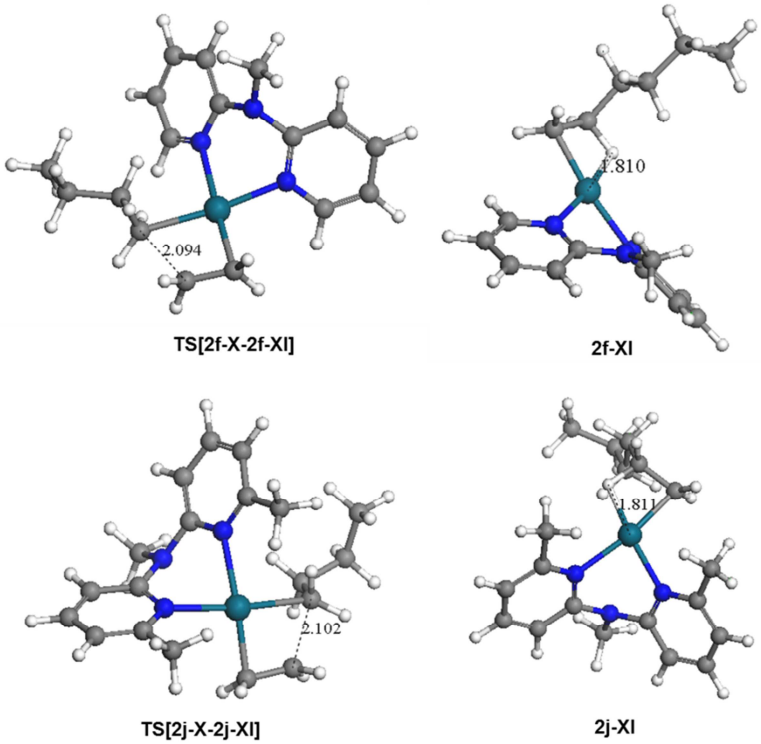

Fig. 3.34 Optimised minima and transition state structures for ethylene insertion from **2f/2j-X$_{\pi\text{-ethylene}}$** to generate the Pd-hexyl species, **2-XI**.

Formation of the Pd-hexyl species, **2-XI**, was calculated to be exothermic relative to **2-IX** by 10.8 kcal/mol (in the case of **2f-XI**) and 26.0 kcal/mol (in the case of **2j-XI**). The geometrically optimised structures, **2f-XI** and **2j-XI**, displayed Pd-H_β agostic interactions with near-identical bond distances of 1.810 Å and 1.811 Å.

3.3.2.8 Reinsertion and elimination of Pd-hydride π-butene species to generate 2-butenes.

Finally, we sought to evaluate the energetics of 1-butene reinsertion and β-hydride elimination from species **2-XII$_{BHE}$**, with a specific emphasis on the effect steric differences would have for these two catalyst precursors, since these complexes catalysed the formation of 2-butenes from ethylene (as discussed above). Scheme 3.10 shows the intermediates we evaluated in terms of relative energies to the Pd-hydride π-butene species, **2f/2j-XII$_{BHE}$**.

Scheme 3.10 Reinsertion and elimination of 2-butenes from species **2-XII$_{BHE}$.**

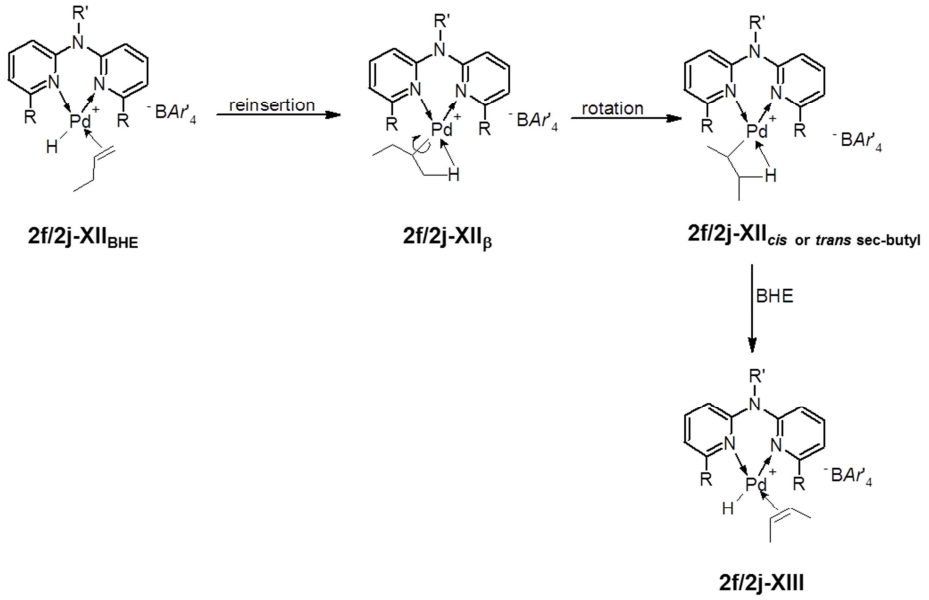

For species **2f-XII$_{BHE}$** and **2j-XII$_{BHE}$** reinsertion of 1-butene with 1,2-regiochemistry was calculated to proceed via transition states **TS[2f-XII$_{BHE}$-2f-XII$_\beta$]** and **TS[2j-XII$_{BHE}$-2j-XII$_\beta$]**, endothermic by 1.6 and 2.8 kcal/mol respectively (Fig. 3.35). The

transition state structures (Fig. 3.36 and 3.37) were characterised by an C_{α}-H distance of 1.881Å (in the case of **TS[2f-XII$_{BHE}$-2f-XII$_{\beta}$]**) and 1.825 Å (in the case of **TS[2j-XII$_{BHE}$-2j-XII$_{\beta}$]**). In the case of **2f**, formation of the Pd-*sec*-butyl$_{(Pd\text{-}CH_3\ agostic)}$ species, **2f-XII$_{\beta}$,** was calculated to be exothermic by 7.6 kcal/mol, relative to **2f-XII$_{BHE}$**.

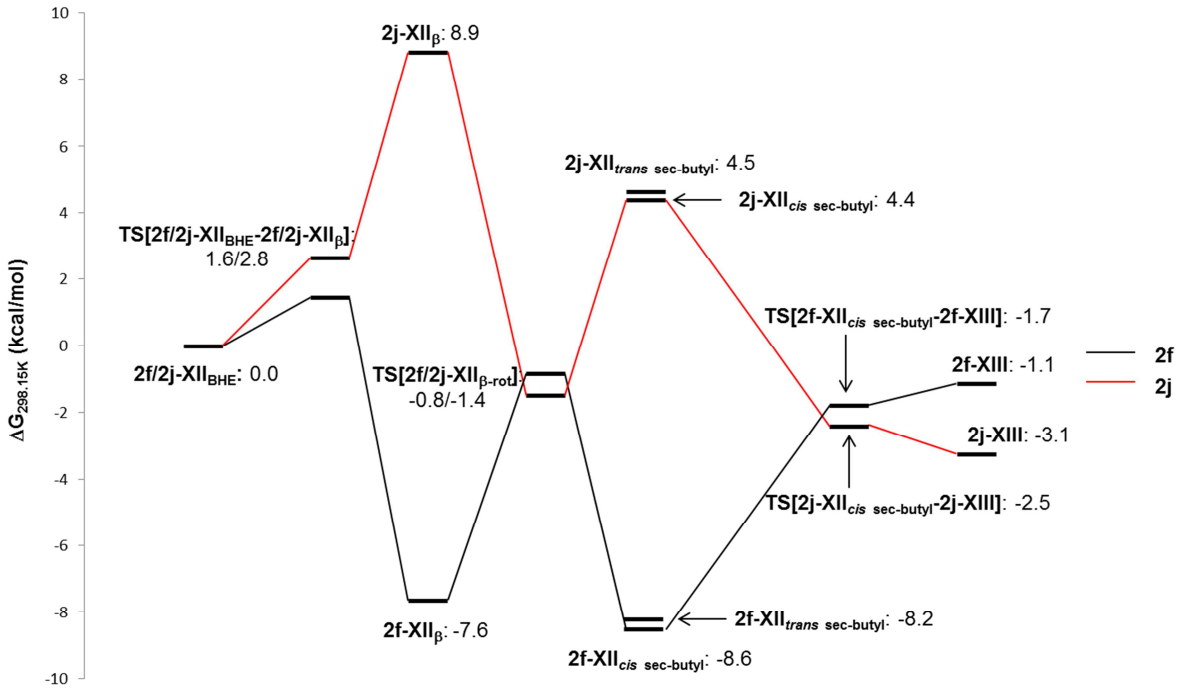

Fig. 3.35 Energy profile of reinsertion and elimination of 1-butene from **2f/2j-XII$_{BHE}$** to generate the Pd-hydride π-2-butene species, **2-XIII**. Calculated Gibbs free energies ($\Delta G_{298.15K}$) reported at 298.15 K and 1 atm.

In contrast, formation of the species **2j-XII$_{\beta}$** was significantly endothermic, with the computed ground state energy endothermic by 8.9 kcal/mol, relative to **2j-XII$_{BHE}$**. This difference may be attributed to increased steric strain in the case of **2j**, with the reinserted alkyl chain positioned in the plane of the palladium coordination sphere. The result thereof is a significant increase in the ground state energy of the insertion product. The effect of steric strain was also observed in the formation of the Pd-*sec*-butyl$_{(Pd\text{-}CH_2\ agostic)}$ species, **2-XII$_{cis/trans\ sec\text{-}butyl}$**. In the case of **2f**, isomerisation via rotation about the Pd-C bond was calculated to proceed via **TS[2f-XII$_{\beta\text{-}rot}$]** with an energy barrier of 6.8 kcal/mol. This value is

lower than the isomerisation barrier (14-16 kcal/mol) determined for sterically bulky Ni(II) and Pd(II) diimine catalysts.[3b,4a]

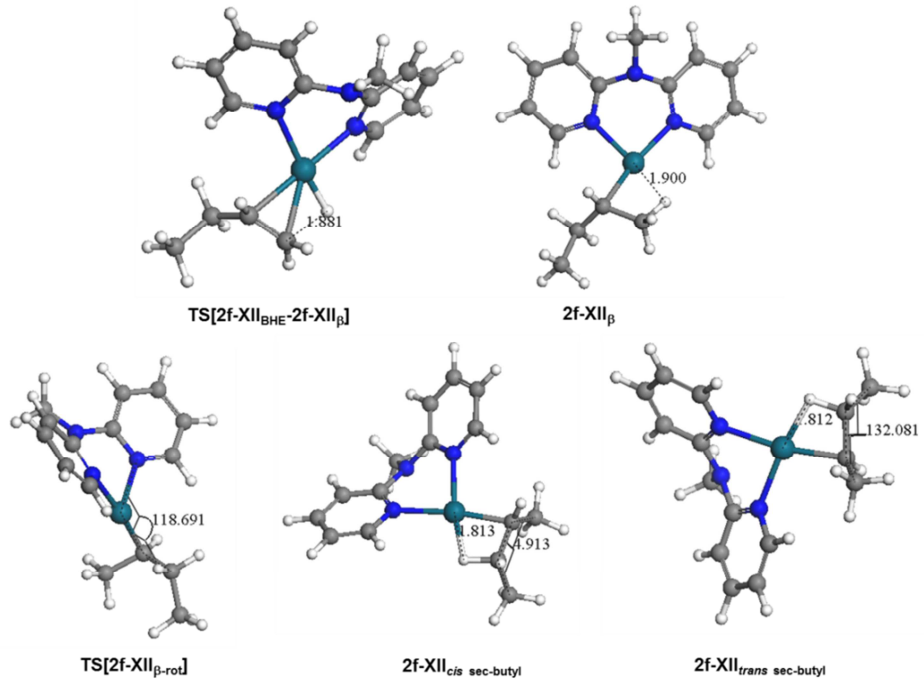

Fig. 3.36 Optimised minima and transition state structures for 1-butene reinsertion and isomerisation from **2f-XII$_{BHE}$** to generate the Pd-*sec*-butyl species, **2f-XII$_{cis}$ or $_{trans}$ $_{sec}$-butyl**.

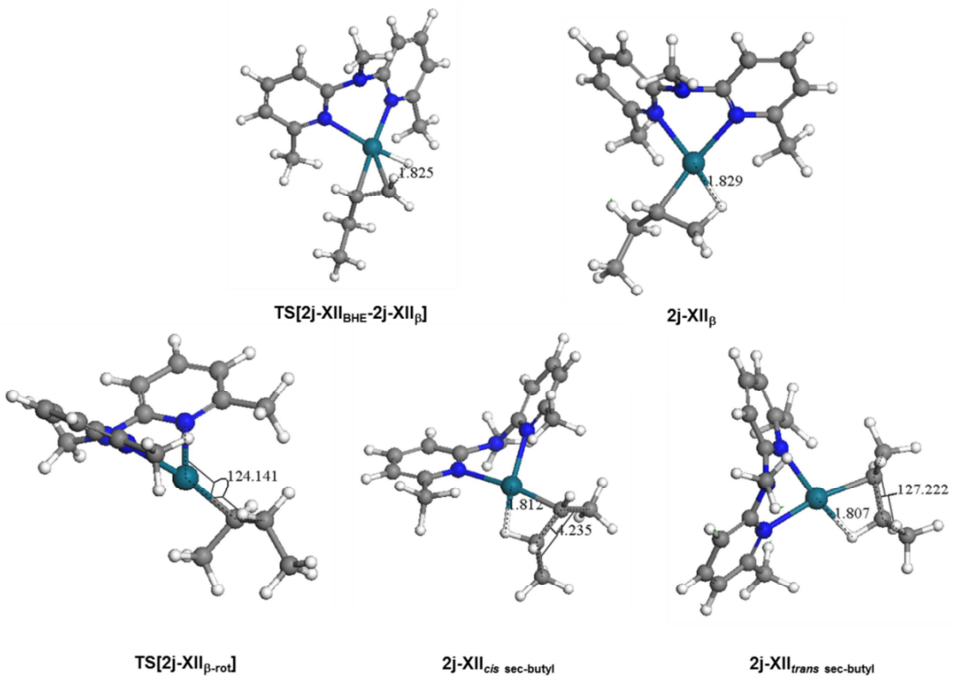

Fig. 3.37 Optimised minima and transition state structures for 1-butene reinsertion and isomerisation from **2j-XII$_{BHE}$** to generate the Pd-*sec*-butyl species, **2j-XII$_{cis}$ or $_{trans}$ $_{sec}$-butyl**.

This difference may be attributed to a lack of axial steric bulk in the current system in comparison to the Brookhart diimine catalyst systems,[3a] which would result in a decrease in the isomerisation energy relative to a sterically encumbered pre-catalyst. Relaxation to the product generated the *cis* and *trans* Pd-*sec*-butyl$_{(Pd\text{-}CH_2\ agostic)}$ species, **2f-XII$_{cis\ sec\text{-}butyl}$** and **2f-XII$_{trans\ sec\text{-}butyl}$**, exothermic by 8.6 and 8.2 kcal/mol respectively (relative to **2f-XII$_{BHE}$**). The optimised geometries displayed a Pd-H$_\beta$ agostic interaction with a distance of 1.813 Å for the *cis* analogue and 1.812 Å for the *trans* analogue. In contrast, for **2j**, isomerisation via rotation the Pd-C bond via **TS[2j-XII$_{\beta\text{-}rot}$]** was calculated to be exothermic by 10.3 kcal/mol (relative to **2j-XII$_\beta$**). This difference in behaviour can be attributed to the release of steric pressure as the alkyl chain is rotated out of the coordination sphere of the palladium centre, as evidenced by a deviation from planarity (N1-Pd-C$_\alpha$-C$_\beta$ dihedral: 124.141 °) in comparison to **2j-XII$_\beta$** (N1-Pd-C$_\alpha$-C$_\beta$ dihedral: -169.508 °). As expected from this rationalisation, formation of the isomerisation products, **2j-XII$_{cis\ sec\text{-}butyl}$** and **2j-XII$_{trans\ sec\text{-}butyl}$**, was calculated to be endothermic by 5.9 and 6.0 kcal/mol respectively. In the case of **2j**, the optimised geometries displayed a Pd-H$_\beta$ agostic interaction with a distance of 1.812 Å for the *cis* analogue and 1.807 Å for the *trans* analogue. For both **2f** and **2j**, the results of our calculations showed no significant energy differences between the *cis* and *trans* isomers.

The elimination of 2-butene via β-hydride elimination was evaluated from the *cis* isomers, **2f/2j-XII$_{cis\ sec\text{-}butyl}$**. Our calculations showed that the elimination proceeded via **TS[2f-XII$_{cis\ sec\text{-}butyl}$-2f-XIII]** and **TS[2j-XII$_{cis\ sec\text{-}butyl}$-2j-XIII]**. In the case of **2f**, the barrier for elimination was found to be endothermic by 6.9 kcal/mol (relative to **2f-XII$_{cis\ sec\text{-}butyl}$**). The product of elimination; the Pd-hydride π-2-butene species, **2f-XIII**, was calculated to be endothermic by 7.1 kcal/mol (relative to **2f-XII$_{cis\ sec\text{-}butyl}$**). The optimised structure (Fig. 3.38)

showed a Pd-H bond distance of 1.555 Å and Pd-C_{β} and Pd-$C_{\beta'}$ distances for the π-bound olefin of 2.271 and 2.298 Å respectively.

In the case of **2j**, the effect of steric strain was once again observed in our calculations. BHE via **TS[2j-XII*cis* sec-butyl-2j-XIII]**, was calculated to be exothermic by 6.9 kcal/mol (relative to **2j-XII*cis* sec-butyl**). Relaxation to the BHE product, **2j-XIII**, was calculated to be exothermic by 3.1 kcal/mol relative to **2j-XII$_{BHE}$**. The optimised structure (Fig. 3.38) showed a Pd-H bond distance of 1.553 Å and Pd-C_{β} and Pd-$C_{\beta'}$ distances for the π–bound olefin of 2.269 and 2.297 Å respectively.

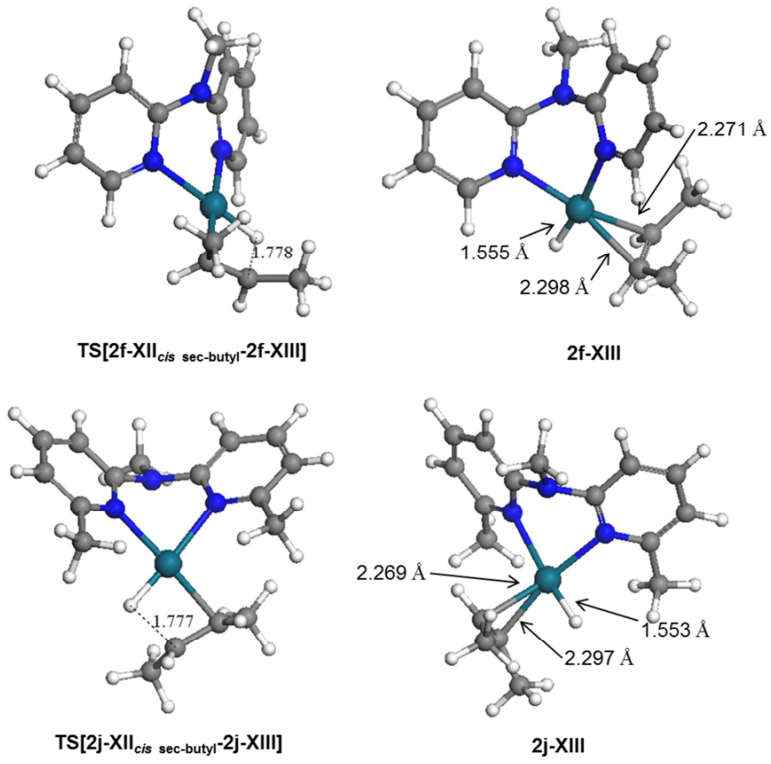

Fig. 3.38 Optimised minima and transition state structures for 1-butene elimination via BHE from **2-XII*cis* sec-butyl** to generate the Pd-hydride π-2-butene species, **2-XIII**.

3.3.3 General Discussion of experimental and theoretical investigations regarding Pd-catalysed ethylene oligomerisation.

The overall energy profile computed for catalytic ethylene dimerisation is shown in Figure 3.39. Our experimental and theoretical investigation showed that the introduction of steric bulk in the *ortho* position of the palladium coordination spheres resulted in a decrease in catalytic activity.

Both the kinetic and DFT investigation identified associative ethylene exchange to generate the Pd-methyl π-ethylene species as a key step, in terms of energy differences between **2f** and **2j**, in the dimerisation cycle. Low-temperature kinetic studies showed that this process was facilitated at higher temperatures (-40 °C) for **2j**, in comparison to **2f**. Computed values for associative olefin exchange from **2f** and **2j**, was consistent with this observation, with the energy difference for this step being 11.6 kcal/mol. Ethylene associative exchange was also identified as playing a crucial role in the formation of the catalyst resting state, from which butene-formation was shown to proceed experimentally. The formation of the five-coordinate intermediate, Pd-hydride π-propylene π-ethylene species; **2-IV$_{int}$**, was calculated to be significantly more endothermic for **2j** than the unsubstituted analogue, **2f**, with an energy difference of 7.8 kcal/mol, which suggests that the formation of the catalyst resting state is energetically more favourable for **2f** in comparison to **2j**. It is these two associative exchange processes which is partially responsible for the experimental observation that complex **2f** oligomerises ethylene with higher activity than **2j**, despite a lower calculated energy barrier for ethylene insertion in **2j** than **2f**. In the case of the Brookhart diimine system, axial steric bulk and decreased insertion barriers synergistically promotes the formation of homo- or co-polymers.

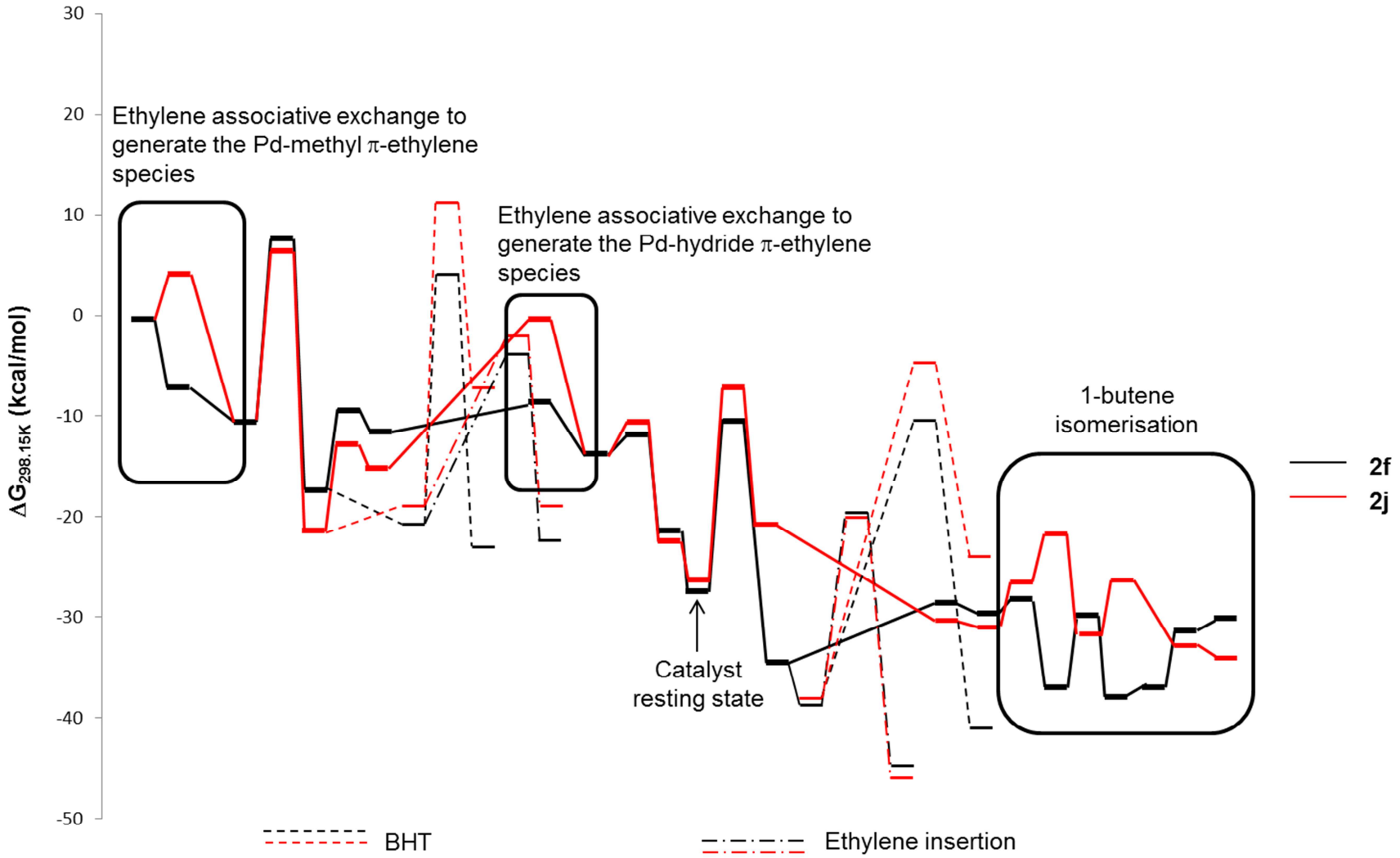

Fig. 3.39 Overall energy profile of the computed steps in the catalytic ethylene oligomerisation of complexes **2f** and **2j**. The most likely pathway is shown in bold. Calculated Gibbs free energies ($\Delta G_{298.15K}$) reported at 298.15 K and 1 atm.

In contrast, the introduction of *o*-Me-groups in the coordination sphere for the evaluated series of complexes, induces steric pressure in only one face of the coordination sphere. Thus, despite a decrease in the calculated ethylene insertion barriers for species derived from **2j**, the lack of axial steric bulk does not decrease associative exchange significantly enough to promote the formation of long-chain olefins or polymer.

Furthermore, our calculations showed that chain transfer proceeded by β-hydride elimination, and that reinsertion and isomerisation to generate Pd-*iso*-butyl species, which would eliminate 2-butenes was facile. No significant energy differences were observed in the computed ground state energies of the *cis* and *trans* isomers, which suggests that the catalyst itself does not influence the selectivity for *cis* or *trans* 2-butene. In addition, our calculations, in the gas phase, showed that 1-butene isomerisation was also governed by steric effects. This was observed in the ground state energy differences for key intermediates. For example the energy difference for **2f-XII$_{\beta}$** relative to **2j-XII$_{\beta}$** is 15 kcal/mol, while the formation of **2f-XII$_{\beta}$** from **2f-XII$_{BHE}$** is energetically favourable in comparison to the formation of **2j-XII$_{\beta}$** from **2j-XII$_{BHE}$**. Despite these calculated energy differences for 1-butene isomerisation, experimentally no significant differences in isomer distribution was observed.

3.4 Conclusions

A series of cationic palladium methyl complexes bearing *N*-alkyl 2,2′-dipyridylaldimine ligands, **2f-2j**, were evaluated as catalyst precursors in ethylene oligomerisation. Our results showed that these complexes catalytically dimerise ethylene with relatively low activity to a mixture of 1- and 2-butenes, with negligible differences in product selectivities. Low-temperature kinetic studies of complexes **2f** and **2j** allowed for the determination of ethylene insertion rates, with **2f** inserting ethylene approximately 1.5x faster

than **2j**. Low temperature spectroscopic techniques also allowed for the identification of the Pd-ethyl π-ethylene species as the catalyst resting state. Complimentary DFT calculations of the catalytic cycle identified two key steps, both involving ethylene associative exchange, which would explain the observed reactivity differences for complexes **2f** and **2j**. Isomerisation via reinsertion, rotation and elimination to form 2-butenes, was calculated to be quite facile for both **2f** and **2j**, even though steric bulk significantly affected the relative energetics associated with each intermediate of the isomerisation process. Consistent with our experimental results, our calculations showed that the nature of the catalyst precursors had a negligible effect on the ratio of *cis* to *trans* 2-butene isomers.

3.5 Experimental Section

All manipulations were performed under an inert atmosphere or vacuum using standard Schlenk techniques. Dichloromethane-d_2 (99.5 % D) was purchased from Sigma-Aldrich and used as received. Low-temperature NMR (^{1}H) spectra were recorded on a Varian Unity Inova 400 MHz spectrometer, with chemical shifts reported in ppm, referenced to the residual protons of the deuterated solvent and trimethyl silane as internal standard.

3.5.1 Preparative-scale catalytic ethylene oligomerisation with complexes 2f-2j.

A 250 ml Parr stainless steel autoclave was sealed under an inert atmosphere in a glovebox. Under a stream of ethylene, a solution of the pre-catalyst (30 µmol) in dichloromethane (20 ml) was added. The reactor was pressurised to the required amount with ethylene and the reaction was allowed to proceed at the required temperature for 18 h. After the allotted time, the reactor was cooled to 0 °C, vented and quenched with MeOH (5 ml). A sample was filtered and analysed by GC-FID employing *p*-xylene as internal standard. Relative amounts of oligomers were calculated from the amount of standard and the response

factors of commercial standards of the analytes. The remainder of the reaction mixture was subjected to work-up to determine whether long-chain oligomers had formed. No long-chain oligomers or polymers were formed during the reactions.

3.5.2 Generation of [PdMe(2,2´-dipyridyl-N-methylamine)(CH_2=CH_2]$^+$[BAr´$_4$]$^-$ (3a)

A valved NMR tube was charged with cationic complex **2f** (30 mg, 0.0248 mmol) and CD_2Cl_2 (0.7 ml). After purging with argon the complex solution was frozen at -196 °C and subjected to three freeze-pump-thaw cycles to remove dissolved oxygen. To the frozen solution was added excess ethylene and the solution warmed to -78 °C. A ^{1}H NMR spectrum recorded (-60 °C) after 90 min showed the quantitative formation of species **3a** (100 % relative to free MeCN). Under these conditions exchange of free and coordinated ethylene was observed to be fast on the NMR chemical shift time scale.

3.5.3 Generation of [PdMe(6,6´-dimethyl-2,2´-dipyridyl-N-methylamine)-(CH_2=CH_2]$^+$[BAr´$_4$]$^-$ (3b)

A valved NMR tube was charged with cationic complex **2j** (30 mg, 0.0248 mmol) and CD_2Cl_2 (0.7 ml). After purging with argon the complex solution was frozen at -196 °C and subjected to three freeze-pump-thaw cycles to remove dissolved oxygen. To the frozen solution was added excess ethylene and the solution warmed to -40 °C. A ^{1}H NMR spectrum recorded (-60 °C) after 300 min showed the quantitative formation of species **3b** (100 % relative to free MeCN). Under these conditions exchange of free and coordinated ethylene was observed to be slow on the NMR chemical shift time scale.

3.5.4 Kinetics of insertion of [PdMe(2,2´-dipyridyl-N-methylamine)(CH_2=CH_2)]$^+$[BAr´$_4$]$^-$ (3a).

A solution of species **3a** was generated as described above in the presence of ethylene. The solution was kept at -10 °C for 5 min, equilibrated at -78 °C for 3 min and an ^{1}H NMR spectrum recorded at -60 °C. This procedure was repeated in 5 min intervals. Values corresponding to $I_{0,PdMe}$ ($I_{0,PdMe}$ = the integral of the Pd-Me resonance at the start of the experiment, δ 0.60 ppm), I_{PdMe} (I_{PdMe} = the integral of the Pd-Me resonance after each 5 min interval) and I_{MeCN} (I_{MeCN} = the integral of free MeCN as internal standard) were determined by careful integration. A plot of ln($A_{PdMe}/A_{0,PdMe}$) versus time (at -10 °C), where $A_{PdMe} = I_{PdMe}/I_{MeCN}$ and $A_{0,PdMe} = I_{0,PdMe}/I_{MeCN}$ was linear with the slope of the line equal to $-k_{insert,Me}$. For **3a** $k_{insert,Me}$ = 9 (± 1) x 10^{-4} s^{-1} at -10 °C.

3.5.5 Kinetics of insertion of [PdMe(6,6´-dimethyl-2,2´-dipyridyl-N-methylamine)-(CH_2=CH_2)]$^+$[BAr´$_4$]$^-$ (3b).

A solution of species **3b** was generated as described above in the presence of ethylene. The solution was kept at -10 °C for 10 min, equilibrated at -78 °C for 3 min and an ^{1}H NMR spectrum recorded at -60 °C. This procedure was repeated in 10 min intervals. Values corresponding to $I_{0,PdMe}$ ($I_{0,PdMe}$ = the integral of the Pd-Me resonance at the start of the experiment, δ 0.60 ppm), I_{PdMe} (I_{PdMe} = the integral of the Pd-Me resonance after each 10 min interval) and I_{MeCN} (I_{MeCN} = the integral of free MeCN as internal standard) were determined by careful integration. A plot of ln($A_{PdMe}/A_{0,PdMe}$) versus time (at -10 °C), where $A_{PdMe} = I_{PdMe}/I_{MeCN}$ and $A_{0,PdMe} = I_{0,PdMe}/I_{MeCN}$ was linear with the slope of the line equal to - $k_{insert,Me}$. For **3b** $k_{insert,Me}$ = 5.5 (± 0.5) x 10^{-4} s^{-1} at -10 °C.

3.5.6 Generation of [PdEt(2,2´-dipyridyl-N-methylamine)(CH_2=CH_2)]$^+$[BAr´$_4$]$^-$ (3e).

A valved NMR tube containing a solution of **3a** and excess ethylene was kept at -10 °C for 90 min. A ^{1}H NMR spectrum was recorded at -60 °C, which showed the complete disappearance of **3a** with concomitant formation of species **3e** and (relative to free MeCN) 1-propylene (82 %), 1-butene (71 %) and *cis* and *trans* 2-butene (652 %).

3.5.7 Generation of [PdEt(6,6´-dimethyl-2,2´-dipyridyl-N-methylamine)-(CH_2=CH_2)]$^+$[BAr´$_4$]$^-$ (3f).

A valved NMR tube containing a solution of **3b** and excess ethylene was kept at -10 °C for 110 min. A ^{1}H NMR spectrum was recorded at -60 °C, which showed the complete disappearance of **3b** with concomitant formation of species **3f** and (relative to free MeCN), 1-propylene (94 %), 1-butene (66 %) and *cis* and *trans* 2-butene (154 %).

3.5.8 Computational Hardware.

Access to computational hardware employed in the molecular modelling study was provided by the Centre for High-Performance Computing (CHPC) via the “Sun Hybrid System”.

3.5.9 Details of computations.

The computational results reported in this chapter were calculated using the Dmol^3 density functional theory (DFT) code[23,27] as implemented in the Accelrys MaterialsStudio (version 5.5) software package. The nonlocal generalised gradient approximation (GGA) exchange-correlation functional was employed in all geometry optimisations, specifically the PW91 functional of Perdew and Wang.[28] The Dmol^3 code utilises a basis set of numeric

atomic functions, which are exact solutions to the Kohn-Sham equations for the atoms.[29] In general these basis sets are more complete than a comparable set of linearly independent Gaussian functions. In addition these basis sets have been demonstrated to have small basis set superposition errors. The computational investigation employed an all-electron polarised split valence basis set, termed double numeric polarised (DNP). All geometry optimisations employed highly efficient delocalised internal coordinates.[30] This has the advantage of significantly decreasing the number of iterations required for larger molecules during geometry optimisation when compared to traditional Cartesian coordinates. The tolerance for convergence of the self-consistent field (SCF) density was set to 1×10^{-5} Hartrees while the tolerance for energy convergence was set at 1×10^{-6} Hartrees. Additional convergence criteria include the tolerance for converged gradient (0.002 Hartrees/Å) and the tolerance for converged atom displacement (0.005 Å).

Optimised geometries were subjected to full frequency analyses at the same GGA/PW91/DNP level of theory to verify the nature of the stationary points. Equilibrium geometries were characterised by the absence of imaginary frequencies while optimised transition state geometries exhibited a single imaginary frequency in the reaction coordinate. Preliminary transition state geometries were obtained by employing either the Dmol^3 PES scan functionality in Cerius[31] or the integrated linear synchronous transit/quadratic synchronous transit (LST/QST) algorithm[32] available in MaterialsStudio.

All computations were performed with the exclusion of solvent effects and the results obtained was mass-balanced for the isolated system in the gas phase. All reported energies incorporate Gibbs free energy corrections to the total electronic energies at 298.15 K and 1 atm.

3.6 References

(1) (a) Drent, E.; Budzelaar, P. H. M. *Chem. Rev.*, **1996**, *96*, 663 (b) Beletskaya, I. P.; Cheprakov, A. V. *Chem. Rev.*, **2000**, *100*, 3009 (c) Ittel, S. D.; Johnson, L. K.; Brookhart, M. *Chem. Rev.*, **2000**, *100*, 1169 (d) Gibson, V. C.; Spitzmesser, S. K. *Chem. Rev.*, **2002**, *103*, 283 (e) Tietze, L. F.; Ila, H.; Bell, H. P. *Chem. Rev.*, **2004**, *104*, 3453 (f) Durand, J.; Milani, B. *Coord. Chem. Rev.*, **2006**, *250*, 542 (g) Nakamura, A.; Ito, S.; Nozaki, K. *Chem. Rev.*, **2009**, *109*, 5215.

(2) Rix, F. C.; Brookhart, M. *J. Am. Chem. Soc.*, **1995**, *117*, 1137.

(3) (a) Johnson, L. K.; Killian, C. M.; Brookhart, M. *J. Am. Chem. Soc.*, **1995**, *117*, 6414 (b) Tempel, D. J.; Johnson, L. K.; Huff, R. L.; White, P. S.; Brookhart, M. *J. Am. Chem. Soc.*, **2000**, *122*, 6686.

(4) (a) Deng, L.; Woo, T. K.; Cavallo, L.; Margl, P. M.; Ziegler, T. *J. Am. Chem. Soc.*, **1997**, *119*, 6177 (b) Deng, L.; Margl, P.; Ziegler, T. *J. Am. Chem. Soc.*, **1997**, *119*, 1094.

(5) Musaev, D. G.; Froese, R. D. J.; Svensson, M.; Morokuma, K. *J. Am. Chem. Soc.*, **1997**, *119*, 367.

(6) (a) Siegbahn, P. E. M.; Stromberg, S.; Zetterberg, K. *Organometallics*, **1996**, *15*, 5542 (b) Stromberg, S.; Zetterberg, K.; E. M. Siegbahn, P. *J. Chem. Soc., Dalton Trans.*, **1997**, *0*, 4147.

(7) Drent, E.; van Dijk, R.; van Ginkel, R.; van Oort, B.; Pugh, R. I. *Chem. Commun.*, **2002**, 744.

(8) (a) Kochi, T.; Noda, S.; Yoshimura, K.; Nozaki, K. *J. Am. Chem. Soc.*, **2007**, *129*, 8948 (b) Nozaki, K.; Kusumoto, S.; Noda, S.; Kochi, T.; Chung, L. W.; Morokuma, K. *J. Am. Chem. Soc.*, **2010**, *132*, 16030.

(9) Weng, W.; Shen, Z.; Jordan, R. F. *J. Am. Chem. Soc.*, **2007**, *129*, 15450.

(10) Ito, S.; Munakata, K.; Nakamura, A.; Nozaki, K. *J. Am. Chem. Soc.*, **2009**, *131*, 14606.

(11) Noda, S.; Nakamura, A.; Kochi, T.; Chung, L. W.; Morokuma, K.; Nozaki, K. *J. Am. Chem. Soc.*, **2009**, *131*, 14088.

(12) Nakamura, A.; Munakata, K.; Ito, S.; Kochi, T.; Chung, L. W.; Morokuma, K.; Nozaki, K. *J. Am. Chem. Soc.*, **2011**, *133*, 6761.

(13) Gott, A. L.; Piers, W. E.; Dutton, J. L.; McDonald, R.; Parvez, M. *Organometallics*, **2011**, *30*, 4236.

(14) Meneghetti, S. P.; Lutz, P. J.; Kress, J. *Organometallics*, **1999**, *18*, 2734.

(15) Doherty, M. D.; Trudeau, S.; White, P. S.; Morken, J., P.; Brookhart, M. *Organometallics*, **2007**, *26*, 1261.

(16) (a) Flapper, J.; Kooijman, H.; Lutz, M.; Spek, A. L.; van Leeuwen, P. W. N. M.; Elsevier, C. J.; Kamer, P. C. J. *Organometallics*, **2009**, *28*, 3272 (b) Flapper, J.; van Leeuwen, P. W. N. M.; Elsevier, C. J.; Kamer, P. C. J. *Organometallics*, **2009**, *28*, 3264.

(17) Conley, M. P.; Burns, C. T.; Jordan, R. F. *Organometallics*, **2007**, *26*, 6750.

(18) Shultz, L. H.; Tempel, D. J.; Brookhart, M. *J. Am. Chem. Soc.*, **2001**, *123*, 11539.

(19) Burns, C. T.; Jordan, R. F. *Organometallics*, **2007**, *26*, 6726.

(20) Rix, F. C.; Brookhart, M.; White, P. S. *J. Am. Chem. Soc.*, **1996**, *118*, 4746.

(21) Milani, B.; Marson, A.; Scarel, A.; Mestroni, G.; Ernsting, J. M.; Elsevier, C. J. *Organometallics*, **2004**, *23*, 1974.

(22) (a) Bühl, M.; Kabrede, H. *J. Chem. Theory Comput.*, **2006**, *2*, 1282 (b) Rydberg, P.; Olsen, L. *J. Phys. Chem. A*, **2009**, *113*, 11949.

(23) (a) Delley, B. *J. Chem. Phys.*, **1992**, *92*, 508 (b) Delley, B. *J. Chem. Phys.*, **2000**, *113*, 7756.

(24) Zheng, F.; Hutton, A. T.; van Sittert, C. G. C. E.; Moss, J. R.; Mapolie, S. F. *Dalton. Trans.*, **2013**, *42*, 11163.

(25) Michalak, A.; Ziegler, T. *J. Am. Chem. Soc.*, **2001**, *123*, 12266.

(26) Woo, T. K.; Margl, P. M.; Blöchl, P. E.; Ziegler, T. *J. Phys. Chem. B*, **1997**, *101*, 7877.

(27) Delley, B. *J. Chem. Phys.*, **1996**, *100*, 6107.

(28) (a) Perdew, J. P. *Physica B*, **1991**, *172*, 1 (b) Perdew, J. P.; Wang, Y. *Phys. Rev. B: Condens. Matter*, **1992**, *45*, 13244.

(29) Delley, B. In *Theoretical and Computational Chemistry*; Seminario, J. M., Politzer, P., Eds.; Elsevier: Amsterdam, The Netherlands, 1995; Vol. 2,

(30) Andzelm, J.; King-Smith, R. D.; Fitzgerald, G. *Chem. Phys. Lett.*, **2001**, *335*, 321.

(31) Vogt, D. In *Applied Homogeneous Catalysis with Organometallic Compounds*; Cornils, B., Herrmann, W. A., Eds.; VCH: Weinheim, Germany, 1996,

(32) Govind, N.; Petersen, G.; Fitzgerald, G.; King-Smith, R. D.; Andzelm, J. *Comput. Mater. Sci.*, **2003**, *28*, 250.

4.1 Introduction

The seminal work by Brookhart, Grubbs and Gibson paved the way for significant research impetus into late transition metal-mediated olefin oligo-/polymerisation.[1] Of particular significance is the work done on Ni(II) systems which display both remarkable activity and selectivity when applied to olefin homo- and co-polymerisation or oligomerisation reactions. These favorable catalytic properties is the main reason why nickel catalyst systems are of the most widely reported in the literature.[2] A few recent examples in the literature is discussed to emphasise this point.

Li and co-workers prepared a series of novel neutral Ni(II) complexes bearing cyclic β-ketiminato ligands (Fig. 4.1, **4-I** and **4-II**) and evaluated these in the polymerisation of ethylene.[3]

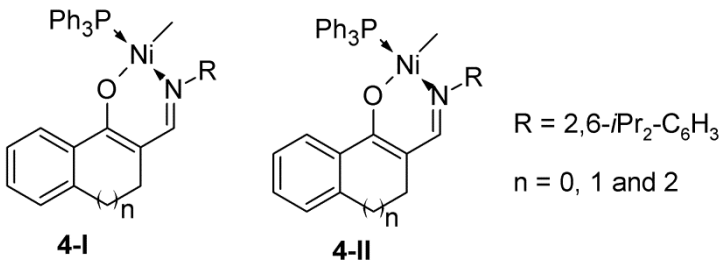

Fig. 4.1 Neutral Ni(II) cyclic β-ketiminato complexes evaluated in catalytic ethylene polymerisation.[3]

Under optimised conditions, in the presence of an activator, activities of up to 71.4 kg PE.mol_{Ni}^{-1}.h^{-1}.atm^{-1} could be obtained. In addition, it was observed that steric bulk *ortho* to the O-atom was not a prerequisite to obtain high activity, in contrast to what is usually observed for neutral Ni(II) salicylaldiminato complexes.[1b,c,4] Moreover, changes in the degree of conjugation had a significant effect on polymer molecular weight and microstructure, with less conjugated systems producing polyethylene with higher molecular weights and lower branch contents than their conjugated counterparts.

Hofmann and co-workers prepared cationic Ni(II) alkyl complexes bearing diphosphinomethane ligands via alkylation of the dichloride complexes and subsequent protonolysis of the di-alkyl analogues (Fig. 4.2, **4-III**).[5]

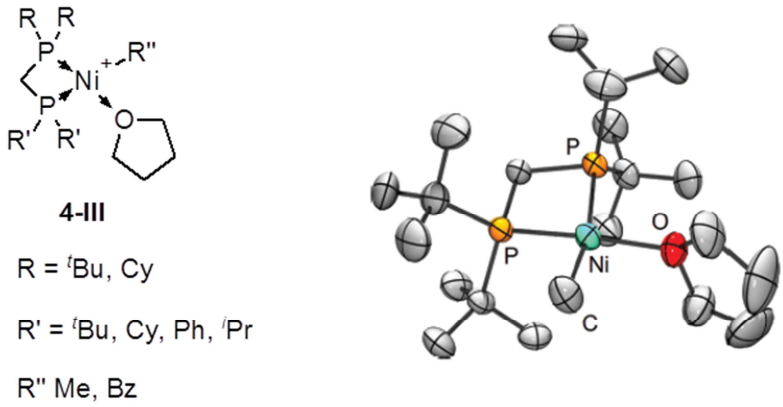

Fig. 4.2 Cationic diphosphinomethane Ni(II)-alkyl complexes prepared by Hofmann *et al*. Copyright 2013 American Chemical Society.[5]

The cationic complexes were found to be self-activating catalysts for ethylene polymerisation, producing polyethylene with high molecular weight and low degrees of branching. An increase in steric bulk at the phosphorus atom resulted in the formation of longer chain polyethylene with a concomitant decrease in chain branching, which is consistent with steric bulk inhibiting associative chain transfer processes.[6]

Sun, Redshaw and co-workers reported a class of Ni(II) complexes bearing 2-(2-benzhydrylbenzenamine)pyridine ligands, in which substituents on the imine nitrogen atom provide significant steric bulk (Fig.4.3, **4-IV** and **4-V**).[7]

Upon activation with MAO or ethyl aluminium sesquichloride (EASC), the Ni(II) complexes exhibited activities of up to 9.30 x 10^3 kg PE.mol_{Ni}^{-1}.h^{-1}. Interestingly, steric bulk was found to result in a decrease in catalytic activity while leading to the formation of higher molecular weight polyethylene with broader molecular weight distributions.

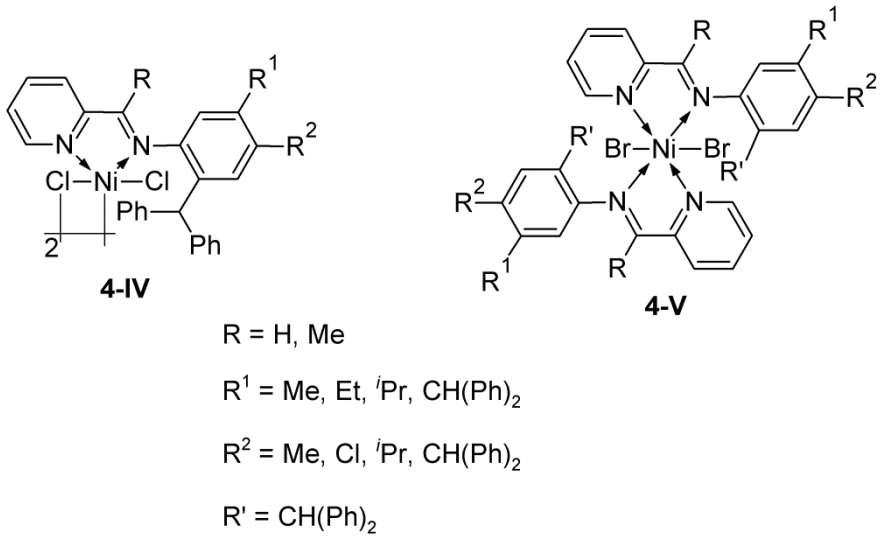

Fig. 4.3 Sterically congested Ni(II) pyridylaldiminato complexes as ethylene polymerisation catalysts.[7]

Ojwach et. al. reported the application of Ni(II) 2,6-bis(di-alkylpyrazol-1-ylmethyl)pyridine complexes in ethylene oligomerisation (Fig. 4.4, **4-VI**, **4-VII** and **4-VIII**).[2a]

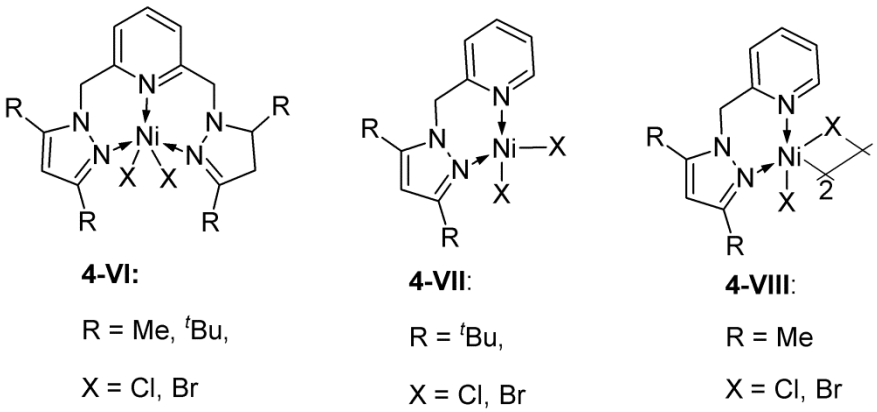

Fig. 4.4 Ni(II) (di-alkylpyrazol-1-ylmethyl)pyridinato complexes as ethylene oligomerisation catalysts.[2a]

In the presence of $EtAlCl_2$ as activator, the Ni(II) complexes oligomerised ethylene C_4-, C_6- and C_8-alkenes, which via a tandem process mediated by the aluminium co-catalyst, were involved in Friedel-Crafts alkylation with the solvent, toluene. Activities of up to 15660 kg alkylated products.$mol_{Ni}^{-1}.h^{-1}$ were obtained. Solvent choice affected both the

catalytic oligomerisation activity as well as the propensity for the formation of alkylated toluene products, since performing catalysis in hexane showed significantly lower catalytic activity toward ethylene oligomerisation, while forming no Friedel-Crafts alkylation products. This was attributed to the need for toluene to act as substrate as well as the need for solvents of sufficient polarity for the generation of catalytically competent species. Finally, they reported that contrary to what was observed previously,[8] the catalyst formed displayed continuous activity without deactivation, as evidenced by performing 1-pentene oligomerisation-tandem-alkylation cycles.

Following the successful preparation of *N*-alkyl-2,2′-dipyridylamine ligands reported in Chapter 2, it was envisaged that this ligand set could be used as a scaffold to prepare neutral Ni(II) pre-catalysts which could be active in ethylene or α-olefin oligo-/polymerisation. Herein we report our synthetic endeavours toward the preparation and characterisation of these Ni(II) *N*-alkyl-2,2′-dipyridylaldiminato complexes and their application as ethylene oligomerisation catalysts.

4.2. Results and Discussion

The *N*-alkyl-2,2′-dipyridylamine ligands (**a-e**, Chapter 2) were reacted with [(DME)$NiCl_2$] to afford dimeric Ni(II) *N*-alkyl-2,2′-dipyridylaldiminato complexes, **4a-4e** (Scheme 4.1) in high yields. The complexes were isolated as blue-green (**4a**), green (**4b** and **4c**) or yellow-green (**4d**) paramagnetic and hygroscopic solids which displayed solubility in polar coordinating solvents and alcohols. In the case of complex **4e**, a pale purple-pink solid was isolated. The complexes were found to be insoluble in ethers, alkanes and chlorinated solvents. Complexes **4a-4e** were characterised by a range of spectroscopic and analytical techniques, the results of which are discussed below.

Characterisation of the complexes by FT-IR spectroscopy showed a shift to higher wavenumbers of the pyridyl ring imine absorption bands, observed in the range 1597-1600 and 1565-1581 cm^{-1} for the complexes (Table 4.1). Analogous shifts have been observed previously for related Ni(II) complexes, which is indicative of ligand coordination to nickel.[9]

Scheme 4.1 Synthesis of Ni(II) *N*-alkyl 2,2′-dipyridylaldiminato complexes.

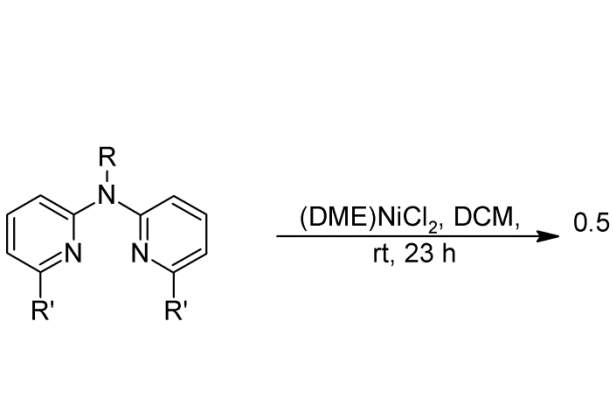

a: R = Me; R' = H

b: R = Bn; R' = H

c: R = MeCy; R' = H

d: R = neopentyl; R' = H

e: R = Me; R' = Me

4a: R = Me; R' = H

4b: R = Bn; R' = H

4c: R = MeCy; R' = H

4d: R = neopentyl; R' = H

4e: R = Me; R' = Me

Characterisation by ESI-MS spectrometry of complexes **4a**-**4e** revealed interesting solvent-dependent fragmentation behaviour.

Table 4.1 Analytical data pertaining to µ-Cl Ni(II) *N*-alkyl-2,2′-dipyridylaldiminato complexes, **4a**-**4e**.

Complex	μ_{eff} (μ_B)[a]	M.p. (dec)[b]	FT-IR (cm^{-1}, C=N)[c]	ESI-MS (*m/z*)[d]
4a	4.15	198-200	1598, 1577	342
4b	3.89	184-186	1597, 1578	418
4c	4.01	200-202	1600, 1577	424
4d	4.32	> 250	1600, 1581	398
4e	4.47	135-136	1600, 1565	370

[a] Measured in the solid state and reported for dimeric complexes. [b] Reported as uncorrected. [c] Recorded as neat spectra on a ZnSe ATR accessory. [d] Reported mass fragment corresponds to $[M + Na + MeOH]^{2+}$.

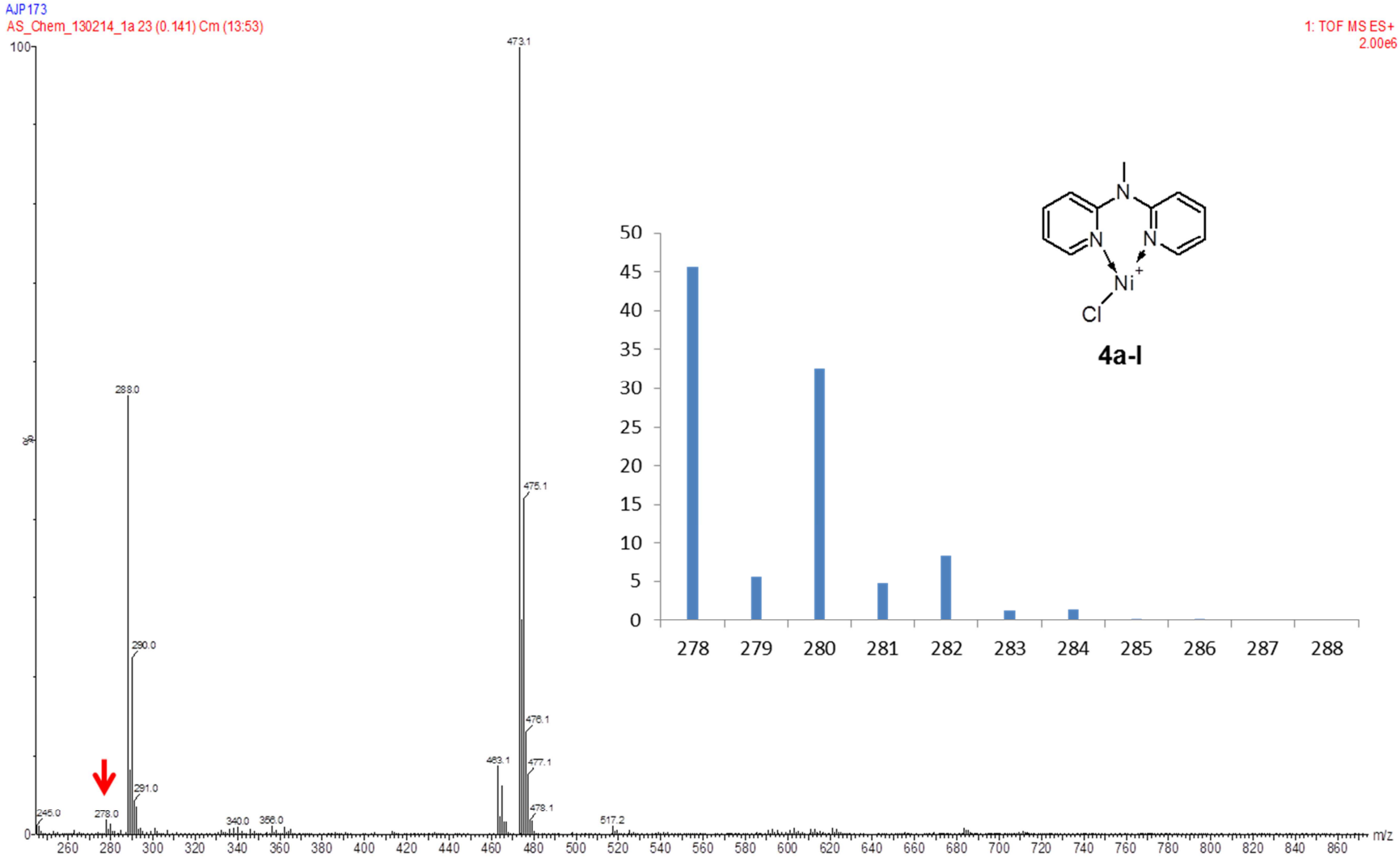

Fig. 4.5 ESI-MS spectrum showing mass fragment at *m/z* 278. Inset shows simulated isotope pattern.

The analysis of complex **4a** will be discussed as a representative example. During ESI-MS analysis, when the sample introduction solvent is MeCN/0.1 % formic acid, a number of low intensity mass fragments were observed. At lower *m*/z values (Fig. 4.5) a mass fragment with low abundance is observed at *m*/*z* 278, assigned to a mononuclear species, **4a-I**, generated by the loss of Cl^-. An additional mass fragment at *m*/z 463 was assigned to the species $[L_2Ni_2Cl_2\text{-}Cl]^+$, **4a-II**, its structure and simulated mass fragment shown in Figure 4.6.

In the range *m*/*z* 500-1000 two mass fragments with very low abundance were observed, which may be assigned. In the first instance, an isotope cluster at *m*/*z* 593 (Fig.4.7) may be assigned to the species, **4a-III**, which is possibly a dimeric μ-Cl $Ni(II)_2$ species, with the fragment generated by loss of Cl^-. Alternatively, **4a-III** may be generated via aggregation of two mononuclear molecules, which then undergoes fragmentation via loss of Cl^-. In the second instance an isotope cluster at *m*/*z* 908 (Fig. 4.8) may be assigned as **4a-IV** which is either a trimeric species, μ-Cl $Ni(II)_3$ or a result of aggregation of three mononuclear species which generates the observed cluster via loss of Cl^-. Species aggregation is a common phenomenon during the ESI-MS experiment and has been reported previously for palladium complexes.[10]

In contrast to what is observed for acetonitrile as solvent, the ESI-MS spectra obtained when employing 100 % MeOH as dissolution and introduction solvent shows the absence of species **4a-III** and **4a-IV**. Instead, an isotope cluster at *m*/z 342 is observed, which may be assigned to a doubly-charged species, **4a-V** (Fig. 4.9). This particular mass fragment is observed in the ESI-MS spectra of the other analogues, **4b** and **4d**, as well.

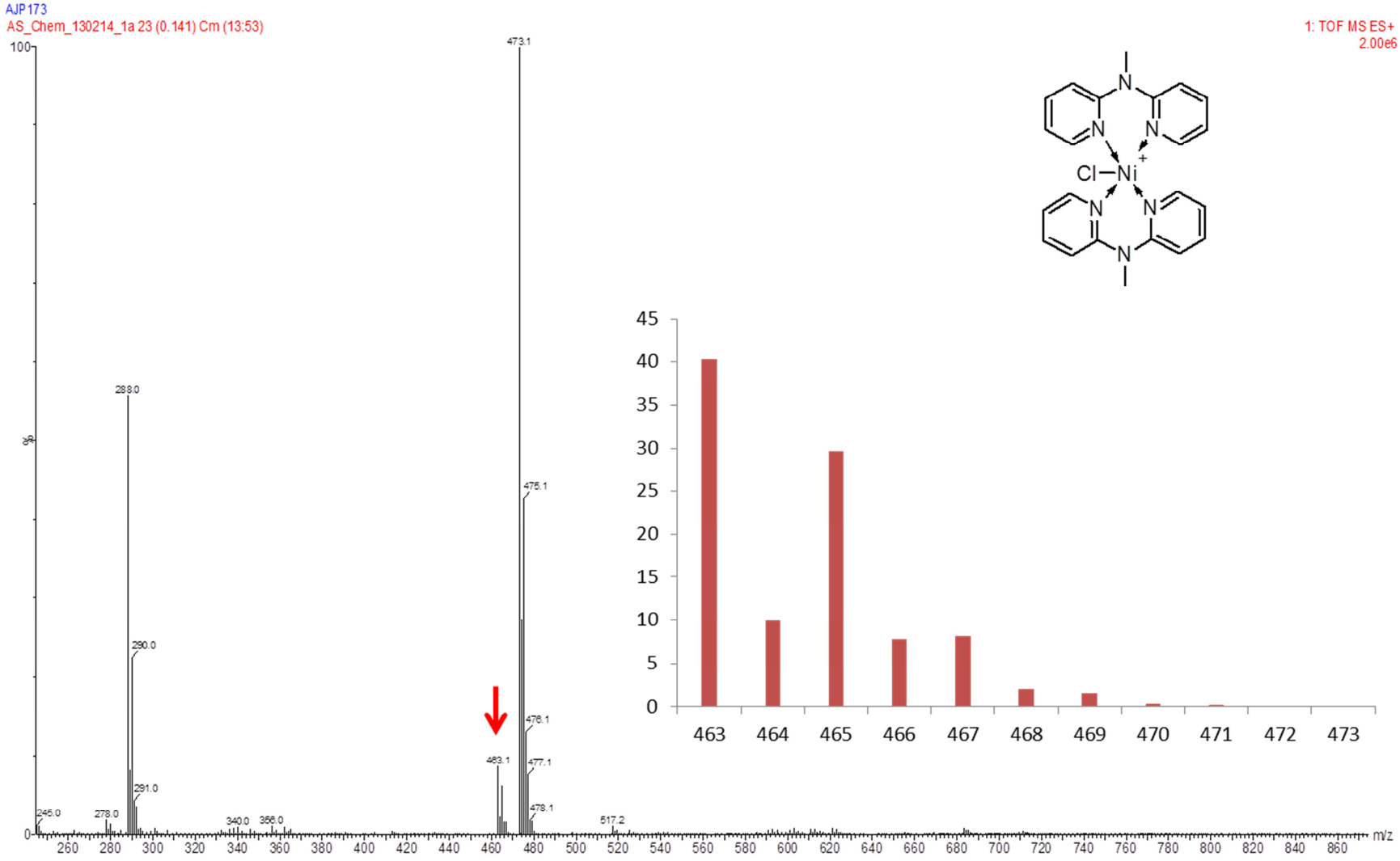

Fig. 4.6 Mass fragment assigned to $[L_2NiCl_2\text{-}Cl]^+$. Inset shows simulated isotope pattern.

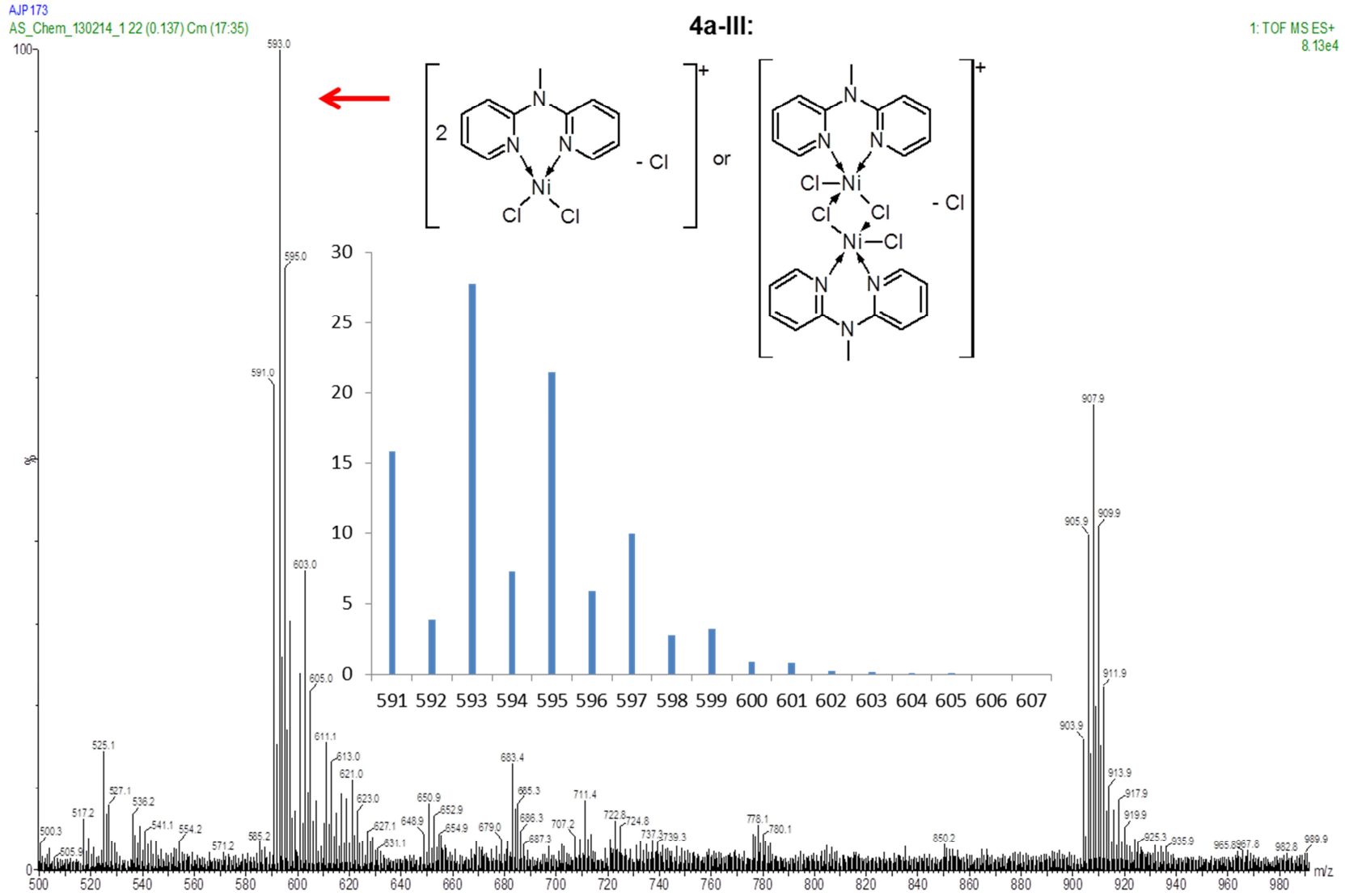

Fig. 4.7 Mass fragment corresponding to species **4a-III**. Inset shows simulated isotope pattern.

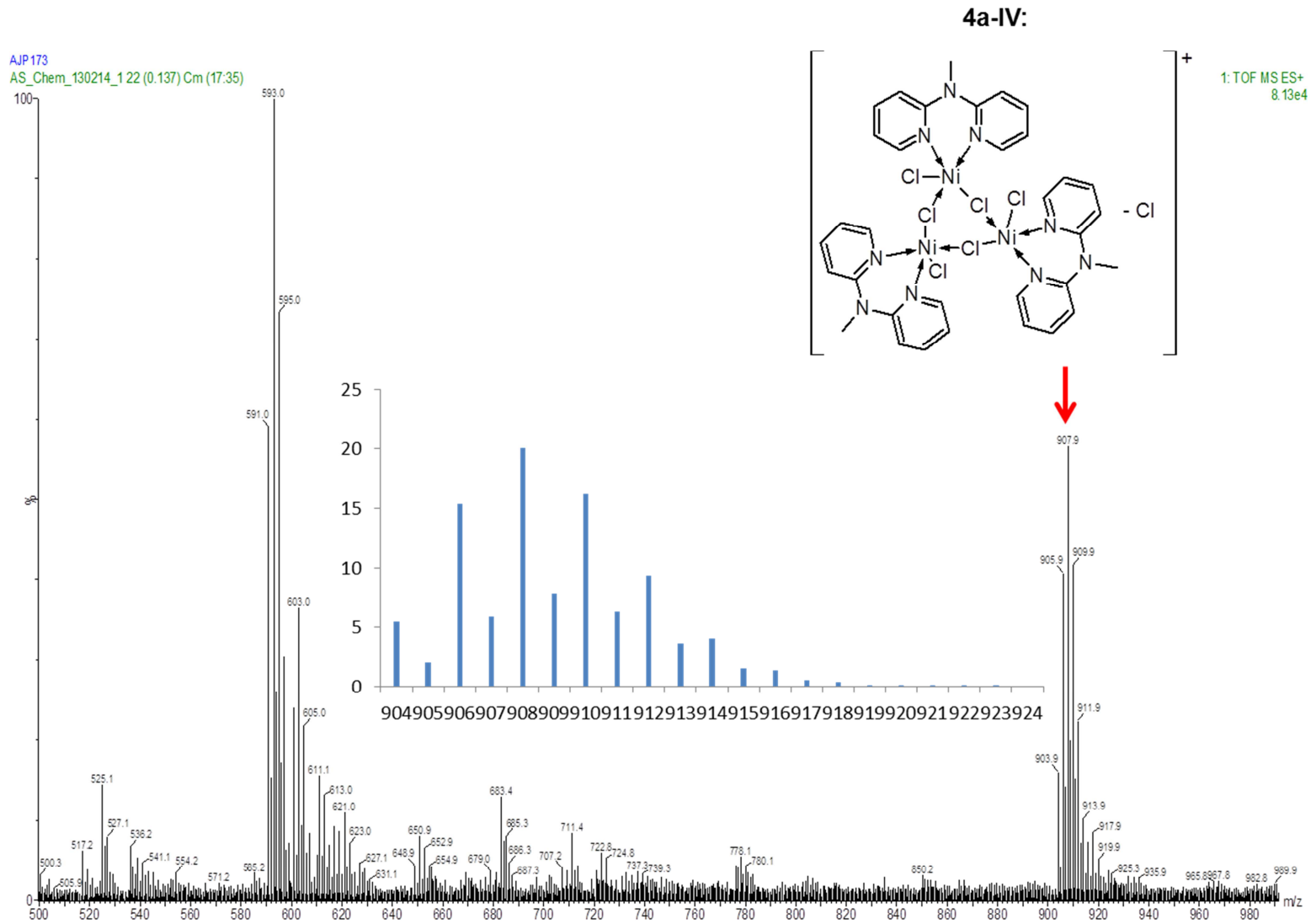

Fig. 4.8 Mass fragment corresponding to species **4a-IV**. Inset shows simulated isotope pattern.

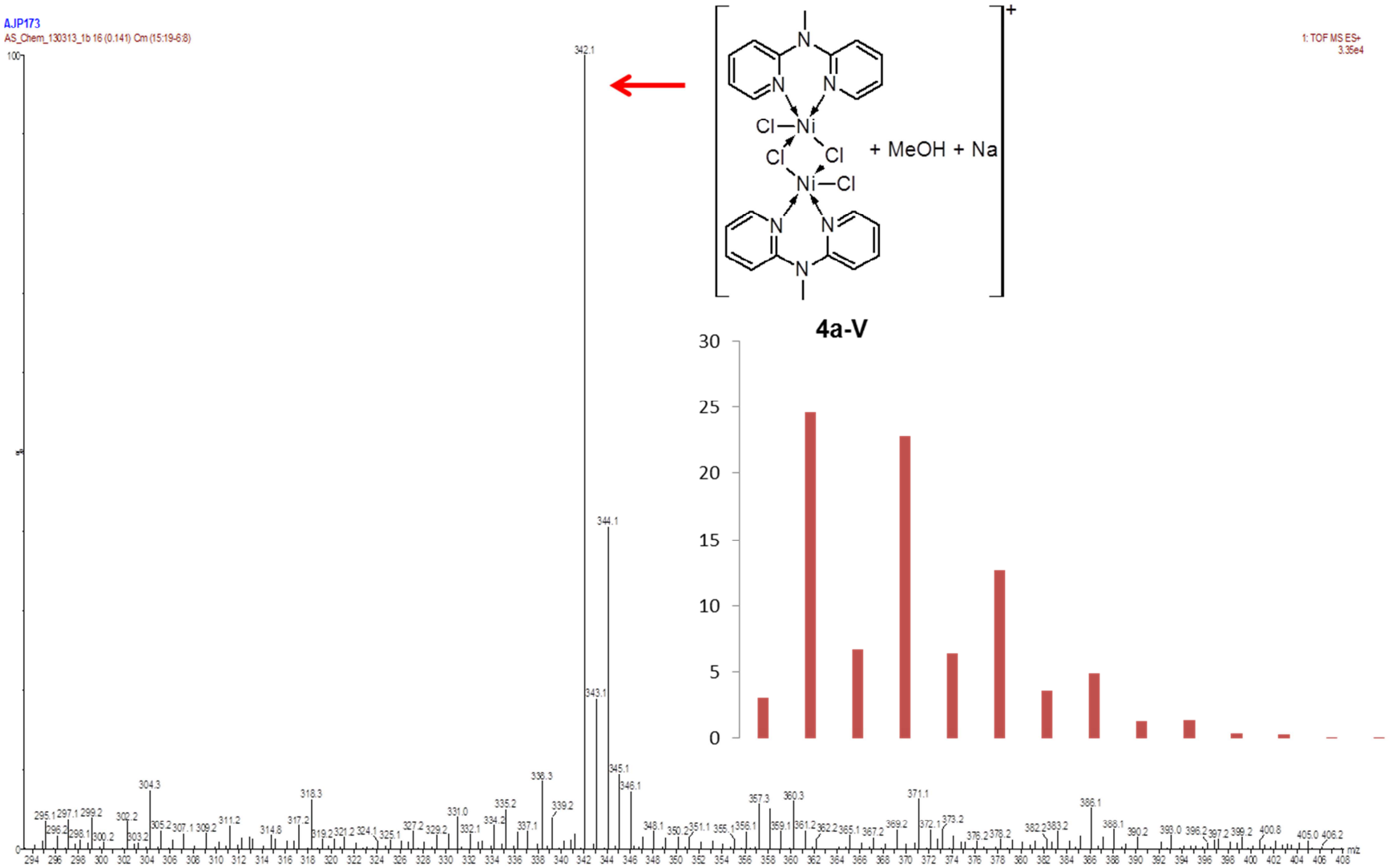

Fig. 4.9. Mass fragment corresponding to species **4a-V**. Inset shows simulated isotope pattern.

From the results discussed it becomes apparent that analyte-solvent interactions are important factors to consider during ESI-MS data interpretation, but is even more so when considering transition metal complexes, and this make unambiguous structural assignment difficult. The experimental solid state magnetic susceptibility values (μ_{eff}, Table 4.1) for complexes **4a**-**4e** are in the range 3.89-4.47 μ_B, higher than the spin-only value of 2.83 μ_B expected for two unpaired electrons.[11] Despite this, experimentally determined values are within the range observed reported for high-spin dimeric Ni(II) complexes with $S = 1$.[12] The results of elemental analyses of complexes **4a**-**4e** were consistent with the formulated dimer with the inclusion of trace amounts of dichloromethane (Experimental Section). The structure of complex **4a** was unambiguously determined by SCD analysis on single crystals grown by vapor diffusion of diethyl ether into a methanol solution of the complex. The molecular structure consists of a MeOH-solvated μ-Cl Ni(II)$_2$ dimer (Fig. 4.10) residing on a crystallographic inversion center. Crystallographic data and metric parameters are tabulated in Table 4.2 and Table 4.3 respectively.

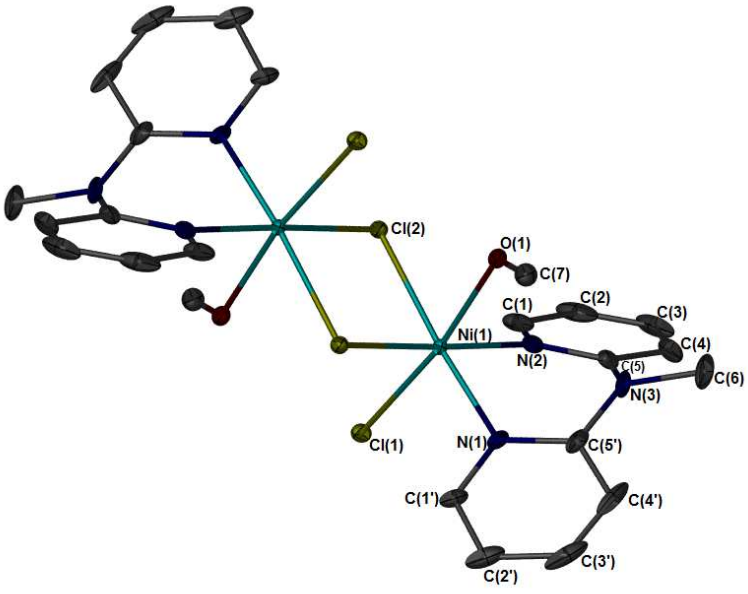

Fig. 4.10 Molecular structure of **4a** drawn at 50 % probability ellispoids. Hydrogen atoms omitted for clarity.

The Ni(II) centre coordination sphere is distorted octahedral with the equatorial plane occupied by two bridging Cl atoms and the N atoms of the chelate ligand while the axial positions are occupied by a terminal Cl atom and a bound MeOH molecule.

Table 4.2 Crystallographic data pertaining to complex **4a.2MeOH**.

Complex	**4a.2MeOH**
Empirical Formula	$C_{24}H_{30}Cl_4N_6Ni_2O_2$
Temperature (K)	100(2)
Wavelength (Å)	0.71073
Crystal System	monoclinic
Space Group	$P_{2/n}$
***a* [Å]**	8.4860(14)
***b* [Å]**	14.430(2)
***c* [Å]**	11.5135(19)
α [°]	90.00
β [°]	95.387(2)
γ [°]	90.00
volume [Å^3]	1403.64
Z	1
calc density [Mg/m^3]	1.6411
abs. coeff [mm^{-1}]	1.757
***F*(000)**	712
crystal dimensions (mm)	0.132 x 0.149 x 0.161
Reflections [Fo > 4(Fo)	3237
Parameters	178
goodness-of-fit on F^2	1.045
Final R indices [I > 2σ/(I)]	R_1 = 0.0208
	wR_2 = 0.0263

The Ni1-Cl1 and Ni1-Cl2 bond lengths of 2.394(6) and 2.415(5) Å respectively fall within the expected range reported for other μ-Cl Ni(II) dimeric structures.[13] In addition the N1-O1 bond length of 2.165(1) Å falls within the range observed for MeOH solvated-Ni(II) complexes.[7,14] The deviation from planarity in the octahedral geometry is as a result of chelation of the ligand to the metal centre, with a N1-Ni1-N2 angle of 85.77 °. The bound MeOH molecule is also slightly tilted within the crystal structure as observed by the O1-Ni1-Cl2 angle of 81.37 °. All other bond lengths and angles fall within the expected range for this class of complexes.

Table 4.3 Selected bond lengths (Å) and angles (°) for complex **4a.2MeOH**.

Bond Lengths (Å)			Bond Angles (°)
Ni1-N1	2.036(2)	N1-Ni1-N2	85.76(6)
Ni1-N2	2.044(1)	N1-Ni1-Cl1	92.51(4)
Ni1-O1	2.165(1)	N1-Ni1-Cl2	175.19(4)
Ni1-Cl1	2.394(6)	N1-Ni1-O1	93.90(5)
Ni1-Cl2	2.415(5)	N2-Ni1-Cl1	94.00(4)
		N2-Ni1-Cl2	173.61(4)

Complex **4e** displayed interesting solution behaviour during attempts at recrystallisation.

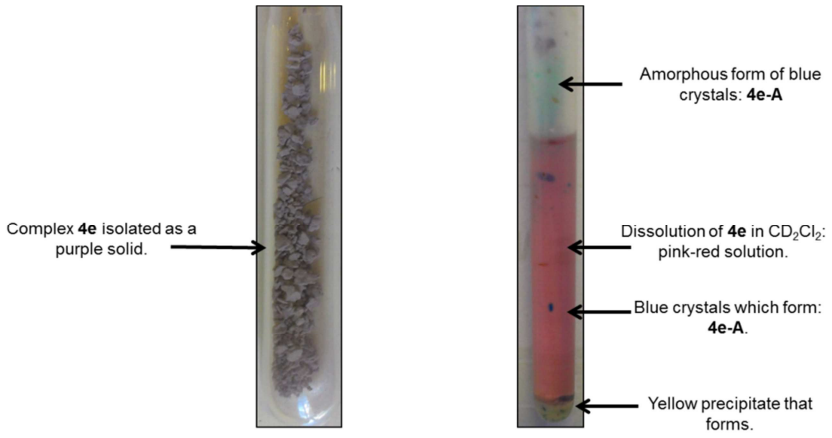

Fig. 4.11 Complex **4e** isolated as a purple solid and dissolution in CD_2Cl_2.

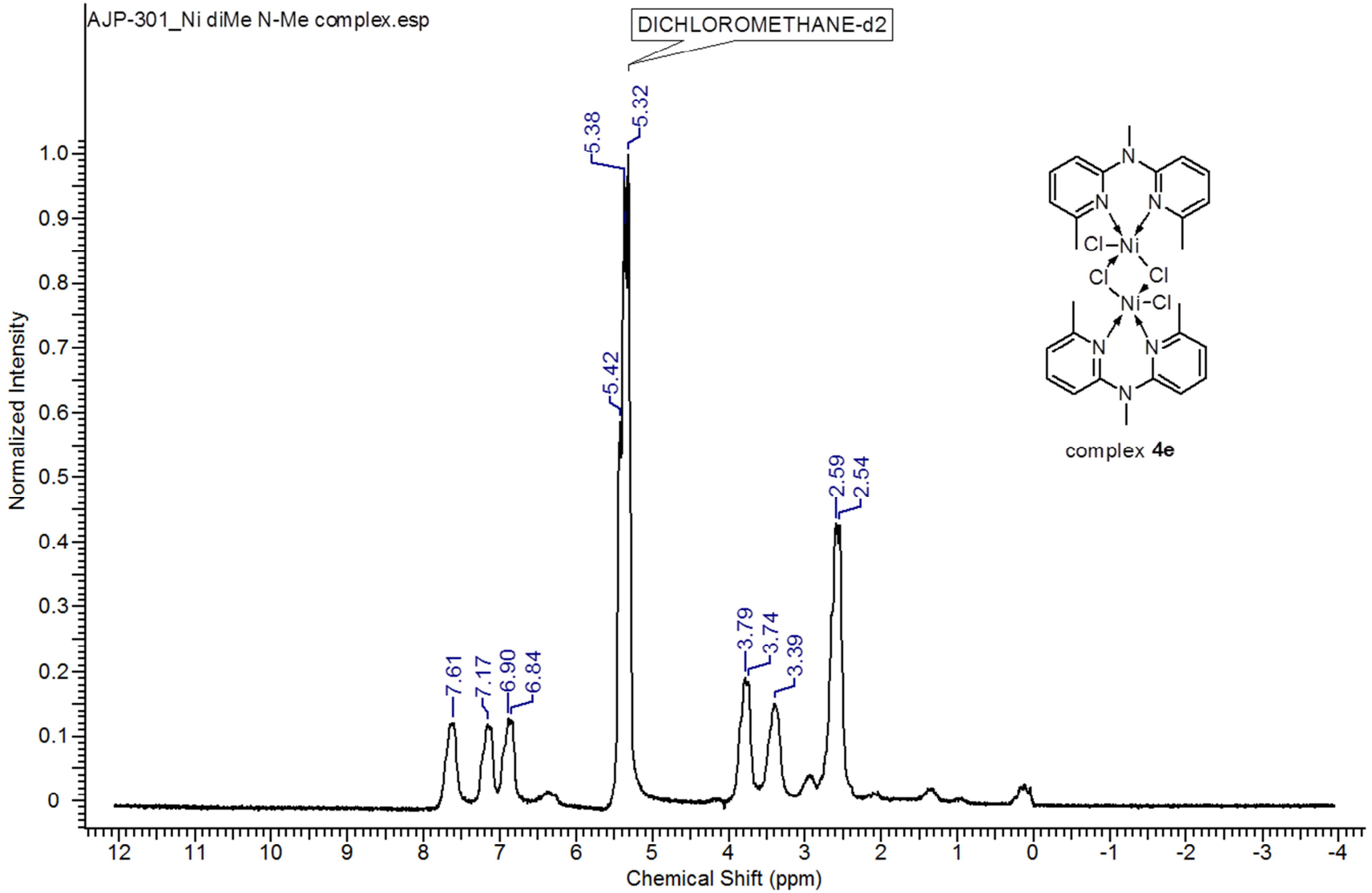

Fig. 4.12 ^{1}H NMR spectrum of complex **4e** in dichloromethane-d_2 at 25 °C.

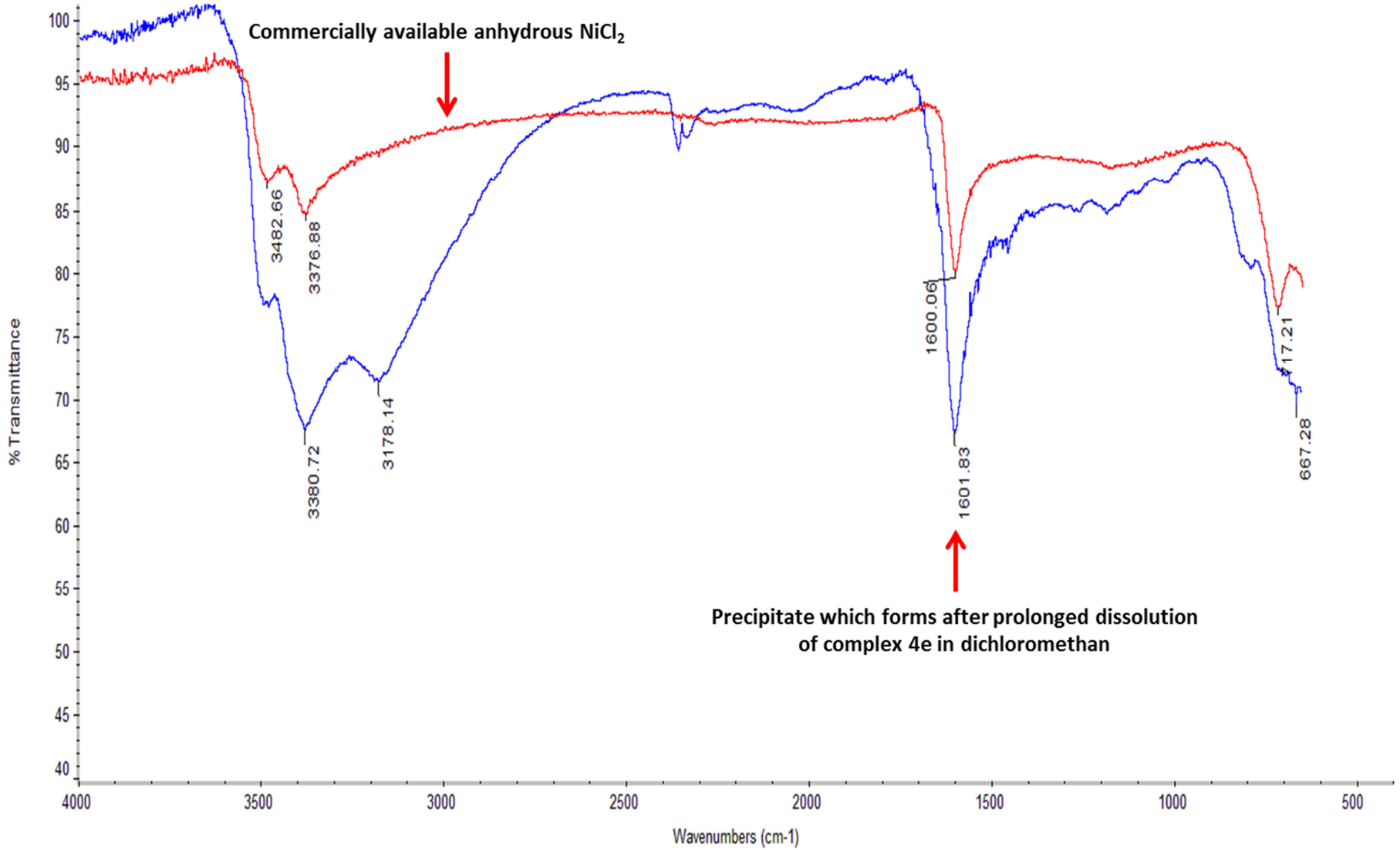

Fig. 4.13 FT-IR spectra of commercial anhydrous $NiCl_2$ (**red**) and the precipitate isolated after prolonged dissolution of **4e** in dichloromethane.

The complex was isolated as a pale purple-pink solid, the colour of which suggested a square planar geometry around the metal centre, in which the ensuing metal centre was diamagnetic (Fig 4.11), while it formed a pink-red coloured solution in dichloromethane. Previous literature reports have described square planar Ni(II) complexes as red or pink coloured solids.[15] However, analytical data, specifically magnetic susceptibility data determined in the solid state, was consistent with a paramagnetic dinuclear chloro-bridged Ni(II) complex (μ_{eff}: 4.47 μ_B). Analysis of the complex by ^{1}H NMR spectroscopy in CD_2Cl_2 showed broad, poorly resolved resonances, consistent with a *paramagnetic* transition metal complex (Fig. 4.12). Prolonged storage of **4e** as a solution in dichloromethane generated a pink-red solution initially, in which the formation of a pale-yellow precipitate and blue crystals were observed (Fig 4.11). Removal of the supernatant and analysis of the pale-yellow precipitate by FT-IR spectroscopy showed absorption bands identical to commercially available $NiCl_2$ (Fig. 4.13). This initial result suggested that the complex dissociates in solution to generate the uncoordinated dipyridylamine ligand and nickel chloride. Layering of the pink-red solution with pentane and storage at 5 °C generated blue crystals (**4e-A**) which were analysed crystallographically (Fig. 4.14).

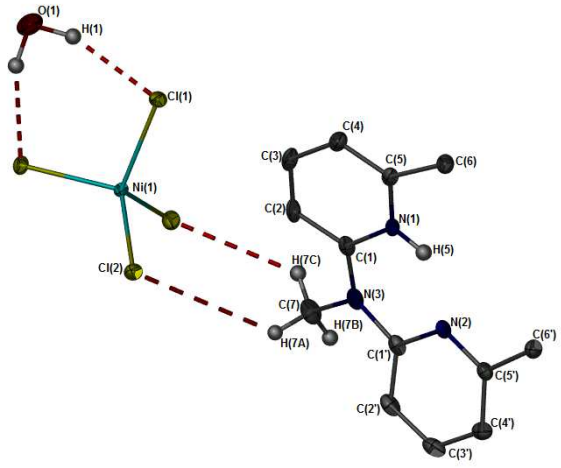

Fig. 4.14 Molecular structure of the crystals isolated as **4e-A**, drawn at 50 % probability. Ni and O atoms located on a centre of inversion. Selected hydrogen atoms omitted for clarity.

Selected crystallographic parameters (Table 4.4), bond lengths and angles (Table 4.5) are tabulated. The assymetric unit consists of a tetrachloronickelate anion which is charge-balanced by two *N*-protonated 6,6′-dimethyl-2,2′-dipyridylamine ligands.

Table 4.4 Crystallographic data pertaining to species **4e-A**.

Species	**4e-A**
Empirical Formula	$C_{26}H_{32}Cl_4N_6NiO$: 2{6,6′-Me_2-2,2′-dipyridylammonium cation}$^{+}${$NiCl_4$}$^{2-}$
Temperature (K)	100(2)
Wavelength (Å)	0.71073
Crystal System	monoclinic
Space Group	$C_{2/c}$
***a* [Å]**	21.751(4)
***b* [Å]**	11.949(2)
***c* [Å]**	13.415(2)
α [°]	90.00
β [°]	123.276(2)
γ [°]	90.00
volume [Å^3]	2915.0(8)
Z	4
calc density [Mg/m^3]	1.6411
abs. coeff [mm^{-1}]	1.064
***F*(000)**	1336
crystal dimensions (mm)	0.209 x 0.115 x 0.137
Reflections [Fo > 4(Fo)	3380
Parameters	180
goodness-of-fit on F^2	1.058
Final R indices [I > 2σ/(I)]	R_1 = 0.0326
	wR_2 = 0.0749

The cationic and anionic portions are effectively dissociated, as evidenced by Ni-N1 and Ni-N1′ bond distances of 5.540 and 5.768 Å. The Ni- and O-atoms are located on an inversion centre and display H···Cl interactions related by symmetry of 2.198 Å. In addition, H···Cl interactions are observed between the *N*-Me and the Cl atoms bound to nickel with a distance of 3.619 Å (Fig. 4.15).

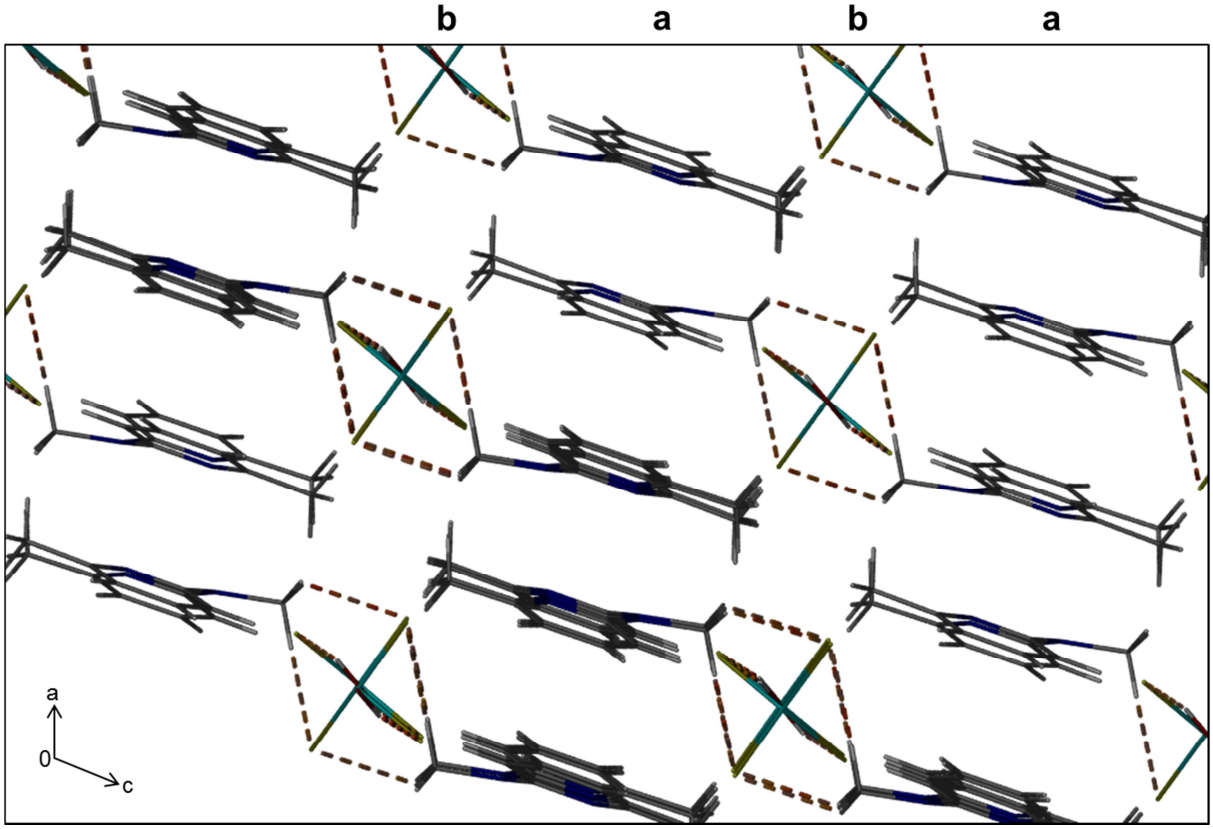

Fig. 4.15 Crystal packing for **4e-A** along the *b*-axis, showing the rhombus-shaped packing around the Ni-centre, with interleaving layers annotated as **a** and **b**.

Table 4.5 Selected bond lengths/interactions (Å) and angles (°) for species **4e-A**.

Bond Lengths and interactions (Å)			Bond Angles (°)
Ni1-Cl1	2.275(6)	Cl1-Ni1-Cl2	116.44(2)
Ni1-Cl2	2.258(7)	Cl1-Ni1-Cl1	100.12(2)
Cl1···H1	2.321		
Cl2···H7A	3.620		

The molecules are packed in rows parallel to the *c* axis, with the rows stabilised by π-π stacking interactions of 3.645 Å and 3.490 Å. Consecutive rows along the *a* axis are linked via H-bonding to each other. Interleaving layers of metal anion, water and ligand pack infinitely along the *b* axis, in an a/b motif. A number of reports in literature detail the crystallographic characterisation of transition metal-/pyridinium ion-pairs,[16] with only five reports corresponding to the preparation of tetrachloronickelate species (Fig 4.16).[17]

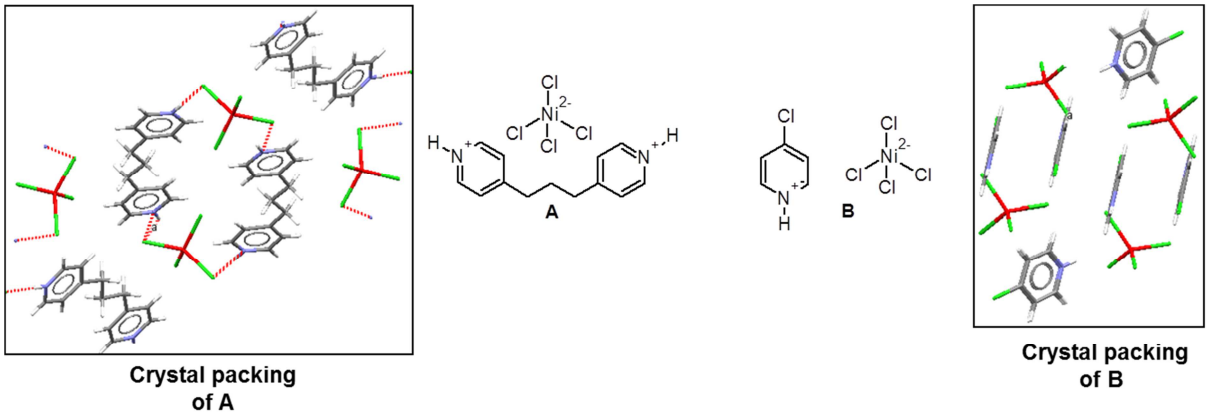

Fig. 4.16 Examples of tetrachloronickelate salts characterised crystallographically.[17b,c]

In all cases, the synthetic procedure for the isolation of the ion-pairs requires the presence of hydrochloric acid to protonate the pyridine ligand and generate the tetrachloronickelate anion.

Scheme 4.2 Hydrochloric acid-promoted formation of species **4e-A**.

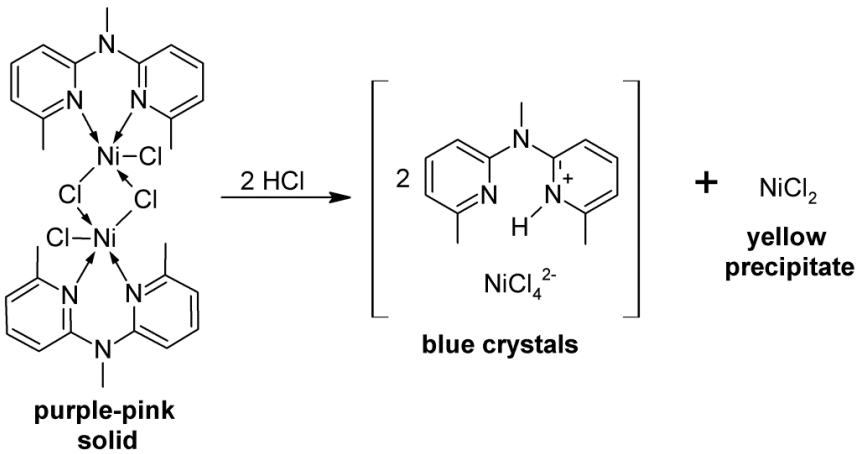

We thus propose that the formation of species **4e-A** is mediated by hydrochloric acid, known to be present in dichloromethane in trace quantities, according to Scheme 4.2.

4.3 Reactivity of complexes 4a-4e toward ethylene.

We evaluated the reactivity of complexes **4a-4e**, in the presence of alkylaluminium reagents as co-catalysts, in ethylene oligo-/polymerisation (Scheme 4.3).

Scheme 4.3 Catalytic activity of complexes **4a-4e**, in the presence of a co-catalyst, to generate ethylene oligomers.

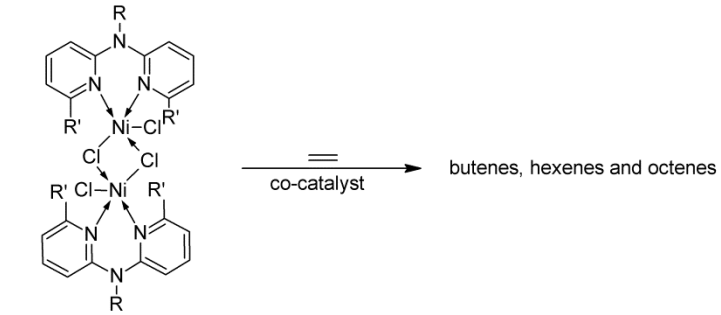

4a: R = Me; R' = H
4b: R = Bn; R' = H
4c: R = MeCy; R' = H
4d: R = Neopentyl; R' = H
4e: R = Me; R' = Me

Our initial catalysis optimisation runs were conducted with complex **4a** as pre-catalyst (Table 4.6). We found that both pre-catalyst/co-catalyst interactions, to generate active species, and Al:Ni ratios had an effect on the generation of an active catalyst system. Initial catalyst screening with complex **4a**/MAO at Al:Ni ratio of 500:1 did not generate an active catalyst system (Table 4.6, Entry 1), as evidenced by the absence of both oligomers and polymers in the reaction mixture. Previous reports demonstrated an increase in catalytic activity when employing chlorobenzene as solvent.[18] When conducting our reactions in chlorobenzene as solvent, no ethylene oligomerisation or polymerisation was observed (Table 4.6, Entry 2).

Table 4.6 Optimisation of co-catalyst and Al:Ni ratios employing complex **4a**, comparative evaluation of complexes **4b-4e** and evaluation of reaction parameters on activity.[a]

Entry	complex	co-catalyst	Al:Ni	Activity ($kg_{oligomers}.mol_{Ni}^{-1}.h^{-1}$)	TOF ($x10^3\ h^{-1}$)	% C_4	% C_6[e]	% C_8[e]	1-C_4: *trans* 2-C_4: *cis* 2-C_4
1	**4a**	MAO	500:1	-	-	-	-	-	-
2[b]	**4a**	MAO	500:1	-					
3	**4a**	MAO	1000:1	123	4	98	2	0	47:42:21
4	**4a**	MMAO	500:1		-	-	-	-	-
5	**4a**	MMAO	1000:1		-	-	-	-	-
6	**4a**	DEAC	125:1	421	10	97	2.5	0.5	33:39:28
7	**4a**	DEAC	250:1	589	21	99	1	0	26:46:28
8	**4b**	DEAC	250:1	662	24	> 99	0	0	36:38:26
9	**4c**	DEAC	250:1	527	19	> 99	0	0	22:48:30
10	**4d**	DEAC	250:1	600	21	> 99	0	0	34:40:26
11	**4e**	DEAC	250:1	499	18	> 99	0	0	98:1.2:0.8
12[c]	**4a**	DEAC	250:1	864	31	> 99	1	0	27:44:29
13[d]	**4a**	DEAC	250:1	249	9	98	2	0	20:50:30

[a] n(pre-catalyst): 10 µmol. Solvent (V): PhMe, 50 ml. Ethylene P: 5 bar. Reaction T: 30 °C. Reaction time: 30 min. TOF: n(ethylene consumed)/n(nickel).h.. MAO: methylaluminoxane. MMAO: modified methylaluminoxane. DEAC: diethyl aluminium chloride. [b] chlorobenzene as solvent. [c] Ethylene P: 10 bar. [d] Reaction time: 90 min. [e] In all cases, the percentage of 1-hexene and 1-octene within the C_6- and C_8-fraction is less than 1 %.

We found that activation of complex **4a** with MAO at Al:Ni ratios of ≥ 1000:1 in toluene generated a catalyst system capable of oligomerising ethylene with activities of 123 $kg_{oligomers}.mol_{Ni}^{-1}.h^{-1}$ and turn-over frequencies of 4 x 10^3 h^{-1} (Table 4.6, Entry 3). The formation of long-chain oligomer or polymer was not observed. The catalyst system displayed high selectivity toward the formation of 1- and 2-butenes (98 %), with up to 47 % 1-butene formed. The formation of small amounts of internal C_6-isomers and C_8-isomers were also observed, with less than 1 % of the higher olefin fraction corresponding to 1-hexene and 1-octene. Contrary to what has been reported previously for Ni(II) phosphinito-imine complexes,[15] activation of complex **4a** with MMAO with Al:Ni ratios of 500:1 and 1000:1 did not generate an active catalyst system (Table 4.6, Entry 3 and 4). Activation of complex **4a** with DEAC at an Al:Ni ratio of 125:1 generated highly active species, capable of oligomerising ethylene with high activities and at low co-catalyst loading (Table 4.6, Entry 5). Increasing the amount of DEAC to an Al:Ni ratio of 250:1 resulted in the formation of an active species capable of dimerising ethylene to butenes with an activity of 589 $kg_{oligomers}.mol_{Ni}^{-1}.h^{-1}$ and a turn-over frequency of 21 x 10^3 h^{-1} (Table 4.6, Entry 6). A selectivity of 99 % to butenes was observed, with the selectivity toward 1-butene found to be 26 %. No significant differences were observed in the selectivity towards butenes and specifically 1-butene, when employing activating complex **4a** with either MAO or DEAC as co-catalyst. The significant difference in catalytic activity as a function of the co-catalyst employed may be as a result of the different active species which is formed during activation employing MAO or DEAC. Brookhart and co-workers demonstrated experimentally that ethylene insertion to produce oligomers and polymers proceed from the catalyst resting state, the Ni-ethyl π-ethylene species.[19] Assuming that an analogous Ni-ethyl π-ethylene species is the catalyst resting state for our catalyst system (established for analogous Pd complexes,

Chapter 3), alkylation and alkyl-abstraction by DEAC, in the presence of ethylene would generate the catalyst resting state directly (Scheme 4.4).

Scheme 4.4 Proposed species generated from complex **4a**, following alkylation and alkyl-abstraction by DEAC.

In contrast, alkylation and alkyl-abstraction by MAO under identical conditions would generate the Ni-methyl π-ethylene species, which would need to undergo a number of chain propagation and termination steps to generate the catalyst resting state (Scheme 4.5).

Scheme 4.5 Proposed species generated from complex **4a**, following alkylation and alkyl-abstraction by MAO.

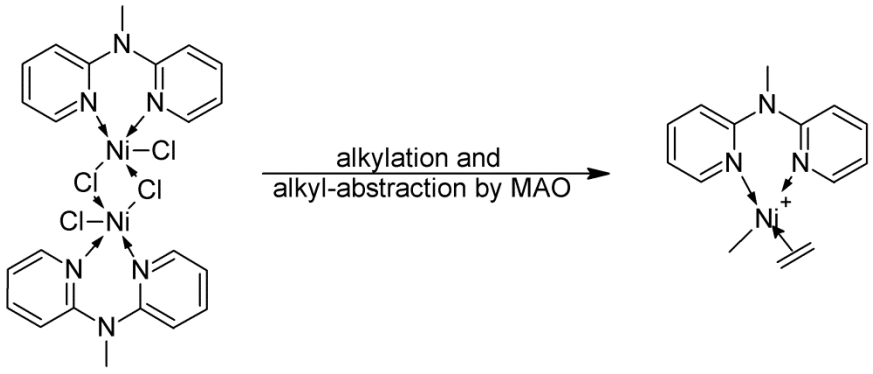

It is this reason which we believe account for the increased catalytic activity for ethylene oligomerisation observed when employing DEAC as co-catalyst.

Next, we evaluated complexes **4a-4e** comparatively in ethylene oligomerisation, employing DEAC as co-catalyst, with an Al:Ni ratio of 250:1 (Table 4.6). Under the evaluated reaction conditions, complexes **4a-4e** were highly active catalysts for the

oligomerisation of ethylene, forming butenes as major products (Table 4.6, Entry 7-11). The observed activity varied between 499-662 $kg_{oligomers}.mol_{Ni}^{-1}.h^{-1}$, while the observed turn-over frequencies varied between 18-24 x 10^3 h^{-1}, in the range observed for previously reported Ni(II) phenyl-ether pyrazole complexes.[20] When considering the activation of complexes **4a-4d** with DEAC as co-catalyst, no clear correlation between the observed reactivity and the bridgehead *N*-alkyl substituents could be established. Thus the effect of the *N*-alkyl substituents on the observed catalytic activity is negligible. On the contrary, comparing the activity of **4a** and **4e**, the introduction of steric bulk in the *ortho* positions of the pyridylamine ligand result in a decrease in activity, from 589 $kg_{oligomers}.mol_{Ni}^{-1}.h^{-1}$ to 499 $kg_{oligomers}.mol_{Ni}^{-1}.h^{-1}$. The observed decrease is as a result of increased barriers to associative exchange and β-hydrogen transfer with increased steric bulk, leading to lower observed catalytic activity, as well as a less electrophilic metal centre which decreases the rate of ethylene insertion.[6c,19,21]

When considering the selectivity toward 1-butene for complexes **4a**-**4d**, no clear trend emerges (Table 4.6, Entry 7-10). This again highlights the negligible effect the bridgehead *N*-alkyl substituents has on the observed selectivity (Fig 4.17). In general, for complexes **4a-4d**, the major isomer formed during catalysis is the thermodynamically favoured *trans* 2-butene, in the range 38-46 % (Table 4.6, Entry 7-10). The percentages of 1-butene and *cis* 2-butene formed was found to vary as well, in the range 22-36 % and 26-30 % respectively. The varying selectivity for 1- and 2-butenes may be attributed to secondary isomerisation reactions which are difficult to control. These processes have been identified employing low temperature spectroscopic techniques,[19] and has been observed previously in Ni(II)-catalysed ethylene oligomerisation.[15]

In contrast, when employing complex **4e** as catalyst, the observed selectivity for 1-butene is 98 % (Table 4.6, Entry 11, Fig 4.18).

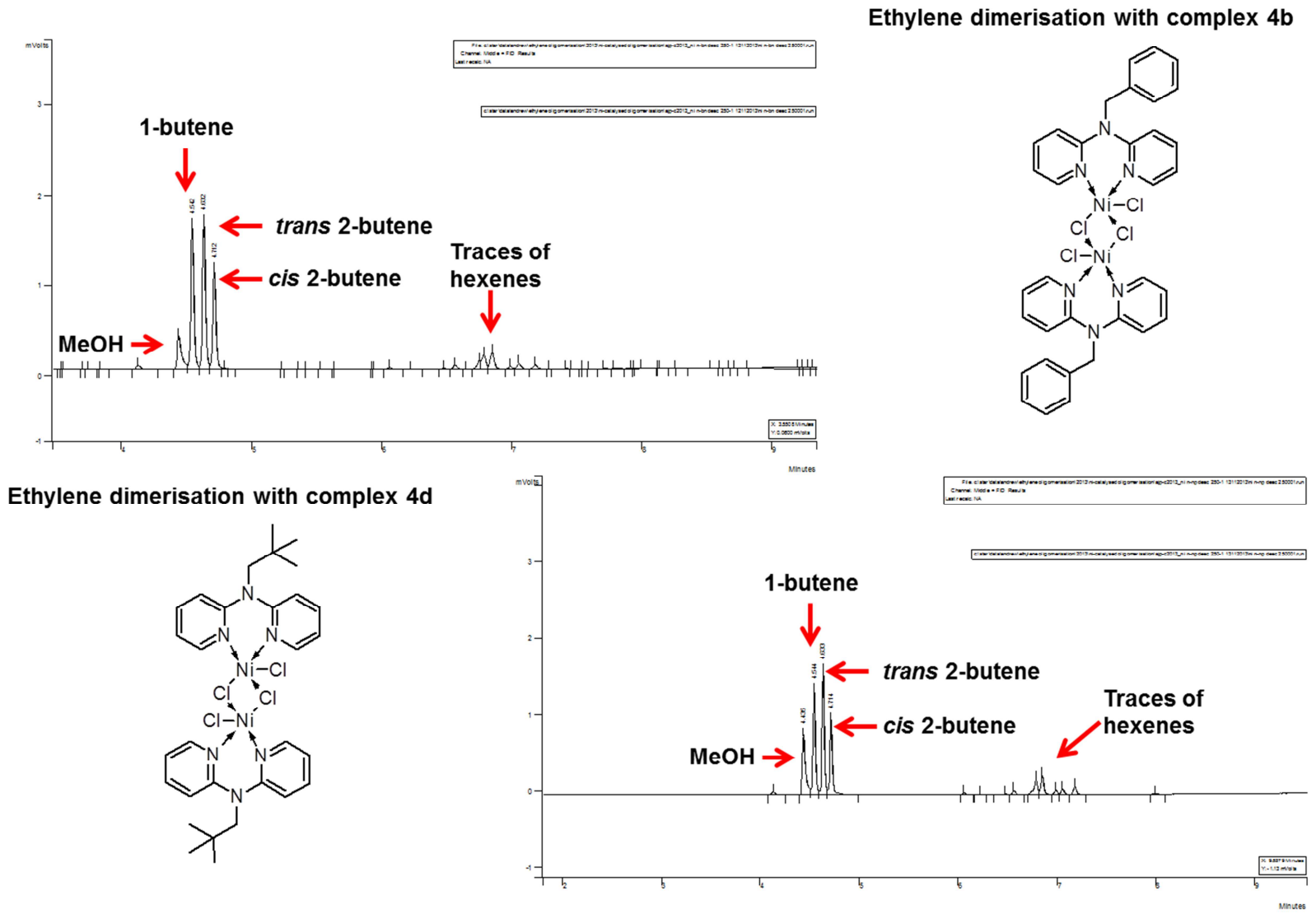

Fig. 4.17 GC chromatograms showing the formation of 1- and 2-butenes catalysed by complexes **4b** and **4d** activated with DEAC.

This marked increase in 1-butene selectivity is attributed to the presence of the *o*-Me substituents which retards the isomerisation of 1-butene, by increasing steric pressure within the nickel coordination sphere. This is as a result of the re-inserted olefin being oriented within the plane of the metal centre prior to elimination, which destabilises the active species and decreases the propensity toward isomerisation Our calculations in Chapter 3, showed that isomerisation of 1-butene via 2,1-insertion and elimination, is less favoured for the mononuclear Pd analogue of complex **4e** in comparison to the mononuclear Pd analogue of complex **4a**. In addition, it has been established by both experiment and theory, that the olefin isomerisation barriers is much higher for sterically bulky Ni-alkyl olefin species, in comparison to their less sterically bulky analogues.[6c,22] It is these factors, a combination of steric and electronic effects, which we believe account for the observed difference in butene selectivity for complexes **4a** and **4e**.

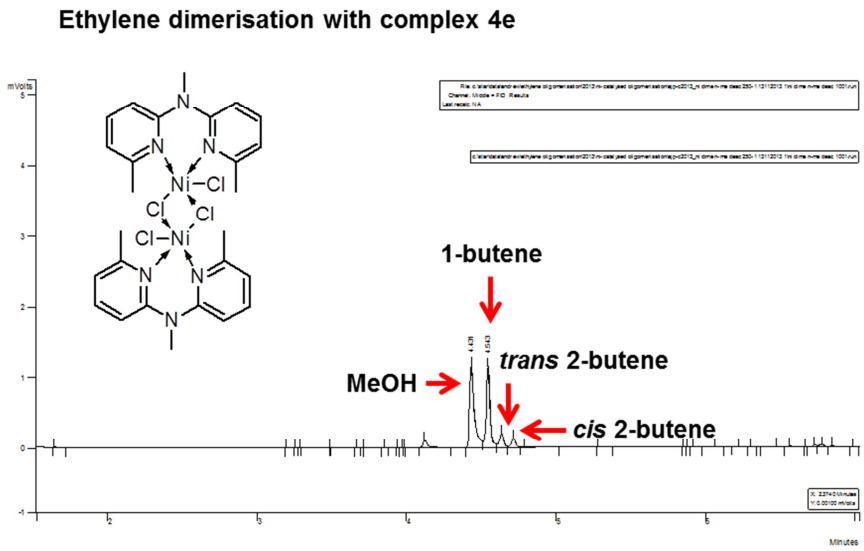

Fig. 4.18 GC chromatogram showing the selective formation of 1-butene, during ethylene dimerisation catalysed by complex **4e** and DEAC.

Finally, we briefly evaluated the effect of varying reaction paramaters on activity employing complex **4a** and DEAC as co-catalyst. It should be noted that we did not evaluate

the effect of temperature due to the highly exothermic nature of the oligomerisation reaction. We found that increasing ethylene pressure from 5 bar to 10 bar, resulted in a significant increase in catalytic activity, found to be 864 $kg_{oligomers}.mol_{Ni}^{-1}.h^{-1}$ and TOF of 31 x 10^3 h^{-1} (Table 4.6, Entry 12). This increase is attributable to an increased equilibrium concentration of monomer present in solution at higher ethylene pressures and has been observed previously for Ni(II) catalyst systems capable of oligomerising and polymerising ethylene.[3,14b,15,23] Increasing the reaction time, from 30 minutes to 90 minutes resulted in a dramatic decrease in catalytic activity, from 589 $kg_{oligomers}.mol_{Ni}^{-1}.h^{-1}$ to 249 $kg_{oligomers.}mol_{Ni}^{-1}.h^{-1}$ (Table 4.6, Entry 13). This decrease is consistent with decomposition of the catalytically active species and is generally observed for nickel- and palladium-catalysed olefin oligo- or polymerisation reactions.[1a] Our results have demonstrated the significant impact that tuning the coordination sphere of the catalyst can have on the observed product selectivity. In this example, the introduction of methyl groups in the *ortho* position of the dipyridylamine ligands increases olefin isomerisation barriers, thereby leading to the preferential formation of 1-butene.

4.4 Conclusions.

A series of chloro-bridged dinuclear Ni(II) complexes, **4a-4e**, ligated by *N*-alkyl dipyridylaldimine ligands were prepared. Characterisation by various spectroscopic and analytical techniques identified the complexes as paramagnetic Ni(II) complexes. During ESI-MS analysis of the complexes, interesting solvent-dependent fragmentation and aggregation processes were identified. In the case of complex **4e** a unique acid-mediated hydrolysis process was identified, the product of which was characterised crystallographically. Following activation with alkylaluminium reagents, complexes **4a-4e** generated species capable of oligomerising ethylene with high activity, up to

864 $kg_{oligomers}.mol_{Ni}^{-1}.h^{-1}$ and high selectivity toward 1-butene, 98 % in the case of **4e**. Consistent with previous literature reports on Ni(II)-catalysed ethylene oligomerisation, an increase in ethylene pressure was found to increase the observed catalytic activity, while an increase in reaction time resulted in a decrease in the observed catalytic activity.

4.5 Experimental Section.

All transformations were performed using standard Schlenk techniques under a nitrogen atmosphere. Solvents were dried by refluxing over the appropriate drying agents followed by distillation prior to use and all other reagents were employed as obtained. ESI-MS (positive ion mode) analyses were performed on Waters API Quattro Micro and Waters API Q-TOF Ultima instruments by direct injection of sample. FT-IR analysis was performed on a Thermo Nicolet AVATAR 330 instrument, and was recorded as neat spectra (ATR) unless otherwise specified. Melting point determinations were performed on a Stuart Scientific SMP3 melting point apparatus and are reported as uncorrected. MAO (1.0 M in toluene, Sigma-Aldrich), MMAO (7 wt % in heptanes, Azko-Nobel) and DEAC (1.8 M in toluene, Sigma-Aldrich) was purchased from commercial sources and used as received. [(DME)$NiCl_2$] was prepared according to a modified literature procedure, while the dipyridylamine ligands were synthesised as outlined in Chapter 2.[24]

4.5.1 Synthesis of [Ni(μ-Cl){2,2′-dipyridyl-N-methylamine}Cl]$_2$, 4a

To a stirring slurry of [(DME)$NiCl_2$] (237 mg, 1.079 mmol) in DCM (20 ml) was added a solution of 2,2′-dipyridyl-*N*-methylamine (200 mg, 1.079 mmol) in DCM (5 ml). The reaction mixture was stirred for 23 h at room temperature. After the allotted time the solvent was removed *in vacuo* and the blue-green solid residue obtained dissolved in MeCN and cannula-filtered into another dry Schlenk tube. The blue-green filtrate was reduced in volume

and layered with Et_2O to form a blue-green solid which was filtered, washed with ether and dried *in vacuo*. Yield: 282 mg, 83 %. % Found (Calc) for [$C_{22}H_{22}Cl_4N_6Ni_2 \cdot 0.5\ CH_2Cl_2$]: C: 40.23 (40.21); H: 3.41 (3.45); N: 12.42 (12.50).

4.5.2 Synthesis of [Ni(μ-Cl){2,2′-dipyridyl-N-benzylamine}Cl]$_2$, 4b

Complex **4b** prepared according to the same synthetic procedure as outlined for complex **4a**, with 2,2′-dipyridyl-*N*-benzylamine employed as ligand. Yield: 272 mg, 90 %. % Found (Calc) for [$C_{34}H_{30}Cl_4N_6Ni_2 \cdot 0.2\ CH_2Cl_2$]: C: 51.82 (51.85); H: 4.33 (4.39); N: 10.75 (10.78).

4.5.3 Synthesis of [Ni(μ-Cl){2,2′-dipyridyl-N-methylcyclohexylamine}Cl]$_2$, 4c

Complex **4c** prepared according to the same synthetic procedure as outlined for complex **4a**, with 2,2′-dipyridyl-*N*-methylcyclohexylamine employed as ligand. Yield: 241 mg, 81 %. % Found (Calc) for [$C_{34}H_{42}Cl_4N_6Ni_2 \cdot 0.6\ CH_2Cl_2$]: C: 48.45 (48.95); H: 4.83 (5.14); N: 10.11 (9.88).

4.5.4 Synthesis of [Ni(μ-Cl){2,2′-dipyridyl-N-neopentylamine}Cl]$_2$, 4d

Complex **4d** prepared according to the same synthetic procedure as outlined for complex **4a**, with 2,2′-dipyridyl-*N*-neopentylamine employed as ligand. Yield: 258 mg, 74 %. % Found (Calc) for [$C_{34}H_{42}Cl_4N_6Ni_2 \cdot 0.3\ CH_2Cl_2$]: C: 45.71 (45.86); H: 4.71 (4.71); N: 11.24 (11.32).

4.5.5 Synthesis of [Ni(μ-Cl){6,6′-dimethyl-2,2′-dipyridyl-N-methylamine}Cl]$_2$, 4e

Complex **4d** prepared according to the same synthetic procedure as outlined for complex **4a**, with 6,6′-dimethyl-2,2′-dipyridyl-*N*-methylamine employed as ligand.

Yield: 196 mg, 53 %. % Found (Calc) for $C_{26}H_{30}Cl_4Ni_6Ni_2$: C: 45.49 (45.54); H: 3.98 (4.41); N: 12.06 (12.06).

4.5.6 X-Ray Crystal structure determination.

Single crystals of complexes **4a** and **4e-A** were mounted on a nylon loop and centred in a stream of cold nitrogen at 100(2) K. Crystal evaluation and data collection were performed on a Bruker-Nonius SMART Apex II CCD diffractometer with Mo K_α radiation (λ = 0.71073 Å). Data collection, reduction and refinement were performed using SAINT[25] and SADABS,[26] which forms part of the APEX II software package. The structures were solved by direct methods and refined by full-matrix least-squares on F^2 using SHELX-97[27] within the X-Seed graphic user interface.[28] All non-hydrogen atoms were refined anisotropically and all hydrogen atoms were placed using calculated positions and riding models.

4.5.7 Procedure for preparative-scale ethylene oligomerisation.

In a glovebox under a nitrogen atmosphere, a 250 ml Parr high-pressure autoclave was charged with the required amount of solvent and co-catalyst, and was sealed prior to being attached to the ethylene feed. The reactor was brought to temperature at which point a dispersion of the pre-catalyst in toluene (total volume: 50 ml) was added via syringe under positive ethylene pressure. The ethylene feed was maintained at the required pressure throughout the catalytic run, with the volume of ethylene consumed monitored throughout the catalytic run. After the allotted time the reactor was cooled to 0 °C, excess ethylene vented and the reaction mixture quenched with acidified MeOH (10 % solution). A sample was filtered and analysed by GC-FID, with *p*-xylene as internal standard. The observed oligomers

were quantified against calibrated standards. Quenching the reaction mixture did not precipitate any polymers and no long-chain oligomers were observed after work-up.

4.6 References

(1) (a) Ittel, S. D.; Johnson, L. K.; Brookhart, M. *Chem. Rev.*, **2000**, *100*, 1169 (b) Wang, C.; Friedrich, S.; Younkin, T. R.; Li, R. T.; Grubbs, R. H.; Bansleben, D. A.; Day, M. W. *Organometallics*, **1998**, *17*, 3149 (c) Younkin, T. R.; Connor, E. F.; Jason, I. H.; Friedrich, S. K.; Grubbs, R. H.; Bansleben, D. A. *Science*, **2000**, *287*, 460 (d) Gibson, V. C.; Spitzmesser, S. K. *Chem. Rev.*, **2002**, *103*, 283.

(2) (a) Ojwach, S. O.; Guzei, I. A.; Benade, L. L.; Mapolie, S. F.; Darkwa, J. *Organometallics*, **2009**, *28*, 2127 (b) Keim, W. *Angew. Chem. Int. Ed. Engl.*, **1990**, *29*, 235.

(3) Song, D.-P.; Wu, J.-Q.; Ye, W.-P.; Mu, H.-L.; Li, Y.-S. *Organometallics*, **2010**, *29*, 2306.

(4) (a) Connor, E. F.; Younkin, T. R.; Henderson, J. I.; Waltman, A. W.; Grubbs, R. H. *Chem. Commun.*, **2003**, 2272 (b) Waltman, A. W.; Younkin, T. R.; Grubbs, R. H. *Organometallics*, **2004**, *23*, 5121.

(5) Schultz, M.; Eisenträger, F.; Regius, C.; Rominger, F.; Hanno-Igels, P.; Jakob, P.; Gruber, I.; Hofmann, P. *Organometallics*, **2011**, *31*, 207.

(6) (a) Svejda, S. A.; Brookhart, M. *Organometallics*, **1999**, *18*, 65 (b) Tempel, D. J.; Johnson, L. K.; Huff, R. L.; White, P. S.; Brookhart, M. *J. Am. Chem. Soc.*, **2000**, *122*, 6686 (c) Deng, L.; Woo, T. K.; Cavallo, L.; Margl, P. M.; Ziegler, T. *J. Am. Chem. Soc.*, **1997**, *119*, 6177.

(7) Sun, W.-H.; Song, S.; Li, B.; Redshaw, C.; Hao, X.; Li, Y.-S.; Wang, F. *Dalton. Trans.*, **2012**, *41*, 11999.

(8) Dyer, P. W.; Fawcett, J.; Hanton, M. J. *Organometallics*, **2008**, *27*, 5082.

(9) (a) Malgas-Enus, R.; Mapolie, S. F.; Smith, G. S. *J. Organomet. Chem.*, **2008**, *693*, 2279 (b) Malgas-Enus, R., *The Preparation and Characterization of Multinuclear Catalysts based on Novel Dendrimers: Application in the Oligomerization and Polymerization of Unsaturated Hydrocarbons*, PhD thesis, Stellenbosch University, 2010.

(10) (a) Ares, R.; López-Torres, M.; Fernández, A.; Vázquez-García, D.; Pereira, M. T.; Vila, J. M.; Naya, L.; Fernández, J. J. *J. Organomet. Chem.*, **2007**, *692*, 4197 (b) Taquet, J.-P.; Siri, O.; Braunstein, P.; Welter, R. *Inorg. Chem.*, **2006**, *45*, 4668.

(11) Miessler, G. L.; Tarr, D. A. *Inorganic Chemistry*; Third Edition ed.; Pearson Prentice Hall: London, United Kingdom, 2004,

(12) Schär, M.; Saurenz, D.; Zimmer, F.; Schädlich, I.; Wolmershäuser, G.; Demeshko, S.; Meyer, F.; Sitzmann, H.; Heigl, O. M.; Köhler, F. H. *Organometallics*, **2013**, *32*, 6298.

(13) (a) Speiser, F.; Braunstein, P.; Saussine, L.; Welter, R. *Inorg. Chem.*, **2004**, *43*, 1649 (b) Peng, J.; Kishi, Y. *Organic Letters*, **2011**, *14*, 86 (c) Yu, J.; Hu, X.; Zeng, Y.; Zhang, L.; Ni, C.; Hao, X.; Sun, W.-H. *New J. Chem.*, **2011**, *35*, 178 (d) Laine, T. V.; Klinga, M.; Leskelä, M. *Eur. J. Inorg. Chem.*, **1999**, *1999*, 959.

(14) (a) Zhao, L.; Niel, V.; Thompson, L. K.; Xu, Z.; Milway, V. A.; Harvey, R. G.; Miller, D. O.; Wilson, C.; Leech, M.; Howard, J. A. K.; Heath, S. L. *Dalton. Trans.*, **2004**, *0*, 1446 (b) Gao, R.; Zhang, M.; Liang, T.; Wang, F.; Sun, W.-H. *Organometallics*, **2008**, *27*, 5641.

(15) Ortiz de la Tabla, L.; Matas, I.; Palma, P.; Álvarez, E.; Cámpora, J. *Organometallics*, **2012**, *31*, 1006.

(16) (a) Tamuly, C.; Barooah, N.; Batsanov, A. S.; Kataky, R.; Baruah, J. B. *Inorg. Chem. Commun.*, **2005**, *8*, 689 (b) Shi, X.-F.; Xing, Z.-Y.; Wu, L.; Zhang, W.-Q. *Inorg. Chim. Acta*, **2006**, *359*, 603 (c) Li, L.; Turnbull, M. M.; Landee, C. P.; Jornet, J.; Deumal, M.; Novoa, J. J.; Wikaira, J. L. *Inorg. Chem.*, **2007**, *46*, 11254 (d) Kuhnert, J.; Cisarova, I.; Lamac, M.; Stepnicka, P. *Dalton. Trans.*, **2008**, 2454 (e) Potter, G. D.; Baird, M. C.; Cole, S. P. C. *J. Organomet. Chem.*, **2007**, *692*, 3508.

(17) (a) Bond, M. R.; Willett, R. D. *Acta Cryst. C*, **1993**, *49*, 861 (b) Cao, L.; Englert, U.; Li, Q. *Acta Cryst. E*, **2008**, *64*, m377 (c) Du, Z.-X.; Qu, J.-P. *Acta Cryst. E*, **2009**, *65*, m1656.

(18) Obuah, C.; Omondi, B.; Nozaki, K.; Darkwa, J. *J. Mol. Catal. A: Chem.*, **2014**, *382*, 31.

(19) Leatherman, M. D.; Svejda, S. A.; Johnson, L. K.; Brookhart, M. *J. Am. Chem. Soc.*, **2003**, *125*, 3068.

(20) Ulbrich, A. H. D. P. S.; Campedelli, R. R.; Milani, J. L. S.; Santos, J. H. Z. d.; Casagrande Jr, O. d. L. *Applied Catalysis A: General*, **2013**, *453*, 280.

(21) (a) Zhang, C.; Sun, W.-H.; Wang, Z.-X. *Eur. J. Inorg. Chem.*, **2006**, 4895 (b) Brookhart, M.; Rix, F. C.; DeSimone, J. M.; Barborak, J. C. *J. Am. Chem. Soc.*, **1992**, *114*, 5894.

(22) (a) Svejda, S. A.; Johnson, L. K.; Brookhart, M. *J. Am. Chem. Soc.*, **1999**, *121*, 10634 (b) Gates, D. P.; Svejda, S. A.; Oñate, E.; Killian, C. M.; Johnson, L. K.; White, P. S.; Brookhart, M. *Macromolecules*, **2000**, *33*, 2320 (c) Jenkins, J. C.; Brookhart, M. *J. Am. Chem. Soc.*, **2004**, *126*, 5827.

(23) (a) Rodriguez, B. A.; Delferro, M.; Marks, T. J. *Organometallics*, **2008**, *27*, 2166 (b) Mu, H.-L.; Ye, W.-P.; Song, D.-P.; Li, Y.-S. *Organometallics*, **2010**, *29*, 6282.

(24) Ward, L. G. L. *Inorg. Synth.*, **1971**, *13*, 154.

(25) SAINT data reduction software, 6.45, Bruker AXS Inc.,Madison, WI, 2003

(26) Blessing, R. H. *Acta Crystallogr. Sect. A: Found. Crystallogr.*, **1995**, *51*, 33.

(27) SHELX-97, 1997

(28) (a) Barbour, L. J. *J. Supramol. Chem.*, **2001**, *1*, 189 (b) Atwood, J. L.; Barbour, L. J. *Cryst. Growth. Des.*, **2003**, *3*, 3.

5.1 Introduction

Chromium-catalysed olefin transformations has garnered significant research interest in recent years, primarily as a result of these catalyst systems having proven to be very amenable to industrial application.[1] Despite numerous reports regarding synthesis and catalytic application of chromium systems, a thorough understanding of the structure-activity relationships in these catalyst systems has been complicated by i) the paramagnetic nature of chromium in its different oxidation states make spectroscopic (NMR) identification of catalytically active intermediates difficult and ii) the redox-dynamism associated with chromium further complicates mechanistic investigations.[2] Despite these complications, specific oxidation states of chromium have been implicated in specific catalytic processes. The Cr(I)/Cr(III) redox cycle has been shown to be operative in selective ethylene trimerisation and tetramerisation via a metallacycle mechanism.[3] Evidence for this has been provided by both experiment[4] and theory.[5] For non-selective ethylene oligomerisation and polymerisation, the active species is generally thought to be a Cr(III) or Cr(II) species, with product formation proceeding via a Cossee-Arlman mechanism. This being said, mechanistic issues regarding the relationship between Cr oxidation states and product formation have not been resolved unequivocally.[1a] In terms of selective oligomerisation, non-selective oligomerisation and polymerisation; the role of ligand has always been of utmost importance. Efficient ligand design in terms of both steric and electronic effects allow for the stabilisation of a particular oxidation state during catalysis, thereby leading to an observed selectivity in product formation. This has been demonstrated by Gambarotta and co-workers who prepared a series of Cr complexes bearing a ligand with the general formula, $(\mu\text{-NR})_2(PN(H)R')_2$, with a N_2P_2 core. They showed that changes in ligand architecture and denticity allowed for the formation of catalysts which displayed switchable selectivity, self-activating behaviour and it

allowed for the formation of polymetallic structures.[4c,d,6] Of particular significance is the reaction of the deprotonated form of the ligand, *cis*{(*t*Bu)N(H)P[μ-N(*t*Bu)]$_2$PN(H)(*t*Bu)}, with $Cr(THF)_3Cl_3$ and its subsequent reductive coupling with vinyl Grignard to form {(*cis*-(*t*Bu)N(H)P[μ-N(*t*Bu)]$_2$PN(H)(*t*Bu)[Li(THF)])}Cr(*cis*-η^4-butadiene).[4d] The isolated complex was found to be a Cr(I) system which displayed self-activating behaviour as a selective ethylene trimerisation catalyst (Fig. 5.1). The key feature of the ligand is that it is an anionic $NP^{III}N$ system which allows for the efficient stabilisation of the metal in the monovalent state.

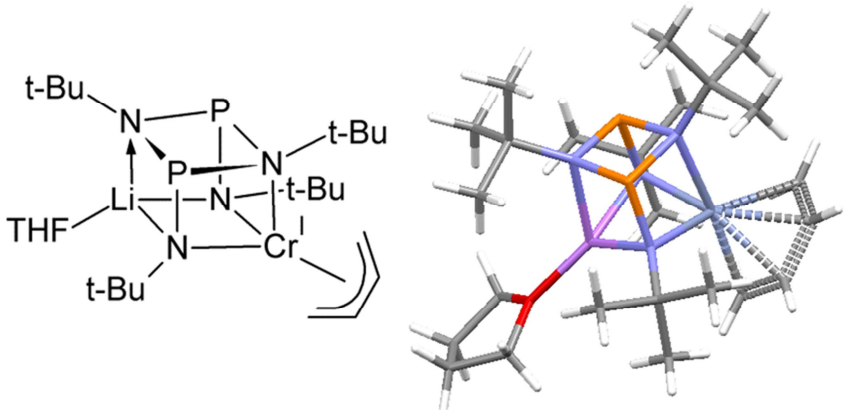

Fig. 5.1 Monovalent Cr-butadiene complex which displays self-activating behaviour in ethylene trimerisation, Copyright Cambridge Structural Database 2013.[4d]

This led us to investigate how the basicity of the N-atom in related N,P ligands may affect the nature of catalysis products. To this end, we prepared a series of iminophosphine ligands and their Cr(III) complexes and evaluated these complexes as catalyst precursors in ethylene oligo-/polymerisation. Herein we report our findings from both an experimental and theoretical perspective.

5.2 Results and Discussion

5.2.1 Preparation of iminophosphine ligands.

A series of known and novel iminophosphine ligands of general formula {[RN=C-(*o*-PPh_2-C_6H_4)]}, **5a**: R = *n*-propyl; **5b**: R = 2,6-*i*Pr_2-C_6H_3; **5c**: R = 2,4,6-Me_3-C_6H_2; **5d**: R = *t*-Bu; **5e**: R = 2,2-$(Me)_2$Pr [2b] were prepared by Schiff base condensation of the corresponding primary amine with *o*-(diphenylphosphino)benzaldehyde (Chart 5.1). Ligands **5a** and **5d** are known[7] whereas ligands **5b**, **5c** and **5e** are novel. The ligands were isolated after work-up in high yields as orange oils (**5a**, **5e**) or pale yellow crystalline solids (**5b**, **5c** and **5d**) and displayed solubility in most organic solvents but were insoluble in alcohols and alkanes. The ligands were characterised by FT-IR and ^{1}H NMR spectroscopy (**5a**, **5d**) as well as $^{13}C\{^{1}H\}$ and $^{31}P\{^{1}H\}$ NMR spectroscopy, ESI-MS spectrometry and elemental analysis (**5b**, **5c** and **5d**).

Chart 5.1 Iminophosphine ligands employed in this study.

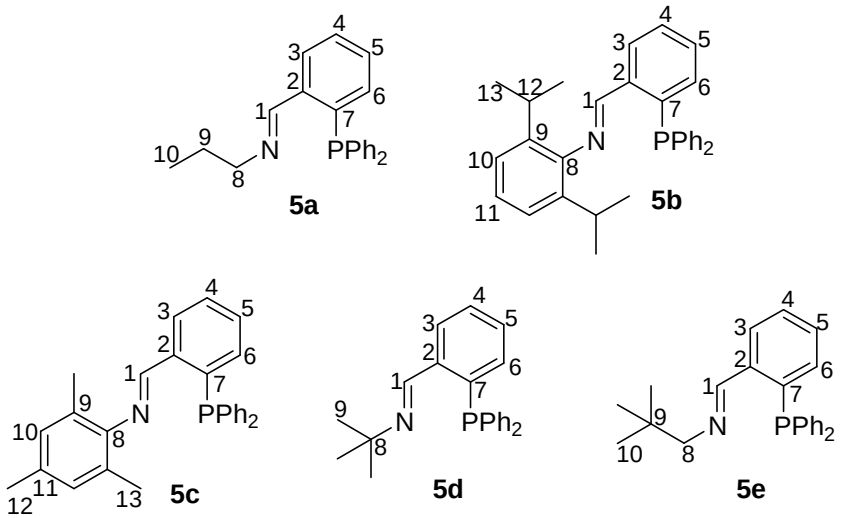

Table. 5.1 ^{1}H NMR spectral data for iminophosphine ligands.[a]

Ligand	Aromatic Region	Aliphatic Region
5a	δ 8.90 (d, 1H, $^{4}J_{H\text{-}P}$ 5.46 Hz, H^{1}); δ 8.43 (m, 1H, H^{3}); δ 7.61 (t, 1H, $^{3}J_{H\text{-}H}$ 7.16 Hz, H^{5}); δ°7.53 (t, 1H, $^{3}J_{H\text{-}H}$ 7.30 Hz, H^{4}); δ 7.40 (m, 6H, *o*-, *p*-H, P*Ph*$_2$); δ 7.31 (m, 4H, *m*-H, P*Ph*$_2$); δ 7.10 (m, 1H, H^{6})	δ 3.46 (m, 2H, H^{8}); δ 1.53 (m, 2H, H^{9}); δ 0.76 (t, 3H, $^{3}J_{H\text{-}H}$ 7.01 Hz, H^{10})
5b	δ 8.94 (d, 1H, $^{4}J_{H\text{-}P}$ 5.86 Hz, H^{1}); δ 8.31 (m, 1H, H^{3}); δ 7.52 (t, 1H, $^{3}J_{H\text{-}H}$ 7.32 Hz, H^{5}); δ 7.40 (t, 1H, $^{3}J_{H\text{-}H}$ 7.32 Hz, H^{4}); δ 7.32 (m, 6H, *o*-, *p*-H, P*Ph*$_2$); δ 7.22 (m, 4H, *m*-H, P*Ph*$_2$); δ 7.05 (m, 3H, $H^{10,11}$); δ 6.95 (m, 1H, H^{6})	δ 2.76 (sept., 2H, $^{3}J_{H\text{-}H}$ 6.83 Hz, H^{12}); δ 1.01 (d, 12H, $^{3}J_{H\text{-}H}$ 6.83 Hz, H^{13})
5c	δ 9.35 (d, 1H, $^{4}J_{H\text{-}P}$ 5.30 Hz, H^{1}); δ 8.73 (m, 1H, H^{3}); δ 7.95 (t, 1H, $^{3}J_{H\text{-}H}$ 7.62 Hz, H^{5}); δ 7.84 (t, 1H, $^{3}J_{H\text{-}H}$ 7.62 Hz, H^{4}); δ 7.79 (m, 8H, *o*-, *p*-H, P*Ph*$_2$, H^{10}); δ 7.71 (m, 4H, *m*-H, P*Ph*$_2$, H^{6}); δ 7.39 (m, 1H, H^{6})	δ 2.72 (s, 3H, H^{13}); δ 2.30 (s, 6H, H^{12})
5d	δ 8.68 (d, 1H, $^{4}J_{H\text{-}P}$ 4.88 Hz, H^{1}); δ 7.83 (m, 1H, H^{3}); δ 7.29 (t, 1H, $^{3}J_{H\text{-}H}$ 7.81 Hz, H^{5}); δ 7.19 (m, 10H, *o*-, *m* and *p*-H, P*Ph*$_2$); δ 7.16 (t, 1H, $^{3}J_{H\text{-}H}$ 7.32 Hz, H^{4}); δ 6.72 (m, 1H, H^{6})	δ 0.96 (s, 9H, H^{9})
5e	δ 8.74 (d, 1H, $^{4}J_{H\text{-}P}$ 4.88 Hz, H^{1}); δ 7.94 (m, 1H, H^{3}); δ 7.39 (m, 1H, H^{5}); δ 7.31 (t, 1H, $^{3}J_{H\text{-}H}$ 7.32 Hz, H^{4}); δ 7.25 (m, 6H, *o*-, *p*-H, P*Ph*$_2$); δ 7.18 (m, 4H, *m*-H, P*Ph*$_2$); δ 6.72 (m, 1H, H^{6})	δ 3.16 (s, 2H, H^{8}); δ 0.76 (s, 9H, H^{10})

[a] Spectra recorded in $CDCl_3$ at 25 °C. Chemical shifts reported as δ ppm values, referenced relative to residual proton signals of the solvent.

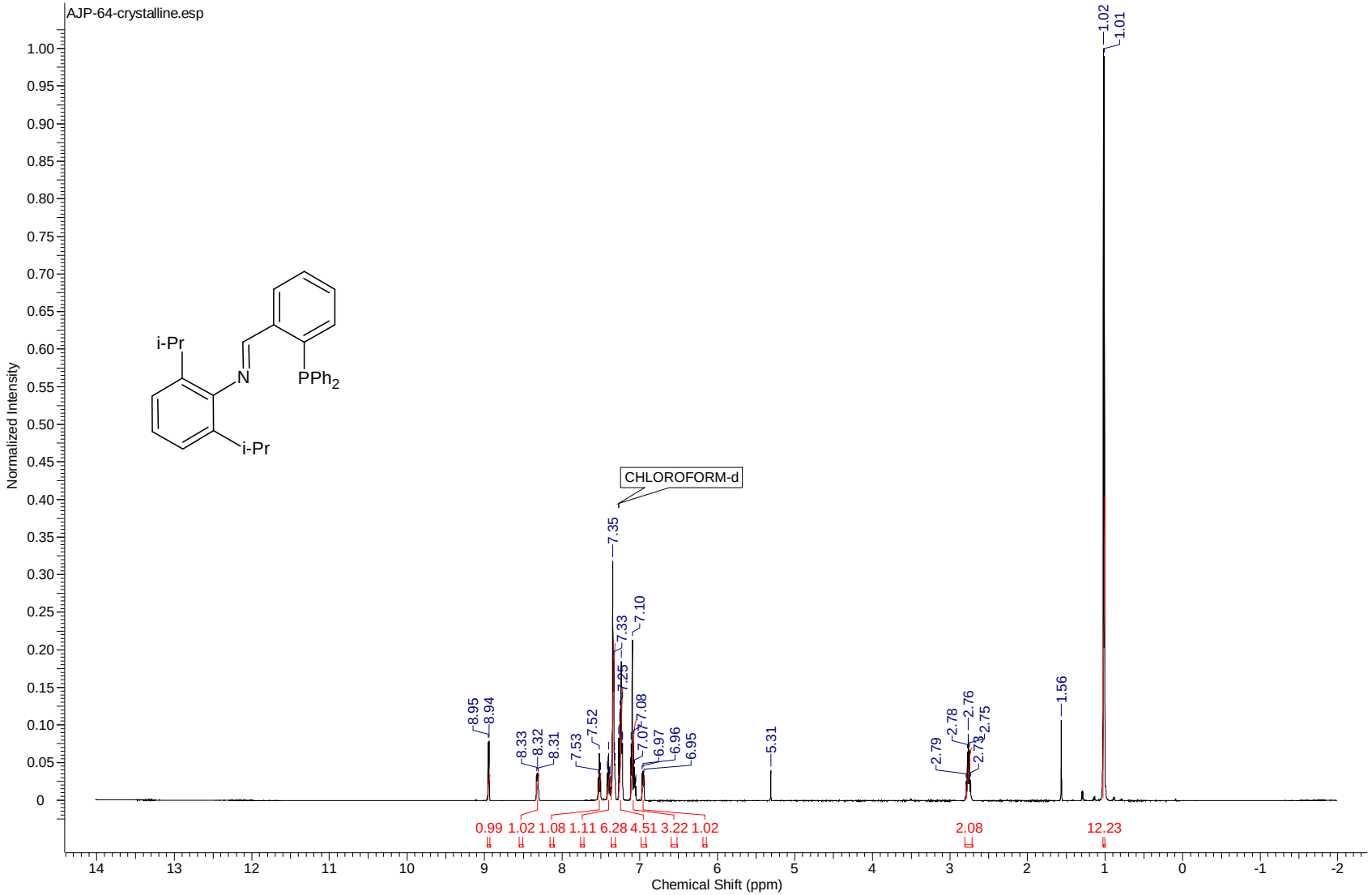

Fig. 5.2 ^{1}H NMR spectrum of iminophosphine ligand **5b** recorded in $CDCl_3$ solution.

FT-IR analysis showed a $\upsilon_{C=N}$ absorption band in the range 1628-1637 cm^{-1} which is indicative of the formation of the Schiff base condensation product (Table 5.2). In the ^{1}H NMR spectra of the iminophosphine ligands (Table 5.1), the imine proton resonance was observed as a doublet in the range δ 8.74-9.35 ppm, due to through-space coupling to the phosphorus substituent ($^{4}J_{H\text{-}P}$ 4.88-5.86 Hz, Fig. 5.2).[8] Further analysis by $^{13}C\{^{1}H\}$ and $^{31}P\{^{1}H\}$ NMR showed the C_{imine} and PPh_2 resonances in the range δ 148.55 ppm and δ -12.26 to -15.61 ppm respectively (Table 5.2), further confirming the isolation of the desired compounds. ESI-MS analysis of ligands **5b**, **5c** and **5e** showed the base peak and molecular ion at *m/z* 450, 408 and 360 respectively, which corresponded to the $[M + H]^+$ ion.

Table 5.2 Analytical data pertaining to iminophosphine ligands **5a-5e**.

Ligand	FT-IR ($\upsilon_{C=N}$, cm^{-1})[a]	$^{31}P\{^{1}H\}$ NMR (PPh_2, δ)[b]	M.p.[c]	ESI-MS[d]
5a	1637	-16.06	oil	n.d.[e]
5b	1628	- 15.61	126-128	450
5c	1631	- 13.88	136-138	408
5d	1634	- 12.26	oil	n.d.[e]
5e	1634	- 13.12	oil	360

[a] Recorded as neat specta on a ZnSe ATR accessory. [b] Recorded in $CDCl_3$ solution, ppm values. [c] Reported as uncorrected. [d] Reported mass fragment corresponds to $[M+H]^+$. [e] n.d.: not determined, literature compound.

5.2.2 Preparation of mononuclear Cr(III) iminophosphine-ligated complexes, 5f-5j.

The ligands **5a-5e** were reacted with the Cr(III) precursor, $[(THF)_3CrCl_3]$, which allowed for the isolation of mononuclear iminophosphinato Cr(III) complexes **5f-5j** (Scheme 5.1). The complexes were isolated as blue-green (**5f**, **5g** and **5h**) or olive-green (**5i** and **5j**) air- and moisture-sensitive solids in high yields. The complexes displayed solubility in polar coordinating solvents and were sparingly soluble in chlorinated organic

solvents and insoluble in ethers, alcohols, aromatic solvents and alkanes. Characterisation of the complexes by ESI-MS analysis in acetonitrile solution showed mass peaks corresponding to $[M\text{-}Cl]^+$, representative of protonation of the mononuclear complex followed by the elimination of HCl, as distinct isotope clusters which compared well to the simulated mass fragments (Table 5.3, Fig. 5.3). The fragmentation process (Scheme 5.2) is analogous to what is generally observed for transition metal-chloro complexes.[9]

Scheme 5.1 Synthesis of mononuclear iminophosphine-ligated Cr(III) complexes.

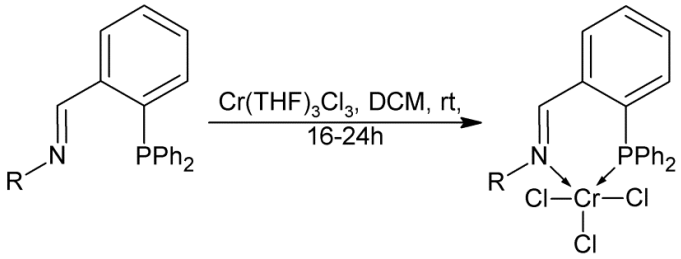

5a: R = *n*Pr
5b: R = 2,6-*i*Pr$_2$-C$_6$H$_3$
5c: R = 2,4,6-Me$_3$-C$_6$H$_2$
5d: R = *t*Bu
5e: R = 2,2-Me$_2$-Pr

5f: R = *n*Pr
5g: R = 2,6-*i*Pr$_2$-C$_6$H$_3$
5h: R = 2,4,6-Me$_3$-C$_6$H$_2$
5i: R = *t*Bu
5j: R = 2,2-Me$_2$-Pr

In addition, higher mass fragments were observed for complexes **5f, 5g** and **5h**, corresponding to $[2M + MeCN]^+$ (Fig. 5.4).

Table 5.3 Analytical data pertaining to mononuclear iminophosphinato Cr(III) complexes, **5f**-**5j**.

Complex	ESI-MS (*m/z*)[a]	μ_{eff} (μ_B)	M.p. (dec)[b]
5f	454	3.33	150-151
5g	572	3.45	205-206
5h	530	3.90	160-161
5i	468	4.08	145-146
5j	482	3.57	170-171

[a] Mass fragment corresponding to [M] - Cl^+; [b] reported as uncorrected.

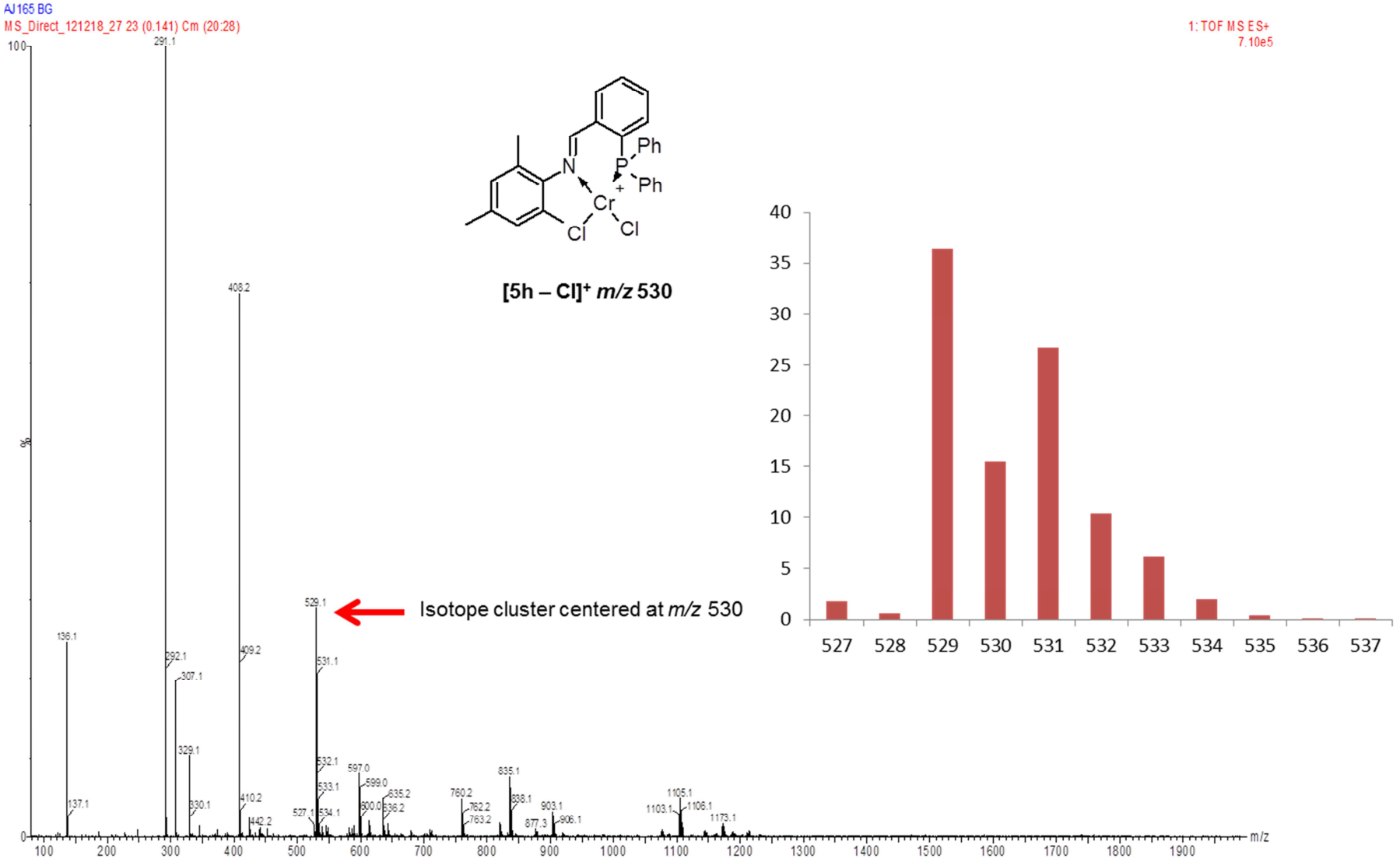

Fig. 5.3 ESI-MS spectrum for complex **5h**, showing the isotope cluster assigned to $[M\text{-}Cl]^+$. Inset shows predicted isotope pattern.

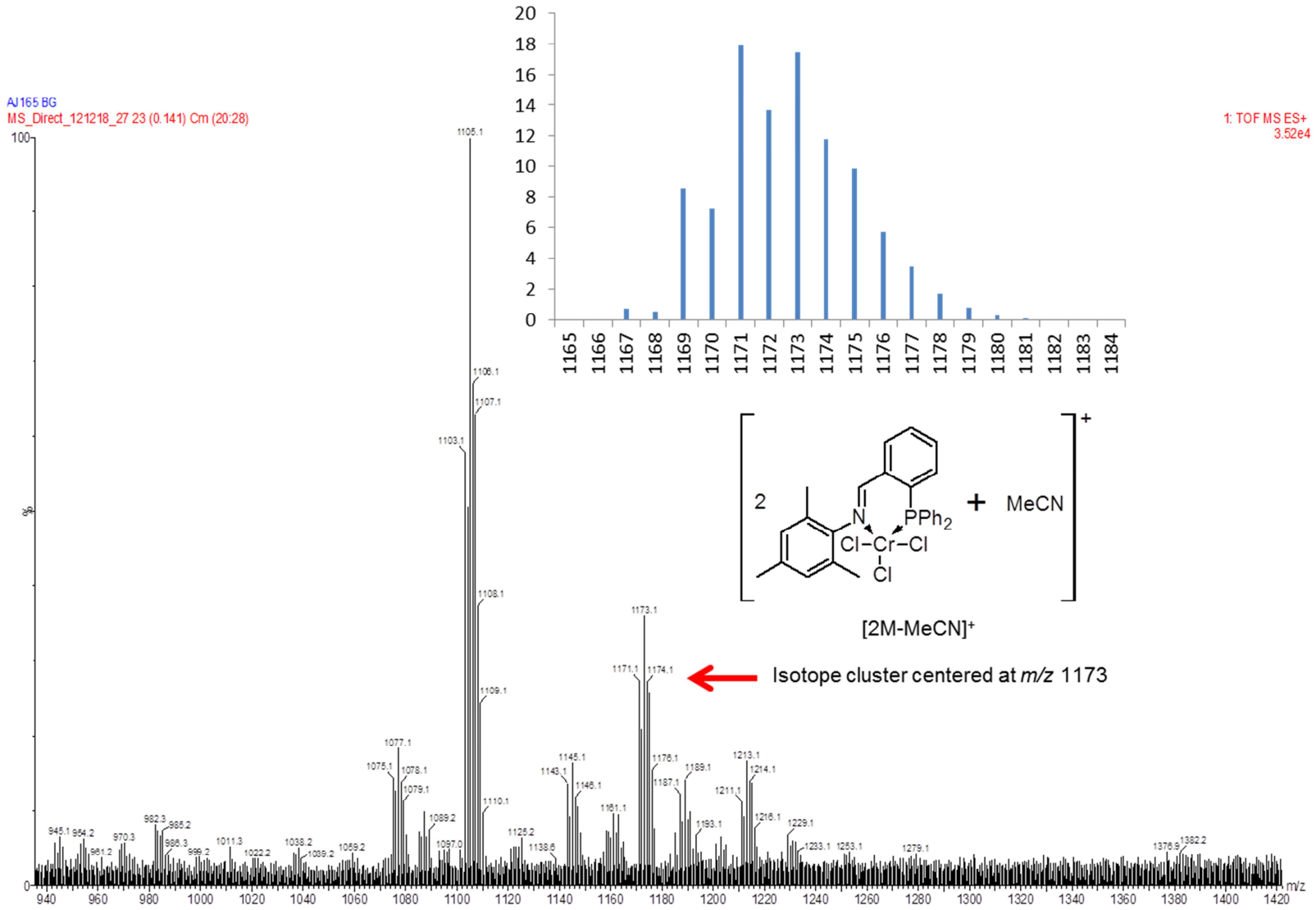

Fig. 5.4 Repesentative ESI-MS spectrum complex **5h** showing the characteristic $[M+MeCN]^+$ isotope cluster. Inset shows simulated isotope cluster.

Scheme 5.2 Observed fragmentation pattern in the ESI-MS spectrum of complex **5h**.

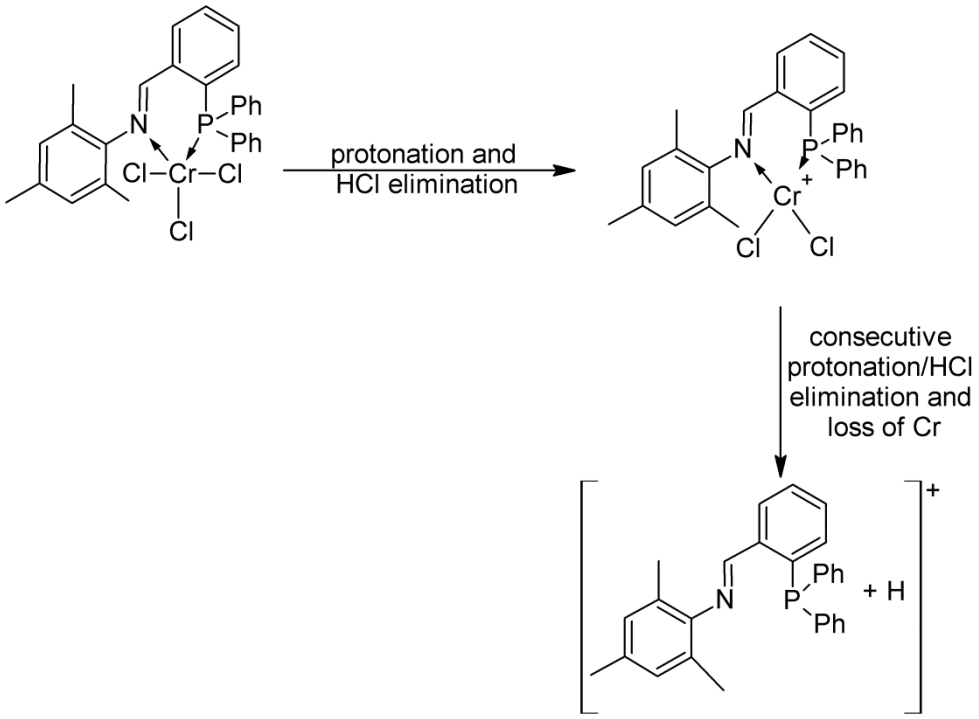

Higher mass fragments due to the formation of aggregates is known to be a common phenomenon during the ESI-MS experiment.[10] Room temperature magnetic susceptibility measurements recorded in the solid state gave μ_{eff} values in the ranging between 3.33-4.08 μ_B, in the range observed for other mononuclear Cr(III) complexes.[11] Elemental analysis confirmed the composition of the complexes (Experimental Section). The molecular structure of the complex **5g** was unambiguously confirmed by SCD analysis. Single crystals of complex **5g** was grown by slow diffusion of pentane into a dichloromethane solution of the complex. The molecular structure of complex **5g** is shown in Figure 5.5 while selected metric (Table 5.4) and crystallographic parameters are tabulated (Table 5.5).

The solid state structure shows the mononuclear Cr(III) iminophosphinato complex with a distorted octahedral geometry about the chromium center. The coordination sphere of the metal is occupied by the chelating N-P ligand occupying the equatorial plane, with a

chlorine atom *trans* to nitrogen and the oxygen atom of a coordinated water molecule *trans* to phosphorus.

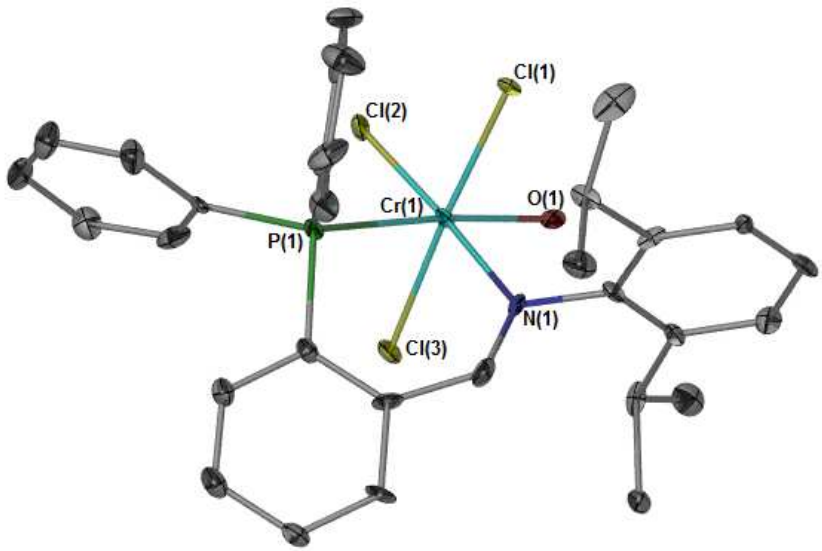

Fig. 5.5 Molecular structure of complex, **5g.H_2O**, drawn at 50 % probability ellipsoids. Hydrogen atoms omitted for clarity.

Table 5.4 Selected bond lengths (°) and angles (Å) for complex **5g.H_2O.**

Bond Lengths (Å)		Bond Angles (°)	
Cr1-N1	2.150(3)	P1-Cr1-N1	85.10(9)
Cr1-P1	2.459(1)	Cl1-Cr1-P1	95.92(4)
Cr1-Cl1	2.330(1)	Cl1-Cr1-N1	90.21(9)
Cr1-Cl2	2.322(1)	Cl1-Cr1-O1	87.54(8)
Cr1-Cl3	2.314(1)	Cl1-Cr1-Cl2	90.46(4)
Cr1-O1	2.051(2)	Cl1-Cr1-Cl3	176.26(5)
		Cl2-Cr1-N1	177.20(1)
		Cl2-Cr1-P1	92.15(4)
		Cl2-Cr1-O1	90.22(8)

The remaining axial coordination sites are occupied by two chlorine atoms. The largest deviation from octahedral geometry is observed in the N1-Cr1-P1 (85.16 °) and P1-Cr1-Cl1 (95.85 °) angles as a result of ligand coordination to the chromium center.

The Cr1-N1 and Cr1-P1 bond lengths are 2.160 Å and 2.461 Å respectively, which are within the range reported for analogous Cr(III) complexes.[12] The Cr1-O1 bond length of 2.050 Å is within the range observed for Cr(III) complexes containing coordinated water molecules and is significantly longer than the length of a Cr=O double bond, which rules out the assignment of a higher oxidation state for chromium.[13] All other bond lengths are within the expected range for these types of complexes.[14] Closer inspection of the intermolecular interactions within the crystal lattice allowed for the identification of H-bonding motifs between the hydrogen atoms on the coordinated water molecule and the Cl-ligands, Cl1 and Cl2 (Fig. 5.6).

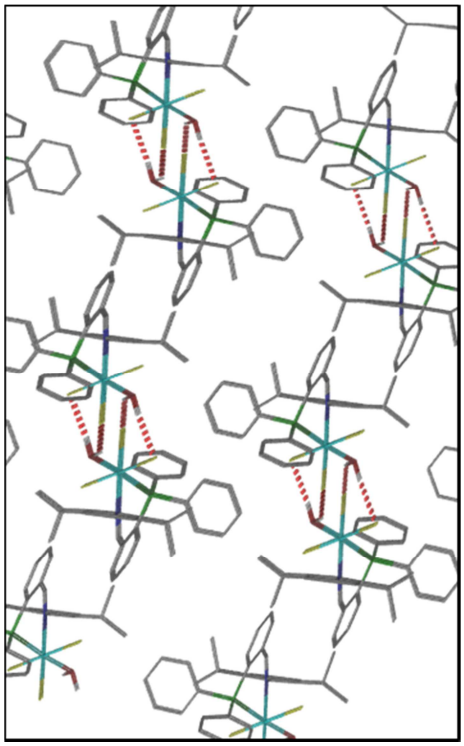

Fig. 5.6 Crystal packing of complex **5g** along the *b*-axis; showing the H···Cl bonding interaction as dashed lines.

The non-bonding interaction between Cl1/Cl2 and the bound water molecule of an adjacent molecule in the unit cell is less than the sum of the Van der Waal's radii (Cl···H: 2.285 Å) and is within the range reported for analogous Cr(III) complexes.[15]

Table 5.5 Crystallographic data for complex **5g.H_2O**.

Complex	**5g.H_2O**
Empirical Formula	$C_{33}H_{36}Cl_7CrNOP$ + disordered solvent
Temperature (K)	100(2)
Wavelength (Å)	0.71073
Crystal System	Triclinic
Space Group	P-1
***a* [Å]**	11.111(3)
***b* [Å]**	11.844(3)
***c* [Å]**	13.938(4)
α [°]	76.508(3)
β [°]	85.441(3)
γ [°]	86.677(3)
volume [Å^3]	1776.5(8)
Z	2
calc. density [Mg/m^3]	1.484
abs. coeff [mm^{-1}]	0.922
***F*(000)**	814
crystal dimensions (mm)	0.090 x 0.050 x 0.02
Reflections [Fo > 4(Fo)	8099
Parameters	349
goodness-of-fit on F^2	0.937
Final R indices [I > 2σ/(I)]	0.0650
	0.1376

5.2.3 Evaluation of mononuclear Cr(III) iminophosphinato complexes in ethylene polymerisation.

The mononuclear iminophosphinato Cr(III) complexes, **5f-5j**, were evaluated as catalyst precursors in the polymerisation of ethylene (Scheme 5.3, Tables 5.6 and 5.7). Optimisation runs were performed with complex **5f** (Table 5.6) yielding only polymer as the product. An Al:Cr ratio ≥ 500:1 is essential to form an active catalyst system (Table 5.6, Entry 2 vs Entry 3), forming neither oligomeric or polymeric products.

Scheme 5.3 General procedure for ethylene polymerisation catalysed by Cr(III) iminophosphine-ligated complexes, **5f**-**5j**.

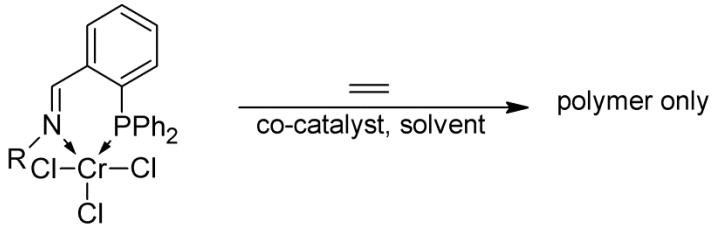

5f: R = *n*Pr

5g: R = 2,6-*i*Pr$_2$-C$_6$H$_3$

5h: R = 2,4,6-Me$_3$-C$_6$H$_2$

5i: R = *t*Bu

5j: R = 2,2-Me$_2$-Pr

For this class of complexes, toluene as solvent generates more active catalyst species in comparison to chlorobenzene (Table 5.6, Entry 3 and 4). The opposite observation has been made previously for chromium ethylene trimerisation catalysts.[16] An increase in Al:Cr ratio led to significant increases in catalytic activity (Table 5.6, Entries 2, 4-6), a trend which has generally been observed in ethylene oligo-/polymerisation catalysis.[6a,17]

Table 5.6 Optimisation runs in catalytic ethylene polymerisation employing complex **5f**.[a]

Entry	complex	Solvent	co-catalyst	Al: Cr	Activity (kg PE. mol$_{Cr}^{-1}$.h^{-1})	T_m (°C)[b]	X_c (%)[c]
1	**5f**	PhCl	MAO	100:1	0	-	-
2	**5f**	PhMe	MAO	100:1	0	-	-
3	**5f**	PhCl	MAO	500:1	35.1	133.1	58.71
4	**5f**	PhMe	MAO	500:1	133.9	134.2	59.34
5	**5f**	PhMe	MAO	1000:1	211.0	134.1	59.02
6	**5f**	PhMe	MAO	2000:1	364.3	135.7	58.65

[a] Reaction conditions: n(complex): 10 µmol; Solvent V: 50 ml; Ethylene P: 10 bar; Reaction T: 30 °C; Reaction time: 1 h. [b] Determined by DSC at a heating rate of 10 °C/min. [c] Determined by DSC. Crystallinity $X_c = \Delta H_f/\Delta H_f°$, $H_f° = 273$ J.g^{-1} for completely crystalline polyethylene.

An Al:Cr ratio of 1000:1 was employed as benchmark to perform a comparative study of the catalytic activity of the complexes **5f-5j**. All the complexes displayed moderate activity (103-235 kg PE. $mol_{Cr}^{-1}.h^{-1}$) in catalytic ethylene polymerisation when activated with MAO; producing polymer as product (Table 5.7, Entry 1-5). GC-analysis of the liquid phase showed no short-chain (C < 20) oligomer-formation (Fig. 5.7). The catalytic activity decreases in the following order:

5j > **5f** > **5g** > **5h** > **5i**

The observed activity trend correlates to a certain extent with an increase in steric bulk at nitrogen, indicative of an increase in steric bulk around the metal centre resulting in a decrease in catalytic activity (Table 5.7, Entry 1-5). Similar results have been observed previously for mononuclear metallocene-derived Cr(III) ethylene polymerisation catalysts.[18]

Table 5.7 Evaluation of complexes **5f-5j** and the effect of various reaction parameters on ethylene polymerisation.[a]

Entry	complex	Solvent	co-catalyst	Al: Cr	Activity (kg PE. $mol_{Cr}^{-1}.h^{-1}$)	T_m (°C)[b]	X_c (%)[e]
1	**5f**	PhMe	MAO	1000:1	211.0	134.1	59.91
2	**5g**	PhMe	MAO	1000:1	186.9	134.8	60.19
3	**5h**	PhMe	MAO	1000:1	140.7	133.7	60.43
4	**5i**	PhMe	MAO	1000:1	103.6	133.4	59.06
5	**5j**	PhMe	MAO	1000:1	235.3	133.6	57.59
6	**5j**	PhMe	DEAC	1000:1	502.7	134.3	57.21
7	**5j**	PhMe	MMAO	1000:1	102.5	132.4	59.45
8[c]	**5j**	PhMe	MAO	1000:1	38.4	134.5	59.32
9[d]	**5j**	PhMe	MAO	1000:1	184.0	133.7	60.01

[a] Reaction conditions: n(complex): 10 µmol; Solvent V: 50 ml; Ethylene P: 10 bar; Reaction T: 30 °C; Reaction time: 1 h. [b] Determined by DSC at a heating rate of 10 °C/min. [c] Reaction T: 60 °C; [d] Ethylene P: 20 bar. [e] Crystallinity $X_c = \Delta H_f/\Delta H_f°$, $H_f° = 273\ J.g^{-1}$ for completely crystalline polyethylene. MAO: methylaluminoxane; MMAO: modified methylaluminoxane; DEAC: diethyl aluminium chloride.

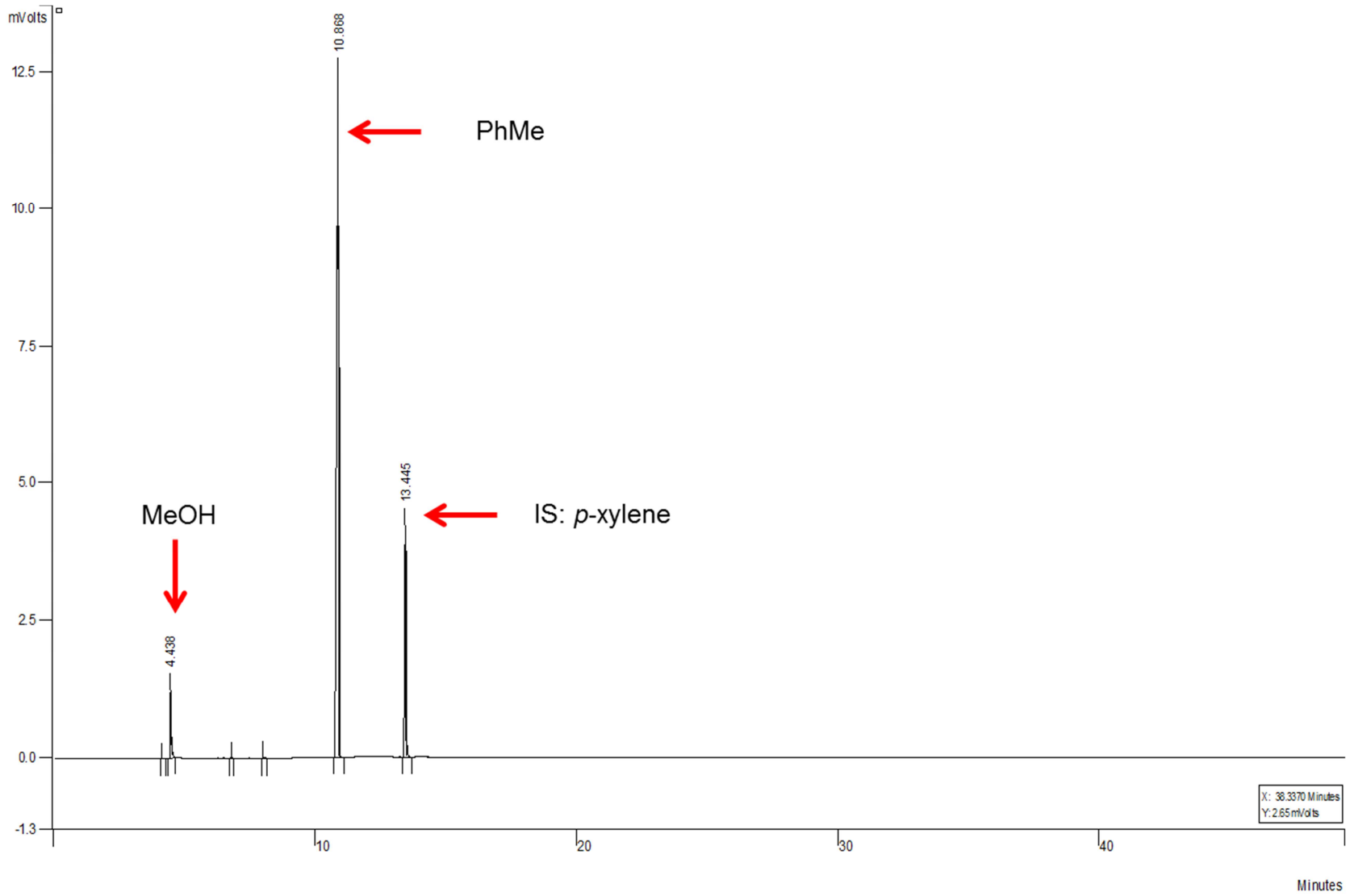

Fig. 5.7 Representative GC-FID chromatogram of the liquid phase after catalytic ethylene polymerisation with complex **5g** (Table 5.7, Entry 2).

This observation is rationalised on the basis that an increase in steric bulk inhibits ethylene coordination and insertion rates leading to an overall decrease in catalytic activity.[18-19] The effects of various reaction parameters were also evaluated employing complex **5j** (Table 5.7, Entry 6-9). Employing more Lewis acidic co-catalysts (DEAC > MAO > MMAO) results in a significant increase in catalytic activity (Table 5.7, Entry 5, 6 and 7). This effect is attributed to the strength of the interaction of the ensuing ion-pair formed during pre-catalyst activation, with weaker ion pairs leading to enhanced catalytic activity. Increasing the reaction temperature from 30 °C to 60 °C (Table 5.7, Entry 5 vs 8) resulted in a significant decrease in catalytic activity, as a result of catalyst decomposition as well as a decrease in ethylene solubility at higher temperatures.[11b,18] Finally, increasing ethylene pressure had no significant effect on catalytic activity (Table 5.7, Entry 9), suggesting that the ethylene insertion rate is zero order in olefin concentration. This is in analogy to what is generally observed for Pd-catalysed ethylene oligomerisation and polymerisation.[20] Under optimised conditions complex **5j** showed the highest activity, producing up to 503 $kg_{PE}.mol^{-1}{}_{Cr}.h^{-1}$ employing DEAC as co-catalyst.

5.2.3.1 Characterisation of the polymer produced.

Solution $^{13}C\{^{1}H\}$ NMR analysis in 1,2,4-trichlorobenzene (TCB) of the polymer at 135 °C showed a single resonance in the range δ 29.56-29.84 ppm, indicative of linear polyethylene (Fig. 5.8) while in all cases the solubility of the polymer in TCB was limited even after prolonged attempts at dissolution at high temperatures. Melt transition temperatures and degrees of crystallinity, determined by DSC, were in the range 132-135 °C and 57.21-60.43 % respectively. These observations suggested that the bulk sample was composed of linear polyethylene (Fig. 5.9).[9d,e]

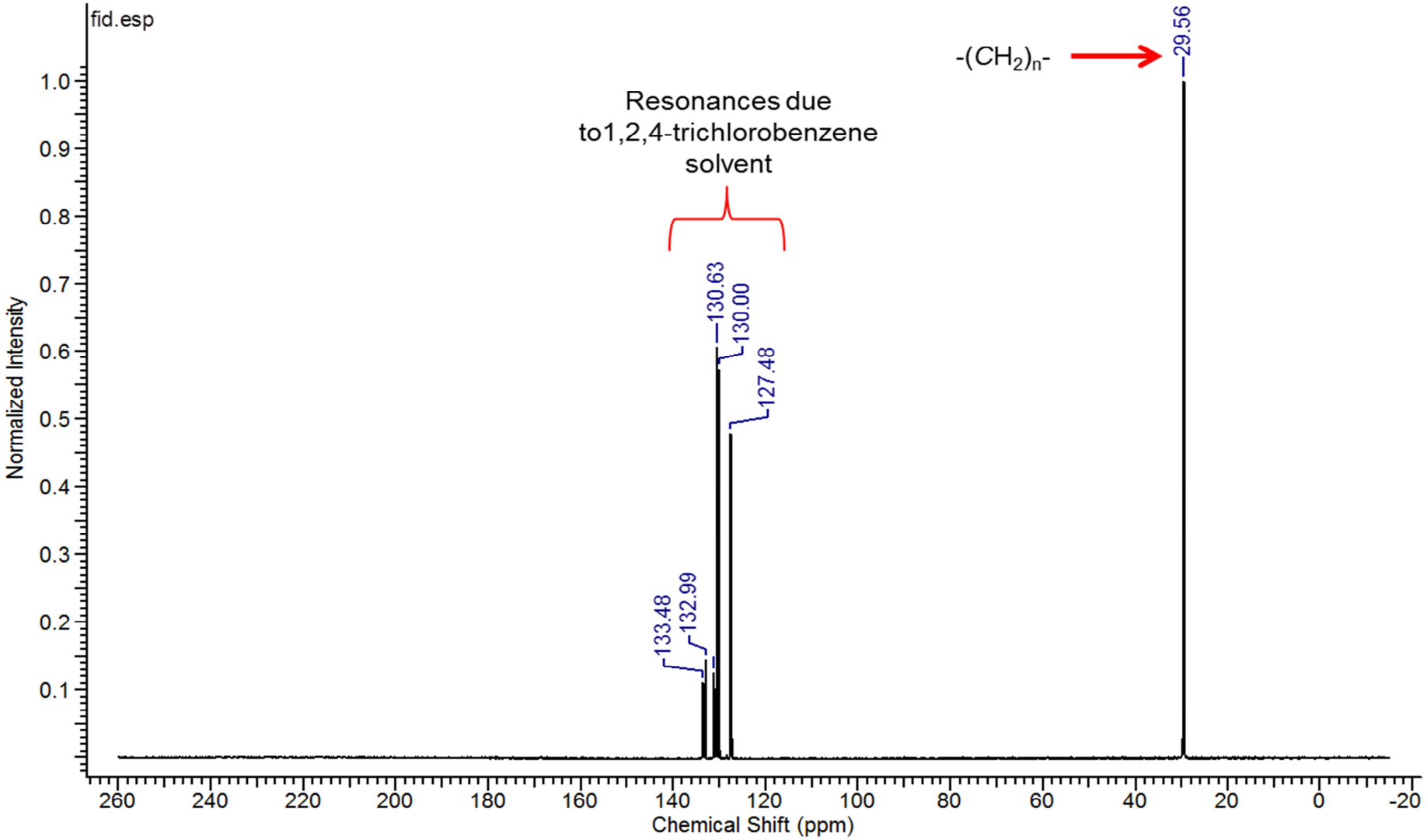

Fig. 5.8 Representative high-temperature $^{13}C\{^{1}H\}$ NMR spectrum of the polyethylene produced during catalysis.

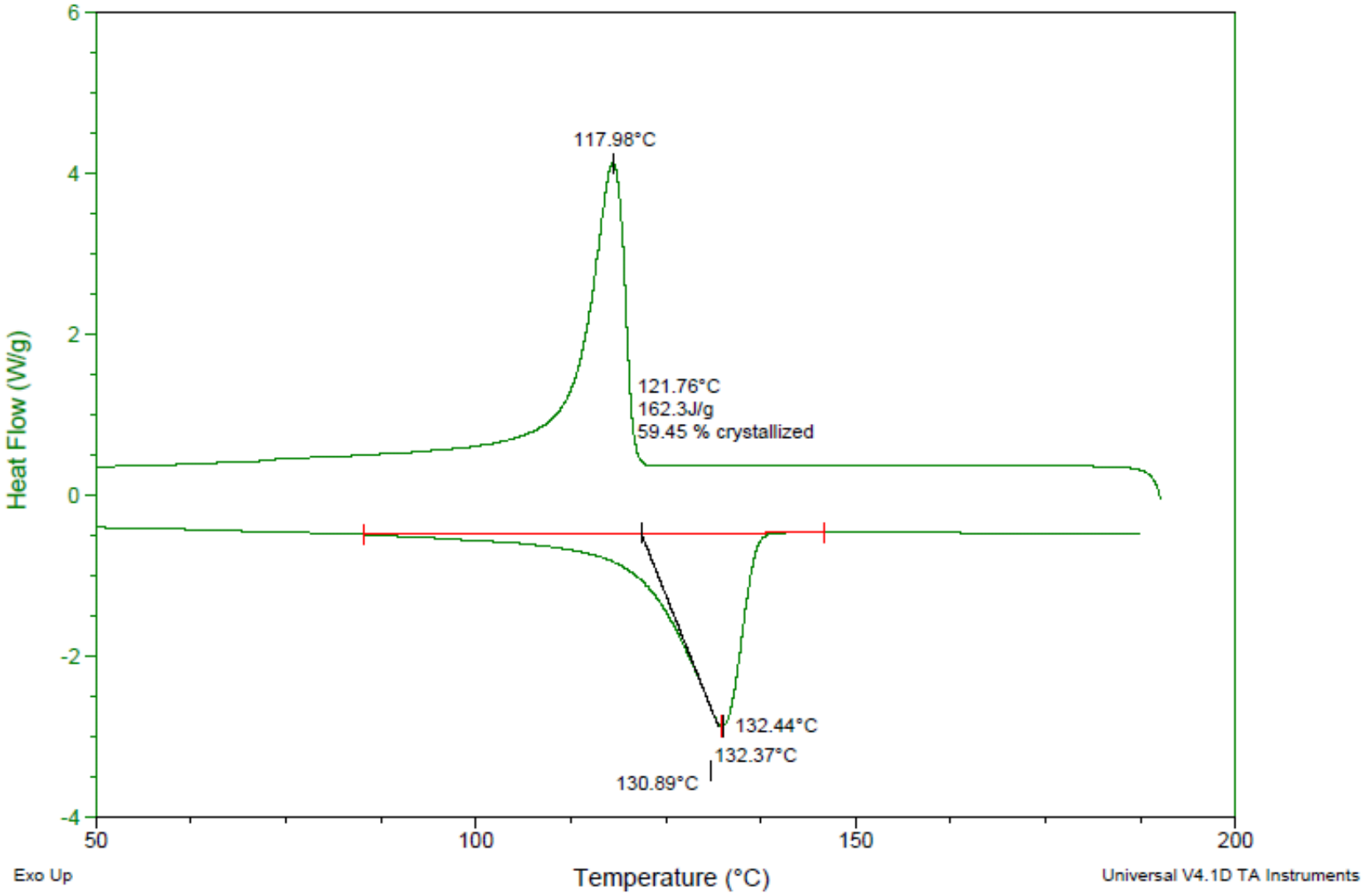

Fig. 5.9 Representative DSC curve of the polyethylene produced during catalysis.

To gain further insight into the microstructure of the isolated polymer, representative samples were analysed by solid state ^{13}C cross polarization magic angle spinning (^{13}C CP/MAS) NMR spectroscopy and wide-angle powder X-ray diffraction (PXRD). The ^{13}C CP/MAS spectrum of the polyethylene product showed two overlapping resonances at δ 32.25 and δ 33.75 ppm respectively, with the former observed as the most intense resonance (Fig. 5.10). Deconvolution of the spectral data (Table 5.8) and assignment of the resonances showed that the polymer is highly crystalline. The most intense carbon resonance at δ 32.25 ppm is due to the polymer chains in the orthorombic phase (OCP), and is as a result of crystallisation of long ethylene sequences.[21] The % contribution of the orthorombic phase to the polymer microstructure is 94 %. The resonance at δ 33.75 ppm is assigned to polymer chains in the monoclinic phase (MCP), as a result of the formation of shorter ethylene sequences. The % contribution of this crystalline phase to the polymer microstructure was determined to be 6 % relative to the orthorombic phase. In general it has been found previously that the contribution of the monoclinic phase very rarely exceeded 10 %.[21b]

Table 5.8 Details of deconvolution of a representative sample of the polyethylene produced by the Cr(III) iminophosphinato complexes.

Component	Peak type	Peak position (ppm)	Ratio (%)
OCP	Lorentzian	32.25	94
MCP	Gaussian	33.75	6

A representative wide-angle PXRD spectrum of the polyethylene produced by the Cr(III) iminophophinato complexes is shown in Figure 5.11.

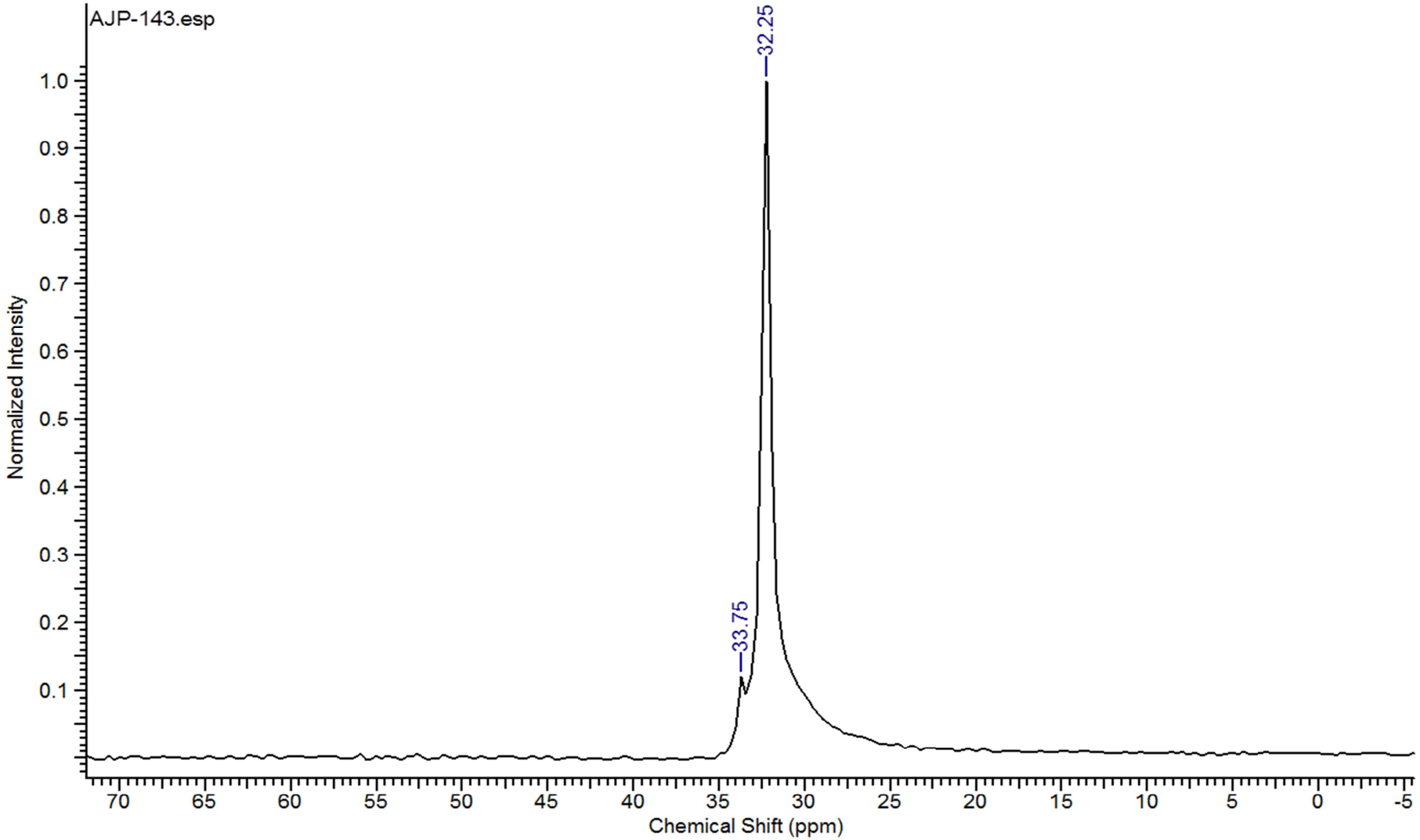

Fig. 5.10 Representative ^{13}C CP/MAS spectrum of a representative sample of the polyethylene produced during catalysis.

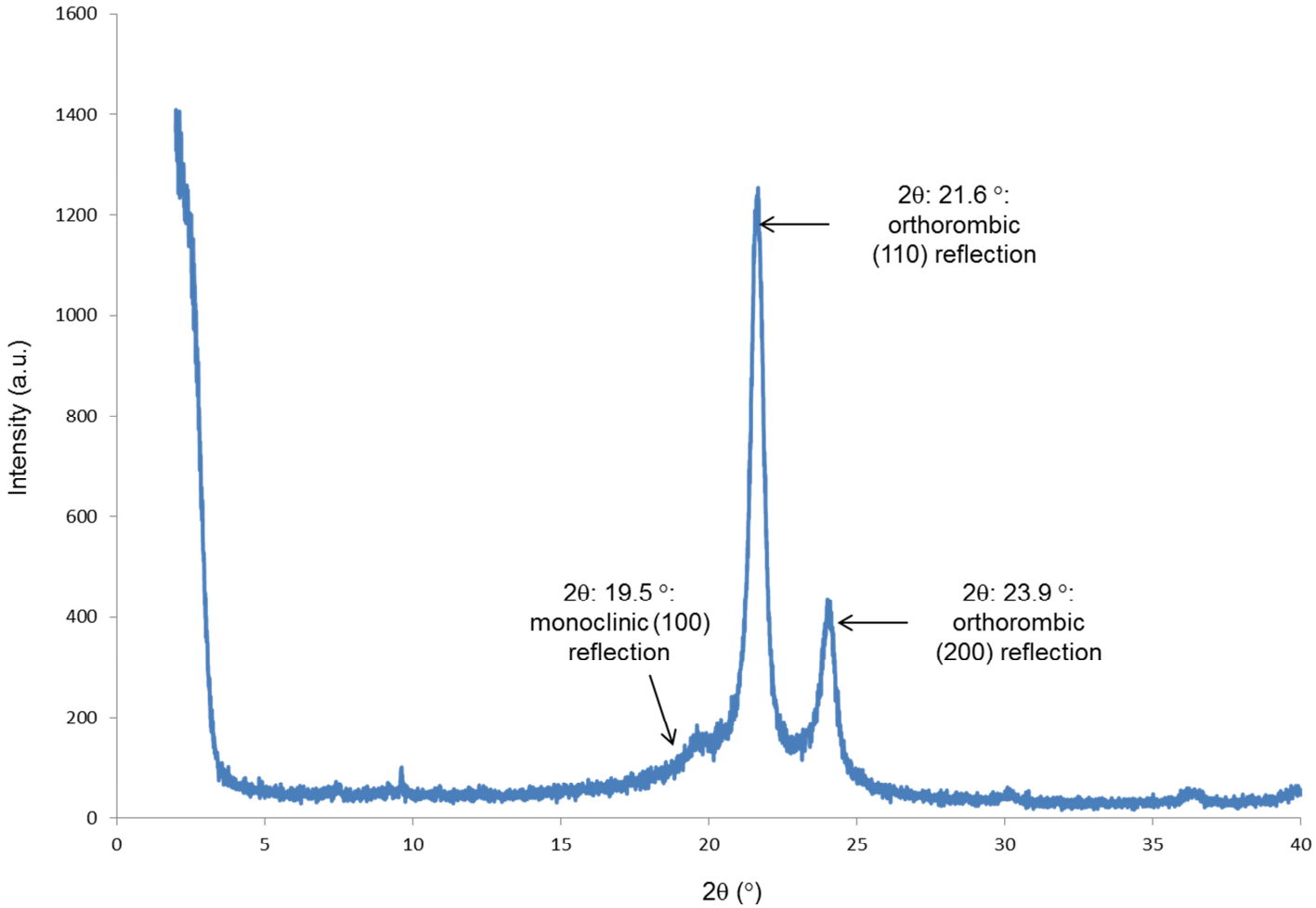

Fig. 5.11 Representative wide-angle PXRD trace of the polyethylene produced employing complex **5j** as pre-catalyst.

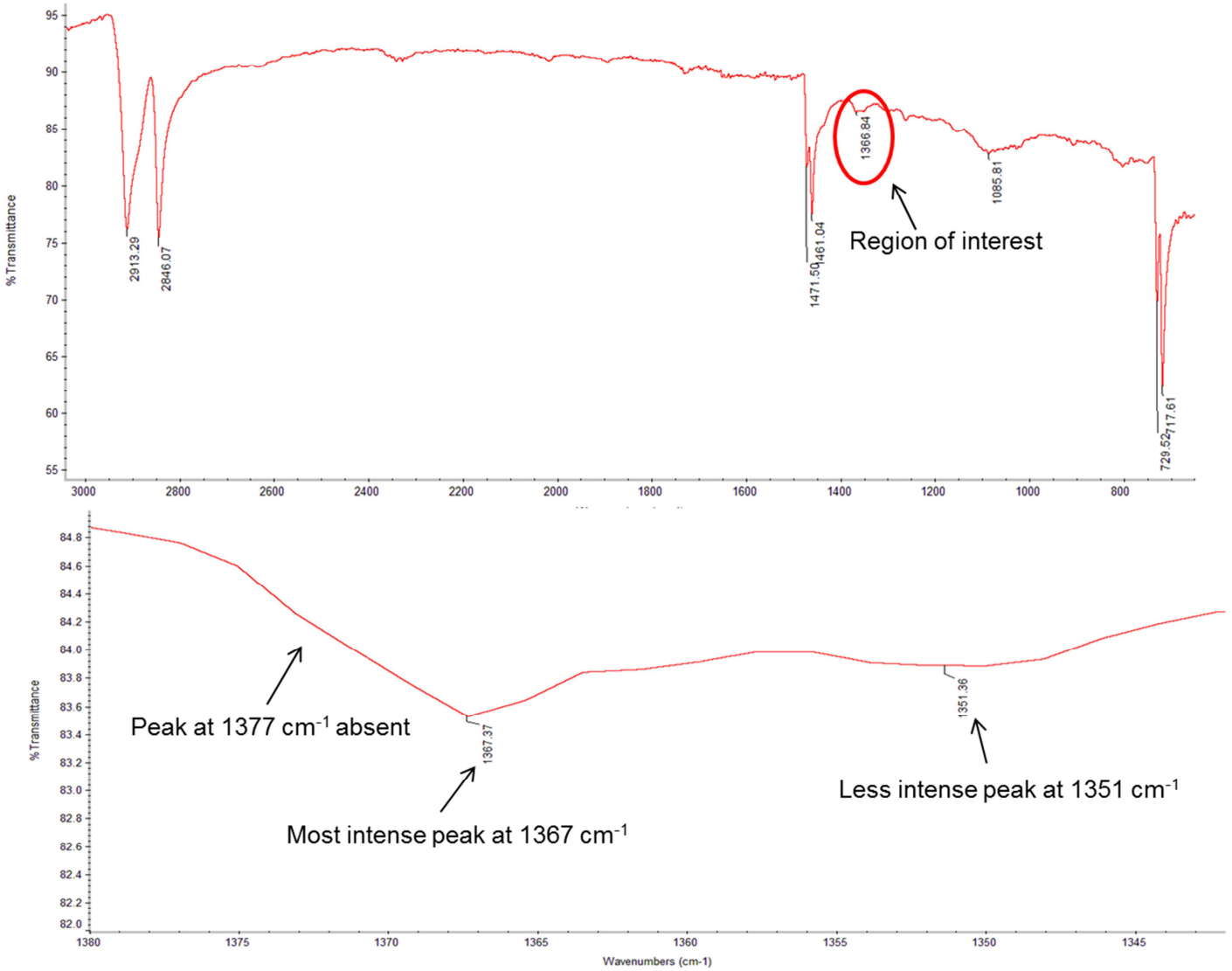

Fig. 5.12 Representative FT-IR spectrum (ATR, film) of the polymer produced.

The PXRD trace shows three reflections at values of 2θ: 19.5° (low intensity); 21.6 ° (highest intensity) and 23.9 ° (medium intensity). The most intense reflection was assigned to the (1 1 0) plane while the medium intensity reflection was assigned to the (2 0 0) plane of the thermodynamically favoured orthorombic phase.[22] The lowest intensity reflection was assigned to the monoclinic (0 0 1) plane.[23] These reflections have been observed previously for ultra high-molecular weight polyethylene produced using Cr(III) half-sandwich complexes as pre-catalysts in the presence of AlR_3 as co-catalyst[24] and corroborates the assigned crystalline phases in the solid state NMR data of the polymer.[25]

The FT-IR spectra of the isolated polyethylene showed strong characteristic methyl and methylene absorption bands at 2913/2846 cm^{-1} and 1471/1461 cm^{-1} respectively (Fig. 5.12). Closer inspection of the absorption bands present in the region between 1400-1300 cm^{-1} allows for the identification of the type of polyethylene that is being analysed. In all cases, the FT-IR spectra of the polyethylene (recorded as thin films) obtained under various reaction conditions showed the most intense absorption band at 1367 cm^{-1}. This relatively intense absorption band, combined with a less intense band at 1351 cm^{-1} and the absence of a band at 1377 cm^{-1} (Fig. 5.12) has been shown to be characteristic of high density polyethylene.[26]

To gain insight into the molecular weight and molecular weight distribution properties of the polymer, three representative polymer samples produced by complexes **5f** (Table 5.7, Entry 1, sample code: **5f-MAO**) and **5j** (Table 5.7, Entry 5, sample code: **5j-MAO**; Table 5.7, Entry 7, sample code: **5j-MMAO**) were analysed by HT-SEC following extended dissolution in TCB at 160 °C (Table 5.9). For all three samples, the molar mass distribution is observed to be very broad (Fig. 5.13). The determined weight-average molecular weight

values are within the same range (Table 5.9, Entry 1-3) suggesting that catalyst structure and co-catalyst has a negligible effect on the molecular weight of the polymer. Additionally, polydispersity indices are observed in the range 68.5-76.0. This observation, combined with the broad molar mass distribution, suggested that the polymerisation may be bi- or multimodal, producing both high and lower molecular weight polyethylene at different catalytic sites.

Table 5.9 Molecular weight and polydispersity values determined by HT-SEC.

Entry	Sample	M_w (x10^6 g/mol)[a]	M_w/M_n[a]
1	**5f-MAO**	2.34	68.5
2	**5j-MAO**	2.58	76.0
3	**5j-MMAO**	2.29	70.3

[a] Determined by HT-SEC analysis.

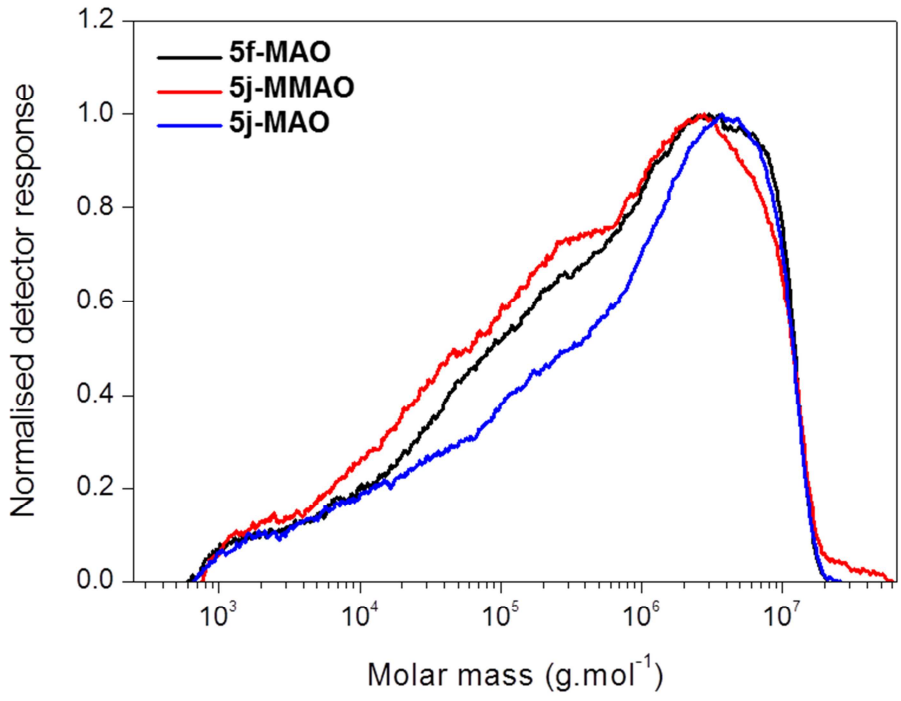

Fig. 5.13 Overlay of the HT-SEC curves obtained for the polymer samples; **5f-MAO, 5j-MMAO** and **5j-MAO**.

Since HT-SEC only provides information about the *average* molecular weight of the polymer, we sought to investigate whether we could fractionate the polymer samples to gain insight into their chemical composition and the resulting distribution.

Crystallisation analysis fraction (CRYSTAF) is a technique developed in the 1990's[27] which measures the distribution of polymer chains with varying crystallisation behaviour in complex semi-crystalline samples.[28] The technique thus provides information about the chemical composition distribution (CCD) of the bulk sample and has been employed extensively in the analysis of ethylene-/α-olefin copolymers.[29] The results of CRYSTAF analysis of three representative polymer samples, **5f-MAO**, **5i-MAO** (Table 5.7, Entry 4) and **5j-MMAO** are shown in Figure 5.14.

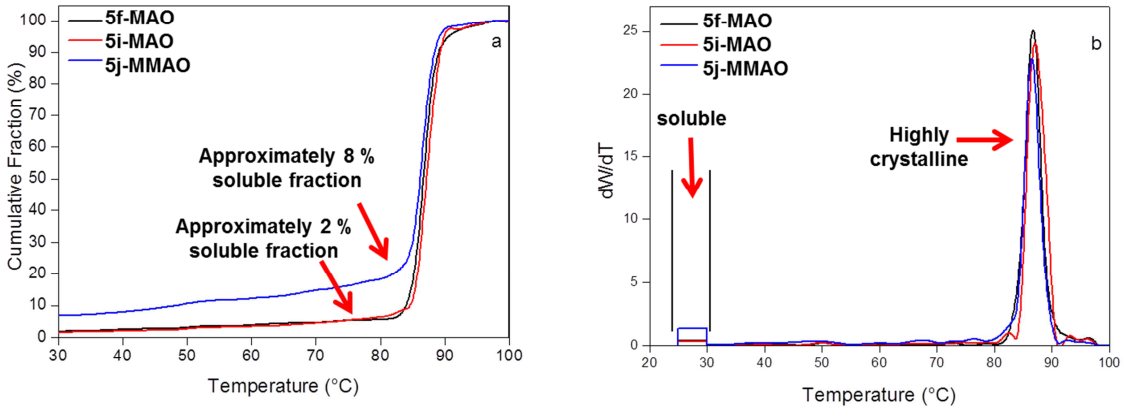

Fig. 5.14 CRYSTAF results obtained for samples **5f-MAO**, **5i-MAO** and **5j-MMAO** displayed as (a) cumulative weight fraction (b) first derivative of the CCD curve.

Figure 5.14a displays the cumulative fraction weight loss detected by IR as a function of temperature, while Figure 5.14b displays the first derivative of the CCD curve and provides a visual representation of the relative chemical composition of the bulk sample. When considering Figure 5.14a, our results show that for polymers produced using **5f-MAO**

and **5i-MAO** approximately 98 % of the total polymer initially in solution crystallises out of solution at approximately 85 °C. In contrast, for samples produced by **5j-MMAO**, the percentage polymer which crystallised out of solution at 85 °C is significantly less than for those produced by **5f-MAO** and **5i-MAO**, at 92 %. This implies that 8 % of the total polymer composition is a soluble fraction that does not precipitate out of solution, even at the lower temperature limit of the analysis of 30 °C. Figure 5.14b shows a narrow chemical composition distribution at a temperature of approximately 85 %, characteristic of highly crystalline high-density polyethylene.[30] This observation supports our interpretation of the solid state NMR, DSC and PXRD analytical data of the bulk sample.

To gain further insight into the composition of the polymer from **5j-MMAO**, preparative fractionation was conducted by dissolving the bulk sample in xylene at 130 °C, followed by cooling of the solution to 30 °C at a rate of 2 °C/min.

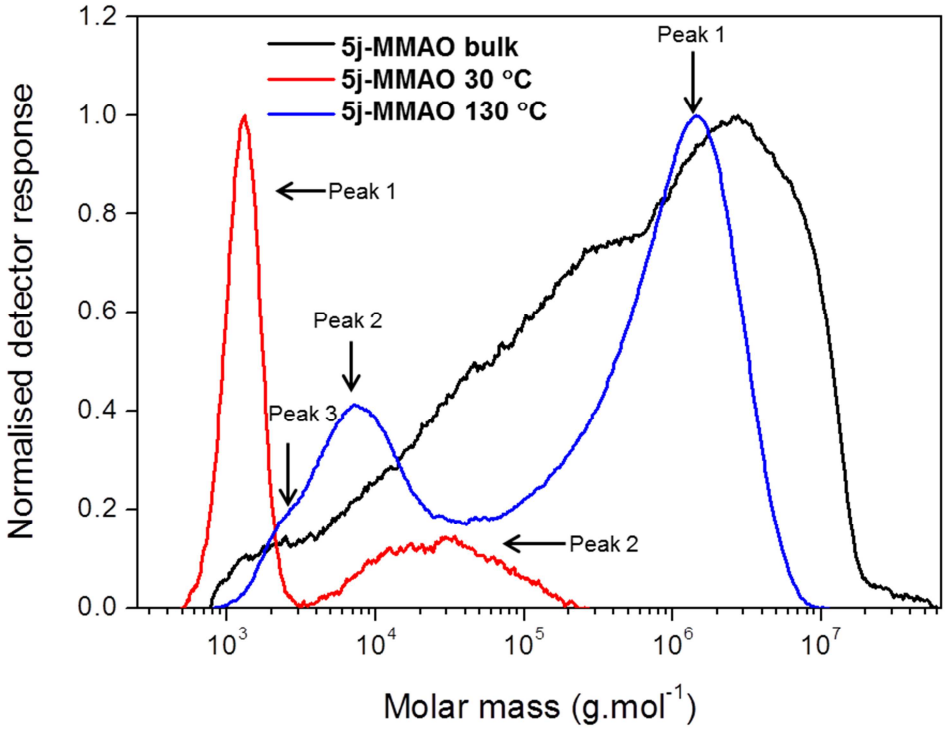

Fig. 5.15 Overlay of the HT-SEC curves obtained for **5j-MMAO** bulk sample and its soluble (30 °C: **5j-MMAO_30 °C**) and highly crystalline (130 °C: **5j-MMAO_130 °C**) fractions.

Soluble (**5j-MMAO_30 °C**) and crystalline fractions (**5j-MMAO_130 °C**) were separated by filtration and analysed by HT-SEC and DSC. Figure 5.15 shows an overlay of the HT-SEC results obtained for the bulk sample (black trace), the soluble fraction (red trace) and the crystalline fraction (blue trace). HT-SEC analysis of the crystalline fraction, **5j-MMAO 130 °C**, showed an average multimodal distribution of polymer molecular weights present in the sample (Table 5.10). The observed molecular weight varied by 4 orders of magnitude, with the highest molecular weight of 1.27 x 10^6 g.mol^{-1} and the lowest molecular weight of 203 g.mol^{-1}. Polydispersity indices were found to be fairly narrow, ranging between 3.59 for the high molecular weight component (**5j-MMAO_130 °C Peak 1**, Table 5.10, Entry 1) and 1.06 for the low molecular weight component (**5j-MMAO_130 °C Peak 3**, Table 5.10, Entry 3). For **5j-MMAO_130 °C Peak 1**, the relatively high PDI value (3.59) is as a result of the formation of multiple active sites with polymeric chains attached, varying slightly in the number of ethylene molecules which have been inserted prior to chain termination. Similar observations have been made previously for phenoxy-iminato Ni(II) and bis-iminopyridyliminato V(III) polymerisation systems.[31]

Table 5.10 Molecular weight and polydispersity values determined by HT-SEC.

Entry	Sample	M_w [b]	M_w/M_n [a]
1	**5j-MMAO_130 °C Peak 1**	1273	3.59
2	**5j-MMAO_130 °C Peak 2**	10.1	1.79
3	**5j-MMAO_130 °C Peak 3**	0.203	1.06
4	**5j-MMAO_30 °C Peak 1**	39.4	2.03
5	**5j-MMAO_30 °C Peak 2**	1.3	1.07

[a] Determined by HT-SEC analysis. [b] M_w: x 10^3 g.mol^{-1}.

In the case of the low molecular weight fraction, **5j-MMAO_30 °C**, analysis by HT-SEC showed a bimodal distribution of polymer chains (Fig. 5.15). Molecular weights varied by one order of magnitude with M_w = 3.94 x 10^4 g.mol^{-1} for **5j-MMAO_30 °C Peak 1** (Table 5.10, Entry 4) and M_w = 1.30 x 10^3 g.mol^{-1} for **5j-MMAO_30 °C Peak 2** (Table 5.10, Entry 5). In both cases, narrow PDI values of 2.03 and 1.07 were observed. Analysis of both fractions by DSC showed broad crystallisation and melting curves, indicative of compositional heterogeneity. For the crystalline fraction, **5j-MMAO_130 °C**, the melting temperature (T_m = 134.8 °C) and degree of crystallinity (X_c = 66.64 %) values determined by DSC are similar to that obtained for the bulk sample (Table 5.7, Entry 7) with slight differences attributed to the removal of the the soluble fraction (Fig 5.16).

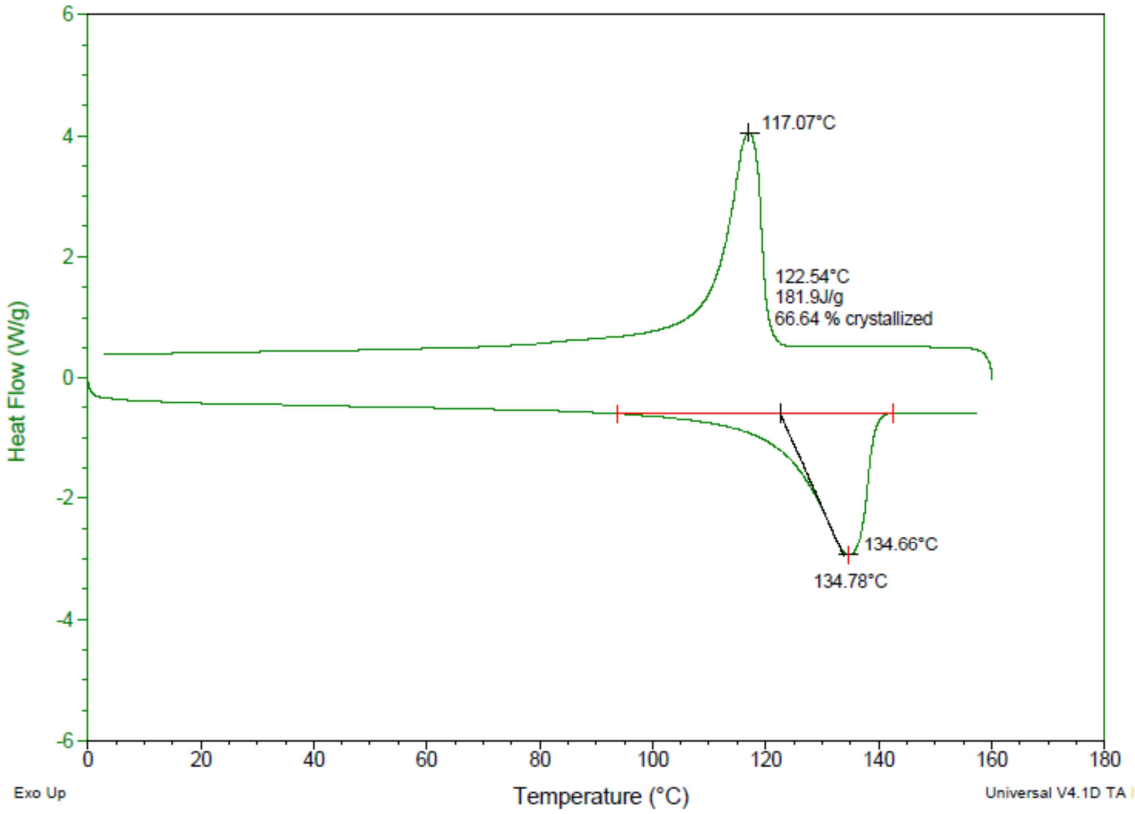

Fig. 5.16 DSC curve of the crystalline fraction, **5j-MMAO_130 °C**.

Interestingly, for the soluble fraction, a low melting temperature of 82.07 °C was observed (Fig 5.17). The observed melting temperature is in the range previously reported for *linear low-density polyethylene* produced by Zr-Ti heterobimetallic catalyst systems.[32] This observation implies that short-chain oligomers may be produced during catalysis and incorporated into the growing polymer chain.

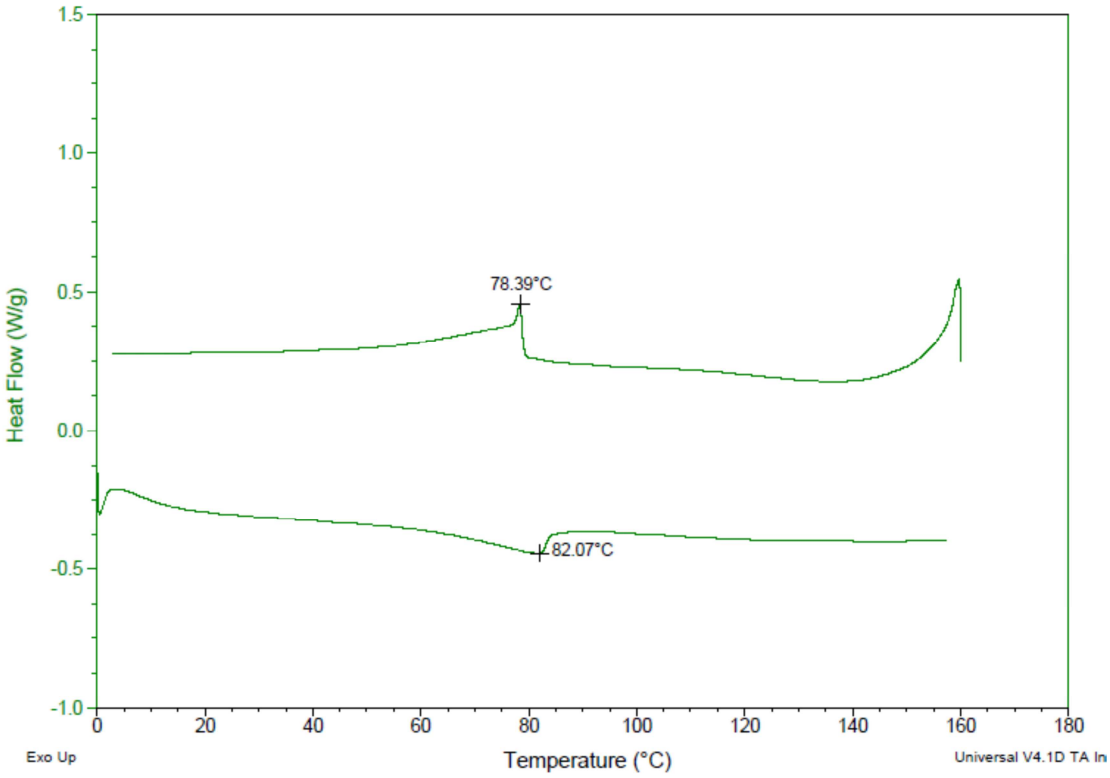

Fig. 5.17 DSC curve of the crystalline fraction, **5j-MMAO_30 °C**.

The fact that no oligomers are detected by GC-FID analysis does not preclude their formation. On the contrary, not detecting oligomers in conjuction with the observation that the soluble fraction is a small percentage of the bulk polymer produced (< 10 %) suggests that the oligomerisation catalyst species may not be long-lived or that only a small percentage of the Cr(III) catalyst precursor is converted to a Cr(I)/Cr(II) ethylene oligomerisation catalyst species. This argument is speculative at present and further analysis is required. Unfortunately, only enough soluble fraction for HT-SEC and DSC analysis was isolated by

preparative fractionation. Analysis by FT-IR and ^{13}C NMR spectroscopy would shed light on the polymer microstructure and provide evidence for the formation of ethylene oligomers during catalysis.

5.3 DFT studies of Cr(III) iminophosphinato complexes in ethylene polymerisation.

As discussed above, the mononuclear Cr(III) iminophosphinato complexes were active catalysts for the polymerisation of ethylene in the presence of an Al co-catalysts. DFT calculations were performed on the Cr(III) iminophosphinato complex/MAO catalyst system to elucidate mechanistic features which governed the catalytic formation of linear high-density polyethylene and what is speculated to be trace amounts of linear low-density polyethylene. Considering the redox dynamism associated with chromium, we decided to employ DFT calculations as a tool to determine the most likely Cr oxidation state responsible for the observed catalytic activity. In general, ethylene polymerisation is considered to proceed via a Cossee-Arlman mechanism from a Cr(III) or Cr(II) active species.[1a,33] Despite this generality, there are a few reports in literature detailing the formation of α-olefins and low-molecular polyethylene, in which a metallacycle mechanism was shown to be operative.[34]

With these considerations in mind, we envisaged employing DFT calculations as a tool to probe:

- Whether Cr(III) or Cr(II) species are predominant in the early stages of the catalytic cycle.
- The propensity for chain growth and termination via a Cossee-Arlman or metallacycle mechanism and how the energetics of chain growth and termination differ between these two mechanisms.

- Finally, to correlate the experimental and theoretical results in terms of the formation of linear high-density and low-density polyethylene.

5.3.1 Spin Multiplicity for Cr(III) and Cr(II) species.

Accurate identification of the ground spin state for chromium in its various oxidation states is important to ensure the location of the lowest energy points on the computed potential energy surface. For Cr(III) species, initial geometric optimisations considered both doublet and quartet multiplicities. In all cases the lowest energy conformation was found for the quartet spin multiplicity. In the case of Cr(II) species, evaluating singlet and triplet multiplicities, the species with the lowest energy had triplet multiplicity.

5.3.2 Methylation aptitude of the iminophosphine Cr(III) and Cr(II) species.

Our DFT investigation employed a simplified analogue of complex **5f** termed complex **1A**, in which the phenyl rings at phosphorus was replaced by methyl groups (Fig. 5.18).

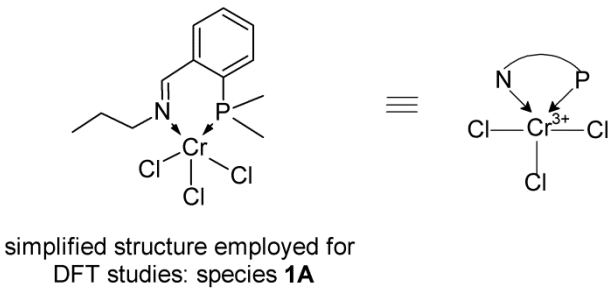

Fig. 5.18 Simplified species, complex **1A**, employed in the DFT studies.

This was in an attempt to minimise the computational time associated with the calculations. Previous DFT investigations of the interaction of MAO with selective trimerisation catalysts showed that trimethyl aluminium (TMA), present in commercial MAO, was responsible for the methylation of the Cr catalyst precursor. Thus we evaluated

the methylation aptitude of complex **1A** by TMA, in which the metal centre is in the +3 (Scheme 5.4, A) and +2 (Scheme 5.4, B) oxidation state. For pathway A, methylation of **1A** generates the (N-P)$CrMe_3$ species, **2A**. In the case of the Cr(II) species, the initial reduction was calculated to proceed by a TMA-assisted one e^- reductive process in which homolytic cleavage of the Cr-Cl bond generates the Cr(II) species and a Me-radical.

Scheme 5.4 Methylation of Cr(III) ad Cr(II) species by TMA.

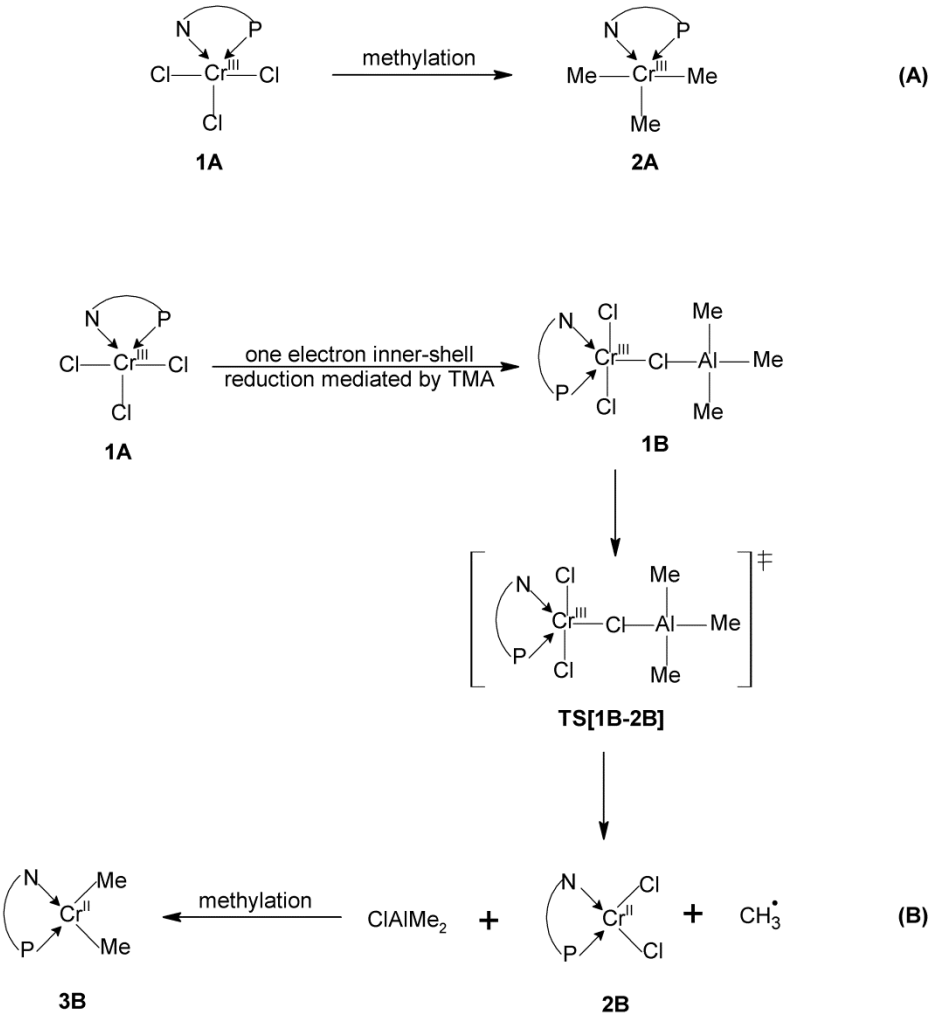

Our calculations showed that the sequential methylation of the Cr(III) complex, **1A**, to species **1B** was exothermic overall by 34.9 kcal/mol (Fig. 5.19). In the case of the +2 oxidation state pathway, the formation of the Cr(II)Cl_2 species, **2B**, proceeds via transition

state structure, **TS[1B-2B]**, in which the Cr-Cl bond length is elongated to 2.837 Å (in comparison to 2.334 Å in **1B**, Fig. 5.20) with a barrier of 9.3 kcal/mol. The methylation of species **2B** to generate the (N-P)$CrMe_2$ species, **3B**, was found to be exothermic by 21 kcal/mol relative to the starting Cr(III) complex, **1A**. With regard to methylation aptitude, our initial calculations thus showed that this process is energetically more favourable for a Cr(III) species in comparison to a Cr(II) species and that the chromium species which enters the catalytic cycle is in the +3 oxidation state.

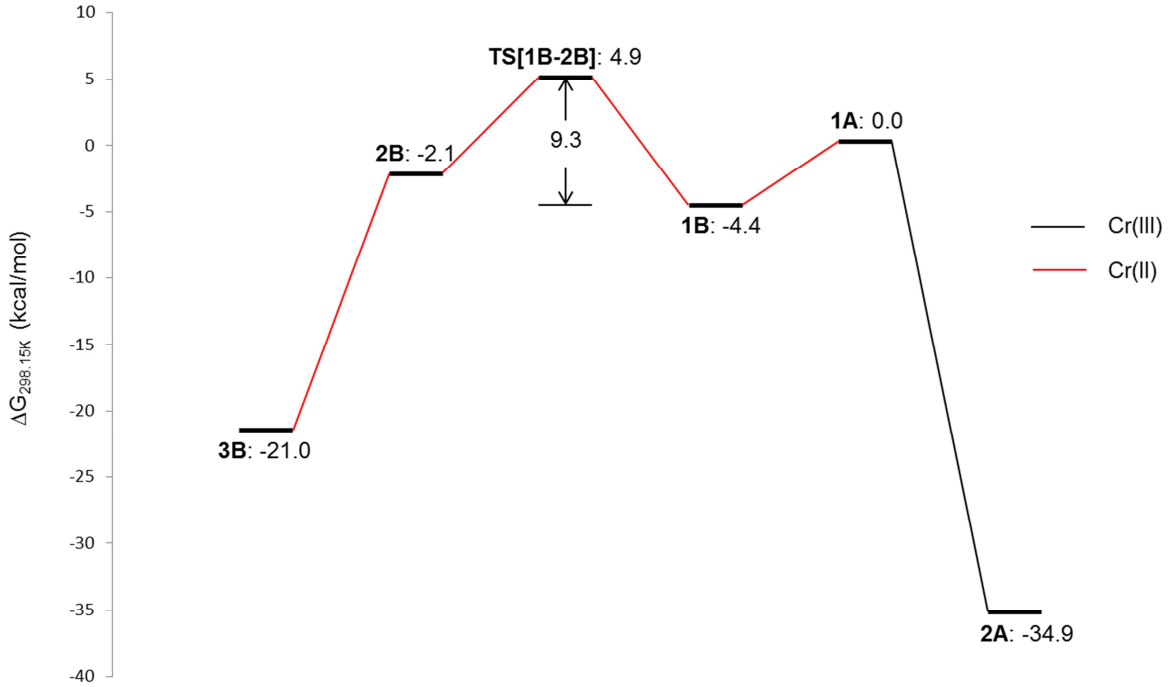

Fig. 5.19 Energy profile of comparative methylation of Cr(III) and Cr(II) species by TMA. Calculated Gibbs free energies ($\Delta G_{298.15K}$) reported at 298.15 K and 1 atm.

5.3.3 Comparative methyl abstraction by MAO and ion-pair formation from Cr(III) and Cr(II) species.

Methyl-group abstraction to generate a vacant coordination site for coordination of the α-olefin is a crucial step in the initiation process for olefin oligo-/polymerisation.[35] In the

current study we evaluated two TMA-expanded MAO models, $(AlOMe)_9$-TMA-*sh* (**MAO2**) and $(AlOMe)_9$-TMA-*ss* (**MAO3**), where *sh* and *ss* represents the square-hexagonal and square-square faces of the cage structure of MAO (Scheme 5.5). These MAO models were previously reported in a computational investigation of Cr-catalysed ethylene trimerisation and are considered to be "realistic" MAO models.[5b]

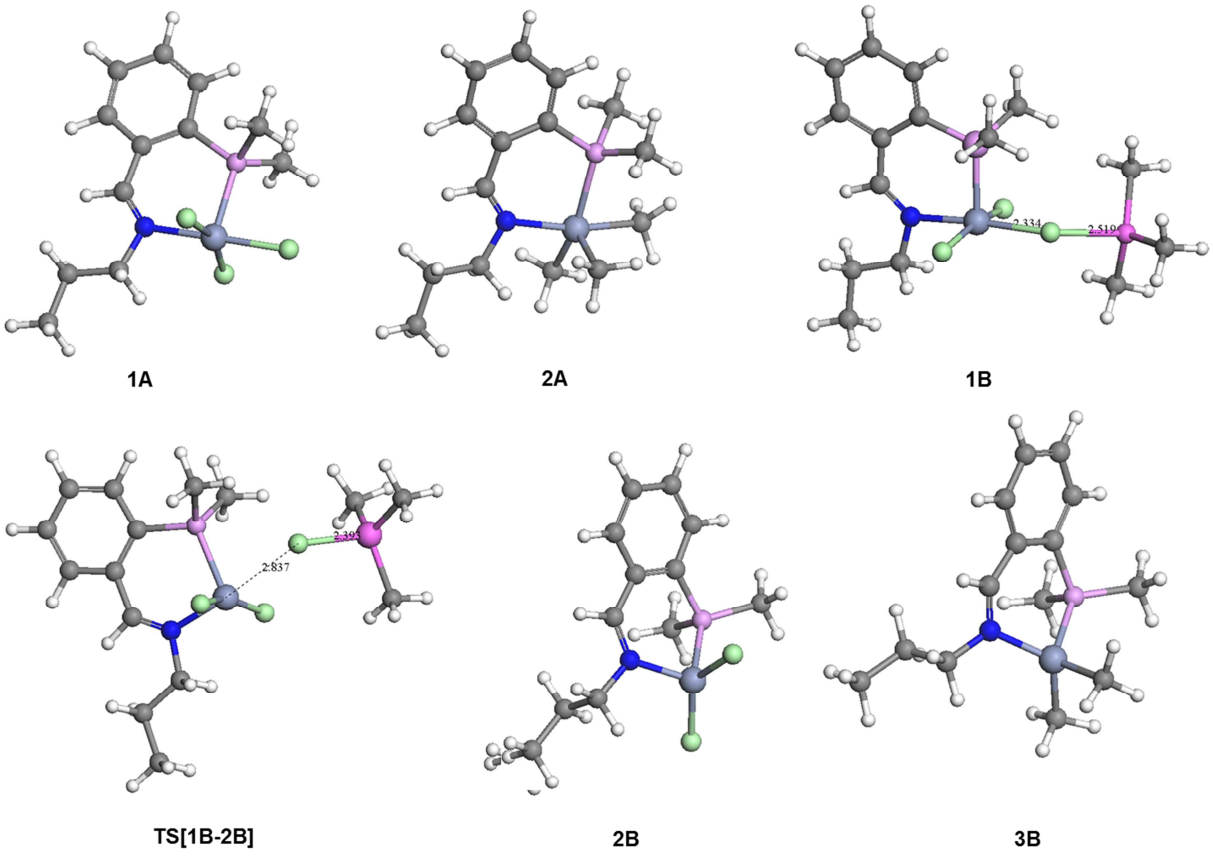

Fig. 5.20 Optimised structures of the species shown in Scheme 6.5.

The use of the $(AlOMe)_9$ cage is further justified by the predicted distribution of cage structures of MAO in which $(AlOMe)_9$ containing a strained square-square Al-O bond was found to be one of the most abundant cage structures.[36] The interaction of MAO with the Cr(III) and Cr(II) species, **2A** and **3B**, via a bridging methyl group between MAO and the Cr metal centre was evaluated computationally. For species **2A** the interaction with both **MAO2** and **MAO3** could be optimised successfully. The formal coordination of MAO to the metal

centre was characterised by an elongated Cr-Me bond distance and a relatively short Me-Al bond distance of 2.118 and 2.357 Å respectively (Scheme 5.6).

Scheme 5.5 The formation of TMA-expanded MAO models, **MAO2** and **MAO3**.

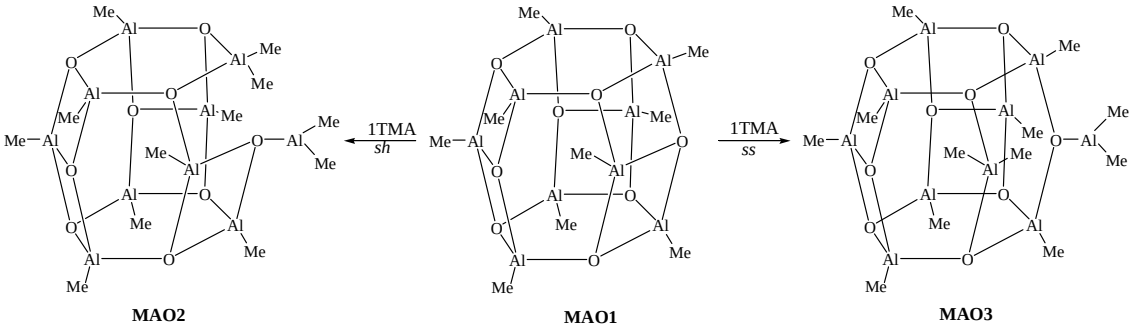

Scheme 5.6 Me-abstraction from Cr(III)Me_3 species, **2A-MAO**.

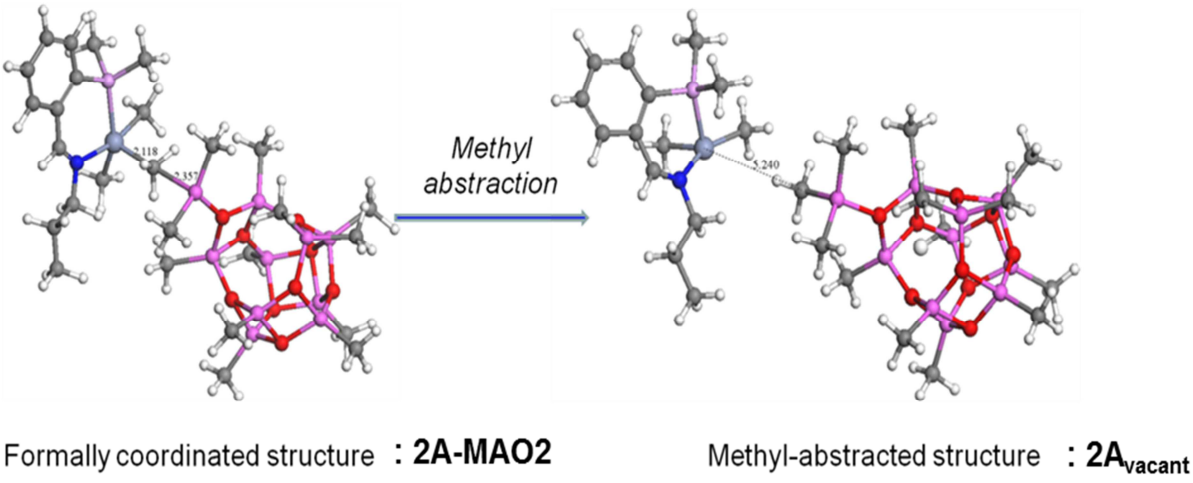

Formal abstraction of the methyl group by **MAO2** and **MAO3** was found to proceed by -4.1 and 5.0 kcal/mol respectively, indicative that methyl-abstraction by MAO from the Cr(III)Me_3 species was quite facile.

On the other hand, the interaction of the Cr(II)Me_2 species, **3B**, with **MAO2** to generate the formally coordinated species could not be successfully optimised. In the case of the interaction with **MAO3**, the formation of the formally coordinated structure was

analogous to **2A-MAO3**, with an observed elongation of the Cr-Me bond distance and a relatively short Me-Al bond distance of 2.204 and 2.116 Å respectively. Figure 5.21 shows the comparative energy profile of Me-abstraction from species **2A** and **3B** as well as the initial chain growth from species **2A**. The optimised structures are shown in Figure 5.22a and 5.22b.

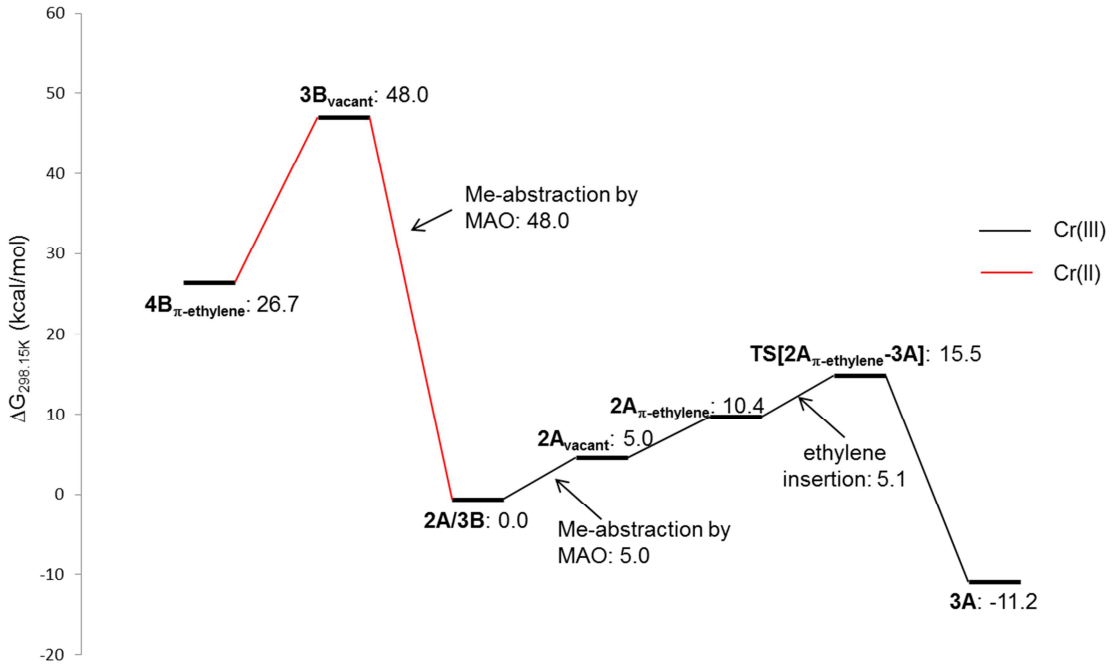

Fig. 5.21 Energy profile of comparative Me-abstraction from **2A** and **3B** by **MAO3**, as well as subsequent chain growth for **2A**. Calculated Gibbs free energies ($\Delta G_{298.15K}$) reported at 298.15 K and 1 atm.

In comparison to the Cr(III) species, Me-abstraction from the Cr(II) species, **3B**, is significantly more endothermic by 43.0 kcal/mol.

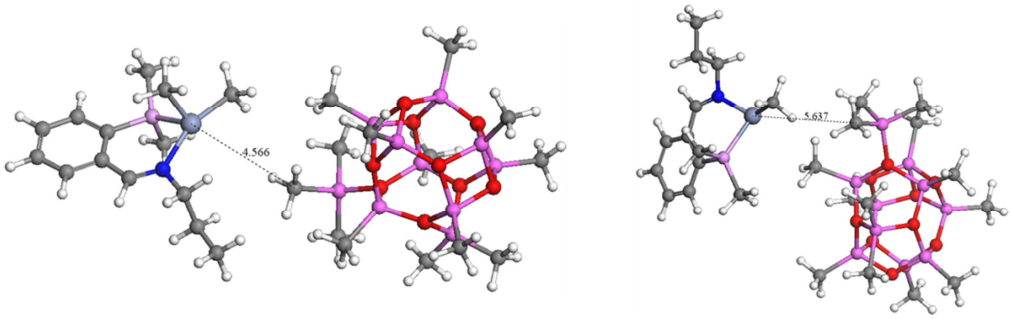

Fig. 5.22a Optimised structures of the Me-abstracted ion-pairs, $\mathbf{2A}_{\mathbf{vacant}}$ (left) and $\mathbf{3B}_{\mathbf{vacant}}$ (right).

In addition, ethylene coordination and insertion from the cationic Cr(III) species, **2A$_{vacant}$**, is more exothermic by 32 kcal/mol relative to Me-abstraction from species **3B**. Thus the results of the initial interaction of the mononuclear Cr(III) species with MAO i.e. methylation and Me-abstraction suggests that the initial active species in the catalytic cycle is the (N-P)CrMe$_3$ species, **2A** and that the formation of polyethylene via a mechanism involving a Cr(II) species is highly unlikely. Also, this result implies that the speculated formation of trace amounts of linear low-density polyethylene is as a result of ethylene oligomerisation at a Cr(I) species.

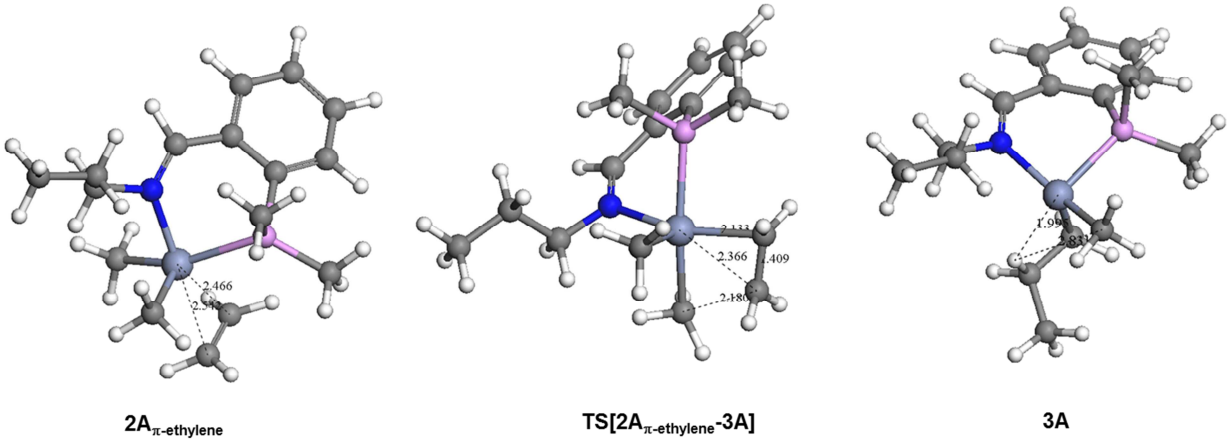

Fig. 5.22b Optimised structures of the intermediates generated during the coordination and insertion of ethylene from **2A$_{vacant}$**.

Ethylene coordination to the vacant coordination site of species **2A$_{vacant}$** was calculated to be endothermic by 5.4 kcal/mol and generated the Cr-methyl π-ethylene species, **2A$_{\pi\text{-ethylene}}$**. Species **2A$_{\pi\text{-ethylene}}$** is characterised by coordination of ethylene in the position *cis* to phosphorus, with Cr-C bond distances of 2.466 and 2.452 Å respectively. Insertion of ethylene into the Cr-Me bond was calculated to proceed via transition state structure, **TS[2A$_{\pi\text{-ethylene}}$-3A]**, in which the coordinated ethylene is rotated in-plane. The transition state structure further displayed a C$_{ethylene}$-C$_{Me}$ bond distance of 2.180 Å. Relaxation of the

transition state to the product side generates Cr-methyl-propyl species, **3A**, exothermic by 11.2 kcal/mol relative to species **2A**. The optimised structure of **3A** shows a stabilising Cr-H_{β} interaction with a bond distance of 1.995 Å.

5.3.4 Comparative chain growth and termination from Cr(III) and Cr(I) catalytic species.

After establishing the nature of the species formed after activation with MAO, we sought to determine whether chain growth and chain termination to generate polyethylene proceeded via a Cossee-Arlman mechanism or whether a Cr(III)/Cr(I) redox cycle could be responsible for oligomer-formation and incorporation to generate LLDPE or for polymer-formation via an extended metallacycle mechanism. The starting point for our comparative evaluation was species **3A**. For a Cr(III)/Cr(I) redox cycle, the Cr(III) species, **3A**, would undergo β-hydrogen transfer from the propyl chain to the coordinated methyl group, eliminating methane and generating a $Cr_{\pi\text{-propylene}}$ species, **4M**, in which the metal centre is reduced to the monovalent state (Scheme 5.7). Ligand exchange of coordinated propylene with the incoming ethylene monomer via the unsaturated species **5M** is expected to generate the Cr(I)-diethylene species, **6M**. Oxidative coupling of the two ethylene molecules via **TS[6M-7M]** would generate the chromacyclopentane species, **7M**, in which chromium is in the +3 oxidation state. Ring expansion via repetitive ethylene coordination-insertion would generate larger metallacycles which would then decompose to generate either ethylene oligomers or polyethylene.

Scheme 5.7 Chain growth and termination via a metallacycle mechanism.

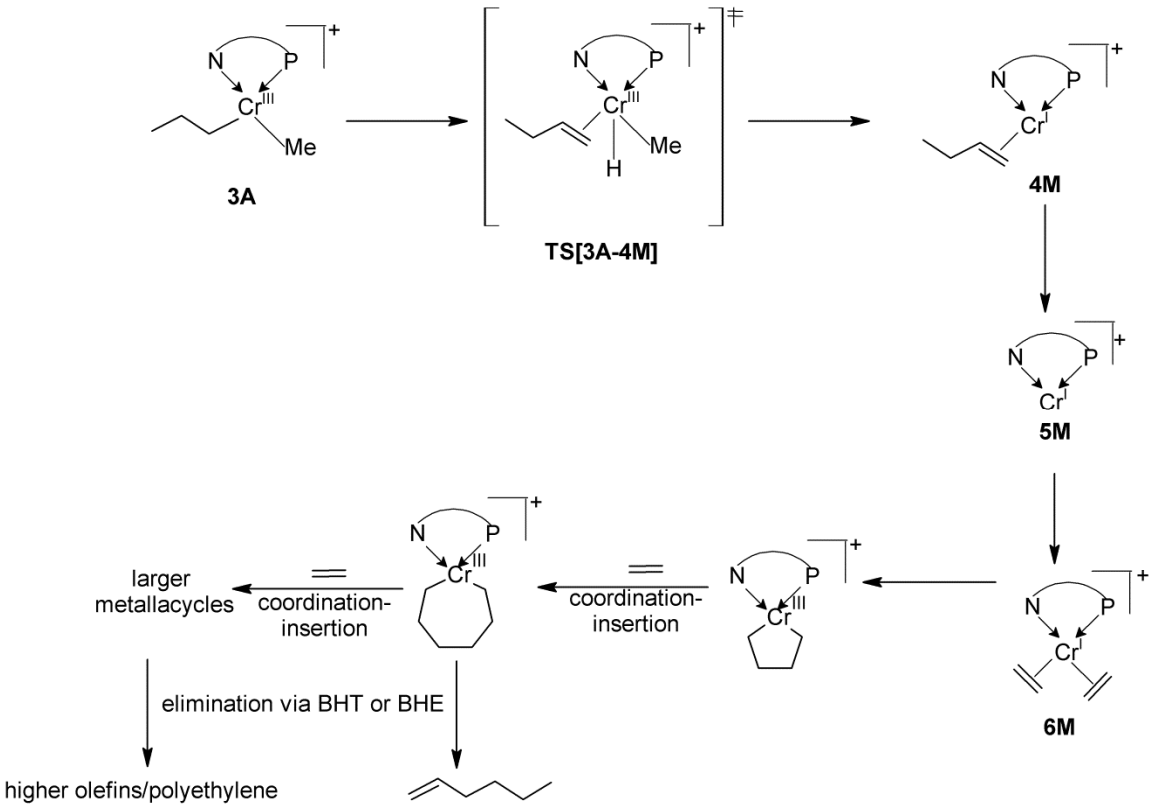

In contrast, for a Cossee-Arlman mechanism, chain growth can proceed directly from species **3A**, in which repetitive ethylene coordination and insertion via species **3A**$_{\pi\text{-ethylene}}$ and **TS[3A**$_{\pi\text{-ethylene}}$**-4A]** followed by elimination of the growing alkyl chain would generate α-olefins or polyethylene (Scheme 5.8). Since both mechanisms are implicated in the results of our polymerisation reactions, we evaluated the chain growth and termination processes for both.

Scheme 5.8 Chain growth and termination via a Cossee-Arlman mechanism.

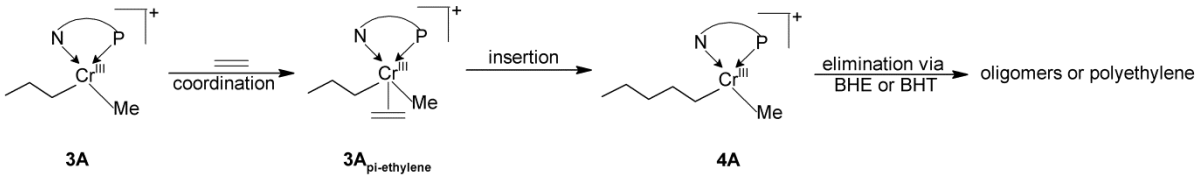

5.3.4.1 Chain growth and termination processes by a metallacycle mechanism.

Figure 5.23 shows the energy profile for chain growth and termination via a metallacycle mechanism, while the geometrically optimised minima and transition states are shown in Figure 5.24 (a and b). The β-hydrogen transfer transition state, **TS[3A-4M]**, was located with an energy of 10.8 kcal/mol above species **3A**. The optimised structure shows a C_{Me}-H_{β} and C_{propyl}-H_{β} interaction of 1.469 and 1.510 Å respectively. Hydrogen transfer proceeds via an agostic hydride shift mechanism, which has been reported previously for early transition metal catalyst systems.[37]

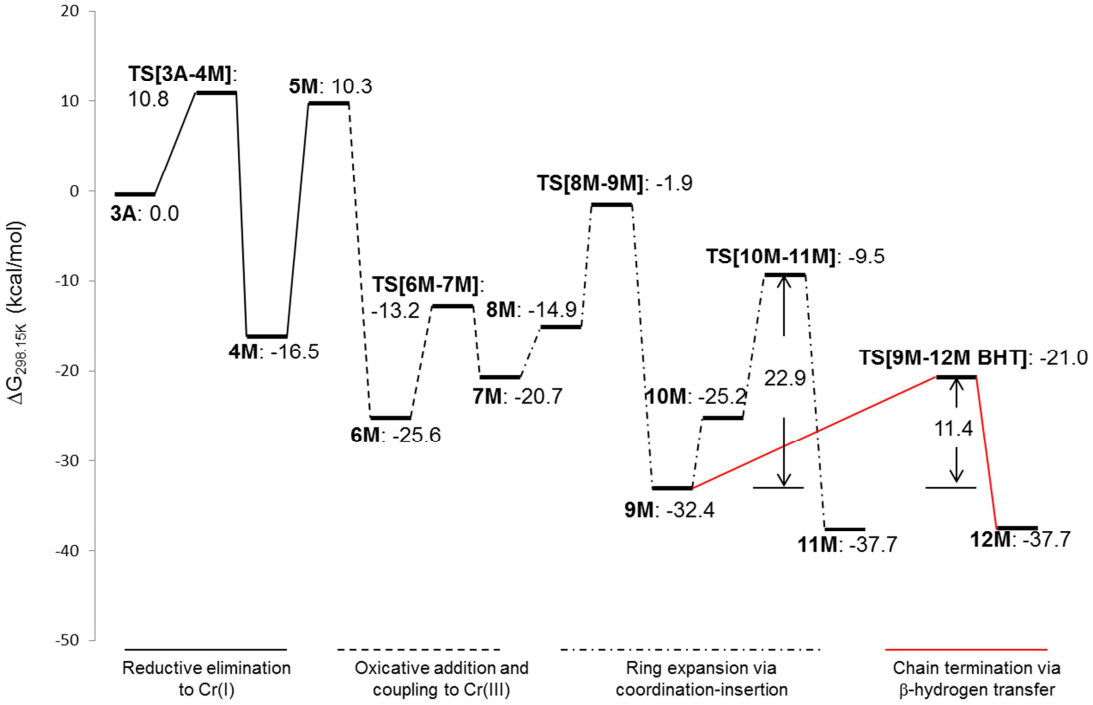

Fig. 5.23 Energy profile for chain growth and termination via a metallacycle mechanism. Calculated Gibbs free energies ($\Delta G_{298.15K}$) reported at 298.15 K and 1 atm.

The formation of the product of elimination, species **4M**, was found to be exothermic by 16.5 kcal/mol, relative to **3A**. The elimination of propylene generates the coordinatively unsaturated species, **5M**, in which the metal centre is in the monovalent state, endothermic by 10.3 kcal/mol relative to species **3A**. The coordination of two ethylene molecules to species

5M generates the Cr(I) di-ethylene species, **6M**, with an energy of -25.6 kcal/mol relative to **3A**. Oxidative coupling generates the Cr(III) metallacyclopentane species, **7M**, which proceeds via **TS[6M-7M]** with a barrier of 12.4 kcal/mol. The transition state structure is characterised by a $C(2)_{ethylene}$-$C(2')_{ethylene}$ bond distance of 1.884 Å. Relaxation of the transition state generates species **7M**, which was found to be exothermic by 20.7 kcal/mol relative to **3A**. The metallacyclopentane moiety is slightly puckered with C2 positioned out of the plane. Species **7M** displays Cr-C1 and Cr-C1′ bond distances of 2.039 and 2.036 Å respectively while the C-C bond distances falls within the same range of approximately 1.50 Å.

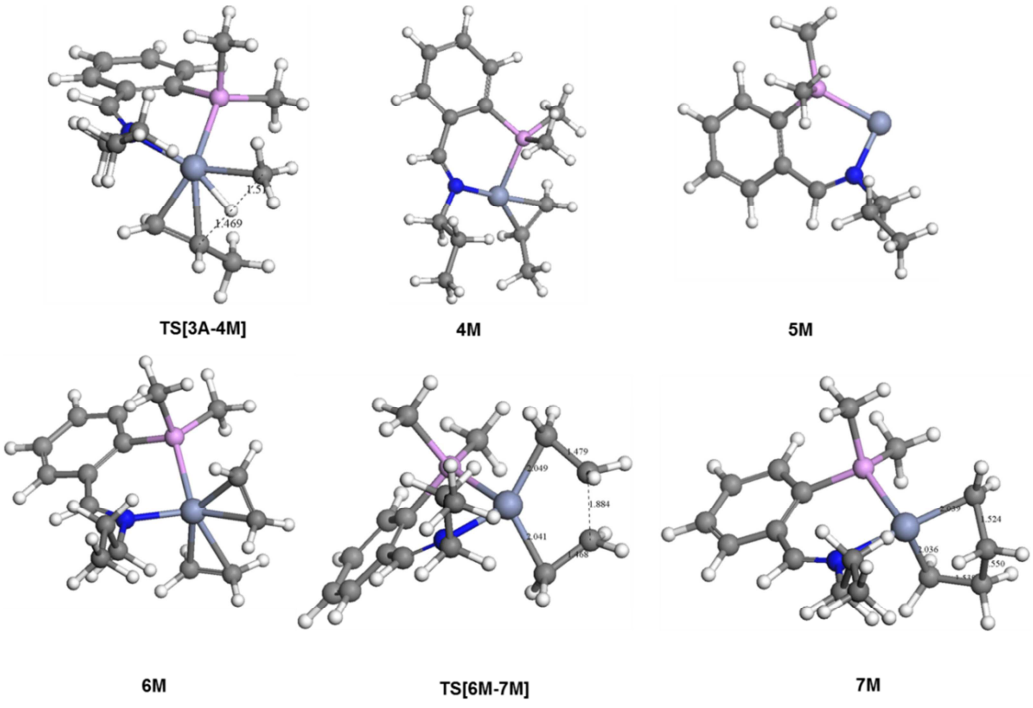

Fig. 5.24a Optimised structures of the intermediates generated during the reductive elimination to Cr(I) and oxidative coupling to Cr(III) for a metallacycle mechanism.

Following the generation of the Cr(I) metallacyclopentane species, **7M**, ethylene insertion and coordination would generate the larger Cr(I) metallacycloheptane (**9M**) and Cr(I) metallacyclononane (**11M**) species. These steps proceed in an analogous manner to the Cossee-Arlman mechanism via transition state species **TS[8M-9M]** and **TS[10M-11M]**

(Fig. 5.24b). The geometry optimised transition states are characterised by $C_{ethylene}$-C_{butyl} (in the case of **TS[8M-9M]**) and $C_{ethylene}$-C_{hexyl} (in the case of **TS[8M-9M]**) bond distances of 2.066 and 2.065 Å respectively in which ring-opening of the metallacycle had occurred. The generation of the Cr(I) metallacycloheptane (**9M**) and Cr(I) metallacyclononane (**11M**) species was calculated to proceed via overall barriers of 18.8 and 22.9 kcal/mol respectively.

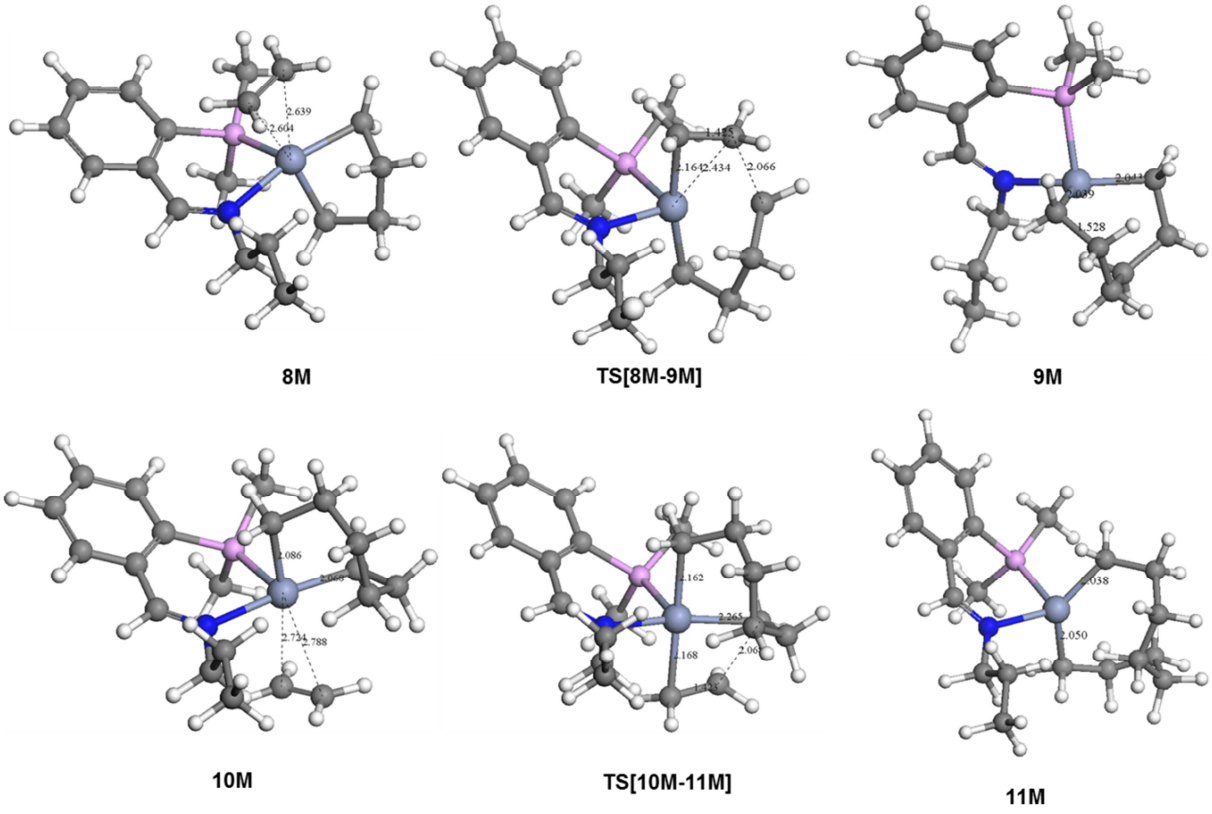

Fig. 5.24b Optimised structures of the intermediates generated during the coordination and insertion of ethylene to generate the Cr(I) metallacycloheptane and Cr(I) metallacyclononane species.

In contrast, the elimination of α-olefin via BHT (all attempts at optimising intermediates associated with BHE failed) was calculated to proceed via the transition state structure **TS[9M-12M BHT]**, with calculated energy barrier of 11.4 kcal/mol relative to **9M**. The transition state is characterised by a Cr-H_β interaction of 2.657 Å as well as C1-H_β and C_β-H_β interactions of 1.517 and 1.476 Å respectively (Fig. 5.25). The formation of the product of β-hydrogen transfer, species **12M**, was calculated to be exothermic by

5.3 kcal/mol, relative to **9M**. Species **12M** is a Cr(I) π-hexenyl species, with Cr-C_α and Cr-C_β bond distances of 2.192 and 2.183 Å respectively. A comparison of the energetics of ring expansion and elimination of α-olefin indicates that the formation of short chain α-olefins, in our calculations 1-hexene, is more energetically favourable than the formation of longer chain α-olefins or polyethylene via ring expansion. Our computational results thus suggest that the formation of LLDPE would be as a result of the incorporation of 1-hexene into the growing polymer chain.

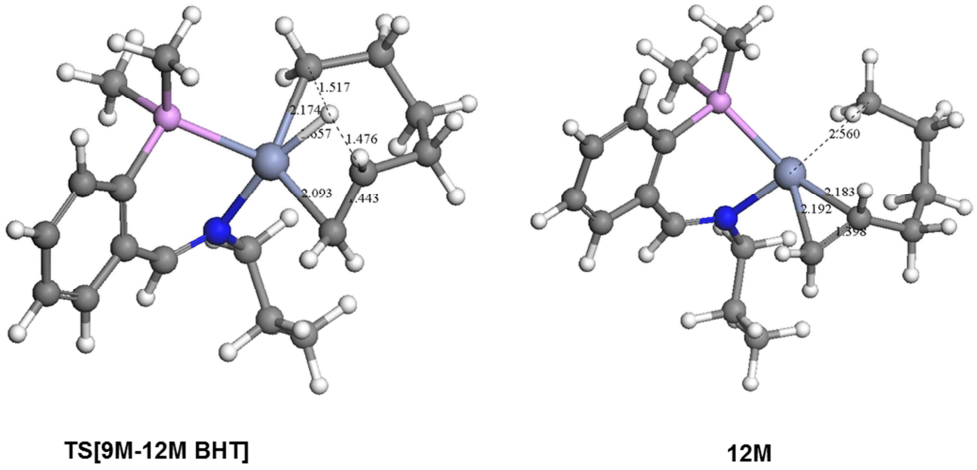

Fig. 5.25 Optimised structures of the transition state and product of β-hydrogen transfer from the Cr(I) metallacycloheptane species, **9M**.

5.3.4.2 Chain growth and termination processes by a Cossee-Arlman mechanism.

Chain growth via a Cossee-Arlman mechanism was calculated to proceed via species **3A**. Ethylene coordination generates the π-ethylene species, $\mathbf{3A_{\pi\text{-ethylene}}}$, calculated to be endothermic by 6.6 kcal/mol with respect to **3A** (Fig. 5.26). Species $\mathbf{3A_{\pi\text{-ethylene}}}$ displays a stabilising β-agostic interaction, with a Cr-H_β bond distance of 1.906 Å (Fig. 5.27). Ethylene

insertion was calculated to proceed via the transition state, **TS[3A$_{\pi\text{-ethylene}}$-4A]**, with an insertion barrier of 4.8 kcal/mol relative to **3A$_{\pi\text{-ethylene}}$**.

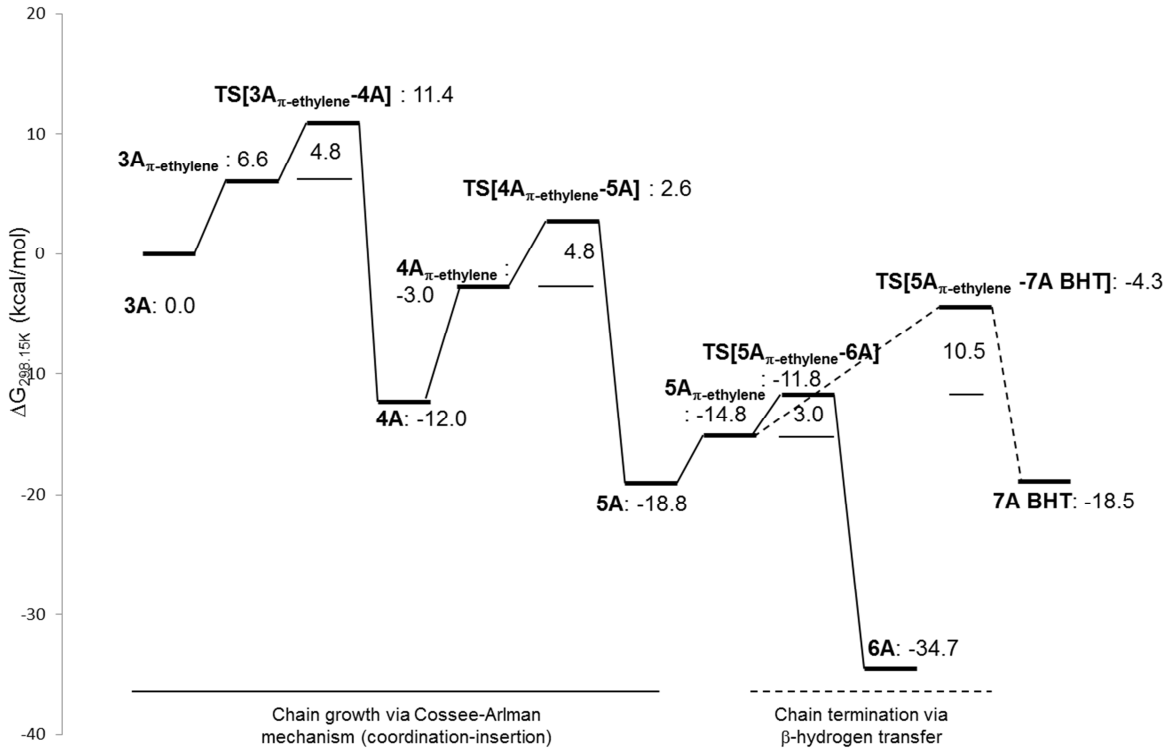

Fig. 5.26 Energy profile for chain growth and termination via a Cossee-Arlman mechanism. Calculated Gibbs free energies ($\Delta G_{298.15K}$) reported at 298.15 K and 1 atm.

The transition state structure is characterised by a C_{α}-$C_{\beta\text{-ethylene}}$ distance of 2.177 Å. The insertion product, species **4A**, was calculated to be more stable than **3A** by 12.0 kcal/mol and was characterised by a stabilising γ-agostic interaction, evidenced by a Cr-H_{γ} distance of 2.184 Å. The propensity for the generation of longer chain olefins in comparison to chain termination via β-hydrogen transfer was modelled by the sequential coordination and insertion of ethylene from **4A** to generate the Cr-heptyl, **5A**, and Cr-nonyl species, **6A**, and the elimination of 1-nonene via BHT. Intermediates **5A** and **6A** are comparable to species **4A**, in terms of geometric aspects, and displays a decrease in the ground state energy with an increase in alkyl chain length (Fig. 5.27).

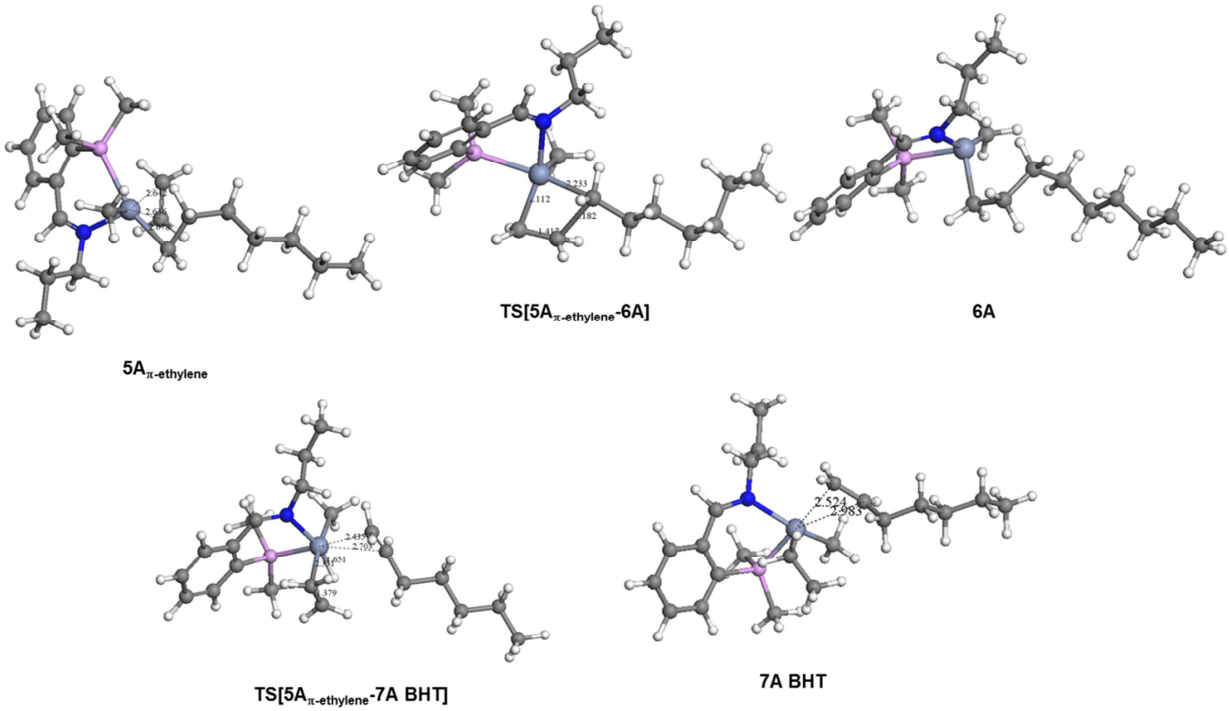

Fig. 5.27 Optimised structures of the transition state and product of ethylene insertion and β-hydrogen transfer from the Cr(III)-heptyl π-ethylene species, $\mathbf{5_{\pi\text{-ethylene}}}$.

In addition, barriers to insertion from the π-ethylene species are comparable to that observed for the coordination-insertion from **3A**. In contrast, chain termination via BHT was calculated to proceed with a barrier of 10.5 kcal/mol via transition state **TS[5A$_{\pi\text{-ethylene}}$-7A BHT]**, characterised by a Cr-H$_\beta$ interaction with a distance of 1.651 Å. Formation of the product of BHT, the Cr(III)-ethyl π-heptene species (**7A BHT**) was calculated to be exothermic by 18.5 kcal/mol relative to **3A**. Species **7A BHT** is characterised by a Cr-C$_\alpha$ and Cr-C$_\beta$ bond distance of 2.524 and 2.983 Å respectively. Our calculations thus show that chain growth is the dominant process in our catalytic cycle via a Cossee-Arlman mechanism.

5.3.4.3 Discussion of experimental and theoretical results.

Evaluation of the two mechanistic pathways showed that the key difference was in the propensity to undergo chain growth or termination. In the case of the Cossee-Arlman mechanism, chain growth via coordination-insertion was favoured while for the metallacycle mechanism chain termination via β-hydrogen transfer was favoured. The initial interpretation of the computational results would suggest that our catalyst system would be display activity and selectivity for ethylene trimerisation to form 1-hexene via a metallacycle mechanism, since the insertion barrier from **3A** (11.4 kcal/mol) is slightly higher than the barrier to form the Cr π-propylene species, **4M** (10.8 kcal/mol). The overriding factor appears to be the formation of the Cr-propyl π-ethylene species, $\mathbf{3A_{\pi\text{-ethylene}}}$, the formation of which requires less energy than formation of the transition state **TS[3A-4M]**, thereby alleviating the energetic requirements for chain growth to occur (Fig. 5.28). This would result in polymer-formation via a Cossee-Arlman mechanism.

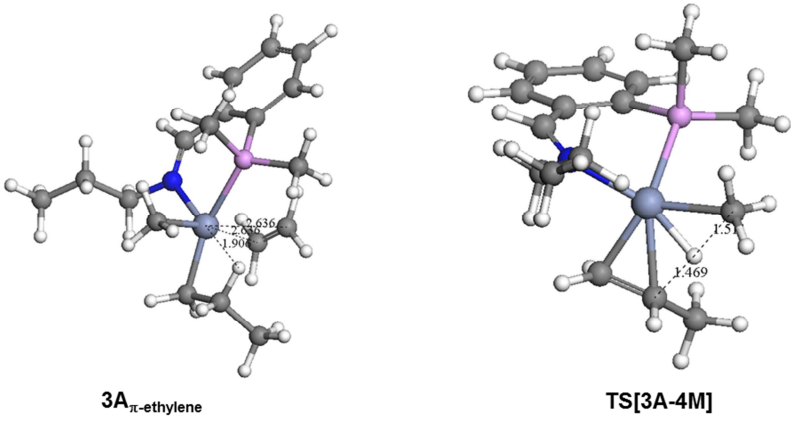

Fig. 5.28 The key intermediates identified within each mechanistic pathway which may affect the selectivity of the catalyst system.

Our experimental results suggest that 1-hexene formation does occur and that the oligomer is incorporated into the polymer backbone soon after its formation. Computationally, 1-hexene formation via a metallacycle mechanism is as facile as

polyethylene formation via a Cossee-Alrman mechanism. Our experimental and theoretical investigation thus suggests that the factors influencing product selectivity is not as clear-cut as initially anticipated and that further investigations is required. The next step in rational catalyst design would be to modify the ligand electronic and steric properties to either destabilise the Cr-propyl π-ethylene species or to decrease the energy of the transition state which generates the monovalent Cr-olefin complex, thereby enhancing the presumed trimerisation activity.

5.4 Conclusions.

A series of iminophosphine ligands, varying in their steric bulk at nitrogen, and their mononuclear Cr(III) complexes have been prepared and characterised. In the presence of Al cocatalysts, the Cr(III) complexes are active catalysts in the polymerisation of ethylene, forming predominantly linear high-density polyethylene. The polymers obtained were characterised by solid state NMR and powder X-ray diffraction which confirmed the high degree of crystallinity of the polymer and provided insight into polymer microstructure. In addition, preparative CRYSTAF, in combination with HT-SEC and DSC analysis, shed light on the molecular weight and molecular weight distribution of the isolated polymer. The catalyst system was observed to produce polymers which display multimodal character, with a broad molecular weight distribution. A low molecular weight fraction was isolated, which is speculated to be a co-polymer of ethylene and 1-hexene produced during catalysis. The effect of varying reaction conditions on catalytic activity was evaluated; under optimised conditions complex **6j** displayed an activity of up to 503 kg PE.mol$_{Cr}^{-1}$.h^{-1}. DFT calculations revealed that polyethylene-formation proceeds via a Cossee-Arlman mechanism and that 1-hexene formation via a metallacycle mechanism was energetically favourable. The comparable energetics of both chain growth mechanisms results in the formation of traces of

LLDPE, the microstructure of which needs to be confirmed by additional analytical techniques. Our theoretical and experimental investigation provided significant insights into Cr-catalysed ethylene oligo-/polymerisation and the factors governing the observed reactivity and selectivity, which would prove useful for future catalyst design.

5.5 Experimental Section.

All transformations were performed using standard Schlenk techniques under a nitrogen atmosphere. Solvents were dried by distillation prior to use and all other reagents were employed as obtained. NMR (^{1}H: 300 and 400 MHz; ^{13}C: 75 and 100 MHz) spectra were recorded on Varian VNMRS 300 MHz; Varian Unity Inova 400 MHz spectrometers and chemical shifts are reported in ppm, referenced to the residual protons of the deuterated solvents and tetramethyl silane (TMS) as internal standard. ESI-MS (positive and negative mode) analyses were performed on Waters API Quattro Micro and Waters API Q-TOF Ultima instruments by direct injection of sample. FT-IR analysis was performed on a Thermo Nicolet AVATAR 330 instrument, and was recorded as neat spectra (ATR) unless otherwise specified. Melting point determinations were performed on a Stuart Scientific SMP3 melting point apparatus and are reported as uncorrected. Magnetic susceptibility measurements were recorded on a Sherwood Scientific magnetic susceptibility balance. Solid samples were weighed in a glovebox in a calibrated sample tube.

5.5.1 Synthesis of N-substituted iminophosphine ligands.

5.5.1.1 [o-(diphenylphosphino)benzylidene]-N-propylamine (5a)

A slurry of *o*-diphenylphosphinobenzaldehyde (400 mg, 0.517 mmol) and propylamine (5 ml, 60.81 mmol) in EtOH (15 ml) was added. The reaction mixture was stirred under reflux for 4 h. After the allotted time the reaction mixture was cooled to room

temperature and the excess amine was removed *in vacuo*. The oily residue obtained was dissolved in dichloromethane (50 ml), the organic layer was washed with water (3 x 20 ml portions), dried over K_2CO_3, filtered and the solvent removed *in vacuo*. The product was isolated as an orange oil. Yield: 398 mg, 87 %. Spectroscopic data discussed in the results and discussion section in agreement with that reported previously.[7]

5.5.1.2 [o-(diphenylphosphino)benzylidene]-N-2,6-diisopropylphenylamine (5b)

The same synthetic procedure as outlined above (**5a**) was employed for the synthesis of **5b**, using 2,6-diisopropylaniline as reagent. Yield: 390 mg, 63 %. $^{13}C\{^1H\}$ (75.38 MHz, $CDCl_3$): δ 160.10 (C^1); δ 147.53 (C^8); δ 138.36 (C^2); δ 134.11 (C-P*Ph*$_2$); δ 132.39 (C^7); δ 131.07 (C^6); δ 130.96 (C^5); δ 129.52 (C^9) δ 129.26 (C^3); δ 128.91 (C^4); δ 128.85 (C-P*Ph*$_2$); δ 128.69 (C-P*Ph*$_2$); δ 128.57 (C-P*Ph*$_2$); δ 128.34 (C-P*Ph*$_2$) δ 126.74 (C^{11}); δ 124.77 (C^{10}); δ 127.50 (C-P*Ph*$_2$); δ 28.04 (C^{12}); δ 22.98 (C^{13}). Found (Calc) for $C_{31}H_{32}NP$: % C: 82.61 (82.82); % H: 7.09 (7.17); % N: 2.85 (3.12).

5.5.1.3 [o-(diphenylphosphino)benzylidene]-N-2,4,6-trimethylphenylamine (5c)

The same synthetic procedure as outlined above (**5a**) was employed for the synthesis of **5c**, using 2,4,6-trimethylaniline as reagent. Yield: 398 mg, 71 %. $^{13}C\{^1H\}$ (75.38 MHz, $CDCl_3$): δ 161.13 (C^1); δ 148.55 (C^8); δ 139.37 (C^7); δ 138.38 (C^6); δ 134.15 (C^2); δ 134.01 (C-P*Ph*$_2$); δ 133.33 (C^5); δ 132.77 (C^9) δ 130.86 (C^{10}); δ 128.95 (C^3); δ 128.90 (C-P*Ph*$_2$); δ 128.66 (C-P*Ph*$_2$); δ 128.62 (C-P*Ph*$_2$); δ 128.48 (C-P*Ph*$_2$); δ 127.52 (C-P*Ph*$_2$); δ 127.04 (C^4); δ 20.68 (C^{12}); δ 17.85 (C^{13}). Found (Calc) for $C_{28}H_{26}NP$: % C: 82.39 (82.53); % H: 6.20 (6.43); % N: 3.17 (3.44).

5.5.1.4 [o-(diphenylphosphino)benzylidene]-N-t-butylamine (5d)

The same synthetic procedure as outlined above (**5a**) was employed for the synthesis of **5d**, using *t*-butylamine as reagent. Yield: 347 mg, 73 %. Spectroscopic data discussed in the results and discussion section in agreement with that reported previously.[7]

5.5.1.5 [o-(diphenylphosphino)benzylidene]-N-2,2-dimethylpropylamine (5e)

The same synthetic procedure as outlined above (**5a**) was employed for the synthesis of **5e**, using 2,2-dimethylpropylamine as reagent. Yield: 371 mg, 75 %. $^{13}C\{^{1}H\}$ (75.38 MHz, $CDCl_3$): δ 160.91 (C^1); δ 137.47 (C^2); δ 133.81 (C-P*Ph*$_2$); δ 132.63 (C^7); δ 132.22 (C^6); δ 131.19 (C^5); δ 129.90 (C^7) δ 129.41 (C^3); δ 128.80 (C-P*Ph*$_2$); δ 128.77 (C^4); δ 128.70 (C-P*Ph*$_2$); δ 128.54 (C-P*Ph*$_2$); δ 128.33 (C-P*Ph*$_2$) δ 126.89 (C^{11}); δ 127.19 (C-P*Ph*$_2$); δ 71.98 (C^8); δ 33.01 (C^9); δ 25.69 (C^{10}). Found (Calc) for $C_{24}H_{26}NP$: % C: 79.98 (80.20); % H: 7.00 (7.29); % N: 3.76 (3.90).

5.5.2 Synthesis of mononuclear Cr(III) iminophosphinato complexes (5f-5j)

5.5.2.1 [$CrCl_3${o-(diphenylphosphino)benzylidene]-N-propylamine}](5f)

To a slurry of [$(THF)_3CrCl_3$] (200 mg, 0.534 mmol) in toluene (20 ml) was added [*o*-(diphenylphosphino)benzylidene]-*N*-propylamine (264 mg, 0.587 mmol). The reaction mixture was stirred under reflux for 18 h. After the allotted time the reaction mixture was cooled to room temperature; filtered; washed with pentane and dried in vacuo. Yield: 170 mg, 65 %. Found (Calc) for $C_{22}H_{22}Cl_3CrNP \cdot 0.3CH_2Cl_2$: % C: 51.67 (51.78); % H: 4.18 (4.41); % N: 2.65 (2.70).

5.5.2.2 [$CrCl_3${o-(diphenylphosphino)benzylidene]-N-2,6-diisopropylphenylamine}](5g)

The same synthetic procedure as outlined above (**5f**) was employed for the synthesis of **5g**, using *o*-(diphenylphosphino)benzylidene]-N-2,6-diisopropylphenylamine as reagent. Yield: 253 mg, 71 %. % Found (Calc) for $C_{31}H_{32}Cl_3CrNP \cdot 0.25CH_2Cl_2$: % C: 59.67 (59.66); % H: 4.98 (5.21); % N: 2.10 (2.23).

5.5.2.3 [$CrCl_3${o-(diphenylphosphino)benzylidene]-N-2,4,6-trimethylphenylamine}](5h)

The same synthetic procedure as outlined above (**5f**) was employed for the synthesis of **5h**, using *o*-(diphenylphosphino)benzylidene]-N-2,4,6-trimethylphenylamine as reagent. Yield: 212 mg, 70 %. % Found (Calc) for $C_{27}H_{24}Cl_3CrNP$: % C: 58.49 (58.77); % H: 4.21 (4.38); % N: 2.20 (2.54).

5.5.2.4 [$CrCl_3${o-(diphenylphosphino)benzylidene]-N-t-butylamine}](5i)

The same synthetic procedure as outlined above (**5f**) was employed for the synthesis of **5i**, using *o*-(diphenylphosphino)benzylidene]-N-*t*-butylamine as reagent. Yield: 215 mg, 80 %.% Found (Calc) for $C_{23}H_{24}Cl_3CrNP \cdot 0.25CH_2Cl_2$: % C: 52.98 (53.19); % H: 4.51 (4.70); % N: 2.40 (2.67).

5.5.2.5 [$CrCl_3${o-(diphenylphosphino)benzylidene]-N-2,2-dimethylpropylamine}](5j)

The same synthetic procedure as outlined above (**5f**) was employed for the synthesis of **5j**, using *o*-(diphenylphosphino)benzylidene]-N-2,2-dimethylpropylamine as reagent. Yield: 232 mg, 84 %.% Found (Calc) for $C_{24}H_{26}Cl_3CrNP$: % C: 55.29 (55.67); % H: 4.81 (5.06); % N: 2.52 (2.71).

5.5.3 General Procedures for catalysis experiments and polymer characterisation.

In a glovebox under a nitrogen atmosphere, a 250 ml Parr high-pressure autoclave was charged with the required amount of solvent and co-catalyst and was sealed prior to being attached to the ethylene feed. The reactor was brought to temperature at which point a dispersion of the pre-catalyst in toluene (total volume: 50 ml) was added via syringe under positive ethylene pressure. The ethylene feed was maintained at the required pressure throughout the catalytic run. After the allotted time the reactor was cooled to 0 °C, excess ethylene vented and the reaction mixture quenched with acidified MeOH (10 % solution). The precipitated polymer was washed with hydrochloric acid, water and acetone and dried at 60 °C *in vacuo* until constant mass. A sample of the organic layer was filtered and analysed by GC-FID to quantify any oligomers which may have formed; none was detected in all catalytic experiments. The crystalline phases of the polyethylene produced was determined by powder X-ray diffraction employing a Bruker D2 Phaser Table-top diffractometer equipped with Cu-Kα radiation at 30 kV and 10 mA, with a step size of 0.02°(2θ) and step time of 4 s between 2 ° and 40° (2θ). The Solid State NMR spectra of the polyethylene produced were acquired on a Varian VNMRS 500 MHz two-channel spectrometer using 3.2 mm zirconia rotors and a 3.2 mm Chemagnetics™ T3 HXY MAS probe. All cross-polarization (CP) spectra were recorded at ambient temperature with proton decoupling and a relaxation delay of 3 s. The power parameters were optimized for the Hartmann–Hahn match; the radio frequency fields were $\gamma_C B_{1C} = \gamma_H B_{1H} \approx 55$ kHz. The contact time for cross-polarization was 2 ms. The free induction decay was 852 points, Fourier transformed with 1704 points and 50 Hz line broadening. Magic angle spinning (MAS) was performed at 15 kHz and Adamantane was used as an external chemical shift standard where the downfield peak referenced to 38.3 ppm. The dipolar dephasing experiments were carried out under

similar conditions with the interrupted decoupling time constant, t1Xidref set to 40 μs after evaluating an array of time constants.

5.5.4 X-Ray Crystal Structure determination.

A single crystal of complex **5g** was mounted on a nylon loop and centred in a stream of cold nitrogen at 100(2) K. Crystal evaluation and data collection was performed on a Bruker-Nonius SMART Apex II CCD diffractometer with Mo K_α radiation (λ = 0.71073 Å). Data collection, reduction and refinement were performed using SAINT[38] and SADABS,[39] which forms part of the APEX II software package. The structures were solved by direct methods and refined by full-matrix least-squares on F^2 using SHELX-97[40] within the X-Seed graphic user interface.[41] All non-hydrogen atoms were refined anisotropically and all hydrogen atoms were placed using calculated positions and riding models. Four disordered dichloromethane solvent molecules were located in the electron density map; the position of which could not be located unambiguously. The contribution of the disordered solvent to the structure factors was secured by back-Fourier transformation using the SQUEEZE function within the PLATON software program.[42] The solvent-accessible void volume was calculated to be 376 $Å^3$/unit cell with an electron count of 165 electrons/unit cell.

5.5.5 High Temperature Size Exclusion Chromatography (HT-SEC).

Molar mass measurements for all samples were performed at 150 °C using a PL GPC 220 high temperature chromatograph (Polymer Laboratories, Church Stretton, UK) equipped with a differential refractive index (RI) detector. The column set used consisted of three 300 × 7.5 mm PLgel Olexis columns together with a 50 × 7.5 mm PLgel Olexis guard column (Polymer Laboratories, Church Stretton, UK). The eluent used was TCB, at a flow rate of 1.0 ml/min with 0.0125% 2,6-di-tert-butyl-4-methylphenol (BHT) added as a

stabiliser. Samples were dissolved at 160 °C in TCB at a concentration of 0.75 mg/ml for 3 h and 200 µl of each sample was injected. Narrowly distributed polystyrene standards (Polymer Laboratories, Church Stretton, UK) were used for calibration.

5.5.6 Differential Scanning Calorimetry (DSC).

Melting and crystallisation behaviours of SCF fractions were measured on a TA Instruments Q100 DSC system, calibrated with indium metal according to standard procedures. A heating rate of 10 °C/min was applied across the temperature range of 0-200 °C. Data obtained during the second heating cycle were used for all thermal analysis calculations. Measurements were conducted in a nitrogen atmosphere at a purge gas flow rate of 50 ml/min.

5.5.7 Crystallisation Analysis Fractionation (CRYSTAF).

CRYSTAF experiments were carried out using a commercial CRYSTAF apparatus Model 200 (Polymer Char, Valencia, Spain). For each sample, approximately 15 mg were dissolved in 35 ml of TCB. Crystallisation was carried out under agitation in stainless steel reactors, equipped with automatic stirring and filtration devices. After dissolution, the temperature was decreased from 100 ºC to approximately 30 ºC at a rate of 0.1 ºC/min. Fractions were taken automatically and the concentration of the solution was determined by an infrared detector, using 3.5 µm as the chosen wavelength.

5.5.8 Preparative Solution Crystallisation Fractionation (prep SCF).

In order to collect sufficient amounts of the soluble fraction, the bulk sample (approximately 600 mg) was dissolved in 200 mL xylene at 130 °C for 3 h under constant stirring of 200 rpm. After complete dissolution the reactor was cooled down to 30 °C at a rate

of 2 °C/ min. The crystallized fractions were collected by filtering the soluble fractions at room temperature. The room temperature soluble fractions (30 °C) were collected and the solvent removed to obtain the components. Both fractions (soluble and crystalline) were washed with acetone and dried in a vacuum oven overnight prior to HT-SEC and DSC analysis.

5.5.9 Computational Hardware.

Access to computational hardware employed in the molecular modelling study was provided by the Centre for High-Performance Computing (CHPC) via the "Sun Hybrid System".

5.5.10 Details of computations.

The computational results reported in this chapter were calculated using the Dmol^3 density functional theory (DFT) code[43] as implemented in the Accelrys MaterialsStudio (version 5.5) software package. The nonlocal generalised gradient approximation (GGA) exchange-correlation functional was employed in all geometry optimisations, specifically the PW91 functional of Perdew and Wang.[44] The Dmol^3 code utilises a basis set of numeric atomic functions, which are exact solutions to the Kohn-Sham equations for the atoms.[45] In general these basis sets are more complete than a comparable set of linearly independent Gaussian functions. In addition these basis sets have been demonstrated to have small basis set superposition errors. The computational investigation employed an all-electron polarised split valence basis set, termed double numeric polarised (DNP). All geometry optimisations employed highly efficient delocalised internal coordinates.[46] This has the advantage of significantly decreasing the number of iterations required for larger molecules during geometry optimisation when compared to traditional Cartesian coordinates. The tolerance for

convergence of the self-consistent field (SCF) density was set to 1 x 10^{-5} Hartrees while the tolerance for energy convergence was set at 1 x 10^{-6} Hartrees. Additional convergence criteria include the tolerance for converged gradient (0.002 Hartrees/Å) and the tolerance for converged atom displacement (0.005 Å).

Optimised geometries were subjected to full frequency analyses at the same GGA/PW91/DNP level of theory to verify the nature of the stationary points. Equilibrium geometries were characterised by the absence of imaginary frequencies while optimised transition state geometries exhibited a single imaginary frequency in the reaction coordinate. Preliminary transition state geometries were obtained by employing either the Dmol^3 PES scan functionality in Cerius[47] or the integrated linear synchronous transit/quadratic synchronous transit (LST/QST) algorithm[48] available in MaterialsStudio.

All computations were performed with the exclusion of solvent effects and the results obtained was mass-balanced for the isolated system in the gas phase. All reported energies incorporate Gibbs free energy corrections to the total electronic energies at 298.15 K and 1 atm.

5.6 References

(1) (a) McGuinness, D. S. *Chem. Rev.*, **2010**, *111*, 2321 (b) Agapie, T. *Coord. Chem. Rev.*, **2011**, *255*, 861.

(2) (a) Temple, C.; Jabri, A.; Crewdson, P.; Gambarotta, S.; Korobkov, I.; Duchateau, R. *Angew. Chem. Int. Ed.*, **2006**, *45*, 7050 (b) Jabri, A.; Temple, C.; Crewdson, P.; Gambarotta, S.; Korobkov, I.; Duchateau, R. *J. Am. Chem. Soc.*, **2006**, *128*, 9238.

(3) (a) Bollmann, A.; Blann, K.; Dixon, J. T.; Hess, F. M.; Killian, E.; Maumela, H.; McGuinness, D. S.; Morgan, D. H.; Neveling, A.; Otto, S.; Overett, M.; Slawin, A.

M. Z.; Wasserscheid, P.; Kuhlmann, S. *J. Am. Chem. Soc.*, **2004**, *126*, 14712 (b) Walsh, R.; Morgan, D. H.; Bollmann, A.; Dixon, J. T. *Applied Catalysis A: General*, **2006**, *306*, 184 (c) Blann, K.; Bollmann, A.; de Bod, H.; Dixon, J. T.; Killian, E.; Nongodlwana, P.; Maumela, M. C.; Maumela, H.; McConnell, A. E.; Morgan, D. H.; Overett, M. J.; Prétorius, M.; Kuhlmann, S.; Wasserscheid, P. *J. Catal.*, **2007**, *249*, 244 (d) Killian, E.; Blann, K.; Bollmann, A.; Dixon, J. T.; Kuhlmann, S.; Maumela, M. C.; Maumela, H.; Morgan, D. H.; Nongodlwana, P.; Overett, M. J.; Pretorius, M.; Höfener, K.; Wasserscheid, P. *J. Mol. Catal. A: Chem.*, **2007**, *270*, 214 (e) Overett, M. J.; Blann, K.; Bollmann, A.; de Villiers, R.; Dixon, J. T.; Killian, E.; Maumela, M. C.; Maumela, H.; McGuinness, D. S.; Morgan, D. H.; Rucklidge, A.; Slawin, A. M. Z. *J. Mol. Catal. A: Chem.*, **2008**, *283*, 114.

(4) (a) Agapie, T.; Schofer, S. J.; Labinger, J. A.; Bercaw, J. E. *J. Am. Chem. Soc.*, **2004**, *126*, 1304 (b) Do, L. H.; Labinger, J. A.; Bercaw, J. E. *Organometallics*, **2012**, *31*, 5143 (c) Thapa, I.; Gambarotta, S.; Korobkov, I.; Murugesu, M.; Budzelaar, P. *Organometallics*, **2011**, *31*, 486 (d) Albahily, K.; Fomitcheva, V.; Gambarotta, S.; Korobkov, I.; Murugesu, M.; Gorelsky, S. I. *J. Am. Chem. Soc.*, **2011**, *133*, 6380.

(5) (a) Yang, Y.; Liu, Z.; Zhong, L.; Qiu, P.; Dong, Q.; Cheng, R.; Vanderbilt, J.; Liu, B. *Organometallics*, **2011**, *30*, 5297 (b) Janse van Rensburg, W.; van den Berg, J.-A.; Steynberg, P. J. *Organometallics*, **2007**, *26*, 1000.

(6) (a) Albahily, K.; Ece, K.; Al-Badawi, D.; Savard, D.; Gambarotta, s.; Burchell, T. J.; Duchateau, R. *Angew. Chem. Int. Ed.*, **2008**, *47*, 5816 (b) Albahily, K.; Licciulli, S.; Gambarotta, S.; Korobkov, I.; Chevalier, R.; Schuhen, K.; Duchateau, R.

Organometallics, **2011**, *30*, 3346 (c) Albahily, K.; Ahmed, Z.; Gambarotta, S.; Koç, E.; Duchateau, R.; Korobkov, I. *Organometallics*, **2011**, *30*, 6022.

(7) Ghilardi, C. A.; Midollini, S.; Moneti, S.; Orlandini, A.; Scapacci, G. *J. Chem. Soc., Dalton Trans.*, **1992**, 3371.

(8) Antonels, N. C.; Therrien, B.; Moss, J. R.; Smith, G. S. *Inorg. Chem. Commun.*, **2009**, *12*, 716.

(9) (a) Flapper, J.; Wormald, P.; Lutz, M.; Spek, A. L.; van Leeuwen, P. W. N. M.; Elsevier, C. J.; Kamer, P. C. J. *Eur. J. Inorg. Chem.*, **2008**, 4968 (b) Flapper, J.; Kooijman, H.; Lutz, M.; Spek, A. L.; van Leeuwen, P. W. N. M.; Elsevier, C. J.; Kamer, P. C. J. *Organometallics*, **2009**, *28*, 3272 (c) Mungwe, N.; Swarts, A. J.; Mapolie, S. F.; Westman, G. *J. Organomet. Chem.*, **2011**, *696*, 3527 (d) Xu, T.; An, H.; Gao, W.; Mu, Y. *Eur. J. Inorg. Chem.*, **2010**, *2010*, 3360 (e) Liu, Z.; Gao, W.; Liu, X.; Luo, X.; Cui, D.; Mu, Y. *Organometallics*, **2011**, *30*, 752.

(10) (a) de Laeter, J. R. *Applications of inorganic mass spectrometry*; J. Wiley: New York, 2001, (b) Henderson, W.; McIndoe, J. *Mass spectrometry of inorganic, coordination and organometallic compounds : tools, techniques, tips*; J. Wiley Chichester, West Sussex 2005,

(11) (a) Conde-Guadano, S.; Danopoulos, A. A.; Pattacini, R.; Hanton, M.; Tooze, R. P. *Organometallics*, **2012**, *31*, 1643 (b) Wang, D.; Liu, S.; Zeng, Y.; Sun, W.-H.; Redshaw, C. *Organometallics*, **2011**, *30*, 3001 (c) Rüther, T.; Braussaud, N.; Cavell, K. J. *Organometallics*, **2001**, *20*, 1247.

(12) (a) McGuinness, D. S.; Wasserscheid, P.; Keim, W.; Hu, C.; Englert, U.; Dixon, J. T.; Grove, C. *Chem. Commun.*, **2003**, 334 (b) Liu, S.; Pattacini, R.; Braunstein, P. *Organometallics*, **2011**, null.

(13) (a) Weeks, C. L.; Levina, A.; Dillon, C. T.; Turner, P.; Fenton, R. R.; Lay, P. A. *Inorg. Chem.*, **2004**, *43*, 7844 (b) Namba, K.; Wang, J.; Cui, S.; Kishi, Y. *Organic Letters*, **2005**, *7*, 5421.

(14) (a) Teo, S.; Weng, Z.; Hor, T. S. A. *Organometallics*, **2008**, *27*, 4188 (b) Kim, S.-K.; Kim, T.-J.; Chung, J.-H.; Hahn, T.-K.; Chae, S.-S.; Lee, H.-S.; Cheong, M.; Kang, S. O. *Organometallics*, **2010**, *29*, 5805.

(15) (a) De Rosa, F.; Bu, X.; Ford, P. C. *Inorg. Chem.*, **2003**, *42*, 4171 (b) Jie, S.; Pattacini, R.; Rogez, G.; Loose, C.; Kortus, J.; Braunstein, P. *Dalton. Trans.*, **2009**, *0*, 97.

(16) Elowe, P. R.; McCann, C.; Pringle, P. G.; Spitzmesser, S. K.; Bercaw, J. E. *Organometallics*, **2006**, *25*, 5255.

(17) (a) Licciulli, S.; Albahily, K.; Fomitcheva, V.; Korobkov, I.; Gambarotta, S.; Duchateau, R. *Angew. Chem. Int. Ed.*, **2011**, *50*, 2346 (b) Albahily, K.; Gambarotta, S.; Duchateau, R. *Organometallics*, **2011**, *30*, 4655.

(18) Xu, T.; Pan, Y.; Lu, X.-B. *Dalton. Trans.*, **2011**, *40*, 8643.

(19) Zhang, L.; Gao, W.; Tao, X.; Wu, Q.; Mu, Y.; Ye, L. *Organometallics*, **2010**, *30*, 433.

(20) (a) Ittel, S. D.; Johnson, L. K.; Brookhart, M. *Chem. Rev.*, **2000**, *100*, 1169 (b) Tempel, D. J.; Johnson, L. K.; Huff, R. L.; White, P. S.; Brookhart, M. *J. Am. Chem. Soc.*, **2000**, *122*, 6686.

(21) (a) Hu, W.; Sirota, E. B. *Macromolecules*, **2003**, *36*, 5144 (b) Gao, X.; Wang, L.; Luo, H.; Zou, Q.; Feng, N.; Feng, J. *Macromolecules*, **2010**, *43*, 5713.

(22) (a) Kim, S.; Kim, J. K.; Park, C. E. *Polymer*, **1997**, *38*, 2113 (b) Joo, Y. L.; Han, O. H.; Lee, H. K.; Song, J. K. *Polymer*, **2000**, *41*, 1355.

(23) Baker, A. M. E.; Windle, A. H. *Polymer*, **2001**, *42*, 667.

(24) Sun, M.; Xu, T.; Gao, W.; Liu, Y.; Wu, Q.; Mu, Y.; Ye, L. *Dalton. Trans.*, **2011**, *40*, 10184.

(25) Thushara, K. S.; Mathew, R.; Ajithkumar, T. G.; Rajamohanan, P. R.; Bhaduri, S.; Gopinath, C. S. *J. Phys. Chem. C*, **2009**, *113*, 8556.

(26) Gulmine, J. V.; Janissek, P. R.; Heise, H. M.; Akcelrud, L. *Polym. Test.*, **2002**, *21*, 557.

(27) Monrabal, B. *J. Appl. Polym. Sci.*, **1994**, *52*, 491.

(28) Soares, J. B. P.; Anantawaraskul, S. *J. Polym. Sci., Part B: Polym. Phys.*, **2005**, *43*, 1557.

(29) Pasch, H.; Malik, M. I.; Macko, T. *Adv. Polym. Sci.*, **2013**, *251*, 77.

(30) (a) Luruli, N.; Heinz, L.-C.; Grumel, V.; Brüll, R.; Pasch, H.; Raubenheimer, H. G. *Polymer*, **2006**, *47*, 56 (b) Wet-Roos, D. D. E.; Toit, A. D. U.; Joubert, D. J. *J. Polym. Sci., Part A: Polym. Chem.*, **2006**, *44*, 6847.

(31) (a) Hu, T.; Tang, L.-M.; Li, X.-F.; Li, Y.-S.; Hu, N.-H. *Organometallics*, **2005**, *24*, 2628 (b) Reardon, D.; Conan, F.; Gambarotta, S.; Yap, G.; Wang, Q. *J. Am. Chem. Soc.*, **1999**, *121*, 9318.

(32) (a) Abramo, G. P.; Li, L.; Marks, T. J. *J. Am. Chem. Soc.*, **2002**, *124*, 13966 (b) Vasile, C. *Handbook of Polyolefins*; Marcel Dekker: New York, 2000, 401-411.

(33) Janse van Rensburg, W.; Grové, C.; Steynberg, J. P.; Stark, K. B.; Huyser, J. J.; Steynberg, P. J. *Organometallics*, **2004**, *23*, 1207.

(34) (a) Tomov, A. K.; Chirinos, J. J.; Jones, D. J.; Long, R. J.; Gibson, V. C. *J. Am. Chem. Soc.*, **2005**, *127*, 10166 (b) Tomov, A. K.; Gibson, V. C.; Britovsek, G. J. P.;

Long, R. J.; van Meurs, M.; Jones, D. J.; Tellmann, K. P.; Chirinos, J. J. *Organometallics*, **2009**, *28*, 7033.

(35) (a) Gibson, V. C.; Spitzmesser, S. K. *Chem. Rev.*, **2002**, *103*, 283 (b) Chen, E. Y.-X.; Marks, T. J. *Chem. Rev.*, **2000**, *100*, 1391.

(36) Zurek, E.; Ziegler, T. *Inorg. Chem.*, **2001**, *40*, 3279.

(37) (a) Blom, B.; Klatt, G.; Fletcher, J. C. Q.; Moss, J. R. *Inorg. Chim. Acta*, **2007**, *360*, 2890 (b) Yu, Z.-X.; Houk, K. N. *Angew. Chem. Int. Ed.*, **2003**, *42*, 808 (c) de Bruin, T. J. M.; Magna, L.; Raybaud, P.; Toulhoat, H. *Organometallics*, **2003**, *22*, 3404.

(38) 6.45 ed.; Bruker AXS Inc.: Madison, WI, 2003.

(39) Blessing, R. H. *Acta Crystallogr. Sect. A: Found. Crystallogr.*, **1995**, *51*, 33.

(40) Sheldrick, G. M., 1997.

(41) (a) Barbour, L. J. *J. Supramol. Chem.*, **2001**, *1*, 189 (b) Atwood, J. L.; Barbour, L. J. *Cryst. Growth. Des.*, **2003**, *3*, 3.

(42) Spek, A. L. *J. Appl. Crystallogr.*, **2003**, *36*, 7.

(43) (a) Delley, B. *J. Chem. Phys.*, **1992**, *92*, 508 (b) Delley, B. *J. Chem. Phys.*, **1996**, *100*, 6107 (c) Delley, B. *J. Chem. Phys.*, **2000**, *113*, 7756.

(44) (a) Perdew, J. P. *Physica B*, **1991**, *172*, 1 (b) Perdew, J. P.; Wang, Y. *Phys. Rev. B: Condens. Matter*, **1992**, *45*, 13244.

(45) Delley, B. In *Theoretical and Computational Chemistry*; Seminario, J. M., Politzer, P., Eds.; Elsevier: Amsterdam, The Netherlands, 1995; Vol. 2,

(46) Andzelm, J.; King-Smith, R. D.; Fitzgerald, G. *Chem. Phys. Lett.*, **2001**, *335*, 321.

(47) Vogt, D. In *Applied Homogeneous Catalysis with Organometallic Compounds*; Cornils, B., Herrmann, W. A., Eds.; VCH: Weinheim, Germany, 1996,

(48) Govind, N.; Petersen, G.; Fitzgerald, G.; King-Smith, R. D.; Andzelm, J. *Comput. Mater. Sci.*, **2003**, *28*, 250.

6.1 General Conclusions

In summary, this thesis investigated the synthesis, characterisation and catalytic application of early and late transition metal complexes in ethylene oligomerisation and polymerisation. More specifically, it envisaged the employment of experimental and computational techniques to rationalise the observed reactivity and selectivity, with the aid of aiding future catalyst design strategies.

A series of neutral (**2a-2e**) and cationic methylpalladium acetonitrile-ligated (**2f-2j**) complexes, bearing *N*-alkyl dipyridylaldimine ligands, were prepared and characterised. The cationic acetonitrile analogues (**2f-2j**) were found to be unstable both in the solid state and solution. To circumvent the observed instability, a series of cationic pyridine-ligated analogues (**2k-2o**) were prepared and characterised. During the synthesis of complexes **2k-2o** it was observed that the ratio of pyridine to neutral complex impacts on the nature of the material isolated. Employing an excess of pyridine allowed for the isolation of the first example of a cationic tris(pyridine) methylpalladium complex (**2o-A**), which was characterised crystallographically. Evaluation of the cationic acetonitrile analogues (**2f-2j**) in preparative scale ethylene oligomerisation showed that these complexes dimerise ethylene to a mixture of 1- and 2-butenes with relatively low activities. The low activity was attributed to decomposition of the cationic complexes at room temperature. Low-temperature spectroscopic investigations employing complexes **2f** and **2j**, established differences in the rate of associative olefin exchange at -78 °C. Associative olefin exchange was found to proceed at lower temperatures for complex **2f** in comparison to **2j**, which was attributed to steric effects. Furthermore, the rate of ethylene insertion into the Pd-Me bond was observed to be faster for complex **2f** in comparison to **2j**, which was attributed to an increase in electrophilicity at palladium in **2f** in comparison to **2j**. The catalyst resting state was

identified as the Pd-ethyl π-ethylene species, from which ethylene insertion into the Pd-Et bond was found to be faster for **2f** in comparison to **2j**. Employing DFT calculations, the overall catalytic cycle could be modelled for **2f** and **2j**. Our calculations corroborated the observed differences in associative olefin exchange, confirmed the formation of the catalyst resting state and identified differences in the energetics of butene isomerisation for **2f** and **2j.**

A series of dinuclear chloro-bridged Ni(II) complexes (**4a**-**4e**), ligated by *N*-alkyl dipyridylamine ligands, were prepared and characterised. Spectroscopic and analytical techniques were consistent with a dimeric structure in which the Ni(II) centres were paramagnetic. During mass spectrometric analysis of the isolated complexes, interesting solvent-dependent fragmentation and aggregation of species present in solution was observed and rationalised. SCD analysis allowed for the unambiguous characterisation of complex **4a**. In the case of complex **4e**, an interesting acid-mediated hydrolysis process was identified, the product of which (complex **4e-A**) was characterised crystallographically. Complex **4e-A** was identified as a salt, with the cation consisting of a singly protonated ligand and the anion consisting of a tetrachloronickelate di-anion, with the general formula $\{2LH\}^{2+}\{NiCl_4\}^{2-}$. Complexes **4a**-**4e**, in the presence of alkyl aluminium reagents, catalysed the oligomerisation of ethylene to a mixture of butenes, hexenes and octenes. In all cases, the selectivity was observed to be toward the formation of butenes, with traces of internal hexenes and octenes being formed. Under optimised conditions, activities of up to 864 $kg_{oligomers}.mol_{Ni}^{-1}.h^{-1}$ and selectivities of up to 98 % 1-butene could be observed.

A series of mononuclear Cr(III) iminophosphine-ligated complexes (**5f**-**5j**), varying in their steric bulk at nitrogen, were prepared and characterised. Upon activation with alkyl aluminium reagents, the complexes were found to be active ethylene polymerisation catalysts, with moderate activity of up to 508 $kg_{PE}.mol_{Cr}^{-1}.h^{-1}$. Characterisation of the

obtained polymer by various solution and solid state analytical techniques identified the bulk polymer as high-density polyethylene. In particular, HT-SEC analysis, showed that the catalytic system produces polyethylene with broad molecular weight and polydispersity indices. To gain more insight into whether the polymerisation was single- or multi-site in nature, CRYSTAF and preparative SCF analyses were conducted on the bulk material. It was found that the majority of the bulk material consists of high-density polyethylene and that the polymerisation was multi-modal in character. A small fraction of the bulk material displayed bimodal polymerisation behaviour, with the analytical results suggesting that the small fraction might be linear low-density polyethylene. The formation of linear low-density polyethylene would require the oligomerisation of ethylene at a particular active site, followed by incorporation of the eliminated α-olefin into the growing polymer chain at another active site. To probe whether our catalyst system would preferentially oligomerise or polymerise ethylene, DFT calculations were performed. Employing a simplified model, our calculations showed that the initial active species entering the catalytic cycle is a Cr(III) species. It was found that for ethylene oligomerisation via a metallacycle mechanism, chain termination was the dominant pathway, which would result in the selective formation of 1-hexene. In the case of ethylene polymerisation via a Cossee-Arlman mechanism, chain growth was found to be the dominant pathway, leading to the formation of polyethylene. Our calculations identified two intermediates, one present in the Cossee-Arlman mechanism and the other present in the metallacycle mechanism, which differ in relative energy by less than 1 kcal/mol. Our computational investigation thus implies that our Cr(III) catalyst system is capable of both selective oligomerisation and polymerisation.

6.2 Future Prospects

As is always the case when conducting research, the current study has generated a number of questions which may be addressed in the future.

6.2.1 Pd(II)-catalysed ethylene oligomerisation.

The low activity observed during room temperature preparative scale ethylene dimerisation, may be circumvented by performing the reactions at low temperatures. We found during our NMR kinetic investigations that ethylene dimerisation proceeds at -10 °C with negligible formation of palladium black. Mimicking these reaction conditions may generate a more long-lived catalyst system, which could display higher activity toward ethylene dimerisation.

In the context of ligand design, it was found computationally that the isomerisation of 1-butene is less facile for **2j** in comparison to **2f**. Our kinetic investigations and preparative scale catalysis reactions showed that the formation of 2-butenes predominates for all the evaluated pre-catalysts. This is likely as a result of low energy barriers for butene isomerisation, which are operative in solution. To probe this hypothesis, a series of ligands may be developed in which the steric bulk of the ortho substituents are gradually increased. This may lead to the isolation of a pre-catalyst which dimerise ethylene selectively to 1-butene.

The isolation of the cationic tris(pyridine) methylpalladium complex, **2o-A**, provides access to a novel class of cationic pre-catalysts which may be active in ethylene dimerisation. It is envisaged that analogues bearing different pyridine derivatives can be prepared and their catalytic activity evaluated in preparative scale ethylene dimerisation reactions. Also, the

kinetics of insertion and the generation of the catalyst resting states may be monitored by low-temperature spectroscopic techniques.

6.2.2 Ni(II)-catalysed ethylene oligomerisation.

An acid-mediated hydrolysis process was proposed for the formation of the tetrachloronickelate salt, **4e-A**. To test this hypothesis, the ligand may be reacted with acid, followed by the addition of a Ni(II) salt such as $NiCl_2 \cdot 6H_2O$, in an attempt to prepare tetrachloronickelate salts. During the evaluation of **4a-4e** as catalyst precursors in ethylene oligomerisation it was hypothesised that the increase in catalytic activity observed when activating the Ni(II) complexes, **4a-4e**, with DEAC in comparison to MAO was as a result of the direct formation of the catalyst resting state in the former. This hypothesis may be probed experimentally, by reacting the Ni(II) pre-catalyst with equimolar amounts of DEAC or MAO in the presence of ethylene at low temperatures, which may allow for the identification of the catalyst resting state by NMR spectroscopy. In addition, comparative insertion kinetics may be determined, particularly for **4a** and **4e**, which would provide evidence of how steric and electronic effects impact on the observed selectivity and reactivity. The experimental investigation may be supplemented with a comparative evaluation of the energetics associated with activation of the pre-catalyst with MAO and DEAC, employing DFT calculations. This would contribute to an understanding of the mechanistic aspects of the catalytic system which has been developed.

6.2.3 Cr(III)-catalysed ethylene polymerisation.

The formation of what is speculated to be traces of LLDPE during ethylene polymerisation by the Cr(III) complexes, **5f-5i**, is very interesting. Future work may include evaluating the formation of polymer in the presence of an α-olefin such as 1-hexene. It is

hypothesised that an increase in co-monomer concentration, in this case 1-hexene, would promote co-monomer incorporation, thereby generating larger quantities of the copolymer which can be isolated and characterised. Specifically, characterisation by NMR spectroscopy would establish the degree of branching within the copolymer. In the context of ligand design, selective trimerisation catalysts may be accessed by reducing the imine functionality in the ligands **5a-5e**. Deprotonation and coordination to Cr(III) precursors may generate a pre-catalyst which possesses sufficient electronic stabilisation to stabilise the Cr(I) oxidation state, known to catalyse selective trimerisation via a metallacycle mechanism.